New Catalysts for Ester Hydrogenation and the Oxygen Reduction Reaction

by

Shuai Xu

A thesis submitted in partial fulfillment of the requirements for the degree of

Doctor of Philosophy

Department of Chemistry
University of Alberta

Abstract

This dissertation reports a crosslinked catalyst organic framework, which was prepared by an alternating ring opening olefin metathesis polymerization (alt-ROMP) between dichloro{*N,N'*-bis({(2-diphenylphosphino)phenyl}methylidene)bicyclo[2.2.1]-hept-5-ene-2,3-diamine}-ruthenium, 1,2-*N*-di(*cis*-5-norbornene-2,3-endo-dicarboximido)-ethane, and *cis*-cyclooctene (COE) catalyzed by $RuCl_2(=CHPh)(PCy_3)_2$ in the presence of a $BaSO_4$ support. The heterogenized catalyst hydrogenated methyl benzoate at a similar rate to the homogeneous catalyst (0.0025 mol% catalyst, 10 mol% KO*t*Bu, 80 °C, 50 bar, THF, 21 h, ~15000 turnovers during the first 1 h). The catalyst was used five times for a total of 121680 turnovers. A study on the reusability of this catalyst showed that ester hydrogenations with bifunctional catalysts slow down as the reaction proceeds. This inhibition is removed by isolating and reusing the catalyst, suggesting that future catalyst design should emphasize avoiding product inhibition.

The *trans*-2,3-Diaminonorborn-5-ene dihydrochloride was resolved using L-menthol as the chiral auxiliary. Four PNNP ligands and their Ru catalyst monomers were synthesized using this resolved precursor. These four catalyst monomers and their alt-ROMP polymers were studied as enantioselective catalysts in the transfer hydrogenation of acetophenone from 2-PrOH (0.5 mol% catalyst, 0.25 mol% KO*t*Bu, rt–45 °C, 2-PrOH) and in the hydrogenation of β-chiral esters via dynamic kinetic resolution (2–2.5 mol% catalyst, 50 mol% NaO*i*Pr, rt, THF, 4 bar H_2); moderate ee's (up to 52%) were obtained within these catalyses.

A base-stable cationic monomer, 4-[6-azonia-spiro[5.5]undecyl]-4-azatricyclo-[5.2.1.0^{2,6}]dec-8-ene-3,5-dione tetrafluoroborate, was designed and synthesized. This monomer (2 equiv.) was copolymerized with [RuCl_2(*N,N'*-bis{2-(diphenylphosphino)benzyl}-

bicyclo[2.2.1]hept-5-ene-2,3-diamine)] (1 equiv.) and COE (3 equiv.) via ROMP by a sequential addition method catalyzed by 0.1 equiv. $RuCl_2(=CHPh)(PCy_3)_2$. The resulting polymeric catalyst contains cationic moieties close to the catalyst metal center and it was immobilized via ROMP over $BaSO_4$ by addition of extra COE and the crosslinker, 1,2-*N*-di(cis-5-norbornene-2,3-endo-dicarboximido)-ethane. It was anticipated that the cationic moiety holds an alkoxide counterion in a reusing ester hydrogenation, which provides a higher local concentration of base that facilitates the hydrogenation. This hypothesis was examined in the hydrogenation of methyl benzoate (S/C = 4200/1, 50 bar H_2, rt, 22 h, THF) in the absence of excess base. The results imply that the proposed local-base assistance does not exist within the current system.

Glancing Angle Deposition (GLAD) was used to prepare 500 nm long Ni nanopillars directly on glassy carbon disc electrodes (Ni_{GLAD}/GC). Ni_{GLAD}[Pt]/GC core-layer nanopillars were prepared by depositing Pt on the Ni_{GLAD} substrate via a novel rotating disc electrode galvanostatic deposition, where a stationary blackened Pt counter electrode served as the Pt source. Scanning electron microscopy, cyclic voltammetry, and inductively-coupled mass spectrometry were employed to characterize the deposits. The results indicated that the Pt was deposited in a conformal manner on the Ni_{GLAD} giving a loading of 11.6 μg. The Ni_{GLAD}[Pt]/GC electrode was about three fold more active than a [Pt]/GC (made with the same deposition in the absence of Ni) towards the oxygen reduction reaction (ORR) in 1.0 M KOH. As well, long term potentiostatic ORR studies showed that the Ni_{GLAD}[Pt]/GC deposit was more durable than the [Pt]/GC, with the former completely retaining its initial performance after 5000 s polarization at 0.85 V vs. RHE, while [Pt]/GC lost 38% of its activity. Subsequent

control experiments in the absence of O_2 showed that such decay was not due to loss of Pt over the prolonged ORR.

Preface

The following is a listing of the contents of each chapter in this thesis.

Chapter 1 is an introductory chapter on catalysis and the catalytic hydrogenation of esters.

Chapter 2 has been copied and/or adapted from the following publication:

Xu, S.; Kalapugama, S.; Rasu, L.; Bergens, S. H., Preparation and study of reusable polymerized catalysts for ester hydrogenation. *ACS Omega*, **2019**, *4*, 12212-12221.

Shuai Xu completed most of the experiments in this project. Suneth Kalapugama did the preliminary study of the ligand synthesis. Dr. Loorthuraja Rasu performed several experiments to address reviewers' comments when the manuscript was under review, and helped the formating of the manuscript. Prof. Steven H. Bergens was the research supervisor of this project.

Chapter 3 is original, unpublished, independent work by the author under the supervision of Prof. S. H. Bergens. Part A of this chapter reports the enantioselective catalyses of a group of RuPNNP complexes. Part B of this chapter is on a polymeric ester hydrogenation catalyst with neighboring base moieties.

Chapter 4 has been copied and/or adapted from the following paper, with a partially re-written introduction:

Xu, S.; Wang, C.; Francis, S. A.; Tucker, R. T.; Sorge, J. B.; Moghaddam, R. B.; Brett, M. J.; Bergens, S. H., Glancing angle deposited Ni nanopillars coated with conformal, thin layers of Pt by a novel electrodeposition: Application to the oxygen reduction reaction. *Electrochim. Acta* **2015,** *151*, 537-543.

Shuai Xu and Dr.Wang were in charge of the electrochemical experiments and data analysis; Dr. Francis did the preliminary study of the project; Dr. Tucker and Dr. Sorge worked on the glancing angle deposition of nickel and scanning electron microscopy characterization; Dr. Moghaddam assisted in the general discussion and the manuscript preparation; Prof. S. H. Bergens and Prof. M. J. Brett were the research supervisors of this project.

Chapter 5 is a summary of the dissertation along with a discussion of future research directions.

Acknowledgements

To my supervisor, Dr. Steven Bergens, I would like to thank you for your guidance in my study and career, it will be a great treasure in my life. Your beautiful verse "Faster, Shuai, Oh-My" will motivate me continuously until I retire. It has been a great experience to learn from, and to work with you.

I sincerely thank my committee members: Dr. Jonathan Veinot, Dr. Derrick Clive, Dr. Rylan Lundgren, Dr. Florence Williams, who help me with my PhD study, review my reports, and attend my candidacy and final defence. I also thank Dr. Brian Sterenberg who kindly agreed to be my external examiner.

A special thanks to Dr. Anna Jordan, who kindly and patiently helped me with editing this thesis. I learned a lot from you.

I sincerely thank Dr. Jason Cooke and Dr. Norman Gee, it was my pleasure to work as a teaching assistant in your labs.

I would like to acknowledge the individuals for the Department of Chemistry. They are Anita Weiler, Mark Miskolzie, Nupur Dabral, Jason Dibbs, Ryan Lewis, and everyone from the analytical laboratory and the mass spectrometry laboratory. I wish to extend my thanks to the Department of Chemistry and the University of Alberta, for providing me such a good place to work.

Thank all my friends in the Bergens group, Prabin Nepal, Dr. Loorthuraja Rasu, Dr. Mona Amiri, Dr. Chao Wang, Dr. Reza Moghaddam, Suneth Kalapugama, Riley Endean, Octavio Martinez, Dr. Jaya Pal, Jinkun Liu, Samuel Varley, Austin Penner, James Pearson, Ben Rennie, Yin Juan Hu, and Wanyue Xu. Thanks for all your company and support during these years.

I am so thankful for my family: my wife, Mingyu, who has been loving and considerate all the time. My mom and dad, who always try to give me everything. My grandpa and grandma, who are still so caring about everything of me in their 90s. To my son, who came to us right in the middle of my thesis-writing months, thank you for bringing so much joy to us and being calm (sometimes) when your dad is working, I promise that your mom and I will figure out a perfect name for you after I submit this thesis.

Table of Contents

List of Schemes

Chapter 1

Chapter 2

Chapter 3

Chapter 5

List of Figures

Chapter 1

Chapter 2

Chapter 3

Chapter 4

Chapter 5

List of Tables

Chapter 2

Chapter 3

Chapter 4

List of Abbreviations

acac   acetylacetonate anion ($CH_3COC^{(-)}HCOCH_3$)

Alt-ROMP   alternating ring-opening metathesis polymerization

BINAP   2,2′-bis(diphenylphosphino)-1,1′-binaphthyl

BINOL   1,1′-bi-2-naphthol

CE   counter electrode

COD   cycloocta-1,5-diene

COE   *cis*-cyclooctene

CV   cyclic voltammogram

de   diastereomeric excess

DFT   density functional theory

DKR   dynamic kinetic resolution

DMA   *N,N*-dimethylacetamide

DPEN   1,2-diphenyl-1,2-ethylenediamine

ECSA   electrochemical active surface area

ee   enantiomeric excess

FAME   fatty acid methyl ester

GC   gas chromatography or glassy carbon

GC-MS   gas chromatography–mass spectrometry

GLAD   glancing angle deposition

HMS   hexagonal mesoporous silica

ICP-MS   inductively coupled plasma mass spectrometry

KHMDS   potassium bis(trimethylsilyl)amide

NBD   2,5-norbornadiene

NHC   N-heterocyclic carbenes

NMR   nuclear magnetic resonance

Norphos   2,3-bis(diphenylphosphino)bicyclo[2.2.1]hept-5-ene

NP   nanoparticle

NW   nanowire

ORR	oxygen reduction reaction
PEG-Oms	polyethylene glycol 2000 monomethyl ether mesylate
PEM	polymer electrolyte membrane
PhanePhos	4,12-bis(diphenylphospino)-[2,2]paracyclophane
PNP, PNNP, PN	refers to a multidentate ligand coordinating via N and P atoms.
PVD	physical vapor deposition
Py	pyridine
RHE	reversible hydrogen electrode
ROMP	ring-opening metathesis polymerization
rt	room temperature
SEM	scanning electron microscopy
Sol	solvento ligand
TMM	trimethylenemethane
TO	turnovers
TOF	turnover frequency
TON	turnover number
Triphos	bis(diphenylphosphinoethyl)phenylphosphine
TsDPEN	*N*-*p*-tosyl-1,2-diphenylethylenediamine
WE	working electrode

Chapter 1

Introduction

1.1 Catalysis and Green Chemistry

Catalysts are substances that facilitate chemical reactions. Catalysis is a natural phenomenon. One example of catalysis is the biological reactions catalyzed by enzymes. It also exists in non-living systems, such as the Cl atom catalysis of ozone depletion ($O_3 + O \rightarrow 2\ O_2$).[1] The phenomenon of catalysis has been observed and utilized for thousands of years. The production of alcohol using a fermentation process is found in the history of most civilizations.[2, 3] Catalysis was recorded scientifically for the first time by Elizabeth Fulhame in 1794, when she found that water facilitated the oxidation of CO, but water did not get changed.[4] In 1817, Davy found that coal gas ignited with oxygen on the surface of Pt or Pd wire without lighting it with a flame.[2] Later, the concept of "catalysis" was proposed by Berzelius in 1835. The word "catalysis" was generated from Greek words, emphasizing the unchanging nature of a substance (a catalyst) which accelerates a reaction.[5-7]

The implementation of catalysis in chemical production took place in the 19th century. In 1831, Phillips[8] patented a method that used Pt to facilitate the oxidation of SO_2 to SO_3, and which eventually was used in the production of sulfuric acid during the late 19th century.[9] One milestone in industrial catalysis was the production of ammonia from nitrogen gas and hydrogen gas: Haber demonstrated the production of ammonia using an Os-based catalyst (later replaced by the Fe-based catalyst found by Mittasch), which was scaled up to production by Bosch in BASF in 1910. Today, 95% (by volume) of all industrial products and 70% of chemical production processes require catalysis.[10] Catalysis provides an 80% added value to chemical industrial products, and it is estimated that more than 35% of the global GDP is related to catalysis.[11] Catalysis itself is a huge market; the value of all catalysts reached 17.2 billion USD in 2014 worldwide, and it is growing.[10]

"Green chemistry" is a modern concept describing a preferable chemical production that should be clean, safe, and environmentally friendly.[12] Twelve principles of green chemistry were formulated by Anastas and Warner in 1998.[13] A simplified summary of these principles is as follows: (1) The formation of waste or byproducts should be as little as possible, especially for those contain toxic substances; (2) The cooperation of each substance in a reaction should be maximized; (3) Ideally, chemical production should proceed in a straightforward route under mild conditions; (4) The consumption of energy should be minimized in a reaction; (5) The reaction process should be safe and properly monitored; (6) Renewable starting materials and non-toxic products are preferred.[14]

Catalysts provide very good solutions to address those concerns.[15] First, catalysis is an alternate pathway for a non-catalytic reaction, it generally requires fewer resources, and it generates less waste. Second, a catalytic process has a lower activation energy compared to the non-catalytic reaction, leading to a faster reaction rate and the possibility of milder conditions (temperature, pressure, etc.). Third, catalysis endows the reactions with better selectivities (chemo-, regio-, diastereo-, and enantio-), which further simplifies the separation and reduces the waste of a reaction.[16-18]

1.2 The Reduction of Esters and Ester Hydrogenations

The reduction of carbonyl compounds is a good example to illustrate how catalysis fits the concept of "green chemistry". Carbonyl compounds, including aldehydes, ketones, esters, amides, and carboxylic acids, can be reduced to alcohols with hydride reducing agents, such as $NaBH_4$ and $LiAlH_4$, in non-catalytic reactions.[19] Several features of this process violate the concepts of "green chemistry". The use of hydride reducing agents produces stoichiometric amounts of waste ($Al(OH)_3$, $B(OH)_3$, etc.), dropping the atom efficiency of the reaction and making the separation tedious. Also, certain hydride reducing agents, such as $LiAlH_4$, are dangerous since they ignite on contact with water.[19, 20]

An alternate is catalytic hydrogenations, in which molecular hydrogen is used to reduce the carbonyl compounds to the desired alcohol in the presence of a catalyst.[19, 20] Hydrogen gas is the cheapest reducing agent.[21] An ideal hydrogenation does not generate any byproducts, making the work-up of the reaction more straightforward, and excess H_2 can be recycled or

used as a fuel.[22, 23] Catalytic hydrogenation can reach a high turnover number (TON, defined as how many substrate molecules can be converted to the product by one catalyst molecule), thus the catalyst loading can be minimal (for example, a TON of 4.5 million was reported in the hydrogenation of acetophenone[24]). Moreover, catalytic hydrogenation can be conducted selectively towards certain desired products.[25] The best example would be Noyori's asymmetrical ketone hydrogenation systems, which reduce prochiral ketones to chiral alcohols with excellent enantioselectivity and efficiency, an example of which is shown in Scheme 1-1.[26, 27]
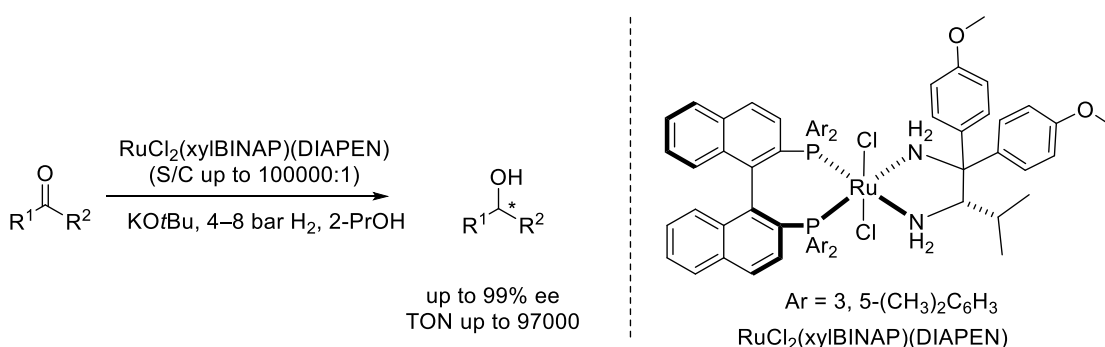
Scheme 1-1. An example of Noyori's asymmetric hydrogenation of ketones.[26, 27]

In the carbonyl compound family, esters are moderately difficult to reduce as the delocalization of the ester group weakens the electrophilicity of the carbonyl carbon (Scheme 1-2). Powerful hydride donors (LiAlH$_4$ and LiBH$_4$) are required for the stoichiometric reduction of esters.[19, 28]
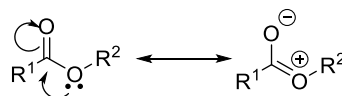
Scheme 1-2. The delocalization of esters.

The reduction of esters to alcohols is an important process in the synthesis of products and building blocks in chemical industry.[19] For example, dodecanol, which is a fatty alcohol used as a non-ionic surfactant, is made by reducing lauric esters via heterogeneous hydrogenation (Scheme 1-3).[29]
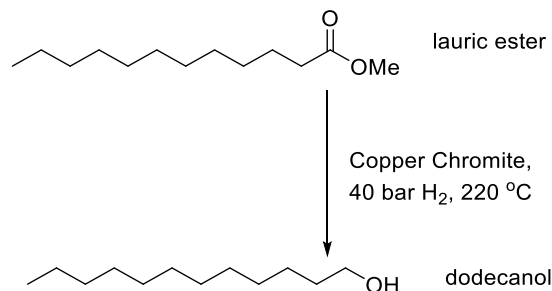
Scheme 1-3. The hydrogenation of lauric ester to produce dodecanol.[29]

Another example is the synthesis of 2-(*l*-menthoxy)ethanol, a cooling compound used in the flavor and fragrance industry. The Takasago International Corporation demonstrated the method to produce 2-(*l*-menthoxy)ethanol using H_2 to reduce methyl *l*-menthoxyacetate with Ru-MACHO (Scheme 1-4).[30]
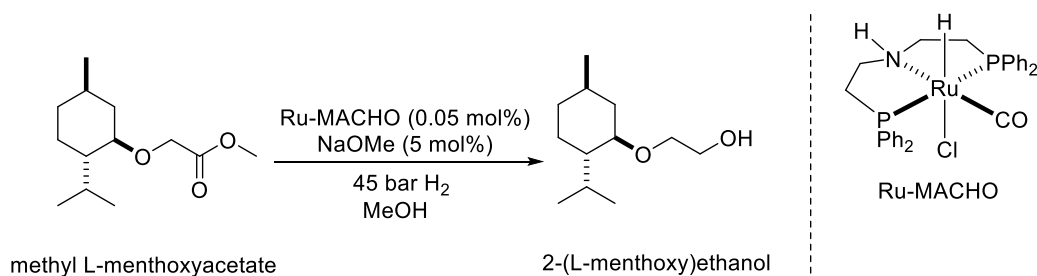
Scheme 1-4. Ester hydrogenation in the synthesis of 2-(*l*-menthoxy)ethanol.[30]

In general, the catalytic hydrogenation of esters is preferred to the stoichiometric reduction using hydride reducing agents. There are two types of ester hydrogenations: heterogeneous and homogeneous. The heterogeneous hydrogenation system was applied to esters first, which operate in harsh conditions.

1.3 Heterogeneous Hydrogenation of Esters

The pioneering study on the heterogeneous hydrogenation of esters was conducted by Adkins and Folkers in 1931.[31] They discovered that copper chromite (formulated as $Cu_2Cr_2O_5$) is a catalyst for ester hydrogenations. With ~10 wt% catalyst loading, several aliphatic esters were hydrogenated to the corresponding alcohols with good yield (80%–98%) under harsh conditions (222 bar H_2, 250 °C).

Later studies[32] demonstrated the poor selectivity of this catalytic system. Two major side reactions were observed, the reduction of other groups and the cleavage of the C–O bond in the alcohol products. For example, 2-methyl cyclohexanol (61.3%) and *o*-cresol (19.2%) were the major products of the hydrogenation of methyl salicylate (Scheme 1-5). The major product (86%) of the hydrogenation of butyl oleate was octadecanol, illustrating the poor selectivity between C=O and C=C bonds.
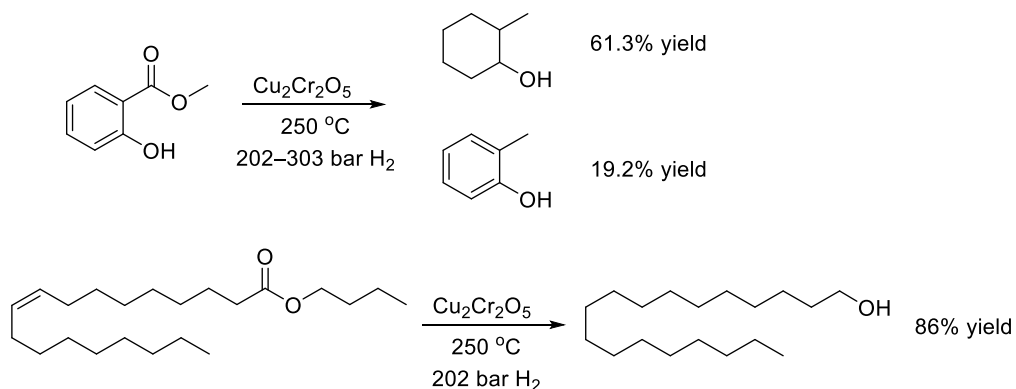
Scheme 1-5. The hydrogenation of methyl salicylate and butyl oleate with copper chromite catalyst.[32]

A comprehensive study on the selectivity of the copper chromite system was conducted in the late 20th century (Scheme 1-6),[33] revealing that when used in the hydrogenation of methyl dodecanoate, the yield of the desired major product (dodecanol) was 82%, with a number of by-products, including fatty ester (C24), aldehyde, ether, ketone, fatty acid, and alkanes (C11 and C12) (1.6 to 10.0 wt% catalyst, 280 °C, 133 bar H_2).
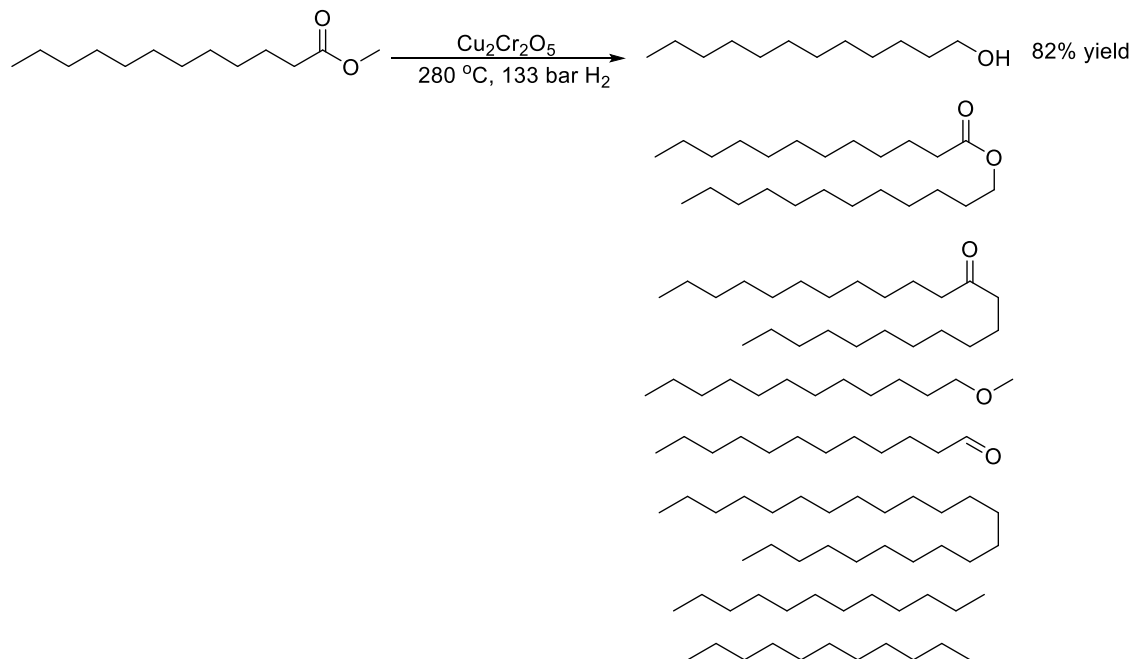
Scheme 1-6. A typical hydrogenation of methyl dodecanoate using the copper chromite catalyst.[33]

Despite the poor selectivity and the extreme conditions, the copper chromite system is still particularly suitable for the hydrogenation of fatty acid methyl esters (FAMEs) and remains as the choice of industry. A recent paper revealed that Procter and Gamble Co. (P&G) has been running FAME hydrogenation with copper chromite catalysts for almost 50 years to produce the fatty alcohol precursors for surfactant manufacture.[34]

Besides the harsh conditions, safety is another major concern when using chromite catalysts since the synthesis of the catalyst involves the reduction of dichromate salts,[35] which contains toxic Cr^{6+} species.[36, 37] Many other heterogeneous catalytic systems for ester hydrogenation were developed by researchers to avoid the use of chromite.

Hattori and coworkers[38] reported a catalyst that was made by co-precipitation of Cu^{2+}, Fe^{2+}, and Al^{3+}, followed by a calcination resulting in a mixture of Fe/Cu/Al oxides. The catalyst was tested in an actual production plant for the hydrogenation of fatty esters (the transesterification products of coconut oil or palm kernel oil with methanol). With 5 wt% catalyst, the desired fatty alcohol was produced steadily in yields above 97% over 20 days (250–270 °C, 120–250 bar, Scheme 1-7); this performance was similar to that of the copper chromite system.

RCOOCH$_3$ $\xrightarrow[\substack{250-270\,^\circ\text{C, }120-250\text{ bar H}_2 \\ 20\text{ days in a production plant}}]{\text{Fe/Cu/Al catalyst}}$ RCH$_2$OH

mixture of fatty acid esters
with different chains
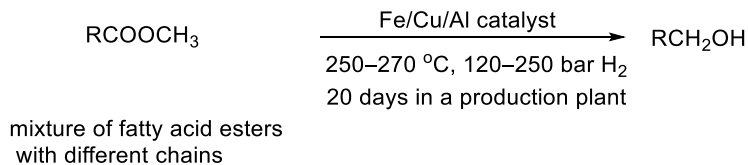
Scheme 1-7. The hydrogenation of fatty esters using a Fe/Cu/Al catalyst.[38]

A copper catalyst supported on hexagonal mesoporous silica (HMS) was reported by the Dai group.[39-41] The catalyst was prepared by wet impregnation of siliceous HMS with Cu^{2+} salts (Cu(NO$_3$)$_2$, Cu(acac)$_2$, CuCl$_2$, Cu$_2$(OH)$_2$CO$_3$, Cu(NH$_3$)$_4$(NO$_3$)$_2$), followed by a calcination process at 450 °C. For the hydrogenation of dimethyl oxalate, up to 98% yield was achieved using the catalyst made from Cu(NH$_3$)$_4$(NO$_3$)$_2$ (200 °C, 25 bar H$_2$, MeOH, in a fixed bed reactor).

Narasimhan and coworkers[42, 43] developed a bimetallic catalytic ester hydrogenation system with Ru and Sn. RuCl$_3$ and SnCl$_2$ were reduced by NaBH$_4$, and the resultant particles were dispersed on Al$_2$O$_3$. The Ru loading on the support was 1.1 wt%. Up to 98% conversion (61–76% yield) was obtained in the hydrogenation of aliphatic esters (2.5 wt% supported catalyst, 270 °C, 44 bar H$_2$). A 61.8% selectivity towards the unsaturated alcohol was observed in the hydrogenation of methyl oleate. The hydrogenation of dimethyl succinate produced 1,4-butanediol in 76% yield in (Scheme 1-8).
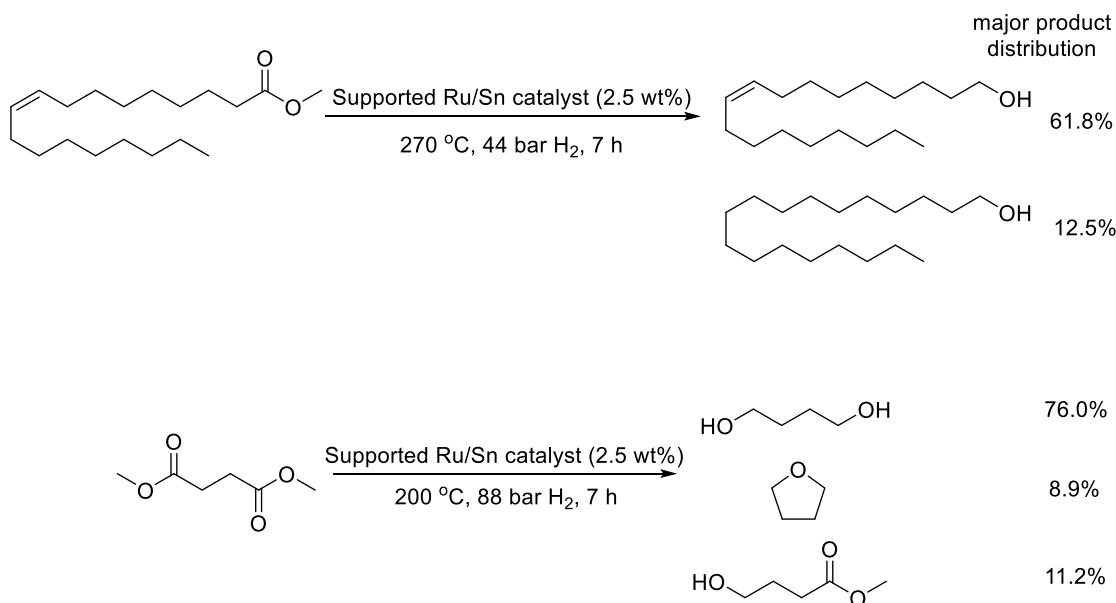
Scheme 1-8. Representative hydrogenations with the Ru/Sn catalyst reported by Patterson et al.[42, 43]

A similar bimetallic catalyst system was developed by the Miyake group[44] and prepared by reducing a precious metal (Ru, Rh, Pt, Ir) salt along with SnCl$_2$ onto Al$_2$O$_3$ using H$_2$ flow. The Rh–Sn system performed better than the other combinations discussed in this paper for the hydrogenation of methyl laurate (Scheme 1-9): 72% conversion was reached with 43% selectivity towards the desired alcohol product. Instead of Sn, Ge also could cooperate with noble metals to promote the hydrogenation of esters. Pieck and coworkers[45, 46] reported that Ru–Ge catalysts supported on Al$_2$O$_3$ were synthesized by reducing Ru and Ge using NaBH$_4$ onto Al$_2$O$_3$. The catalytic performance was evaluated for the hydrogenation of methyl oleate. The best selectivity was reached when the molar ratio between Ru and Ge was 0.5. However, only 19% yield of the desired oleyl alcohol was obtained (28 wt% supported catalyst, 290 °C, 50 bar H$_2$, n-dodecane).
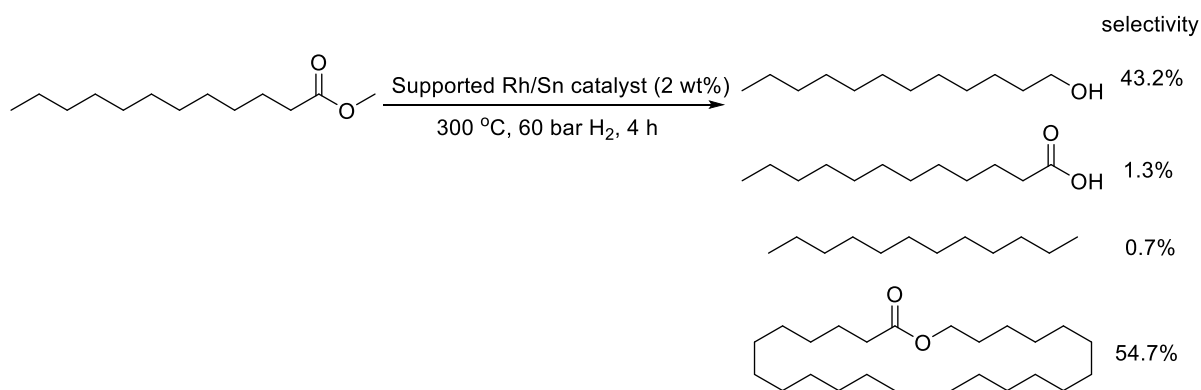
Scheme 1-9. The hydrogenation of methyl laurate reported by Miyake et al.[44]

Yuan's group[47] reported a catalyst system prepared by reducing Au and Ag sequentially onto a mesoporous silica, SBA-15. The resulting nanoalloy Au–Ag catalyst hydrogenated dimethyl malonate and dimethyl succinate to the mono-reduced products (or the lactone after intramolecular esterification) with 87.8% and 86.5% conversion, respectively (Scheme 1-10). The author believed that the ester substrates were activated on Au, whereas the H$_2$ was incorporated to the reaction on the Ag surface.
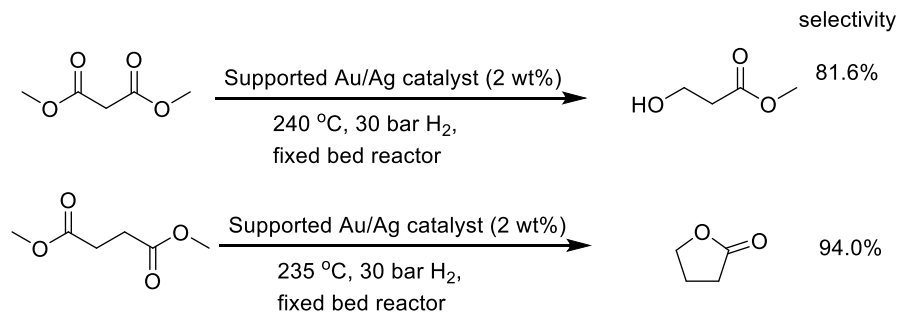
Scheme 1-10. The ester hydrogenations performed with a Au/Ag catalyst reported by Yuan et al.[47]

A Ni–Re catalytic system was reported by Pidko et al.[48] The best catalyst in this paper was made by reducing $HReO_4$ and $Ni(NO_3)_2$ with H_2 on TiO_2 at 300 °C. Methyl hexanoate was hydrogenated to hexanol with 76% selectivity and 70% conversion (Scheme 1-11). The catalyst was recycled and regenerated using H_2 flow at 300 °C for 1 h. No significant loss in activity or selectivity was observed in the reusing experiment of methyl hexanoate hydrogenation under the same conditions.
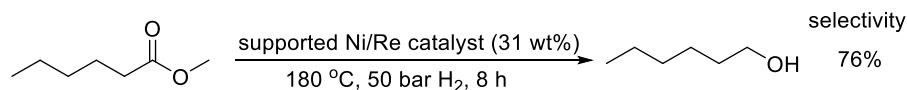
Scheme 1-11. The hydrogenation of methyl hexanoate using Ni/Re catalyst reported by Pidko et al.[48]

In summary, the heterogeneous hydrogenation of esters requires harsh conditions and high catalyst loading, and it is mainly used in the reduction of biomass-derived substrates. Recent research focuses on the improvement of the catalyst activity, functional group tolerance, and selectivity. The strategies include changing the composition of bimetallic systems, optimizing the morphology of the catalyst surface, modifying the support materials, etc.[20] Some representative heterogeneous catalytic systems for the hydrogenation of esters are summarized in this section. However, this is a topic beyond the scope of this dissertation, and the interested reader is directed to review articles on the subject in the literature.[20]

1.4 Homogeneous Ester Hydrogenations

In general, homogeneous ester hydrogenation catalysts operate with a broader substrate scope, require lower temperature and pressure, and give higher efficiency than the heterogeneous systems.

1.4.1 Inner Sphere Ester Hydrogenation Catalysts

In the early 1980s, Grey, Pez, and their coworkers reported the potassium hydrido(phosphine) ruthenate complex **1** and a roughly-defined complex **2** (Scheme 1-12) as the first effective homogeneous ester hydrogenation catalyst precursors.[49-51] Both catalysts could hydrogenate activated esters, i.e., with electron-withdrawing groups. For example, methyl trifluoroacetate and trifluoroethyl trifluoroacetate were converted to alcohols under mild conditions (0.3 or 0.6 mol% Ru, 90 °C, 6.2 bar H_2, toluene, 4 or 12 h) with up to 100% conversions and a TON of 333. Complex **1** was inactive and complex **2** showed minimal activity for the hydrogenation of non-activated esters. For example, methyl acetate was hydrogenated to methanol and ethanol with 22% conversion and a TON of 37 by **2**, whereas aromatic esters, such as methyl benzoate, were not hydrogenated by **2**. The hydrogenations carried out with **1** or **2** were fully shut down when 18-crown-6 was added, which effectively trapped the K^+. This result implied that K^+ was necessary to activate this hydrogenation.
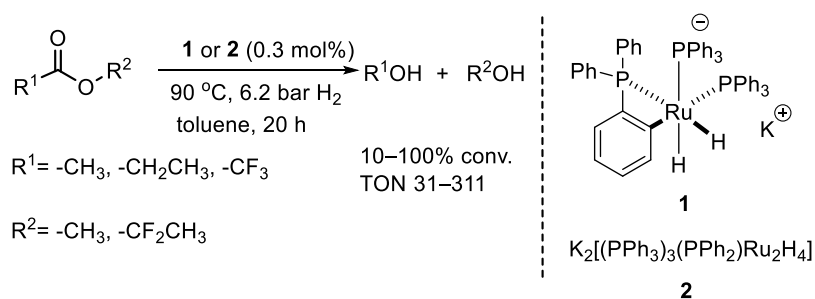
Scheme 1-12. Ester hydrogenation with the catalysts invented by Grey and Pez.[49-51]

Around the same time, Bianchi and coworkers found that δ-valerolactone was hydrogenated to 1,5-pentanediol with the Ru cluster complex formulated as $H_4Ru_4(CO)_8(PnBu_3)_4$ (**3**) (1.3 mol% Ru, 180 °C, 131 bar H_2, toluene/diethyl ether), to give 22% conversion after 48 h.[52] The same group also reported using **3** to hydrogenate diesters to hydroxyl esters via a mono-hydrogenation process.[53] For example, dimethyl oxalate was

hydrogenated to methyl glycolate (51.1% yield, a TON of 41 relative to Ru; 0.31 mol% **3**, 131 bar H_2, 180 °C, benzene, 144 h). Another catalyst precursor, formulated as $Ru_2(CO)_2(CH_3COO)_2(PnBu_3)_2$[54] (**4**)**,** hydrogenated dimethyl oxalate to a mixture of methyl glycolate and ethylene glycol under similar conditions.

In 1992, Wada et al reported an active catalyst prepared by mixing 1 equiv. $Ru(acac)_3$ and 10 equiv. $P(nC_8H_{17})_3$ in situ,[55] which catalyzed the hydrogenation of γ-butyrolactone with a TON of 234 (0.064 mol% $Ru(acac)_3$, 0.64 mol% $P(nC_8H_{17})_3$, 200 °C, 50 bar H_2, tetraglyme, 3 h). By adding NH_4PF_6 or H_3PO_4 as a promoter (5 equiv. to Ru), the TON was improved to 452 or 421, respectively. A variety of lactones were hydrogenated to the corresponding diols with good selectivity (up to 99%), as shown in Scheme 1-13. The activity of the catalyst towards the hydrogenation of EtOAc was significantly lower; only 30 turnovers were obtained under the same conditions. The active catalyst is believed to be the octahedral dihydride species $RuH_2[P(nC_8H_{17})_3]_4$ (**5**) together with the mono-solvento species $RuH_2[P(nC_8H_{17})_3]_3(sol)$ (**6**). Both **5** and **6** were observed by NMR spectroscopy when $Ru(acac)_3$ and $P(nC_8H_{17})_3$ reacted under H_2 (the author did not specify the geometry of **5** and **6**).
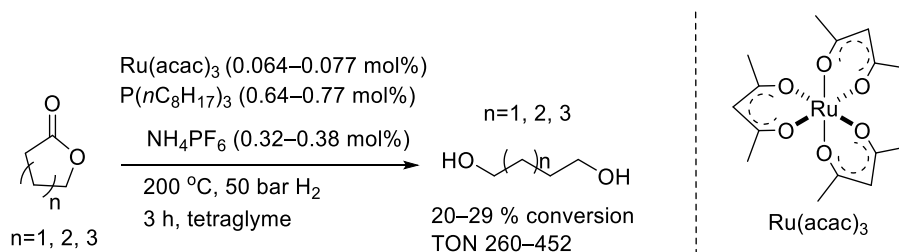
Scheme 1-13. The hydrogenation of lactones using the catalyst developed by Wada et al.[55]

Nomura optimized this catalytic system using methyl phenylacetate as the standard substrate (Scheme 1-14).[56] The catalytic performance improved extensively when 2-dimethoxyethane (dme) was used as the solvent and zinc metal was added as a promoter. The highest TON of 179 was reached under only 10 bar hydrogen pressure (0.2 mol% Ru, 2 mol% $P(nC_8H_{17})_3$, 1 mol% Zn metal, 200 °C, 10 bar H_2, dme, 20 h). The role of Zn is not clear.
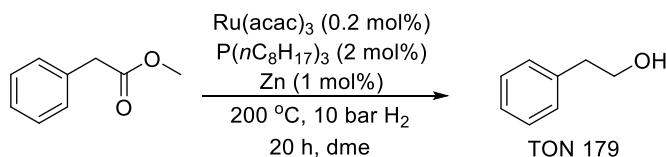
Scheme 1-14. Ester hydrogenation reported by Nomura.[56]

The authors proposed a catalytic cycle without the cooperation of Zn for ester hydrogenations (Scheme 1-15), although very limited experimental evidence for the mechanism was reported. The authors proposed that the active species was a Ru dihydride complex (**7**) formed in situ. The hydride transfers to the carbonyl carbon with a concerted Ru–O bond formation (**8**) in a metathesis pathway, forming the aldehyde and the Ru alkoxide (**9**). It is proposed that **9** undergoes alkoxide-hydride reductive elimination to form **10** and MeOH, with one $P(nC_8H_{17})_3$ coordinated to Ru to substitute the MeOH. An oxidative addition of H_2 regenerates the dihydride species. The aldehyde intermediate underwent a similar reducing process to the alcohol product.
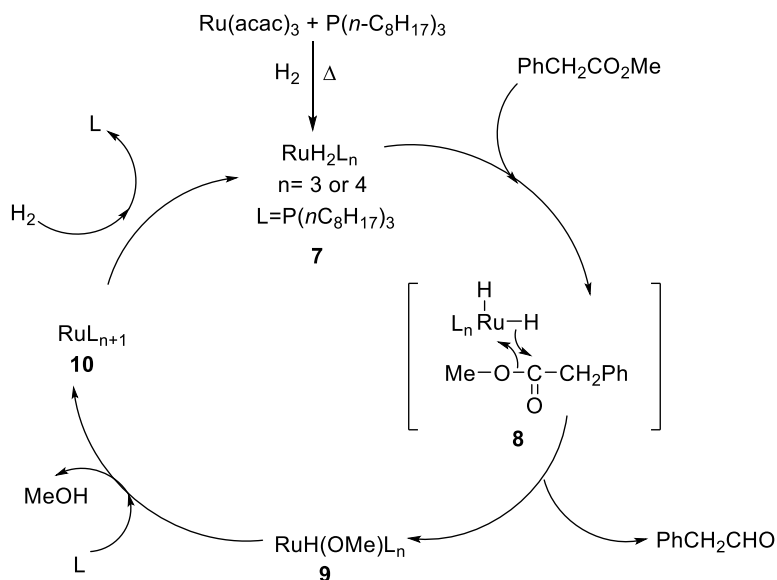
Scheme 1-15. The mechanism of ester hydrogenation with Ru-phosphine catalyst.[56]

The first use of triphos, the tridentate phosphine ligand $MeC(CH_2PPh_2)_3$ (**11**), in catalytic ester hydrogenation was by Teunissen and Elsevier.[57, 58] This breakthrough was discovered by screening $Ru(acac)_3$ with a variety of phosphine and amine ligands. Multidentate

12

phosphines (**11** to **14**, Figure 1-1) were more active, with **11** being the most active. Using **11**, dimethyl oxalate was hydrogenated to ethylene glycol in up to a TON of 160 (in ester groups) under practical conditions (1.19 mol% Ru, 0.26 mol% Zn metal, 100 °C, 70 bar H_2, MeOH, 16 h). A *fac-* configuration of the active Ru(triphos) species was believed to be important as **11** was more active than **13** or **14**, which can coordinate to Ru in both the *fac-* or *mer-* configuration. The TON was improved to 857 with lower Ru loading (0.20 mol% Ru, 0.07 mol% Zn metal, 100 °C, 70 bar H_2, MeOH, 16 h).
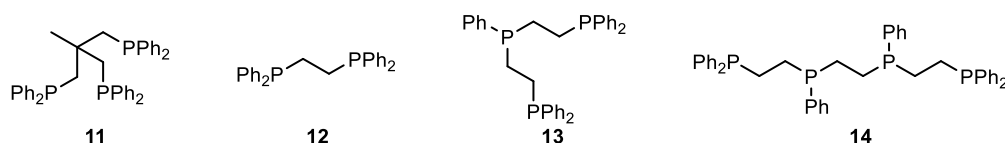
Figure 1-1. Screened ligands with Ru(acac)$_3$ by Teunissen, Elsevier, and their coworkers.[57, 58]

The role of zinc is undetermined, and a later study[59] illustrated that zinc did not always have a positive effect on the hydrogenation of diester compounds with the Ru-triphos system. On the other hand, triethylamine or HBF$_4$ greatly improved the hydrogenation of dimethyl phthalate, by ~300%. Acidic alcohol solvents, such as CF_3CH_2OH or $CF_3CHOHCF_3$, also improved the Ru–triphos system. As shown in Scheme 1-16, the highest TON of 2071 was obtained for the hydrogenation of benzyl benzoate using $CF_3CHOHCF_3$ as the solvent and triethylamine as the additive (0.046 mol% Ru, 9 mol% triethylamine, 120 °C, 85 bar H_2, 16 h). The hypothesis that acidic solvents promoted the hydrogenation by transesterification was excluded by the observation that the hydrogenation proceeded faster in hexafluoro-2-propanol than in 2,2,2-trifluoroethanol, but transesterification took place faster with the primary alcohols. The authors implied an "ionic hydrogenation" interaction such that the hydrogen atom in the fluorinated alcohols weakly bonded to the hydride in the Ru, promoting the hydrogenation reaction, as shown in Scheme 1-16.
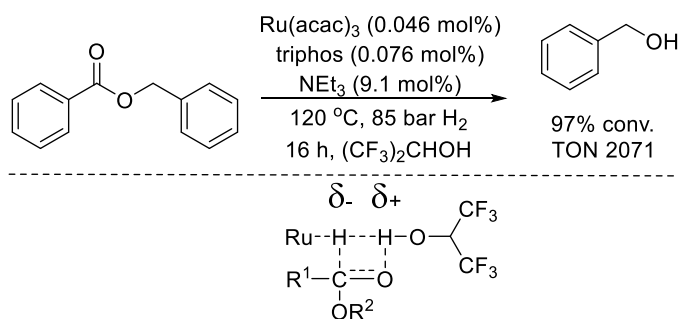
Scheme 1-16. The hydrogenation of methyl benzoate with Ru–triphos catalysts and the proposed mechanism of how the acid alcohol solvents promoted the hydrogenation of esters.[59]

Leitner's group isolated the Ru–triphos complex, Ru(triphos)(TMM) (**15**, Scheme 1-17, TMM=trimethylenemethane), as an ester hydrogenation catalyst precursor.[60] A range of carboxylic derivatives were hydrogenated with **15**, including ketones, esters, amides, anhydrides, and carboxylic acids. Methyl benzoate was converted quantitively to benzyl alcohol with 1 mol% catalyst without any other additives (Scheme 1-17). A similar activity was obtained in the hydrogenation of other esters, such as dimethyl succinate, dimethyl itaconate, γ-valerolactone, and methyl levulinate.
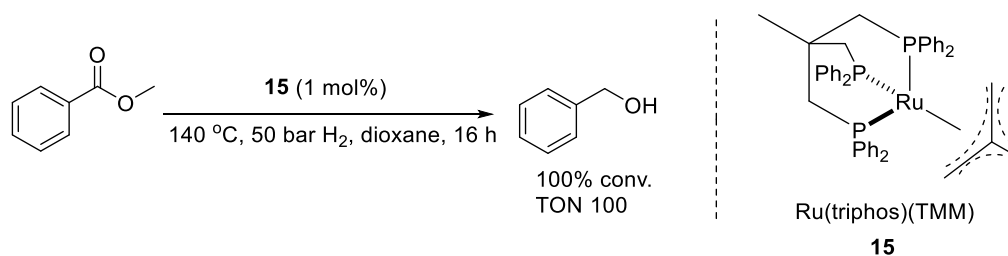
Scheme 1-17. Ester hydrogenation using isolated Ru(triphos)(TMM) catalyst.[60]

This report also presented the first detailed study on the mechanism of ester hydrogenation with Ru–triphos complexes using density functional theory (DFT) calculations. A ruthenium triphos dihydride solvento species, **16** (Scheme 1-18), was proposed as the active catalyst, which was formed when the catalyst was placed in THF under an H$_2$ atmosphere. A vacancy site was generated after dissociation of the solvent ligand and then was occupied by the carbonyl oxygen to form **17**. The hydride transferred from Ru to the carbonyl carbon with the formation of the Ru–O bond and without changing the oxidation state of Ru; this was described as a migratory insertion-type pathway (**17** to **18**). Then, H$_2$ coordinated to Ru (**19**),

and the Ru–O bond was hydrogenolyzed by the coordinated H_2, generating the hemiacetal bonding to the Ru dihydride species (**20**). The dissociation of the hemiacetal recovered the active dihydride species **16**. The hemiacetal decomposed to aldehyde, which was hydrogenated to alcohol following a similar catalytic cycle. This catalytic cycle is classified as an "inner sphere" mechanism since all the atom transfer processes are accomplished with the direct cooperation of the Ru, in contrast to the outer-sphere catalytic cycles of the later-found bifunctional catalysts, which are described in the following section.
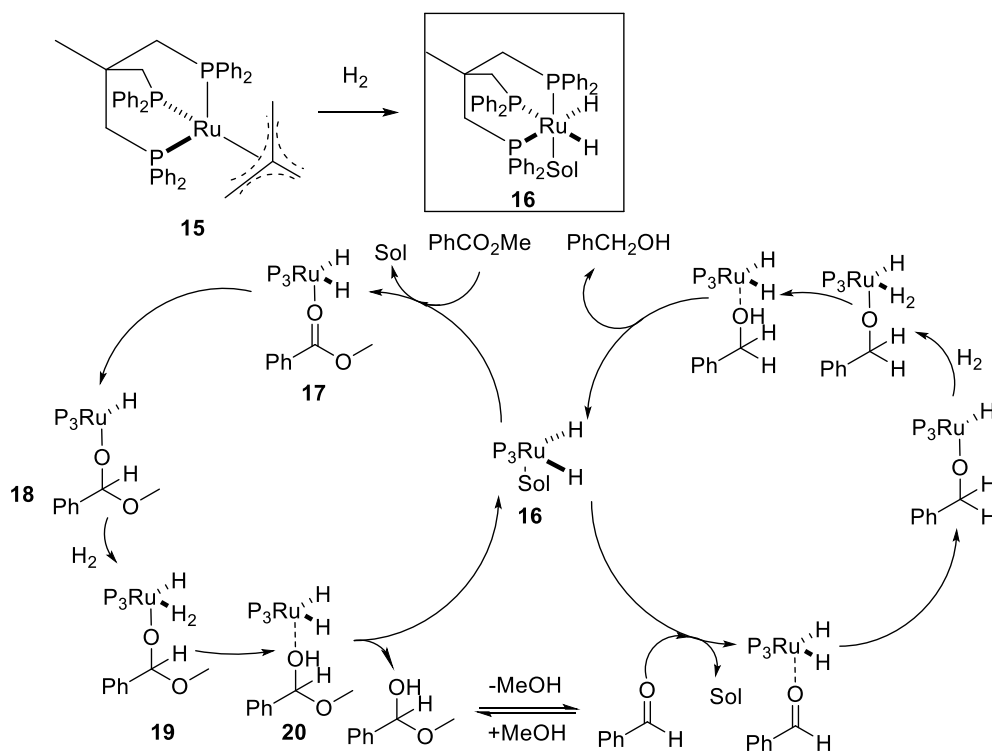
Scheme 1-18. Catalytic cycle for the ester hydrogenations with Ru(triphos) systems.[60]

Homogeneous catalysts in inner-sphere mechanisms work under milder conditions than heterogeneous catalysts. However, more improvements are needed in the activity and selectivity of these catalysts. The later invented bifunctional hydrogenation catalysts are recognized as better systems because of their higher efficiency.

1.4.2 Bifunctional Ester Hydrogenation Catalysts

Bifunctional ester hydrogenation catalysts are generally believed to work by cooperation between an acidic proton on the ligand and a hydride on the metal center of the catalyst. These catalysts represent the state of the art of the ester hydrogenation.

More than a decade after the bifunctional $Ru(H)_2(diphosphine)(diamine)$ catalysts for ketone hydrogenations was reported by Noyori, Milstein first applied a bifunctional catalyst to the hydrogenation of esters in 2006.[61] The catalyst was the well-defined distorted square-pyramidal Ru monohydride carbonyl complex **21** (Scheme 1-19) with a pincer type PNN ligand. Catalyst **21** hydrogenated a series of non-activated esters with up to a TON of 100 under 5.4 bar H_2 at 115 °C in dioxane, without any other additives (Scheme 1-19).
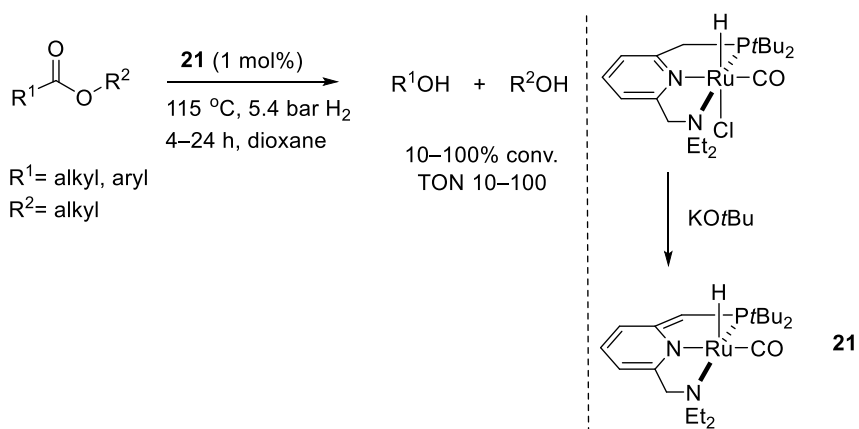
Scheme 1-19. Ester hydrogenation with Milstein's catalyst.[61]

The mechanism of this hydrogenation was proposed to be a combination of an aromatization/dearomatization process and a bifunctional hydride/proton transfer (Scheme 1-20). Dihydrogen addition to the square-pyramidal complex **21** forms the aromatized dihydride complex **22**, then the saturated amine dissociates from the Ru center, allowing the ester to coordinate through the carbonyl oxygen to form **23**. Next, one hydride transfers from Ru to the carbonyl carbon (**23** to **24**). Deprotonation at the acidic methylene group by the hemiacetalate ligand in **24** generates the hemiacetal and **21**. The hemiacetal eliminates an aldehyde, which is hydrogenated to alcohol via a similar process. This bifunctional catalytic cycle is different from the classic Noyori $RuH_2(diamine)(diphosphine)$ bifunctional ketone hydrogenation mechanism where the proton transfer occurs with an NH group.
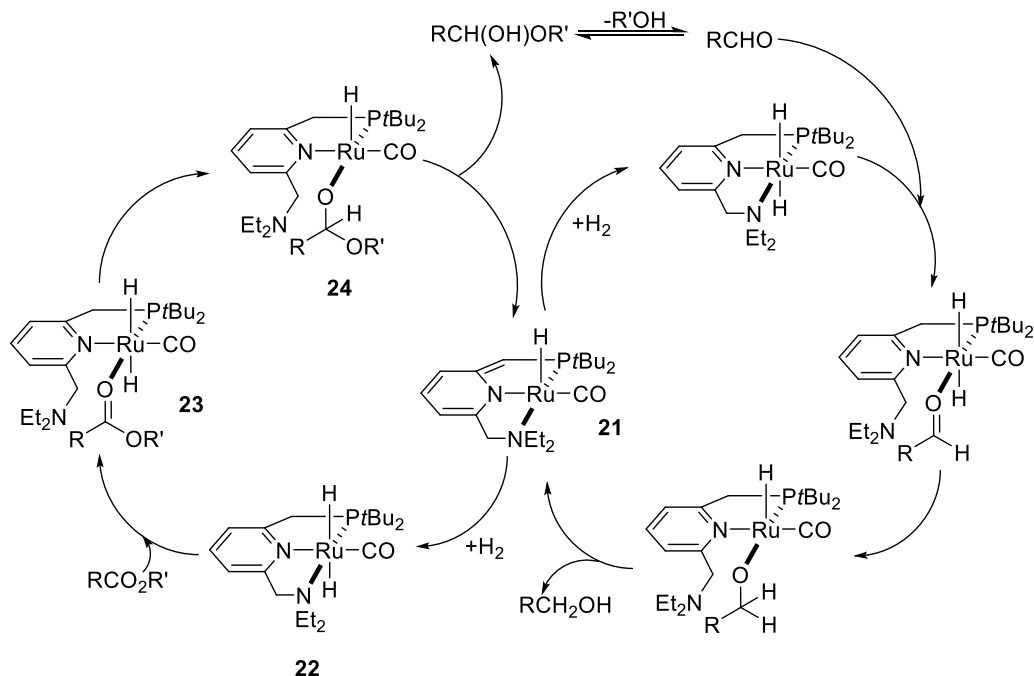
Scheme 1-20. The proposed catalytic cycle of Milstein's ester hydrogenation catalyst.[61]

One year after Milstein's catalyst was reported, Saudan's team from Firmenich reported their Ru catalysts made from amino-phosphine ligands, and which were believed to operate by a mechanism similar to Noyori's ketone hydrogenation.[62] The most active catalysts are shown in Scheme 1-21. Complex **25** hydrogenated isopropyl benzoate with up to a TON of 9900 (99% yield) with low catalyst loadings (0.01 mol% **25**, 5 mol% NaOMe, 100 °C, 50 bar H_2 pressure, THF, 4 h). Complex **26** showed similar activities to **25**. Excellent selectivity towards carbonyl reduction was observed in reactions with unsaturated substrates containing an alkene group. For example, methyl cyclohex-3-ene-1-carboxylate was hydrogenated to cyclohex-3-enylmethanol in 90% yield and a TON of 1800 with only 2% saturated byproduct (0.05 mol% **25**, 5 mol% NaOMe, 100 °C, 50 bar H_2, THF, 2.5 h). The authors found that increasing the number of substituents on the alkene group increased the selectivity towards carbonyl reduction.
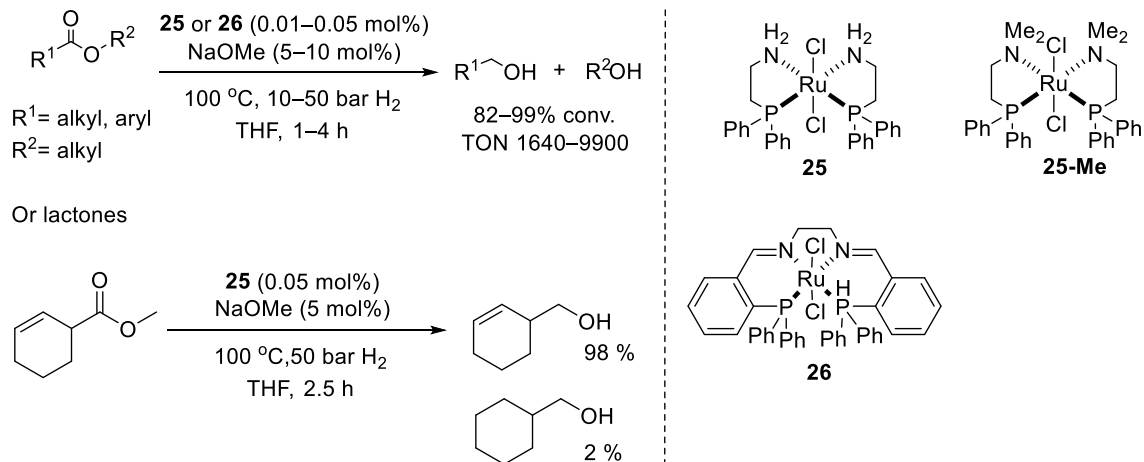
Scheme 1-21. Ester hydrogenation with Firmenich's catalysts.[62]

The proposed mechanism was a typical NH assisted bifunctional carbonyl reduction. Specifically, the dichloride precatalysts **25** and **26** were activated by dihydrogen and base, forming the dihydride species $RuH_2(PN)(PN)$ or $RuH_2(PNNP)$ (PN and PNNP are the multidentate ligands coordinate via N and P atoms), respectively, and the ester reacted with the catalyst by a classical Noyori type bifunctional addition of H_2 to form hemiacetal intermediate (Scheme 1-22).[63, 64] A control experiment showed that a catalyst analog of **25** with tertiary amine ligand (**25-Me**) did not provide any activity towards ester hydrogenations, which supported the bifunctional hypothesis. The authors implied that NH groups would be generated during the initiation of **26** under the hydrogenation conditions. This paper showed that Noyori type ruthenium catalysts with aminophosphine ligands can be used as ester hydrogenation catalysts with excellent activities.
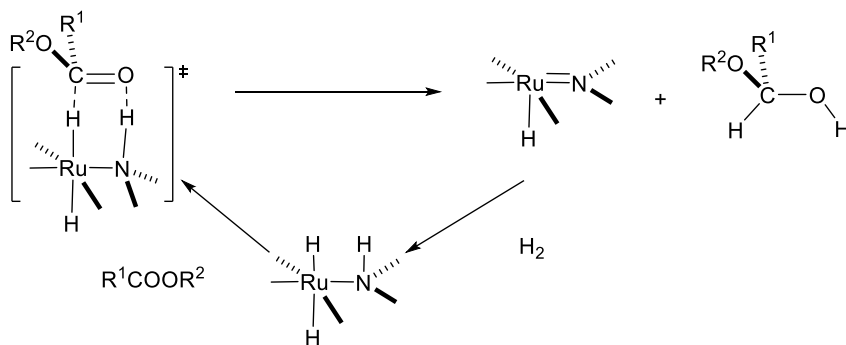
Scheme 1-22. Generalized mechanism for Firmenich's ester hydrogenation catalysts.[63, 64]

18

Most catalysts for ester hydrogenations contain either the pincer type tridentate ligands or tetradentate ligands. The proposed mechanisms can be classified into two major types based on the proton source in the bifunctional addition: 1) the proton source is an acidic methylene group with an aromatization/dearomatization process, exemplified by Milstein's catalyst whose mechanism is shown in Scheme 1-20; 2) the proton source is an NH group, exemplified by Firmenich's catalysts.

Clarke and coworkers[65] screened several ruthenium complexes as ester hydrogenation catalysts. The three most active catalysts had similar activities and are **27**, **28** and **29**, shown in Figure 1-2. The activity of these catalysts is modest compared to Firmenich's catalysts. Almost quantitative conversion with a TON of ~200 was achieved with 0.5% catalyst loading for the hydrogenation of a variety of aliphatic and aromatic esters (25 mol% KOtBu, 50 °C, 50 bar H_2, Me-THF, 16 h).
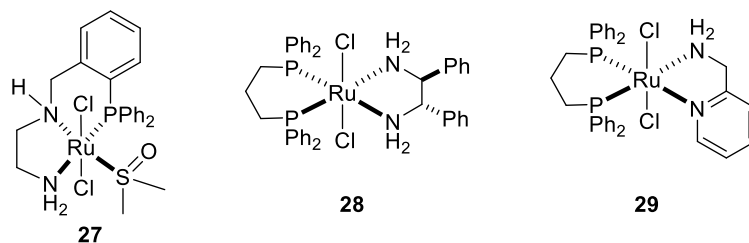
Figure 1-2. Active ester hydrogenation catalysts developed by the Clarke group.[65]

In a later report,[66] **27** was used to degrade poly(ethylene terephthalate) via ester hydrogenation. Up to 73% of the polymer was converted into diol (2 mol% **27**, 80 mol%, KOtBu, 100 °C, 50 bar H_2, THF/anisole, 48 h, Scheme 1-23).
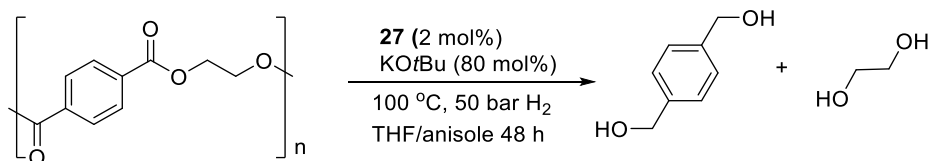
Scheme 1-23. Degeneration of polyesters using hydrogenation method.[66]

Kuriyama and the coauthors from Takasago International Corporation synthesized a pincer Ru-PNP carbonyl complex (Ru-MACHO, **30**, Scheme 1-24) for catalytic ester

hydrogenations.[30] Up to a TON of 980 was achieved with **30** for the hydrogenation of benzoate esters (0.1 mol% **30**, 10% NaOMe, 100 °C, 50 bar, MeOH, 16 h). The large-scale hydrogenation of the near optically pure substrate methyl (*R*)-lactate with **30** was demonstrated; 1477 kg (*R*)-1,2-propanediol was produced from 2200 kg methyl (R)-lactate, and the optical purity was retained after the hydrogenation (Scheme 1-24).
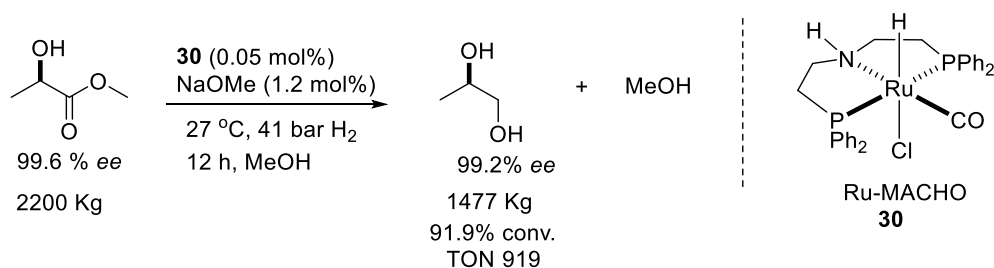
Scheme 1-24. The large-scale hydrogenation of methyl (*R*)-lactate with Ru-MACHO.[30]

Milstein synthesized a series of Ru-PNN or Ru-PNP borohydride complexes that catalyzed the hydrogenation of aromatic and aliphatic esters under mild conditions (Scheme 1-25).[67] Up to a TON of 200 was obtained with the most active catalyst, **31**, in 12 h. The advantage of introducing the borohydride moiety was that it initiates the catalyst precursor without base, forming the Ru-hydride complex directly. Dehydrogenative coupling of primary alcohols to esters and H_2, the reverse reaction of an ester hydrogenation, also could be catalyzed by **31**.
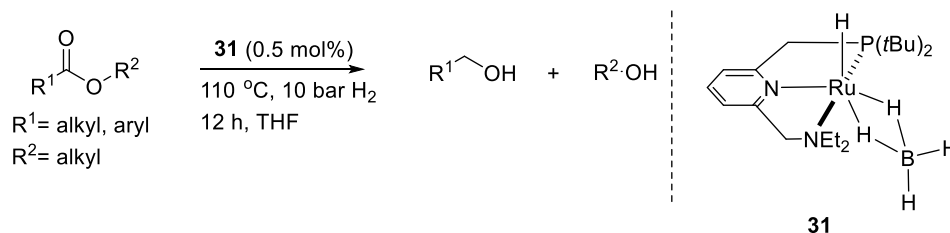
Scheme 1-25. Ester hydrogenation with Milstein's Ru-PNN-borohydride complex.[67]

Ikariya and coworkers reported a Ru catalyst bearing diamine ligands, (**32**, Scheme 1-26).[68] This catalyst hydrogenates a variety of lactones to the diol product with large amount of base, in almost quantitative conversions with TONs of 100.
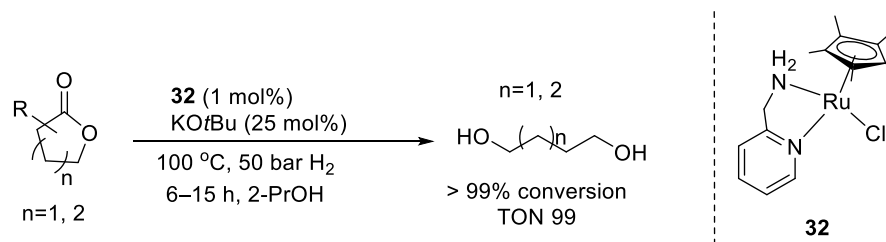
Scheme 1-26. The hydrogenation of lactones reported by Ikariya et al.[68]

N-heterocyclic carbenes (NHCs) are cyclic nitrogen-containing carbene ligands, which are stabilized by bulky substituents on the nitrogen atoms. They are considered to be phosphine mimics with stronger coordination to metals.[69] Because of the stronger metal–ligand interaction, NHC complexes also generally are more stable towards oxidation by air than phosphine complexes.[70, 71] Since 2010, several groups have employed NHCs to replace a phosphorus moiety in ester hydrogenation catalysts.

In 2010, Morris and coworkers reported a Ru–NHC complex (**33**, Figure 1-3) which catalyzed the hydrogenation of carbonyl compounds with good activity.[72] Methyl benzoate was the only ester studied in this paper, and its hydrogenation was carried out under moderate conditions with a TON of 1170 and 78% conv. (0.07 mol% catalyst, 0.5 mol% KOtBu, 50 °C, 25 bar H$_2$, THF, 2 h). A later study expanded the substrate scope, and several aliphatic and aromatic esters as well as lactones were hydrogenated by **33** with TONs of 88–1480 and 6–98% conv. (0.07 mol% **33**, 0.5 mol% KOtBu, 50 °C, 25 bar H$_2$, THF, 3–17 h).[73]
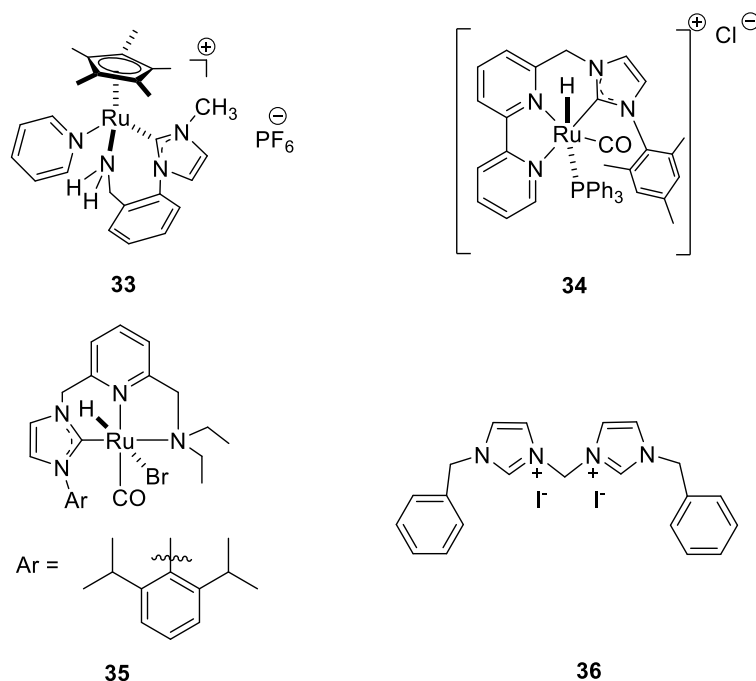
Figure 1-3. Some ester hydrogenation catalysts with NHC ligands or NHC ligand precursors.

Milstein and co-workers synthesized a CNN pincer type catalyst with a bipyridine-NHC ligand (**34**, Scheme 1-27).[74] With a catalytic amount of base (1 equiv. to Ru), **34** exhibited moderate activity in the hydrogenation of benzoate esters with TONs of 90–100 (1 mol% **34**, 1 mol% KOtBu, 135 °C, 5.4 bar H_2, toluene, 2 h). A TON of 2880 was obtained in the hydrogenation of ethyl benzoate at elevated temperature and under 50 bar H_2 (0.025 mol% **34**, 0.025% KOtBu, 110 °C, 50 bar H_2, toluene, 12 h). Dearomatization was observed when **34** was treated with potassium bis(trimethylsilyl)amide (KHMDS) (Scheme 1-27), indicating a similar active species in the catalytic cycle compared to the **21** (Scheme 1-19).
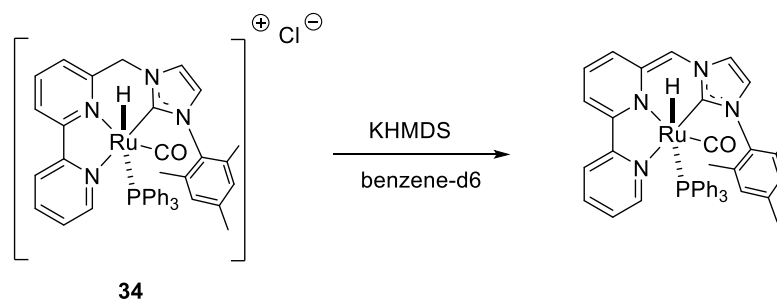
Scheme 1-27. Dearomatization of **34** with KHMDS.[74]

A Ru-CNN catalyst with a trialkylamine group, **35**, was reported by the Song group.[75] The catalyst generally exhibited comparable activities to Milstein's catalyst **34**. The authors stressed the performance of this catalyst towards the hydrogenation of bulky esters. For example, the hydrogenation of *tert*-butyl acetate occurred with a TON of 92 under mild pressure (1 mol% **35**, 8 mol% KO*t*Bu, toluene, 5.2 bar H_2, 105 °C, 2 h). In an NMR mechanistic study, the methylene group on the NHC side was more acidic, and it deprotonated first, along with the dearomatization of the pyridine moiety, when the **35** was treated with KHMDS, shown in Scheme 1-28. The resultant square pyramidal complex could split D_2 to form a Ru-hydride-deuteride species even at -78 °C, and its hydride and methylene hydrogen on the both arms also were accessible to H–D exchange at rt.
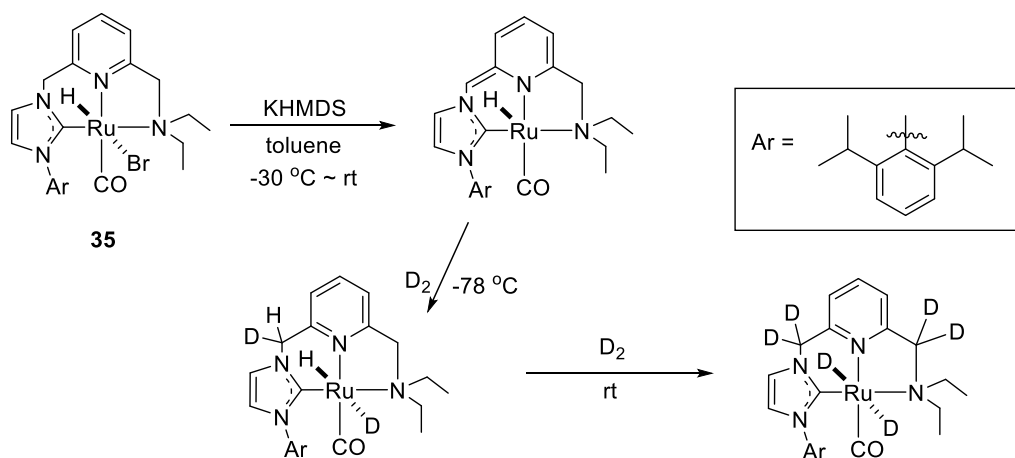
Scheme 1-28. Dearomatization of **35** and its H–D exchange with D_2.[75]

Beller et al studied the activity of a series of Ru-carbene complexes[76] formed by mixing [Ru(p-cymene)Cl$_2$]$_2$ and imidazolium carbene precursors in situ. The catalysts obtained from bidentate carbenes were more active than monodentate carbenes. A range of aliphatic and aromatic esters were converted to alcohols by the best carbene precursor **36** (Figure 1-3) with moderate TONs of 32–92 (1 mol% Ru, 30 mol% KO*t*Bu, 1,4-dioxane, 50 bar H_2, 100 °C, 6 h).

The Beller group also reported the first iridium catalyst for ester hydrogenations.[77] The cationic pincer type iridium catalyst (**37**, Scheme 1-29) hydrogenated both aromatic and aliphatic esters and lactones with moderate activity. It was believed that **37** worked by a classical Noyori type bifunctional mechanism, with the NH moiety providing the proton in the catalytic cycle.
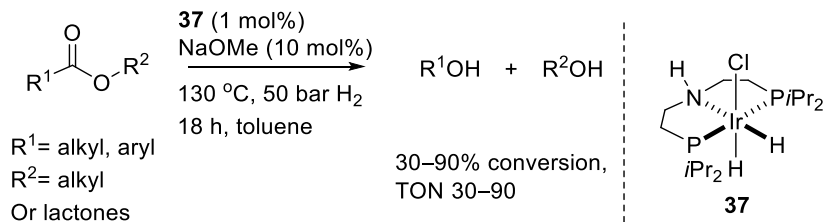
Scheme 1-29. Ester hydrogenation catalyzed by an Ir complex reported by Beller group.[77]

The major parameters to evaluate an ester hydrogenation catalyst are the turnover number and the conditions. An industrially applicable homogeneous catalytic reaction usually requires >50000 TON for low-value products; in some cases a TON >1000 is sufficient for the manufacture of high-value products.[78] Several remarkable catalysts that catalyze ester hydrogenation with TONs of tens of thousands were reported.

Gusev reported a series of Ru or Os catalysts in 2012.[79] Remarkably, two dimeric catalysts, **38** and **39**, were exceptionally active for the hydrogenation of esters under neutral conditions (Scheme 1-30). For example, with 0.025 mol% Os dimer catalyst **38**, ethyl benzoate was hydrogenated almost fully to benzyl alcohol within 1.6 h (100 °C, 50 bar H_2, THF) without any addition of base with a TON of 1980. The highest TON of 18000 (per Ru) was achieved with the Ru dimer **39** for the hydrogenation of methyl hexanoate (0.0025 mol% **39**, 100 °C, 50 bar H_2, 17 h). The authors were uncertain about whether the catalysis operated by an outer-sphere or an inner-sphere mechanism. Also, the reverse reaction, dehydrogenation of alcohols to esters catalyzed by these complexes was studied. Alkyl alcohols (C2–C7) were refluxed with **38** under neat conditions, giving ester products and releasing hydrogen gas.
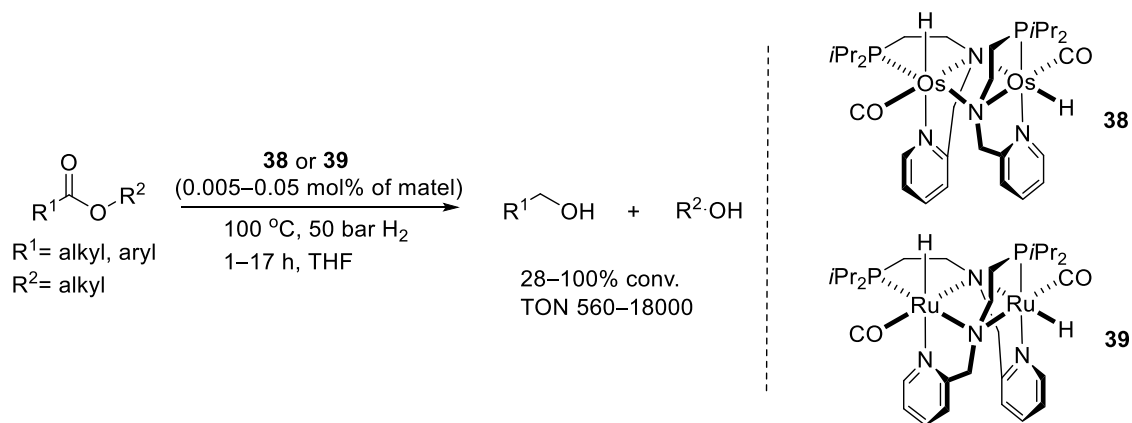
Scheme 1-30. Ester hydrogenation catalyzed by Ru and Os dimerized complexes.[79]

The Gusev group later found that highly active ester hydrogenation catalysts could be made by replacing the phosphorus ligands in the pincer Ru-PNP catalyst with sulfur.[80] The resultant Ru-SNS catalysts (**40**, Scheme 1-31) presumably cost less than the Ru-PNP catalysts and had outstanding activity. Methyl benzoate was hydrogenated with a TON of 3800 and 95% conv. (0.025 mol% **40**, 1 mol% KOtBu, 40 °C, 50 bar H$_2$, THF, 6 h). The highest TON, 58400 (73% conv.), was obtained for the hydrogenation of ethyl acetate under neat conditions (0.00125 mol% **40**, 0.125 mol% NaOEt, 40 °C, 50 bar H$_2$, 21 h). The dehydrogenation of alcohols also was catalyzed by **40**. An interesting transformation was observed when **40** was treated with base and ethanol. The dichloride species **40** forms the alkoxide-monohydride Ru intermediate **41**, which may have formed via the Ru-amide species. Complex **41** would be further transformed to the *fac*-dihydride species **42**. Both **41** and **42** were isolated, and their structures were confirmed in the solid-state. It is believed that **42** is the active species for both the ester hydrogenations and the dehydrogenation of alcohols.
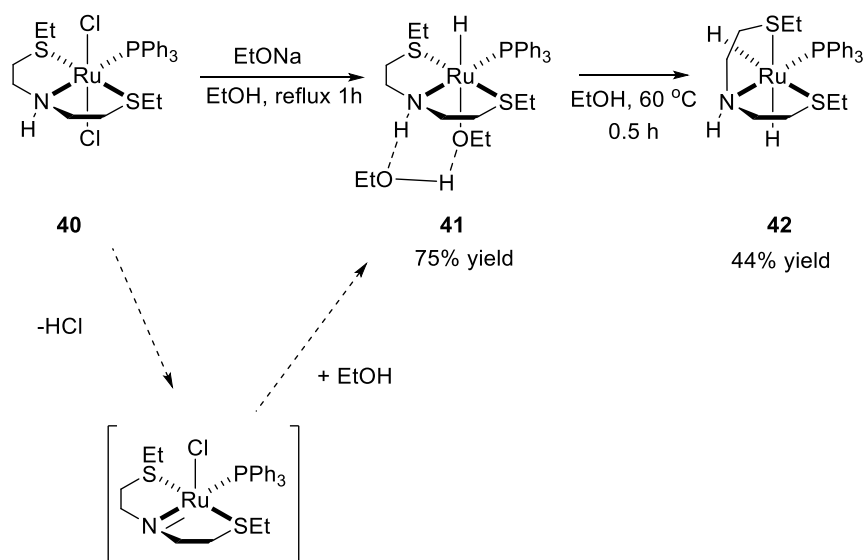
Scheme 1-31. Sulphur containing catalyst for ester hydrogenation invented by Gusev et al and its transformation to active species.[80]

A later study in the Gusev group focused on the selectivity towards carbonyl reduction during the hydrogenation of unsaturated esters bearing olefin groups. A novel Os catalyst (**43**, Scheme 1-32)[81] exhibited excellent selectivity: 98% of the olefin group remained after the

hydrogenation of 10-undecenoate (0.01 mol% **43**, 2 mol% NaOMe, 100 °C, 50 bar H$_2$, neat, 5 h). This catalyst showed excellent selectivity (96–100% towards unsaturated alcohol products) and good activity with a TON of 2000–9800 over a large scope of non-conjugated aliphatic unsaturated substrates (0.01–0.05 mol% **43**, 1 mol% base, 100 °C, 50 bar H$_2$, 2-PrOH or in neat, 2–24 h). However, the α,β-unsaturated ester substrates were still fully hydrogenated to saturated alcohols.
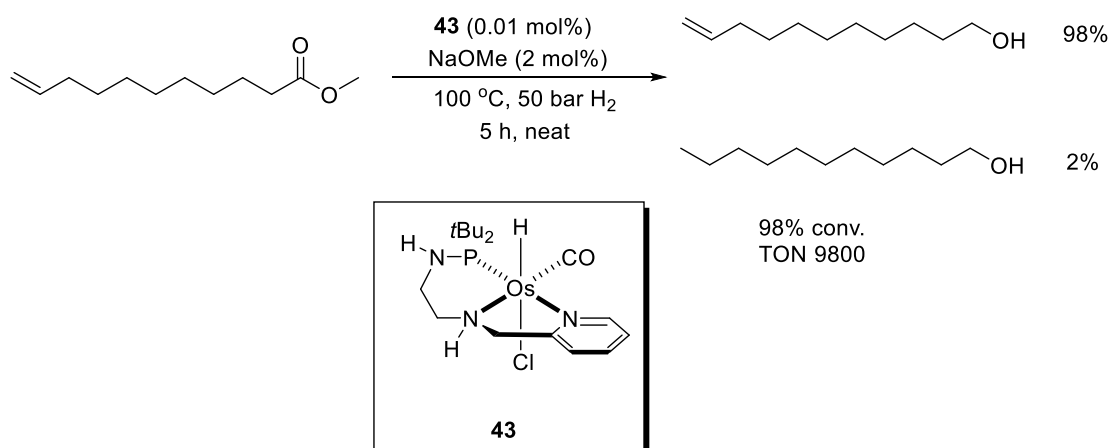
Scheme 1-32. Hydrogenation of 10-undecenoate with excellent selectivity reported by Gusev et al.[81]

The active species of this system are believed to be the dihydride complexes **44** and **45** (cis/trans mixture), shown in Scheme 1-33, which are obtained by treating **43** with NaOMe under H$_2$ or lithium triethylborohydride. The activity of isolated active dihydride complexes was independent of the presence of base, indicating that the only function of base in this catalytic system was to initiate the catalyst precursor.
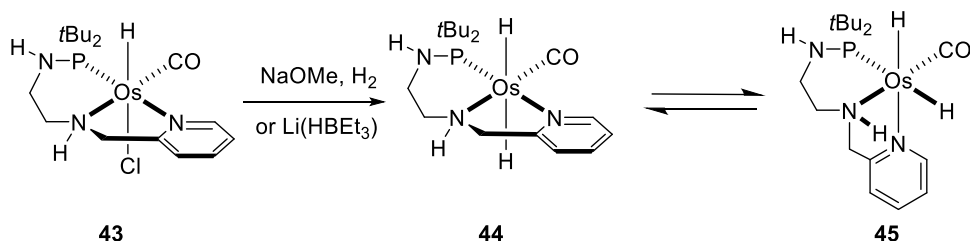
Scheme 1-33. Os-based catalyst with excellent selectivity and its active dihydride species.[81]

The Ru analogue of this system also was studied by tuning the "Y" group in the pincer PNY ligands[82] and with methyl undecenoate as the substrate. The catalyst precursor **46** had the highest activity and selectivity with a TON of 1680 and 84% conv. (96% selectivity towards unsaturated alcohol, 0.05 mol% **46**, 1 mol% KO*t*Bu, 100 °C, 50 bar H_2, THF, 2.5 h). This system's best activity was worse than that of the Os analogue **43** with a TON of 1900 (98% selectivity, same conditions). The nature of the Y group profoundly influenced the catalyst performance. Catalysts made from more labile groups, such as **47** (less stable 6-member ring) and **48** (weaker coordination through O), were less active or inactive in ester hydrogenations, leading to the conclusion that partial ligand dissociation likely was not involved in this catalytic system. The key proposed steps of the catalytic cycle based on the computational results are shown in Scheme 1-34. A rearrangement of the bifunctional adduct **50** resulted in the Ru–ether complex intermediate **51**. Cleavage of the C–O bond formed the Ru alkoxide **52** and released the aldehyde. This mechanism is in contrast with the formation of a Ru-amide and hemiacetal as predicted by the classic Noyori's mechanism. It was proposed that **52** then undergoes Ru–O hydrogenolysis to generate MeOH and **49**. Similar mechanisms also were presented in other reports regarding mechanism studies in the hydrogenation of esters.[73, 83-85]

The Bergens group carried out a mechanistic investigation on the hydrogenation of esters with Noyori's ketone hydrogenation catalyst, *trans*-Ru(H)$_2$((*R*)-BINAP)((*R*,*R*)-DPEN) (BINAP = 2,2′-bis(diphenylphosphino)-1,1′-binaphthyl, DPEN = 1,2-diphenyl-1,2-ethylenediamine).[86] As part of this investigation, they prepared Noyori's catalyst in solution and for the first time, directly observed the bifunctional of an ester-type substrate. They found that the bifunctional addition of γ-butyrolactone occurs at a remarkable -80°C to form the corresponding Ru-hemiacetaloxide. This result demonstrates the high intrinsic reducing power of these catalysts towards esters. Indeed, the acyclic ester, ethyl hexanoate underwent catalytic hydrogenation with this catalyst at -20 °C under 4 bar H_2 (60 equiv. ester, 4 equiv. KHMDS, 23% conversion after 4 h). More details on this research are discussed in Chapter 3.
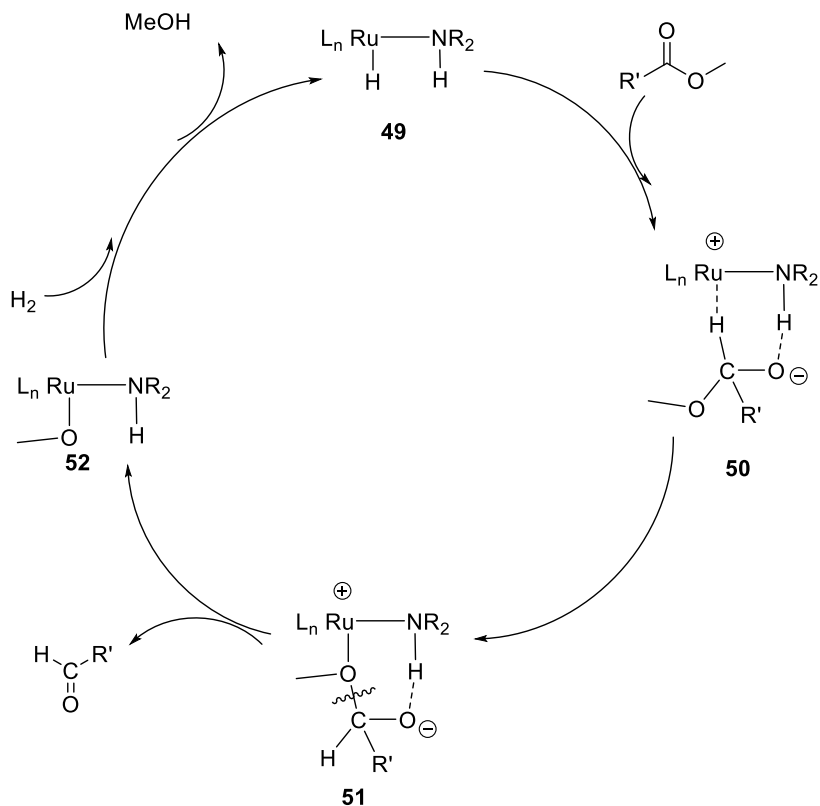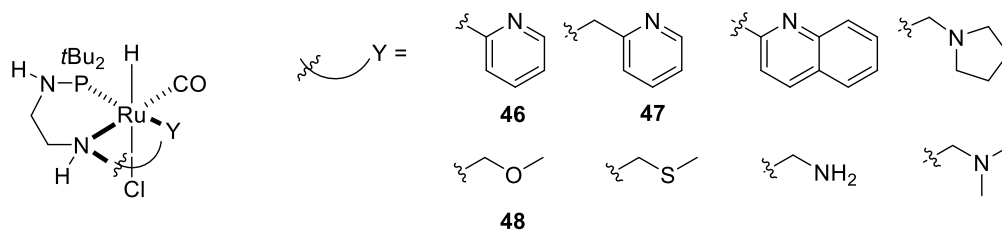
Scheme 1-34. A series of Ru catalysts studied by the Gusev group and the proposed catalytic cycle ester hydrogenations.[82]

In 2014, Zhou reported a Ru-PNNN complex (**53**, Scheme 1-35) that catalyzes the hydrogenation of a variety of esters.[87] A variety of lactones, aliphatic or aromatic esters and diesters were hydrogenated by **53** with conversions > 95% and TONs of 950–1940 (conditions as shown in Scheme 1-35). The highest TON of 91000 was obtained for the hydrogenation of γ-valerolactone (0.001 mol% **53**, 10 mol% NaOMe, 25 °C, 101 bar, 2-PrOH, 48 h) and methyl benzoate (0.001 mol% **53**, 10 mol% NaOMe, 25 °C, 101 bar, 2-PrOH, 64 h). The authors' preliminary NMR study confirmed the formation of a trans dihydride species when mixing **53** with 10 equiv. KO*t*Bu under 51 bar H₂ (THF, rt). The authors proposed a mechanism adapted

from Milstein's aromatization–dearomatization catalytic cycle, with the dissociation of the NEt$_2$ arm, as shown in Scheme 1-35.
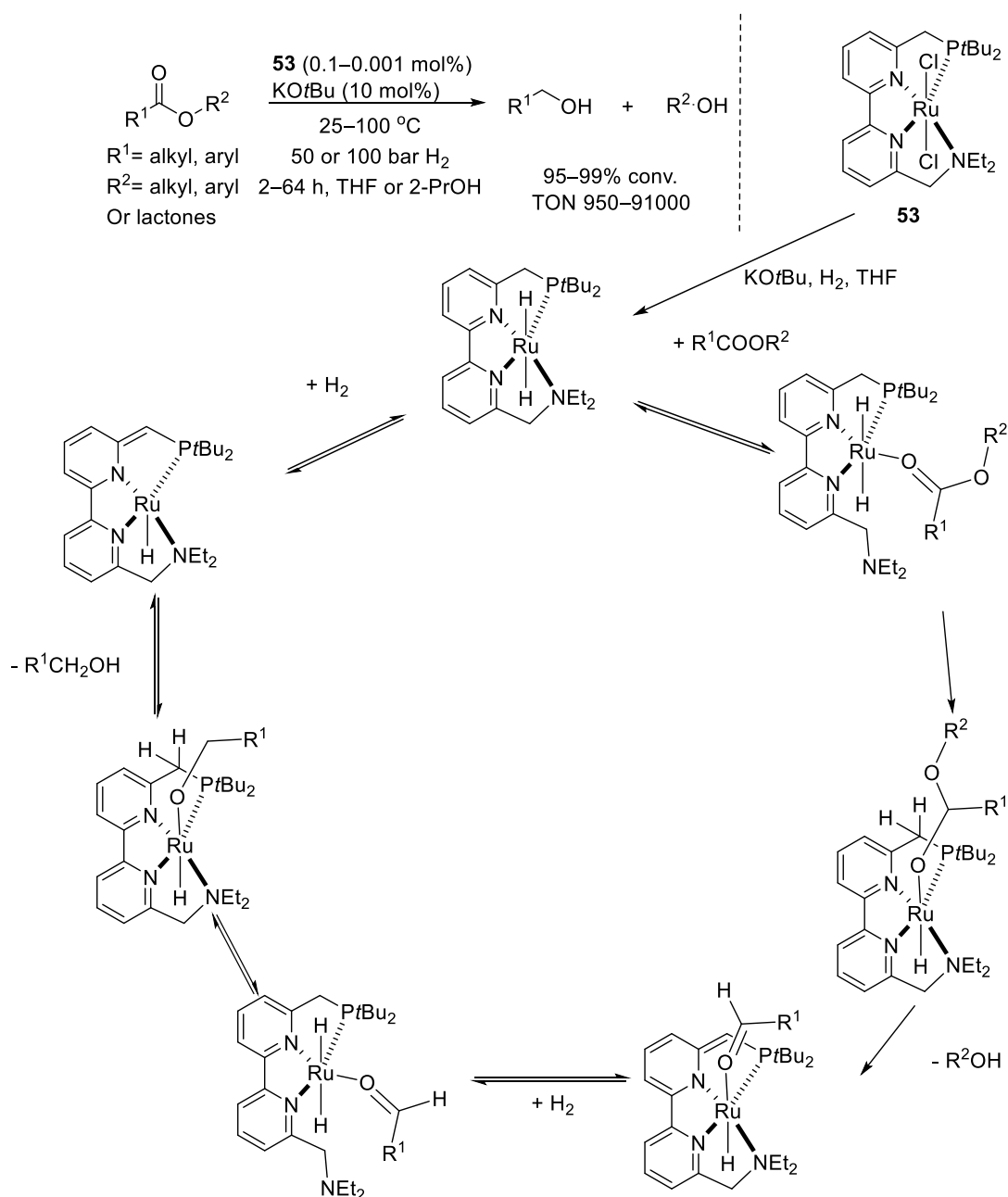
Scheme 1-35. Ester hydrogenation catalyst and its mechanism proposed by Zhou et al.[87]

Milstein's group modified their pincer type catalyst by introducing an NH moiety to the Ru complex center (**54**, Scheme 1-36).[88] Compound **54** underwent a double-deprotonation to form **55** when it was treated with 2.5 equiv. KH, which provided two possible pathways for

the catalytic cycle: the classical Noyori-type bifunctional addition with the NH moiety to form **57** and Milstein's aromatization/dearomatization process, in which the transfer of the proton takes place on the benzyl methylene group to form **56**. Ester hydrogenation experiments were performed in a wide scope of substrates, including aliphatic esters, aromatic esters, and lactones. The loading of **54** could be as low as 0.02 mol% to obtain a decent conversion of 93–99%, with a TON of 4650–4950 (1–1.1 mol% KOtBu, 19–25 °C, 50 bar, THF, 24–72 h).
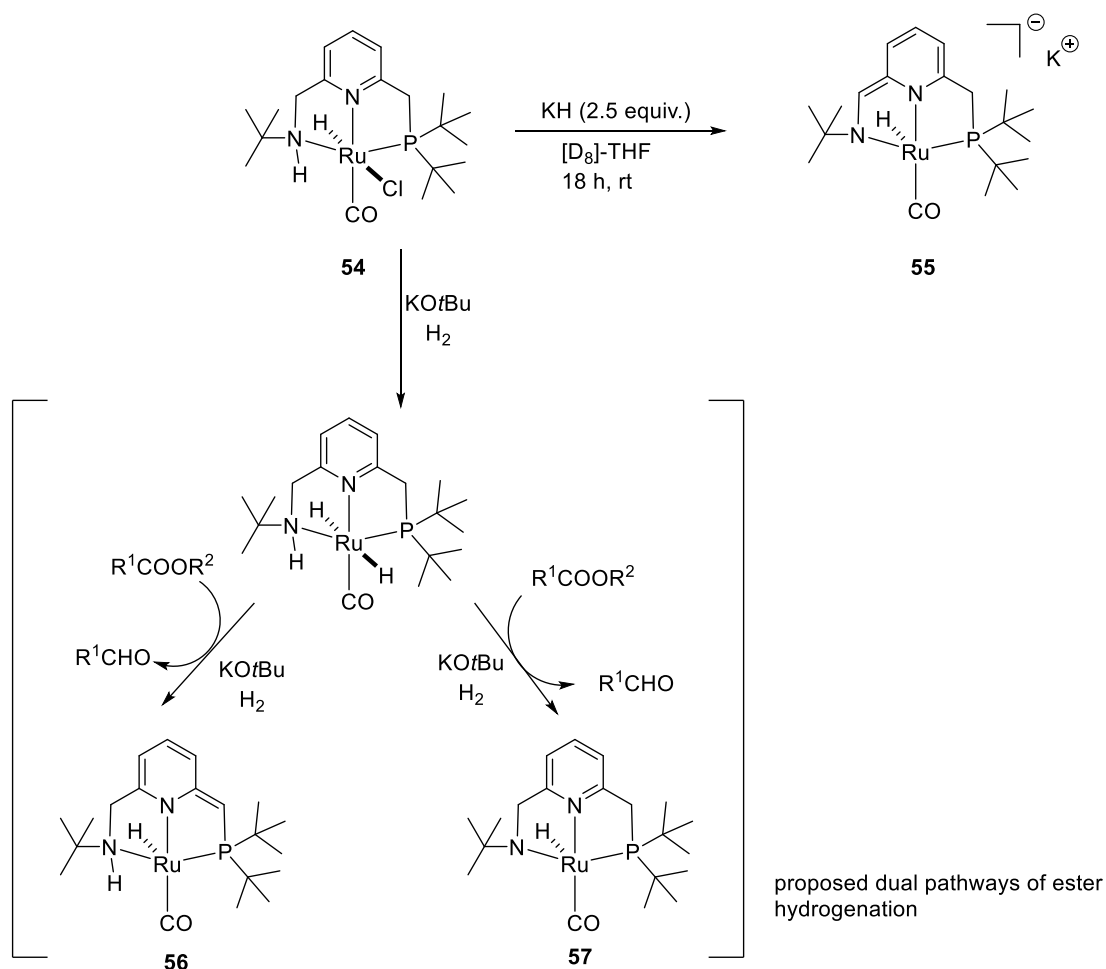
Scheme 1-36. Ru Pincer catalyst which could be deprotonated in two pathways.[88]

The Pidko group also replaced the phosphorus ligands with NHC groups in Ru ester hydrogenation catalysts.[89] A cationic, dimeric Ru CNC catalyst with three chloro-bridges showed outstanding activity (**58**, Figure 1-4). Some representative aromatic, aliphatic esters and lactones were hydrogenated with this catalyst in quantitative yield with TONs of 2000–15000. The highest TON of 79680 was achieved in the hydrogenation of ethyl hexanoate

(0.00125 mol% Ru in **58**, 0.02 mol% KO*t*Bu, 80 °C, 50 bar H$_2$, THF, 30 h). In a preliminary mechanistic study, an anionic intermediate bearing a 1-ethoxyethanolate ligand (**59**) was observed in the hydrogenation process of ethyl acetate, indicating that the active species was a monomeric Ru CNC hydride complex.
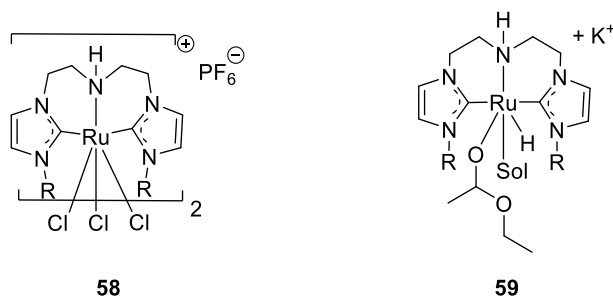
Figure 1-4. Pidko's dimeric ester hydrogenation catalyst precursor and its monomeric species in the EtOAc hydrogenation process.[89]

Zhang's group introduced hydrazine-containing ligands to prepare Ru ester hydrogenation catalysts.[90] The catalyst precursor was made by mixing the hydrazine-containing ligand **60** (Scheme 1-37 a) with [RuCl$_2$(*p*-cymene)]$_2$ in dioxane, then precipitating by adding diethyl ether to afford the solid catalyst as a non-well defined mixture (**61**). A wide substrate scope was studied, including aliphatic/aromatic esters and lactones. Up to 17200 turnovers (TO) and 86% conv. was obtained for the hydrogenation of methyl benzoate (0.005 mol% **61**, 5 mol% NaOEt, 50 bar, 80 °C, dioxane, 16 h).
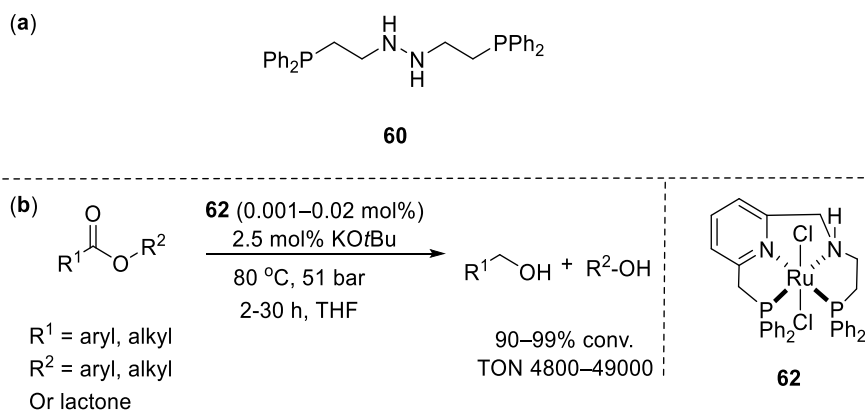
Scheme 1-37. (a) and (b) two catalytic systems reported by Zhang and coworkers.[90, 66]

Zhang's group also reported the catalyst **62** (Scheme 1-37 b), which was exceptionally active towards ester hydrogenations.[66] A range of aliphatic and aromatic esters were hydrogenated with TONs of 19800–80000 (0.0016–0.005 mol% **62**, 2.5 mol% KO*t*Bu, 51 bar, 80 °C, THF, 5 h). The highest TON of 80000 with 80% yield was obtained for the hydrogenation of ethyl acetate (0.001 mol% **62**, 2.5 mol% KO*t*Bu, 51 bar, 80 °C, in neat, 30 h). An outstanding TON of 49000 with 98% yield also was achieved in the hydrogenation of methyl benzoate (0.002 mol% **62**, 2.5 mol% KO*t*Bu, 51 bar, 80 °C, THF, 5 h). The author attributed this remarkable activity to the strong hydricity of the metal-hydrides when there are two phosphorus ligands, and on the improved acidity of the NH when the NH is next to a benzyl group. The proposed mechanism involved a bifunctional addition with a deprotonated NH in the presence of base, which was consistent with a study reported by Bergens et al.[91]

Chianese reported their pincer type Ru-CNN catalyst (**63**, Scheme 1-38) bearing an NHC group in 2016.[28] The activity of this catalyst was only moderate: TONs of 120–980 were achieved when hydrogenating a variety of aromatic and aliphatic esters (0.1–0.8 mol% **63**, 0.6–4.8 mol% NaO*t*Bu, 105 °C, 6 bar H_2, toluene, 20 h). An interesting result showed that **63** was much less active in the hydrogenation of methyl esters (A TON <10 was obtained in similar conditions) compared to ethyl, benzyl, or hexyl esters. A reasonable hypothesis was that the methanol byproduct was more poisoning than other primary alcohols. This speculation was investigated (Scheme 1-38): for the hydrogenation of methyl decanoate, adding benzyl alcohol increased the rate of production of 1-decanol, regardless of methanol formation by the transesterification. This experiment proved that benzyl esters were intrinsically more active than the methyl analog within this catalytic system. Later research[92] showed that tuning the substitution on the NHC and the amine arm greatly influenced the activity of the catalyst. The best combination was shown as **64** in Scheme 1-38. A TON of 1960 was achieved in the hydrogenation of ethyl benzoate (0.05 mol% **64**, 0.3 mol% NaO*t*Bu, 105 °C, 6 bar, toluene, 20 h).

equiv. benzyl alcohol added:	yield of 1-decanol
0	5%
0.2	25%
0.5	98%
1.0	99%
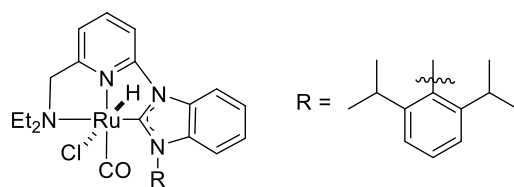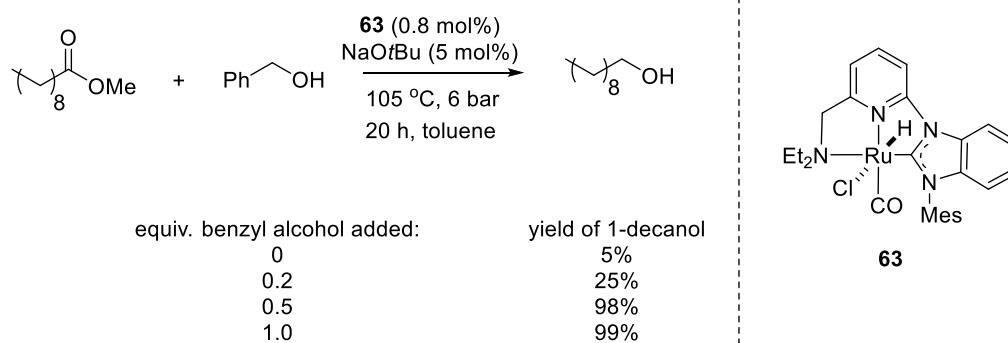
Scheme 1-38. Catalytic systems for ester hydrogenation reported by the Chianese group.[28, 92]

Instead of the commonly used alkoxide base, $NaBH_4$ was employed to facilitate the ester hydrogenation by the Yang and Sun groups.[93] A multitude of esters were hydrogenated using complex **65** (Scheme 1-39) as the catalyst, with 5–10 mol% $NaBH_4$. The highest TON of 56000 was obtained for the hydrogenation of methyl 4-trifluoromethyl benzoate (0.001 mol% **65**, 10 mol% $NaBH_4$, 140 °C, 50 bar, THF, 30 h). The η^1-BH_4 complex **66** was isolated when **65** was treated with H_2 and $NaBH_4$. A computational mechanistic study illustrated that the *trans*-dihydride complex **67** was the active species, which was generated from **66** through a cis/trans rearrangement (Scheme 1-39). The Ru-amido complex **68** was generated after one bifunctional addition to esters. An alcohol molecule (MeOH) and $NaBH_4$ would assist the regeneration of **67** via the formation of the Ru-alkoxide complex **69**. However, this catalytic cycle also indicated that $NaBH_4$ was consumed to form an alkoxide base (NaOMe), which should result in similar conditions to the hydrogenations conducted with alkoxide base.
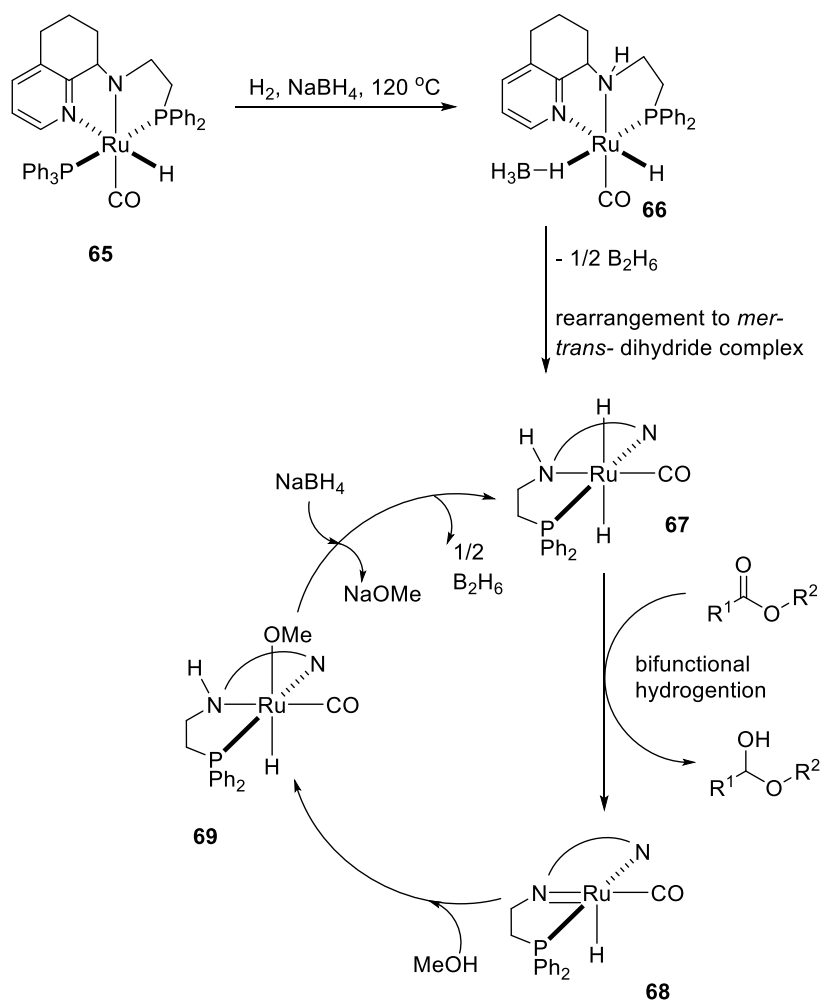
Scheme 1-39. NaBH$_4$-facilitated ester hydrogenation reported by Yang's and Sun's groups.[93]

The latest Ru-based ester hydrogenation was reported by the de Vries group, who invented another pincer type catalyst (**70**, Scheme 1-40) with a sulfur moiety on the ligand to replace the commonly used phosphorus moiety.[94] An interesting feature was that **70** selectively hydrogenated the carbonyl group of α,β-unsaturated esters; 87–100% selectivity was obtained to give unsaturated alcohol products, with up to 99% conversions (Scheme 1-40).
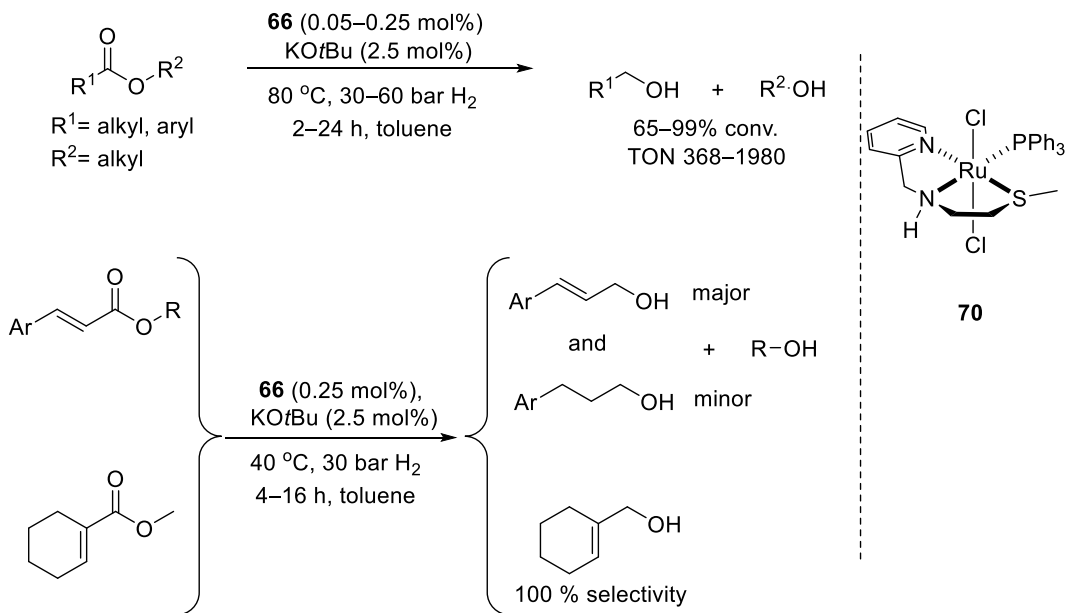
Scheme 1-40. Ru-NNS catalyst reported by the de Vries group.[94]

In summary, bifunctional catalysts made of 2nd or 3rd row transition metals (Ru, Ir, Os) are the most active catalysts for ester hydrogenations. Remarkable TONs of above 10000 have been reported by several research groups. Despite the use of noble metals, these catalysts are highly suitable for industrial applications.

1.4.3 Hydrogenation of Esters with Non-precious Metal Catalysts

In the perspective of "green chemistry", abundant, inexpensive and environmentally benign metal catalysts are preferred to potentially toxic precious metal catalysts. Since 2014, many studies focused on replacing Ru with other metals, including Fe, Mn, and Co.

In 2014, Milstein applied a pincer PNP ligand to Fe, affording a catalyst for ester hydrogenations (**71**, Scheme 1-41).[95] The highest TON of 1280 was reached for the hydrogenation of 2,2,2-trifluoroethyl trifluoroacetate using 1% KO*t*Bu, at 40 °C, 10 bar H_2 in 1,4-dioxane in 90 h. Notably, this pioneering catalyst only worked with highly activated trifluoroacetates and was not active for difluoroacetates. The proposed mechanism involved an outer-sphere hydride transfer onto the carbonyl carbon, followed by the proton transfer via dearomatization to reduce esters to aldehydes, as shown in Scheme 1-41.
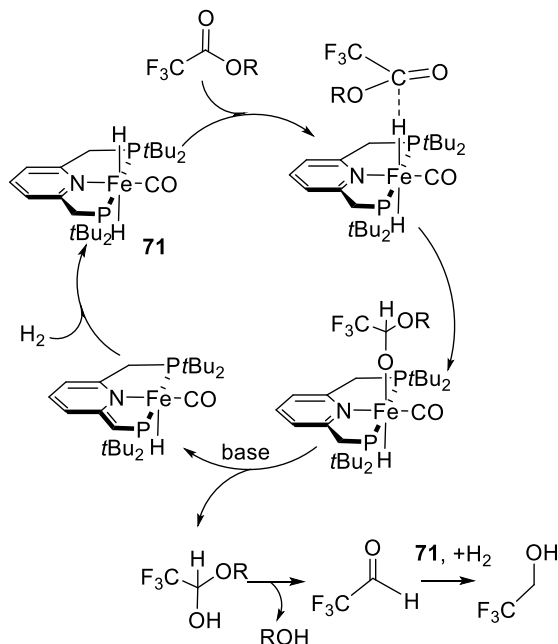
Scheme 1-41. Fe-based ester hydrogenation catalyst reported by Milstein and coworkers and its proposed catalytic cycle in the ester carbonyl reduction.[95]

Almost the same time, Beller et al[96] and Guan et al[97] reported another PNP pincer type Fe catalyst (**72**, Scheme 1-42) for ester hydrogenation. The major progress of these studies compared to Milstein's work was that the substrate scope was expanded to non-activated esters. TONs of above 80 (reported by Beller) were obtained with various substrates under base-free conditions (1 mol% **72**, 100 or 120 °C, 30 bar, THF, 6 or 19 h). The Beller group later studied the effects of different alkyl substituents on the phosphine motif,[98] showing that the catalyst with an ethyl group (**73**) gave the best activity. A TON of 100 can be achieved with various substrates under milder conditions (1 mol% **73**, 60 or 100 °C, 30 bar, THF, 6 or 18 h) compared to the earlier study.
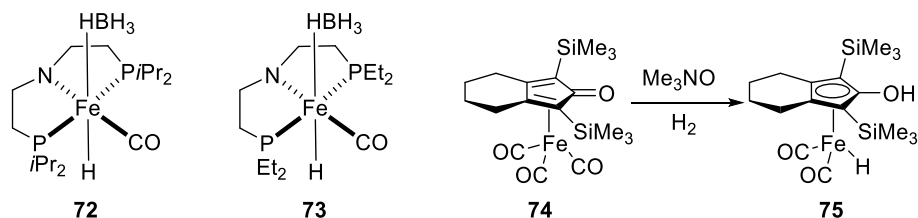
Scheme 1-42. Iron-based ester hydrogenation catalysts reported by Beller et al, Guan et al, and Lefort et al.

Another unique iron catalyst (**74**), shown in Scheme 1-42, was reported by the Lefort group in 2016.[99] This catalyst is the Fe-analog of the (cyclopentadienone)ruthenium carbonyl complexes for ketone hydrogenations, which was reported first by Shov in the 1980s.[100-101] This catalyst exhibited moderate activity with a TON up to 336 (0.25 mol% **74**, 90 °C, 70 bar, toluene, 17 h) towards trifluoroacetates esters, with Me_3NO as the initiator. The authors believed that the active catalyst was **75**, obtained from **74** by the decarbonylation and the split of H_2, which worked as a bifunctional catalyst, where the -OH group functioned as the acidic proton source like the NH moiety in Noyori-type catalysts.

A cobalt/triphos system was studied as an ester hydrogenation catalyst by Elsevier, Bruin, and coworkers.[102] The catalyst was prepared in situ by mixing 1 equiv. $Co(BF_4)_2 \cdot 6H_2O$ and 1 equiv. triphos (**11**). Remarkable activity with the selected carboxylic acids and modest hydrogenation activity with benzoate esters, aliphatic esters and lactones with a TON of 8–20 (5 or 10 mol% Ru, 100 °C, 80 bar, toluene, 22 h) were observed.

Milstein then applied pincer type ligands to Co complexes.[103] Three PNP or PNN cobalt precatalysts (Figure 1-5) were synthesized, and they were all active towards ester hydrogenation. The most active in the screening reactions was **76**: A TON of 42 was obtained in the hydrogenation of cyclohexyl hexanoate in THF, (2 mol% **76**, 4 mol% $NaHBEt_3$ and 25 mol% KOtBu, 50 bar, 130 °C).

76
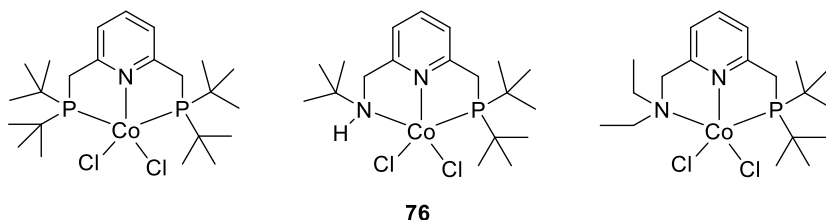
Figure 1-5. Co-based ester hydrogenation catalysts reported by Milstein et al.[103]

Interestingly, since **76** was inactive towards the hydrogenation of methyl benzoate under similar conditions, this mechanism was proposed uniquely to be an enolate hydrogenation, made by deprotonation of the esters, as shown in Scheme 1-43.
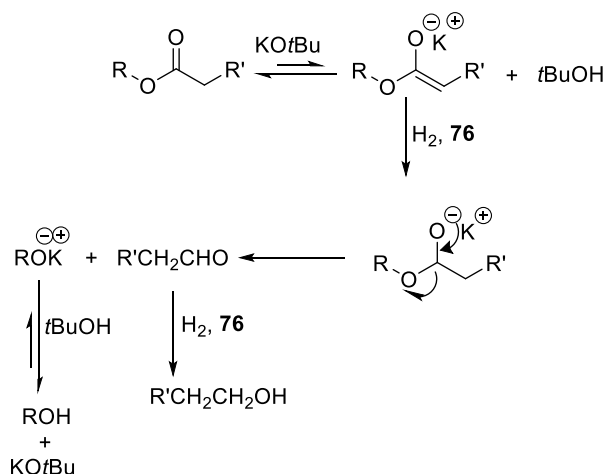
Scheme 1-43. Proposed mechanism of Milstein's Co-based ester hydrogenation catalyst.[103]

Another cobalt system for hydrogenation of esters was reported by the Jones group.[104] The Co-PNP pincer complex **77** (Scheme 1-44) was active towards the hydrogenation of a variety of aliphatic and aromatic esters without additives. Modest activity with 24–100% conv. and a TON of 12–50 was obtained in the hydrogenation of a variety of aromatic and aliphatic esters (2 mol% **77**, 55 bar, 120 °C, 20 h, THF). Remarkable performance was achieved with the hydrogenation of γ-valerolactone, giving a TON of 3890 and 38.9% yield under neat conditions (0.01 mol% **77**, 55 bar, 120 °C, 72 h). The derivative of **77** using an N-Me to replace the NH moiety, **78**, showed very close activity in the hydrogenation of methyl benzoate and γ-valerolactone. Based on this result, the authors believed that **77** adapted to a classic inner sphere mechanism, starting with the initiation under H_2 by releasing tetramethylsilane to form the monohydride species **79**.
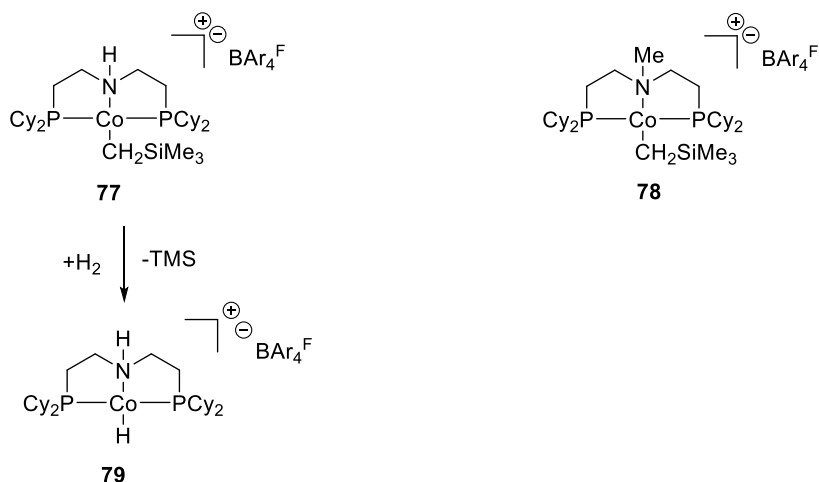
Scheme 1-44. Co catalysts reported by the Jones group, and the proposed active species.[104]

Beller reported their Co-PNP catalysts for ester hydrogenation in 2017.[105] Four Co-PNP complexes were synthesized by tuning the substituents on the phosphorous atoms and the halide ligands. The most active catalyst was found to be **80** (Figure 1-6) in this report. This catalyst was mildly active with a TON up to 20 for the hydrogenation of aliphatic/aromatic esters and lactones (5 mol% catalyst, 20 mol% NaOMe, 120 °C, 50 bar H_2, dioxane, 6–48 h). The -NMe version of this catalyst, **80-Me**, was inactive, implying that the catalysis underwent an outer-sphere mechanism. However, the DFT calculations did not exclude the inner-sphere mechanism.

Figure 1-6. Co catalysts reported by the Beller et al.[105]

Researchers turned their focus on Mn-based ester hydrogenation catalysts in 2016 since manganese is the third most abundant transition metal in earth's crust after iron and cobalt. The first Mn-catalyzed ester hydrogenation was reported by Beller.[106] The catalyst was made by reacting a PNP tridentate ligand with Mn(CO)₅Br. As shown in Scheme 1-45, the resulting complex is a mixture of a *cis*-dicarbonyl Mn complex with a Br⁻ ligand (**81**) and a *mer*-tricarbonyl Mn complex with a Br⁻ counter ion (**82**). Both **81** and **82** could be isolated and had

identical activity towards the hydrogenation of methyl benzoate. In addition, **82** hydrogenates a large scope of esters, including aliphatic/aromatic esters and lactones with a TON up to 50. The key step of the proposed mechanism is a bifunctional addition of the ester to the H-Co-NH in the active catalyst.
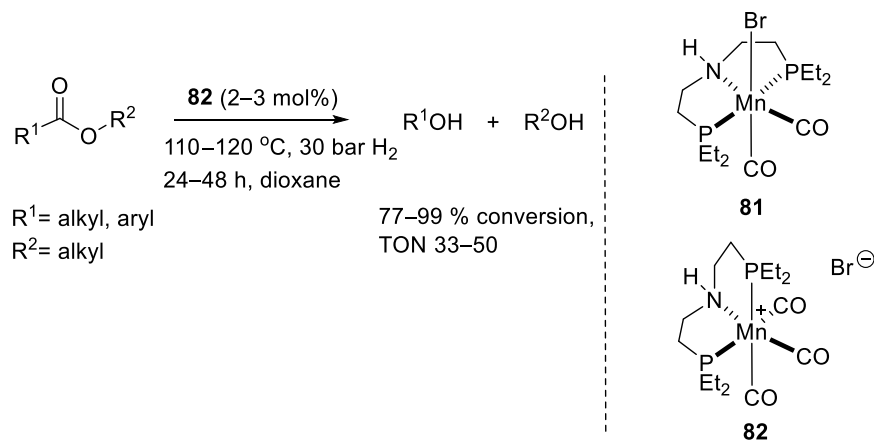
Scheme 1-45. Mn ester hydrogenation catalysts reported by the Beller group.[106]

Milstein et al reported their Mn-based catalyst with a pincer PNN ligand bearing an NH group for ester hydrogenations in 2017 (**83**, Scheme 1-46).[107] The catalyst operated with a strong base cocatalyst. The best performance was obtained with 2 mol% KH. A wide scope of esters, including aromatic esters, aliphatic esters, and lactones, can be hydrogenated quantitively to alcohols with a TON of 100 (1 mol% **83**, 2% KH, 20 bar, 100 °C, toluene, 21–60 h). A preliminary study of the mechanism was carried out, confirming the formation of the Me-amido complex **84** when **83** was treated with base. Compound **84** is believed to be the active species in the catalytic cycle. The dearomatization was not observed with this catalyst, indicating that the operative mechanism was likely to be the outer-sphere process that involved the proton transfer with the NH moiety.
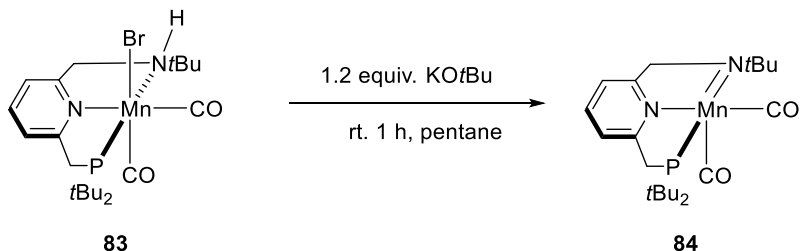
Scheme 1-46. Mn ester hydrogenation catalyst reported by Milstein et al. and its transformation with base.[107]

Clarke and coworkers reported a Mn-tricarbonyl catalyst for ketone and ester hydrogenations with a PNN ligand in a cis configuration (**85**, Scheme 1-47).[108] Above 82% conv. with a TON of 90–820 was achieved in the hydrogenation of a range of aromatic esters with **85** in 2-PrOH with KO*t*Bu base (Scheme 1-47).
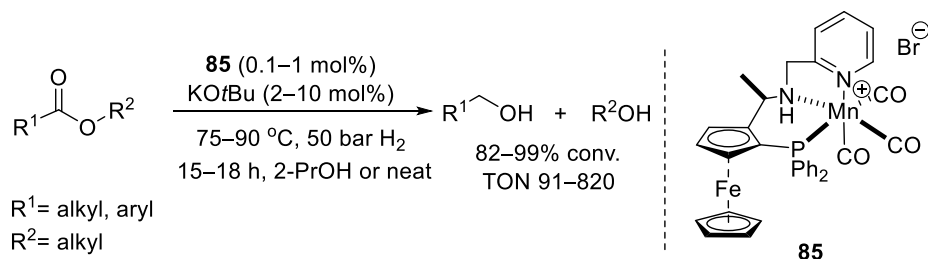
Scheme 1-47. Mn catalyst reported by Clarke et al.[108]

The first Mn catalyst with bidentate ligands for ester hydrogenation was reported by the Pidko group.[109] Three Mn complexes were synthesized, and they were all able to hydrogenate methyl benzoate at a considerable rate in the screening studies. Compound **86** (Scheme 1-48) was the most active. A variety of aromatic and aliphatic esters can be converted to the corresponding alcohols with a large percent of base and a TON up to 495 (Scheme 1-48).
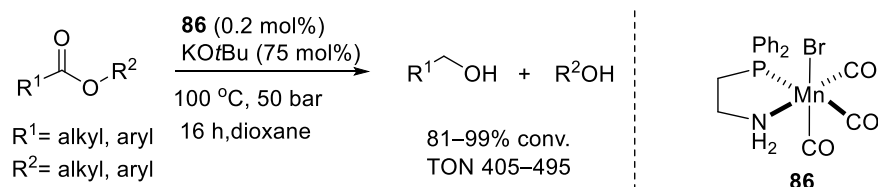
Scheme 1-48. Non-pincer type Mn catalyst reported by the Pidko group.[109]

The catalyst also had good chemoselectivity towards carbonyls. Non-conjugated unsaturated esters were hydrogenated to unsaturated alcohols without reducing the olefin bonds. Kinetic experiments proved the great dependency on base of this catalyst. Product inhibition effect also was observed, consistent with previous studies on the ruthenium catalytic system. A plausible mechanism of the product inhibition is shown in Scheme 1-49.[86] The amido metal complex is formed after bifunctional reduction of esters, which may either split the H_2 to form the active dihydride species or react with the alcohol product to generate the inactive alkoxide species, which lower the concentration of the active catalysts in a hydrogenation.
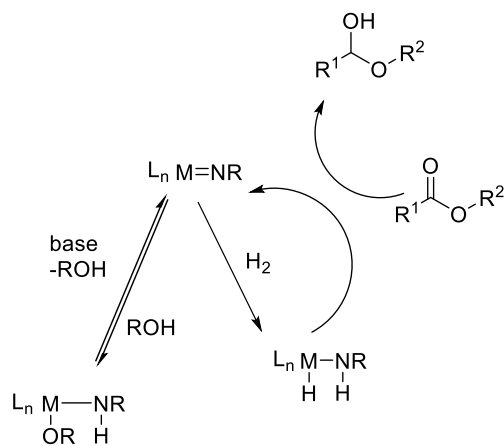
Scheme 1-49. A plausible mechanism of the product inhibition of ester hydrogenations.[86]

In summary, the use of non-precious metal catalysts is a promising solution to the concerns regarding the cost and environmental impact of noble metal catalysts for ester hydrogenations. However, given that the ligands also contribute greatly to the cost and toxicity of a catalyst, the efficiency of non-precious metal catalysts likely needs to be improved before industrial implementation.

1.5 Immobilized Catalysts for the Hydrogenation/Transfer Hydrogenation of Carbonyl Compounds

Despite the high efficiency of homogeneous catalysts, there are remaining concerns about their applications in industrial productions. First, many organometallic catalysts are made of expensive ligands and metals, but the recycling of these catalysts generally is unachievable. Second, transition-metal-based catalysts may contaminate the desired products, which is particularly unwanted in the pharmaceutical and other fine chemical industries, and the separation of the catalyst residuals leads to extra processes and costs. One approach to address those issues is to anchor the molecular homogeneous catalysts onto insoluble solid supports so that the catalysts can be removed from the reaction by simple filtration and, ideally, be reused to improve their overall efficiency.[110-112]

The support materials can be either inorganic materials,[113, 114] such as silica, alumina, zeolites, clay, etc., or organic polymers.[115, 116] The support materials should be inert and provide a high surface area to maximize the rate of mass transfer. Catalysts can be attached onto the supports via physical interactions (electrostatic, adsorption, hydrogen-bonding, etc.) or by covalently bonding to the supports. A great amount of research has been devoted to the immobilization of homogeneous organometallic catalysts. To focus on the topic of this dissertation, only polymer-supported catalysts for the hydrogenation/transfer hydrogenation of carbonyl compounds are discussed extensively in this chapter. For other immobilized catalytic systems, interested readers are directed to recent review papers.[112, 117-121]

The pioneering work on polymer-immobilized catalysts was reported by Grubbs in 1971.[122] As shown in Scheme 1-50, crosslinked polystyrene beads were functionalized with a diphenylphosphine group and then metallated with Wilkinson's catalyst, $RhCl(PPh_3)_3$, to obtain the polymer-bound catalyst **87**, which showed a loading of 0.13 mmol Rh/g beads (the characterization technique was not reported). Catalyst **87** was reused 10 times with only ±5% variation in activity in the hydrogenation of cyclohexene in benzene (1 bar H_2). In this pioneering report, the detailed characterization of the metallated polymer, the catalyst loading in the hydrogenation, and the leaching of the catalyst were not reported; hydrogenation activity was obtained by the H_2 consumption, but the details of this measurement were not specified.
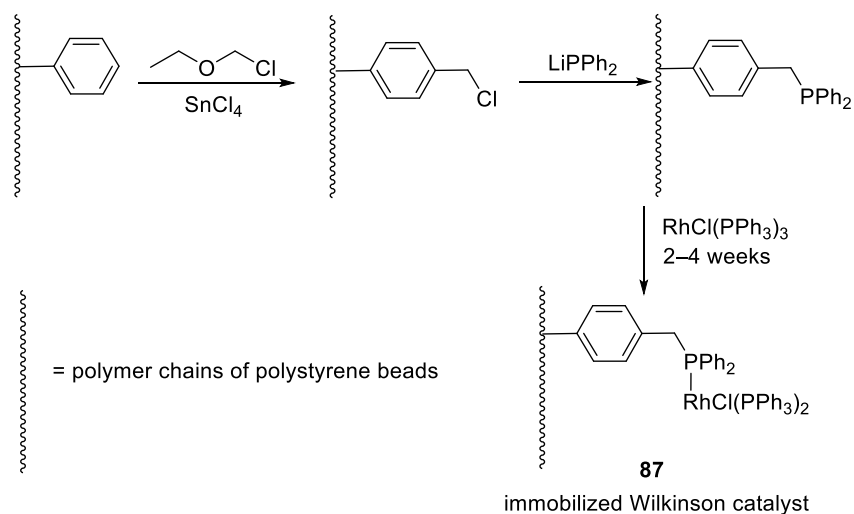
Scheme 1-50. The polymer-based immobilized catalyst for olefin hydrogenations.[122]

Noyori et al reported several series of homogeneous Ru catalysts with outstanding performance for the enantioselective hydrogenation/transfer hydrogenation of ketones in the late 20th century. The representative catalysts include Ru(Cl)$_2$BINAP[123], Ru(OAc)$_2$BINAP[124] (BINAP = 2,2′-bis(diphenylphosphino)-1,1′-binaphthyl), RuCl$_2$(diphosphine)(diamine),[125, 126] and RuCl(η^6-mesitylene)(TsDPEN).[127, 128] These catalytic systems hydrogenate a massive variety of prochiral ketones and β-keto esters with excellent activity and selectivity; representative catalysts and reactions are shown in Scheme 1-51. These systems have been used widely in fine chemical industry[129], and Noyori was awarded the Nobel Prize in Chemistry in 2001 for his contributions in asymmetrical catalysis. Following these breakthroughs, researchers began to study the immobilization of these systems on polymer supports. The most common strategy is to attach the diphosphine or diamine ligand covalently to the backbone of a polymer.
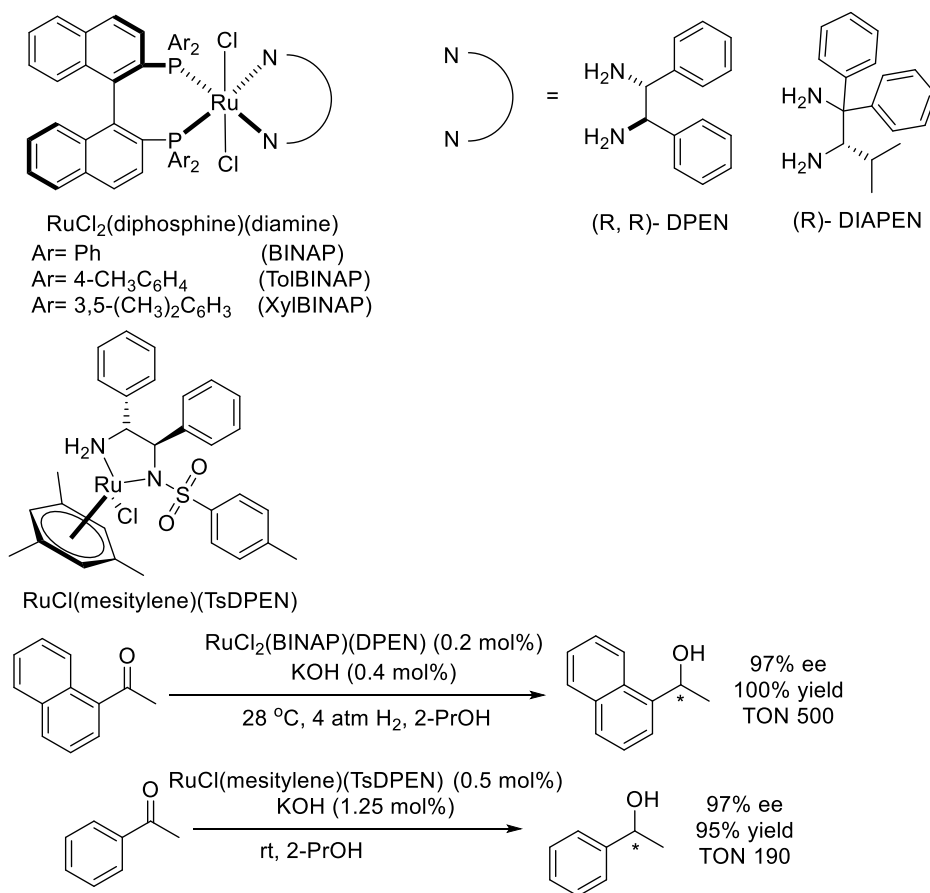
Scheme 1-51. Representative Ru catalysts for the asymmetrical hydrogenation/transfer hydrogenation of prochiral ketones.[123-128]

The first attempt to immobilize a catalyst through a diphosphine ligand for ketone reductions was reported by Bayston and coworkers.[130] Compound (*R*)-BINOL (**88**, Scheme 1-52) was modified via Friedel–Crafts acylation, ketone hydrogenation over Pd/C, hydrogenolysis with methanesulfonic acid, and demethoxylation to incorporate a pendent ester group onto the naphthyl backbone (**89**). Conversion to the ditriflate, and then displacement by Ph$_2$PH catalyzed by Ni formed the (*R*)-BINAP derivative, **90**. Ligand **90** was grafted onto the polymer support by condensation between the ester and the aminomethylated polystyrene (**91**). The active catalyst **92** was prepared by metalation of **91** with [(COD)Ru(bis(2-methallyl))] and HBr in acetone. Catalyst **92** is an analog of the homogeneous [RuBr$_2$(BINAP)] catalyst, which catalyzes the hydrogenation of β-keto esters with high ee,[123] however, no detailed characterization of the catalyst was reported. The activity and reusability of **92** were evaluated with the hydrogenation of methyl acetoacetate to produce methyl (*R*)-3-hydroxybutyrate (2 mol% **92**, 10 bar, 70 °C, THF/MeOH, 18–36 h). Three runs were carried out with a simple

45

filtration between to isolate the product. The yield of each run was 99%, 99%, and 82%, respectively. The reaction time increased from 18 h to 24 h to 36 h, and the ee dropped from 97% to 90%. The leaching of Ru in this catalysis was less than 1%.
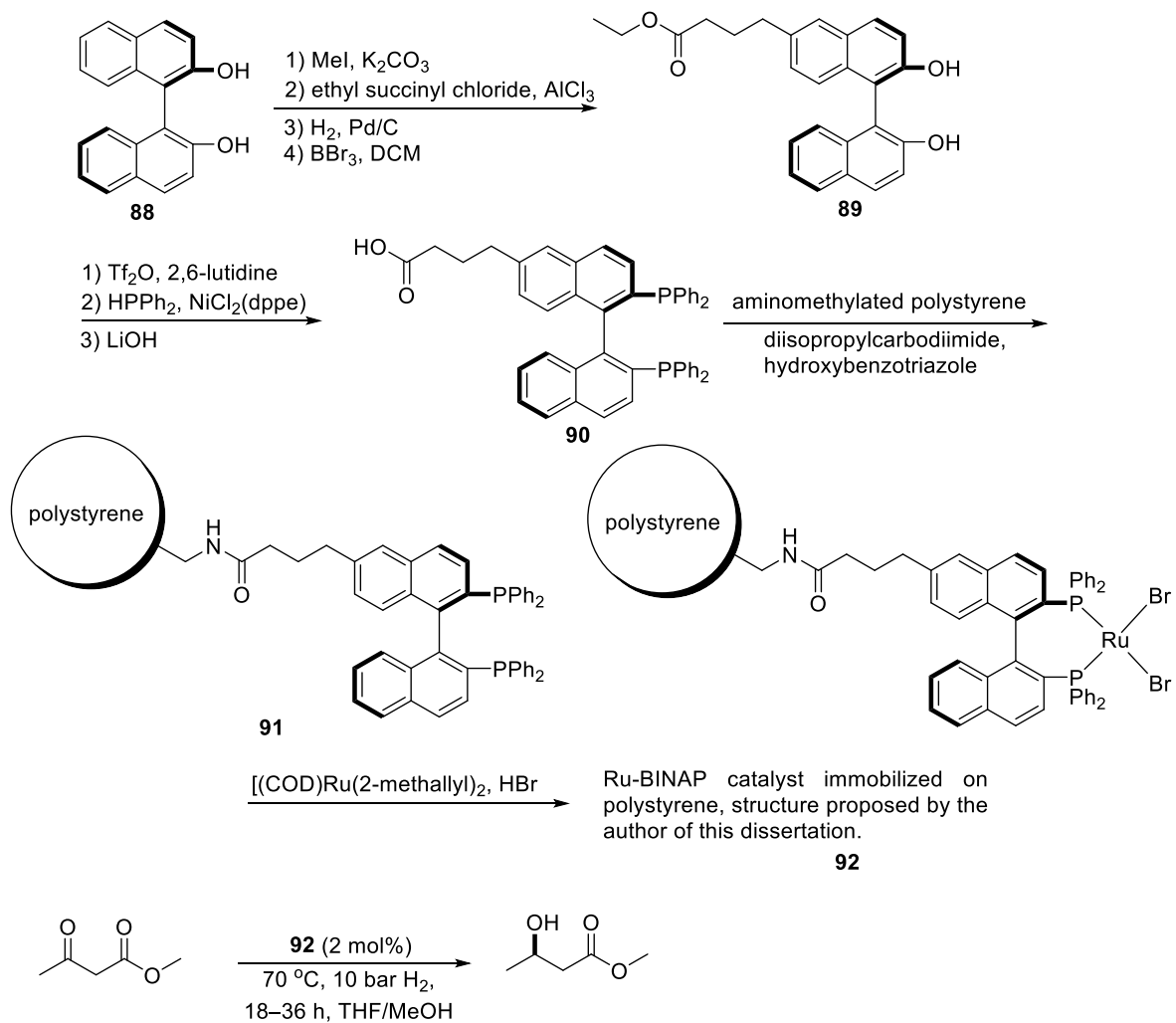
Scheme 1-52. Immobilized Ru-BINAP catalyst made by Bayston and coworkers and its hydrogenation.[130]

Soon after, Noyori and coworkers prepared a RuCl$_2$(BINAP)(DPEN) catalyst supported on polystyrene beads using **91**.[131] As shown in Scheme 1-53, **91** was metallated by reaction with [RuCl$_2$(η^6-benzene)]$_2$ in *N,N*-dimethylacetamide (DMA), followed by reaction with (*R*, *R*)-DPEN to afford **93**, which was confirmed as a mixture of trans and cis isomers (7:1) using solid state ^{31}P NMR. It possessed excellent activity and stability for the reusing hydrogenation of 1'-acetonaphthone: 99%–100% conversion with a TON of ~2500 / run was achieved within the first nine runs with excellent ee (97–98%), indicating that the modification on the ligand

did not affect the enantioselectivity of this catalyst (0.04 mol% **93**, 2% KOtBu, 8 bar, 25 °C, 2-PrOH/DMF, 20–36 h). DMF was used as a cosolvent to swell the polymer and maximize mass transfer. By the 10th run, the catalysts required a significantly longer reaction time (50–86 h) to maintain the high conversions. The total TON was 33000 after 14 consecutive runs.
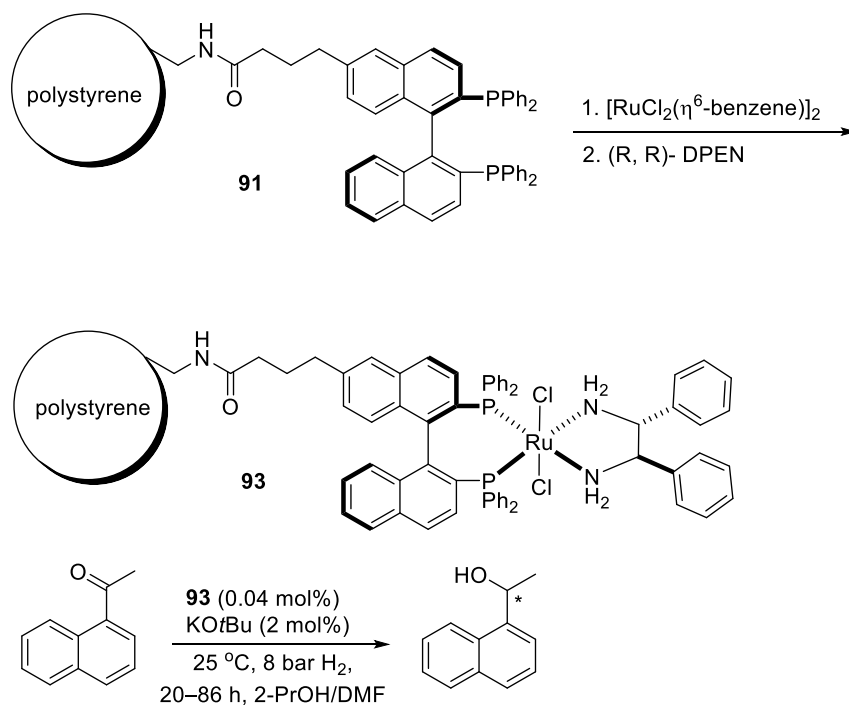
Scheme 1-53. Polystyrene-supported RuCl$_2$(BINAP)(DPEN) catalyst reported by Noyori et al.[131]

The diamine ligands also can be linked to polymers to immobilize these types of catalysts. Xiao's group reported the first example of the immobilization of the DPEN ligand onto polymer supports. The TsDPEN derivative was also prepared.[132-134] As shown in Scheme 1-54, the researchers started from the di-BnO-substituted ligand **94** and the monotosylated derivative TsDPEN **95**. After protecting the amine groups with Boc, **94** or **95** were converted to di-hydroxyl derivatives **96** or **97** by hydrogenolysis. Then, these were immobilized onto polyethylene glycol 2000 monomethyl ether mesylate (PEG-OMs) by the nucleophilic substitution of the mesylate. The immobilized DPEN **98** and the immobilized TsDPEN **99** were obtained after removal of the Boc protecting group.
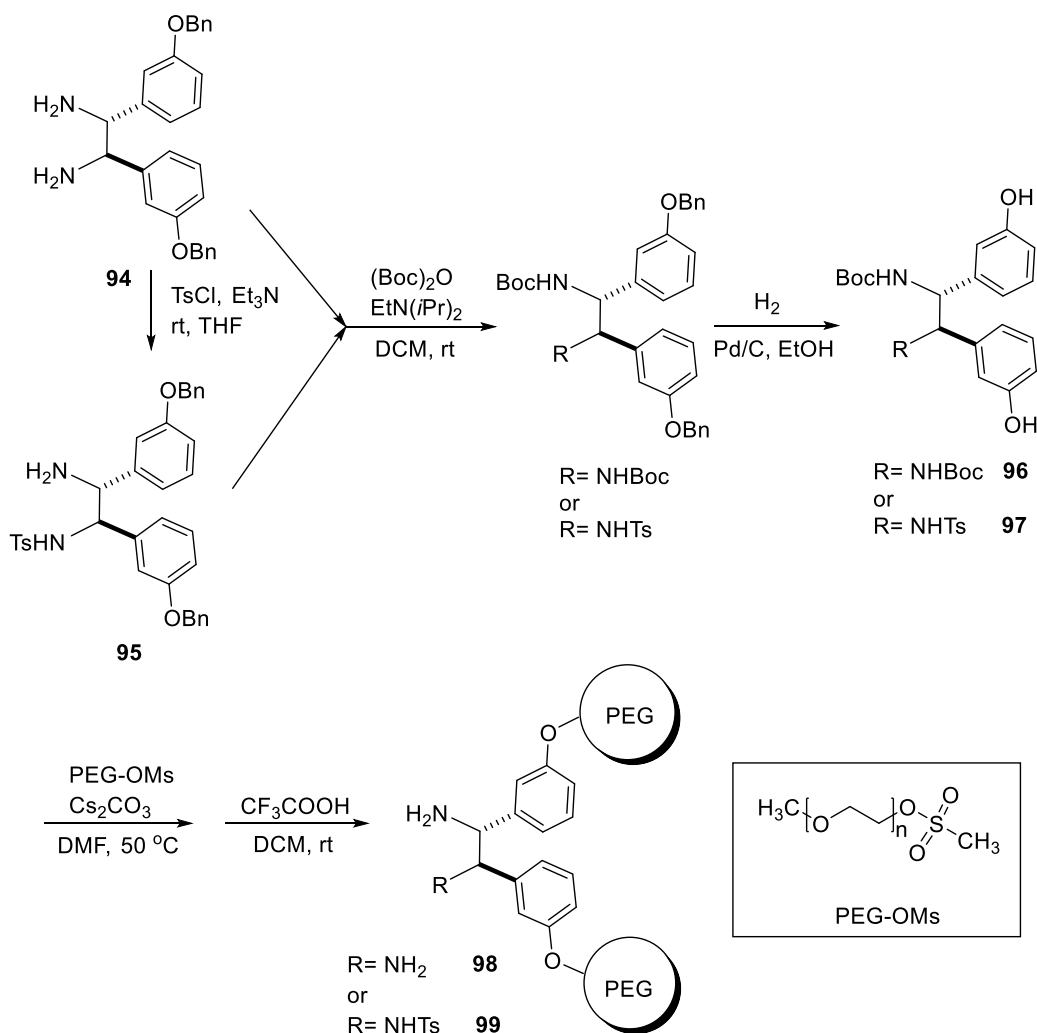
Scheme 1-54. The immobilization of DPEN onto PEG reported by Xiao et al.[132-134]

The supported ligand **98** was metallated with [RuCl₂(η⁶-benzene)]₂ and PhanePhos (PhanePhos = 4,12-bis(diphenylphospino)-[2,2]paracyclophane) to form the immobilized RuCl₂(diphosphine)(diamine) precatalyst (**100**). The proposed structure of **100** is shown in Scheme 1-55, but no characterizations were reported. It was examined as a reusable catalyst for the hydrogenation of 1'-acetonaphthone to (*S*)-1-(1'-naphtyl)ethanol (0.1 mol% **100**, 1.2% KO*t*Bu, 9 bar, rt, 2-PrOH, 3 h, Scheme 1-55). Although **100** was soluble in the reaction media, it was precipitated between runs by addition of diethyl ether. Three consecutive reactions were carried out with conversions >96% and ee ~96%. The amount of Ru leached in the reaction was 2.7 ppm (~18% of total Ru loading, calculated based on the numbers in the paper).
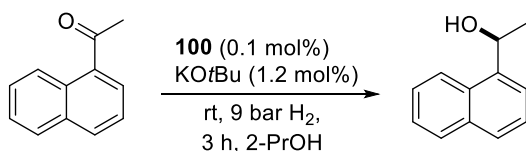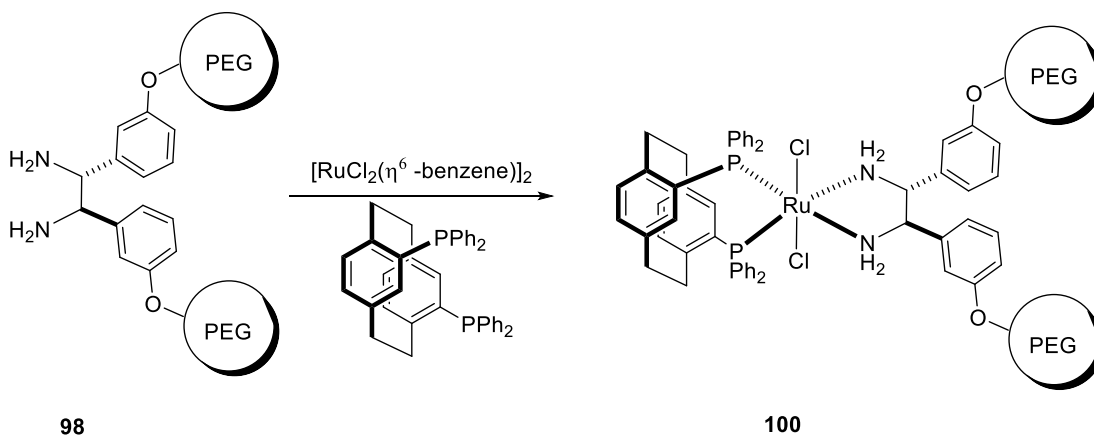
Scheme 1-55. Reusable hydrogenation with immobilized catalyst **100**.[132]

In other reports,[133, 134] **99** was metallated with $[RuCl_2(p\text{-cymene})]_2$ to prepare the heterogeneous analog of the RuCl(TsDPEN) catalyst (as shown in Scheme 1-56). The resulting supported complex (**101**) catalyzed the enantioselective transfer hydrogenation of ketones in both $HCOOH/Et_3N$ azeotrope media and in aqueous solution. The best performance of reuse was recorded as 11 consecutive runs without significant loss in activity (conv. >95%) and selectivity (ee >91%) for the transfer hydrogenation of acetophenone to (R)-1-phenylethanol (1 mol% **101**, 1000 mol% HCOONa in the first run, 100 mol% HCOOH in the following runs, 40 °C, H_2O, reaction times are missing). The catalyst was precipitated by adding water, and it was separated by extraction. Inductively coupled plasma mass spectrometry (ICP-MS) analysis confirmed that 0.4% Ru was leached out. The total TON was above 1300. It was comparable to the homogeneous RuCl(mesitylene)(TsDPEN) catalyst (structure see Scheme 1-51), which reduces acetophenone with a TON of 990 in a single reaction (0.1 mol% catalyst, $HCOOH/Et_3N$, 28 °C, 60 h).
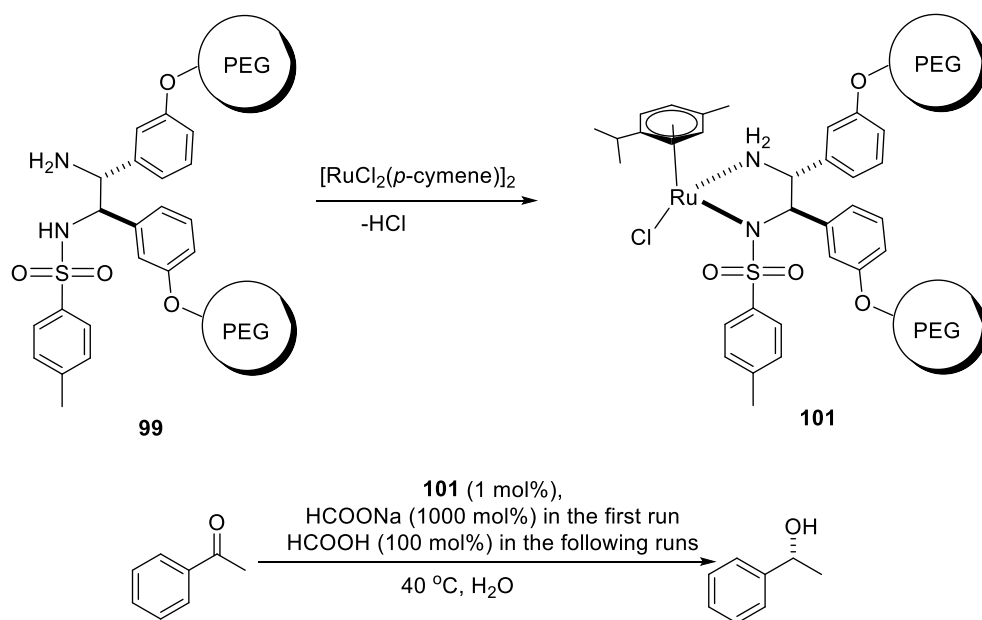
Scheme 1-56. Reusable transfer hydrogenation reported by Xiao et al.[133, 134]

Another strategy to immobilize diamine ligands onto polymers is to polymerize monomers bearing the diamine ligand. The first example was by Lemaire and coworkers,[135] who successfully introduced DPEN into a styrene-based monomer via a facile one-step sulfonation reaction, as shown in Scheme 1-57. The resultant monomer, **102**, underwent radical copolymerization either with styrene to form the linear polymer **103** or with both styrene and divinylbenzene to produce the crosslinked network **104**. The metalation reagent [Ir(COD)Cl]$_2$ (COD = 1, 5-cyclooctadiene) was reacted with **103** to prepare the active catalyst (**105**), which was able to catalyze the transfer hydrogenation of acetophenone with 2-PrOH in two successive reactions with decreasing yields (96% to 18%) and ee (94% to 80%) (experimental details were not reported comprehensively in the manuscript).
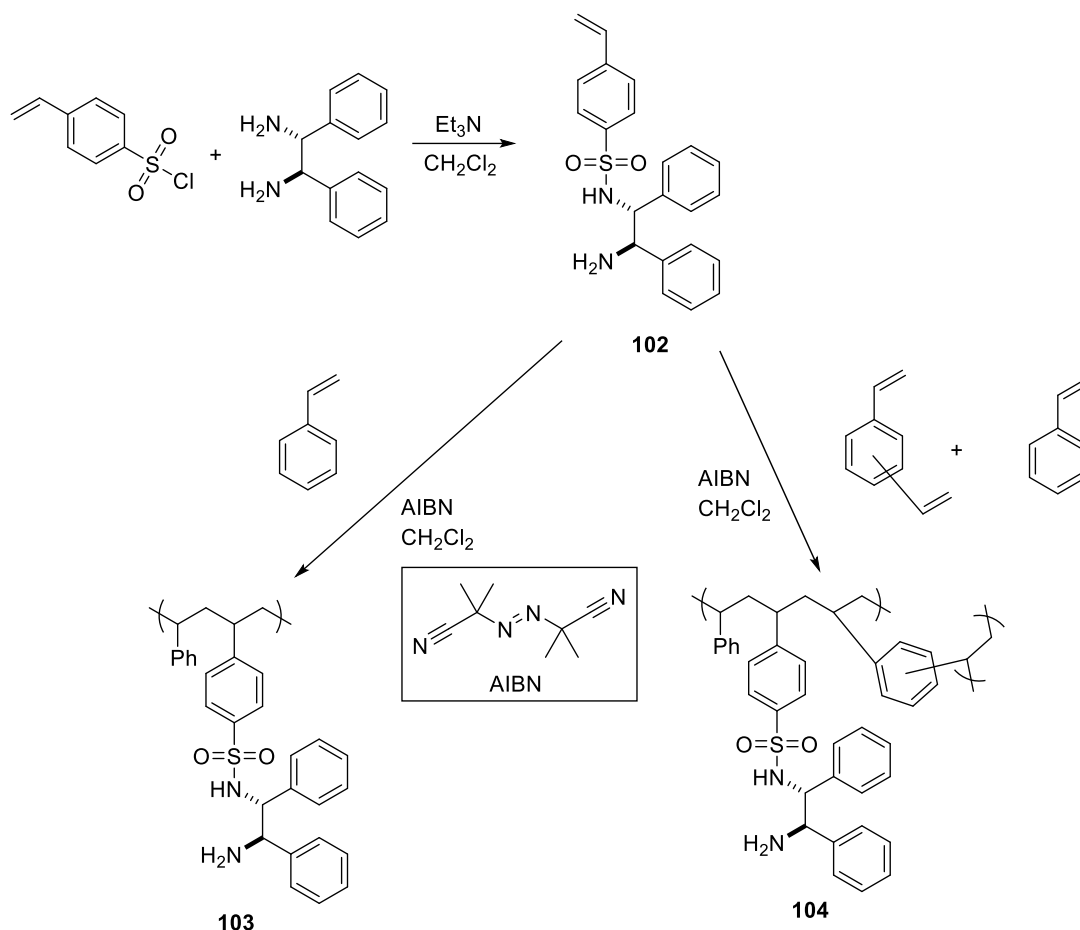
Scheme 1-57. The synthesis of polystyrene-based TsDPEN reported by Lemaire et al.[135]

Xiao's group prepared **104**[136] by a method called solvothermal synthesis.[137] The copolymerization was conducted at rt in DMF first, then heated at 100 °C for 24 h, resulting in a mesoporous morphology. After metalation with [RuCl$_2$(*p*-cymene)]$_2$, the resultant mesoporous self-supported catalyst, with a BET surface area of 481 m^2/g, was able to catalyze the transfer hydrogenation of acetophenone from formate in good stability over 14 successive runs in aqueous media (conv. >94%, ee = 93~94%, 1 mol% Ru, 500% HCOONa, 40 °C, H$_2$O, 1.5 h). No detectable leaching of Ru was found in those heterogeneous reactions. This showed comparable activity to the homogeneous analogs in ketone transfer hydrogenations, for example, RuCl(mesitylene)(TsDPEN) (discussed above).

The Itsuno group conducted research with the same styrene-based TsDPEN monomer **102** to prepare immobilized catalysts for transfer hydrogenation of ketones.[138, 139] Copolymerizing monomers with hydrophilic pendent groups and **102** to make the polymeric

catalysts allows them to swell better in water, facilitating the transfer hydrogenation of ketones in aqueous media. The best system was prepared by copolymerizing **102**, divinylbenzene, and benzyltributylammonium *p*-vinylphenylsulfonate, resulting in a crosslinked polymer **106** (Scheme 1-58). Metalation with [RuCl$_2$(*p*-cymene)]$_2$ afforded **107**. The author stated that the NMR of **107** was different from that of **106**, but no further analysis was given. The transfer hydrogenation of acetophenone was carried out five times using **107** in water without losses in activity or ee (1 mol% **107**, 500% HCOONa, 40 °C, H$_2$O, 3 h). Without introducing the anionic monomers, the polymer catalyst prepared via the same methodology showed much less activity (7% in 17 h) and lower enantioselectivity (80% ee) compared to that with **107**, illustrating the importance of the hydrophilicity of the polymer in this catalysis.
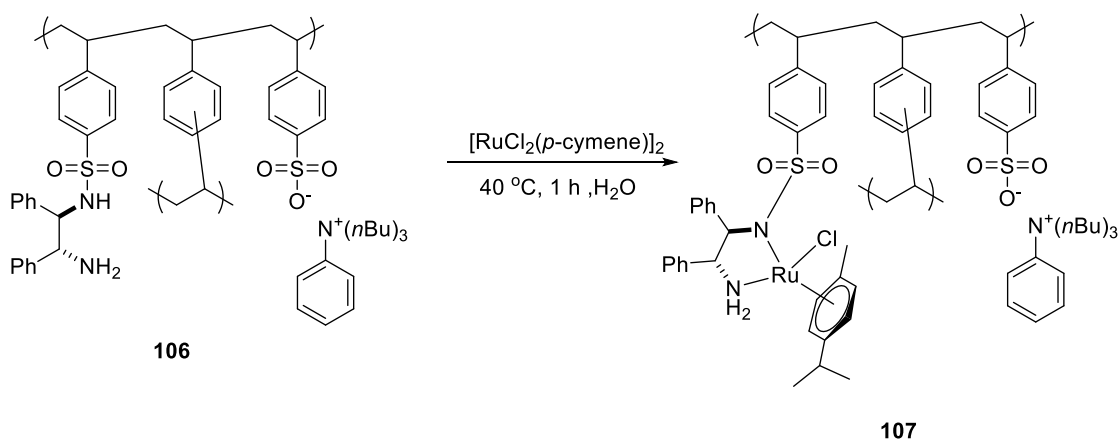
Scheme 1-58. Supported Ru-TsDPEN catalyst worked in aqueous media reported by the Itsuno group.[138, 139]

Hou's group copolymerized **102** with dimethyl aminopropyl acrylamide to afford **108**, which was metallated to form **109** as a pH-responsive polymer catalyst (Scheme 1-59).[140] The optimized ratio between **102** and dimethyl aminopropyl acrylamide was 1:1.2, and the characterization of **109** indicated that 74% of the ligand on the polymer was metallated by Ru. Compound **109** remained soluble in acidic aqueous media due to the protonation of the pendent tertiary amine but precipitated once the pH was raised above ~7. The transfer hydrogenation of ketones was carried out using HCOOH as the proton/hydride source. The pH of the reaction media increased with the consumption of HCOOH so that the dissolved polymer catalyst precipitated upon completion of the reaction. This reversible pH-responsive feature was utilized for the recycling of the catalyst. The transfer hydrogenation of acetophenone was

performed in eight consecutive runs with a consistent ee of 95% and with some loss in activity (100–87% conv.) (1 mol% **109**, 400% HCOOH/HCOONa with initial pH = 3.64, 40 °C, H$_2$O, reaction time was not specified).
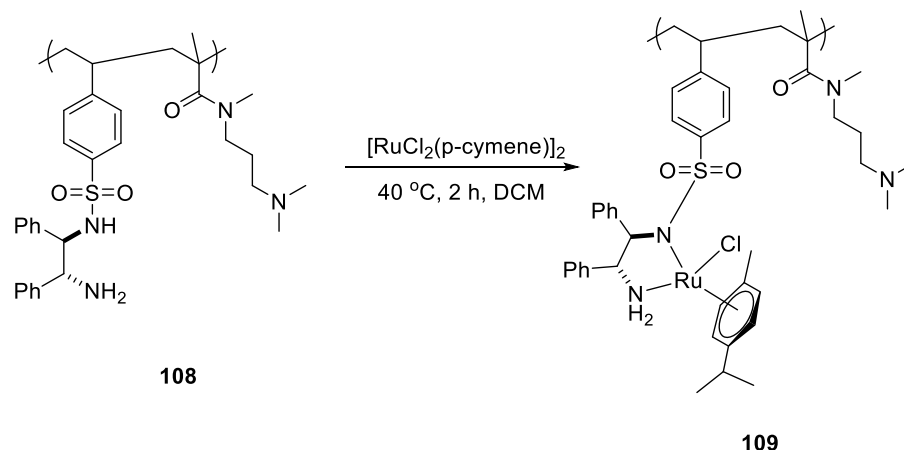
Scheme 1-59. pH-responsive supported catalyst reported by Hou et al.[140]

As introduced above, there are two steps commonly employed for the immobilization of hydrogenation/transfer hydrogenation catalysts: 1) linking the ligand to the polymer support or polymerizing a ligand-containing monomer, and 2) metalation of the supported ligands. The characterization of the actual complexes formed after the metalation is not easy, and a number of studies[131, 139-145] indicated that the heterogeneous metalation hardly proceeds to completion. An ideal alternate pathway is to prepare the complexes first, then link them onto monomers or polymers covalently.

The Bergens group demonstrated another strategy to immobilize a catalyst by preparing a catalyst monomer bearing strained alkyne groups and anchoring the catalyst onto polymers via ring opening metathesis polymerization (ROMP). ROMPs catalyzed by the family of Grubbs catalysts proceed in mild conditions without the need of any bases or radicals, providing a friendly environment for the hydrogenation catalyst to survive. The first example was a RuCl$_2$(Norphos)(DPEN) catalyst used for the asymmetric hydrogenation of 1'-acetonaphthone.[146] The Ru compound RuCl$_2$(Norphos)(Py)$_2$ (**110**, Scheme 1-60) was prepared as the catalyst monomer for ROMP. The polymerization of **110** as the only monomer with 1st generation Grubbs catalyst (**111**) did not proceed since the metathesis catalyst center was severely crowded after the ring-opening of one **110** molecule blocking the next **110** from

interacting with the metathesis catalyst center. To facilitate the polymerization, *cis*-cyclooctene (COE) was added as a spacer, providing a less crowded environment around the metathesis catalyst center. The resultant copolymer was crosslinked by the addition of dicyclopentadiene to afford **112**, followed by the incorporation of (*R*,*R*)-DPEN to afford the active hydrogenation catalyst, which was deposited on a fine powder of $BaSO_4$ to increase the surface area and to maximize the mass transport, resulting in the supported catalyst **113**.

With the catalysis of **113**, 1'-acetonaphthone was hydrogenated to (*S*)-1-(1'-naphtyl)ethanol in good ee of 84.9 to 79.6% in 11 successive runs (0.2 mol% Ru in **113**, 0.8% KO*t*Bu, 4 bar, 22 °C, 2-PrOH, 2–15 h). Except for the first four exploratory runs with a shorter reaction time (2–14 h), quantitative conversion was achieved in the following 15-hour runs, until the conversion slightly decreased to 97% in Run 11. The catalytic rate of **113** was ~40% that of the homogeneous monomer **110** under the same conditions, showing that the heterogeneity did not slow down the mass transport significantly. The ee of the hydrogenation of 1'-acetonaphthone with **110** was only 48% (*S*). The drastic change in ee could be attributed to both the introduction of DPEN and the chiral environment change of opening the Norphos backbone.
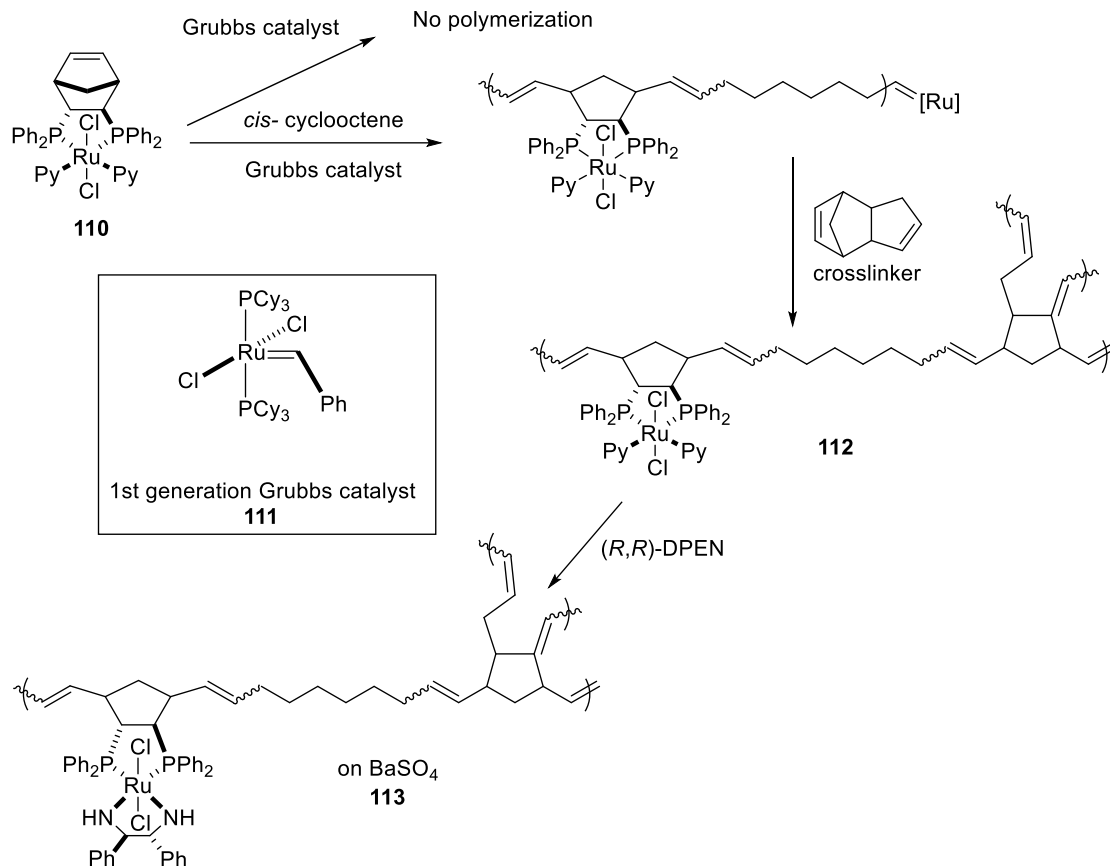
Scheme 1-60. The supported RuCl$_2$(Norphos)(DPEN) catalyst reported by the Bergens group.[146]

Another supported catalyst system with better activity and selectivity was developed using a similar methodology.[147] As shown in Scheme 1-61, (*R*)-5,5'-diamino-BINAP was condensed with *cis*-5-norbornene-2,3-endo-dicarboxylic anhydride to form the ROMP-active ligand **114**, which reacted with *trans*-RuCl$_2$(NBD)Py$_2$, (**115**, NBD = 2,5-norbornadiene, Py = pyridine), to prepare the ROMP-active catalyst monomer **116**. With 5 mol% **111**, the copolymerization of **116** and COE proceeded smoothly, resulting in a self-crosslinked polymer **117**, in which the bis-pyridine ligands were replaced by (*R*,*R*)-DPEN. The deposition of the polymer on BaSO$_4$ resulted in the immobilized RuCl$_2$(BINAP)(DPEN) catalyst **118**.
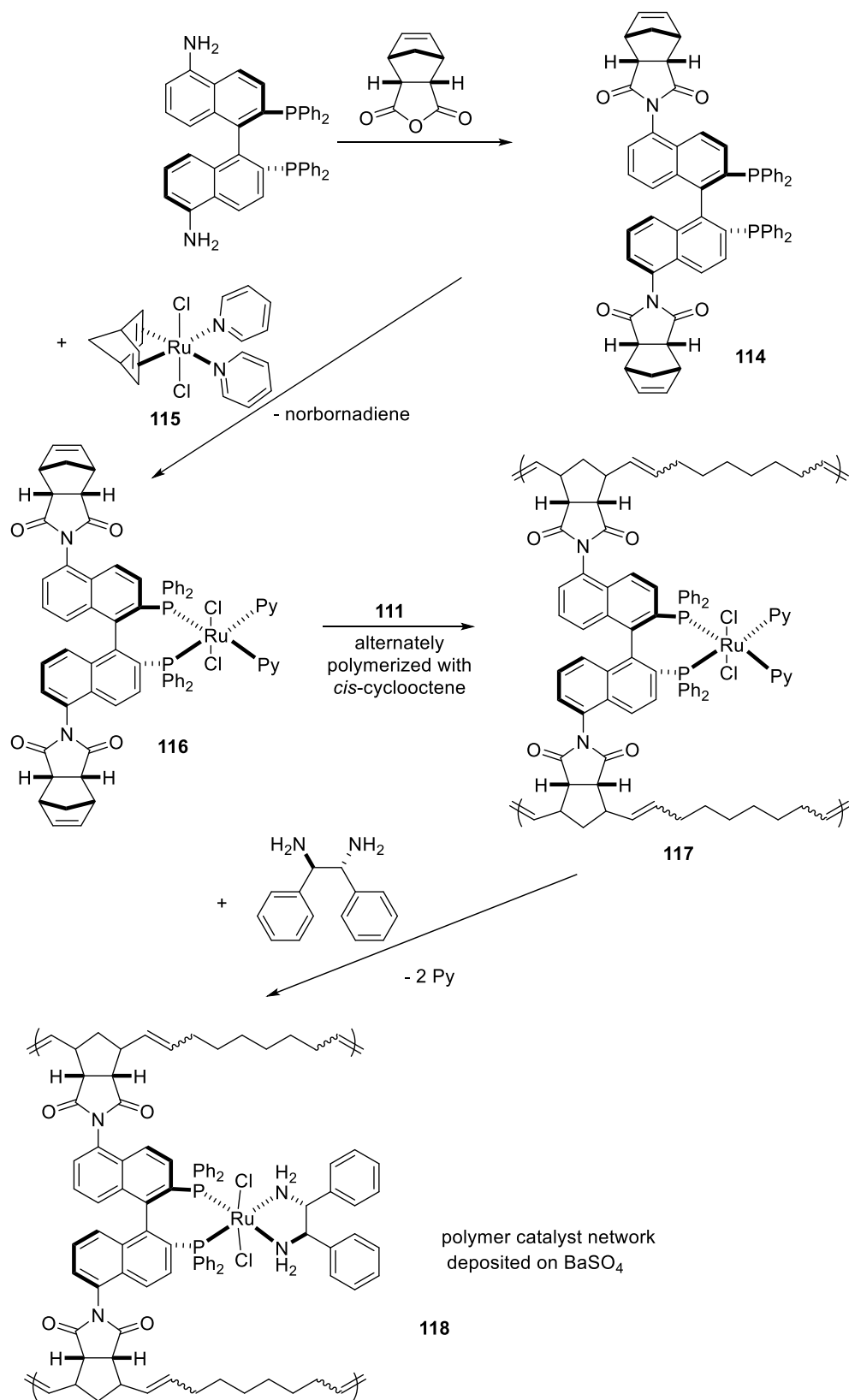
Scheme 1-61. Immobilized RuCl₂(BINAP)(DPEN) reported by the Bergens group.[147]

Although it took a few days to initiate **118** under the hydrogenation conditions (0.1 mol% Ru in **118**, 2% KO*t*Bu, 10 bar, 40 °C, 2-PrOH, 19–73 h), the polymer network became swollen slowly in 2-PrOH, and **118** exhibited a highly reliable activity (100% conv.) and selectivity (ee = 94–96%) in the following 25 consecutive runs. The initial TOF of these 25 runs was comparable to the TOF of the homogeneous RuCl$_2$(BINAP)(DPEN) catalyst, showing that the mass transport was not hindered by the heterogeneity of **118**. Eventually, the reaction was stopped mechanically as the catalyst powder was splashed onto the top of the reactor, indicating that **118** might not reach the best reusability in the reported experiments. The ICP-MS study of the representative runs confirmed that only a negligible amount of Ru had leached into the reaction (below 0.016% in each tested run). All these results illustrated that immobilizing organometallic catalysts via ROMP followed by the deposition of the polymer on inert supports is a highly promising methodology to prepare reusable catalysts. Immobilized catalytic systems with Rh were developed also in the Bergens group with similar strategies for catalytic intramolecular cycloisomerization[148] and the isomerization of allylic alcohols[149].

1.6 Research Objectives

Inspired by the previous achievements of immobilizing catalysts via ROMP, one of the research projects presented in this dissertation was to address the immobilization of a homogeneous ester hydrogenation catalyst. The polymer catalyst was made of a well-defined, ROMP-active Ru-(PNNP) catalyst monomer with the copolymerization of a newly designed crosslinker. No further metalation or ligand substitution was needed after preparing the polymer with the presence of a BaSO$_4$ support. One point that diminishes the significance of immobilizing homogeneous catalysts is that most resultant heterogeneous catalysts eventually provide less TONs compared to a single reaction with their homogeneous analogs. We overcame this drawback of immobilized catalysts since our ester hydrogenation catalyst hit the highest TON ever reported in the literature. This project is introduced in Chapter 2.

Two other projects were derived from the project in Chapter 2. Firstly, the ROMP-active Ru-PNNP catalyst was a chiral molecule. This catalyst and its derivatives were resolved successfully and tested for the asymmetrical hydrogenation/transfer hydrogenation of ketones,

as well as the asymmetrical hydrogenation of α-chiral esters, via dynamic kinetic resolution (DKR). Secondly, since the hydrogenation of esters generally requires a large amount of base to facilitate the reaction, we introduced a grafting strong base moiety into the polymer chain of our polymeric ester hydrogenation catalyst. We expected that this neighboring base would work as an intramolecular promoter to accelerate the hydrogenation reaction greatly without the addition of a large excess of base. The background information and the results of these two exploratory projects are summarized in Chapter 3.

I also worked on electrochemical catalysis with a project on Pt–Ni nanostructured catalysts for the electrochemical oxygen reduction of fuel cells. The core of the catalyst was made via the glancing angle deposition (GLAD) of Ni, and the shell was prepared through the counter electrode deposition of Pt. This part of the work is discussed in Chapter 4 independently, with a brief introduction on the cathode catalysts of fuel cells as well as the GLAD technology.

Chapter 2

A Reusable Polymer-based Ru Catalyst for the Hydrogenation of Esters

2.1 Introduction

As discussed in Chapter 1, catalytic hydrogenation is an atom-economic alternative to the stoichiometric reduction of esters using main-group hydride reagents.[92, 93] The first ester hydrogenation catalysts were heterogeneous copper chromite species[31, 32, 150] that required harsh conditions (250–300 °C, 130–202 bar H_2) and high catalyst loadings (~10 wt%).[34] Current heterogeneous[20] ester hydrogenation catalyst systems are more active, and include Ru-ZrO_2,[151] Ru-Sn,[42, 43] Ru-Ge,[46] and Ag-Au[47] bimetallic systems (typical conditions: 30–50 bar H_2, 140–300 °C).[47] The first homogenous catalysts were ruthenate complexes **1** and **2** that hydrogenated activated esters under moderately forcing conditions (10–100% conv., 0.6 mol% Ru, 90 °C, 6.2 bar, toluene, 4–20 h).[49] The Milstein group reported a breakthrough in 2006 with the ruthenium PNN pincer compound **21** that hydrogenated a number of esters with turnover numbers (TONs) ranging from 82–100 (5.3 bar H_2, 1 mol% **21**, 4–12 h, 115 °C).[61] Saudan et al reported shortly thereafter that ruthenium-based bifunctional catalysts **25** and **26** hydrogenate a variety of esters with TONs as high as 9900 under practical conditions in the presence of base (0.01–0.05 mol% **25** or **26**, 5 mol% NaOMe, 100 °C, 50 bar H_2, THF, 1–4 h).[62] Many ester hydrogenation catalysts have been developed since these discovery reports. The more active catalysts in the literature contain Ru[28, 30, 34, 65, 72, 74, 76, 81, 94] or Os[79] metal centers, the most active hydrogenate esters with TONs ranging between 49,000 and 91,000 (typical conditions: 0.001–0.002 mol% catalyst, 2–10 mol% alkoxide base, 25–80 °C, 50–101 bar).[66, 80, 87, 89]

Milstein and co-workers reported the first iron-based catalyst **71** for ester hydrogenations in 2014.[95] This catalyst hydrogenated 2,2,2-trifluoroethyl trifluoroacetate with TONs up to 1280 (0.05 mol% **71**, 1 mol% KOtBu, 40 °C, 10 bar H_2, 1,4-dioxane, 90 h). Several groups have since then developed with earth-abundant metal centres including Co,[102, 103, 105] Fe,[95-98] and Mn.[106-109] These systems are highly promising, with TONs ranging from the tens to a few hundreds (30–50 bar H_2, 70–120 °C). Jones et al recently reported 3890 turnovers for the hydrogenation of the lactone γ-valerolactone with a cobalt catalyst **77** (0.01 mol% **77**, 55 bar, 120 °C, 72 h, neat).[104]

Another strategy to lower the cost and toxicity of homogeneous catalysts is to immobilize them by covalent bonding to polymers and dedrimers.[112, 152-176] There are a number reports describing polymerized Ru catalysts for the hydrogenations and transfer hydrogenations of ketones.[130, 136, 177] For example,[136] a mesoporous, polystyrene-based, self-supported catalyst **104** that catalyzed the transfer hydrogenation of acetophenone over 14 runs (total ~1300 TON) without significant loss in activity or enantioselectivity (ee = 93~94%, 1 mol% Ru in **104**, 500% HCOONa, 40 °C, H_2O, 1.5 h/run). Our group previously reported a highly reusable Ru-BINAP catalyst-polymer framework **118** that was crosslinked with the Ru-BINAP monomer.[147] The solid catalyst operated continuously over 25 runs (1000 TON/run) for the enantioselective hydrogenation of 1-acetonaphthone (0.1 mol% Ru in **118**, 2 mol% KOtBu, 40 °C, 10 bar H_2 pressure, 2-PrOH, 21 h) without loss in activity (100% yield) or enantioselectivity (95% ee). The leaching of this catalyst in any representative run analyzed by ICP-MS was <0.016% of the total Ru loading. The reaction stopped after 34 runs because the solid catalyst accumulated on the roof of the bomb. Several alt-ROMP Rh[148, 149] and Ru[146] polymeric systems have been reported by our group.

To the best of our knowledge, there is only one report on polymer-based catalysts for the hydrogenation of esters. Kamer and coworkers[178] immobilized tridentate PNN ligands on Merrifield resin (crosslinked polystyrene bearing -CH_2Cl group) and then metallated them with Ru (Scheme 2-1), which was moderately active in the hydrogenation of esters. The first three runs leveled around a TON of 75 when reused in the hydrogenation of methyl benzoate (0.9 mol% Ru, 10 mol% KOtBu, 40 °C, 50 bar, THF, 2 h), and the fourth run dropped to a TON of 50, resulting in a total TON of 285.
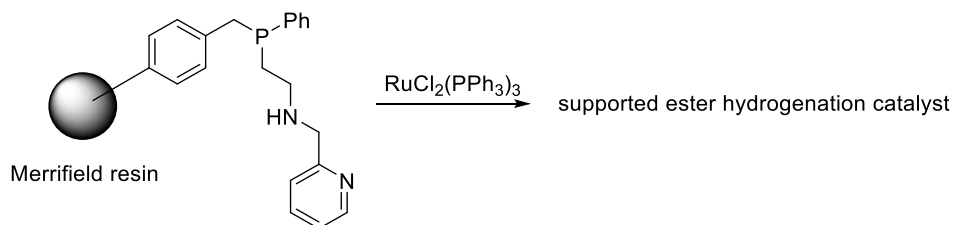
Scheme 2-1. Ru-PNN catalyst immobilized on Merrifield resin for ester hydrogenation reported by Kamer et al.[178]

Ruthenium complexes with tetradentate PNNP ligands are active catalysts for a variety of enantioselective reactions, including hydrogenations and transfer hydrogenations of ketones,[179] epoxidations of olefins,[180] Diels–Alder reactions,[181] and cyclopropanations.[182] Saudan et al reported that the **26** is active for ester hydrogenations (0.05 mol% **26**, 5 mol% NaOMe, 100 °C, 50 bar H_2, THF, 1 h, TON = 1980).[62] Although **26** does not contain N-H groups, it is quite reasonable to expect that the imine groups are reduced to the corresponding amines during the initial stages of the hydrogenation.[62, 183] We now report a facile synthesis of a ROMP-active Ru-PNNP analogue of **26**, its polymerization by alt-ROMP, and its performance as a reusable catalyst for ester hydrogenations

2.2 Results and Discussion

2.2.1 The Synthesis of the Supported Catalyst

As shown in Scheme 2-2, we prepared a ROMP-active analog of **26** by condensing the known diamine, *trans*-5-norbornene-endo-2,3-diamine (**119**)[184], with 2 equiv. 2-diphenylphosphinobenzaldehyde to give the norbornene-containing PNNP tetradentate ligand *N,N'*-bis({(2-diphenylphosphino)phenyl}methylidene)bicyclo[2.2.1]hept-5-ene-2,3-diamine (**120**). Reaction between **120** and *trans*-RuCl$_2$(NBD)Py$_2$ (**115**)[185] gave the *trans*-dichloride **121** in 53% yield after purification. Figure 2-1 shows the solid-state structure of **121** as determined by X-ray diffraction. The solid-state structure confirms the *trans*-configuration of the chlorides, as is similar to the reported structures for these types of compounds. [62, 179, 183]
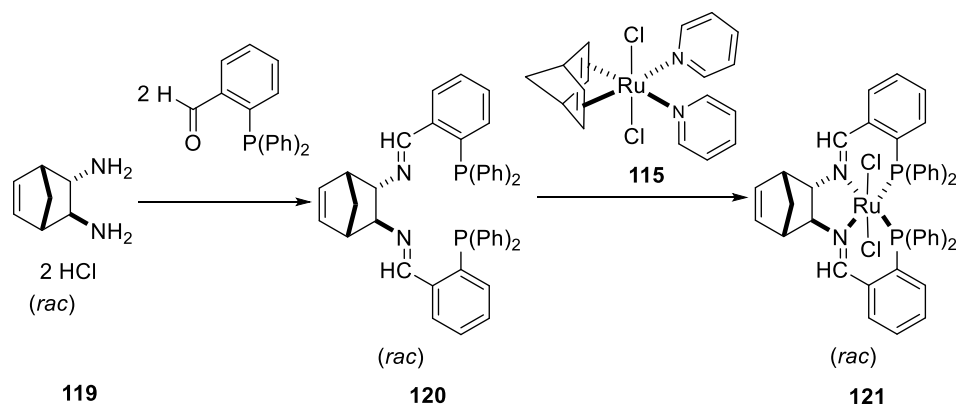
Scheme 2-2. Syntheses of **120** and **121**.
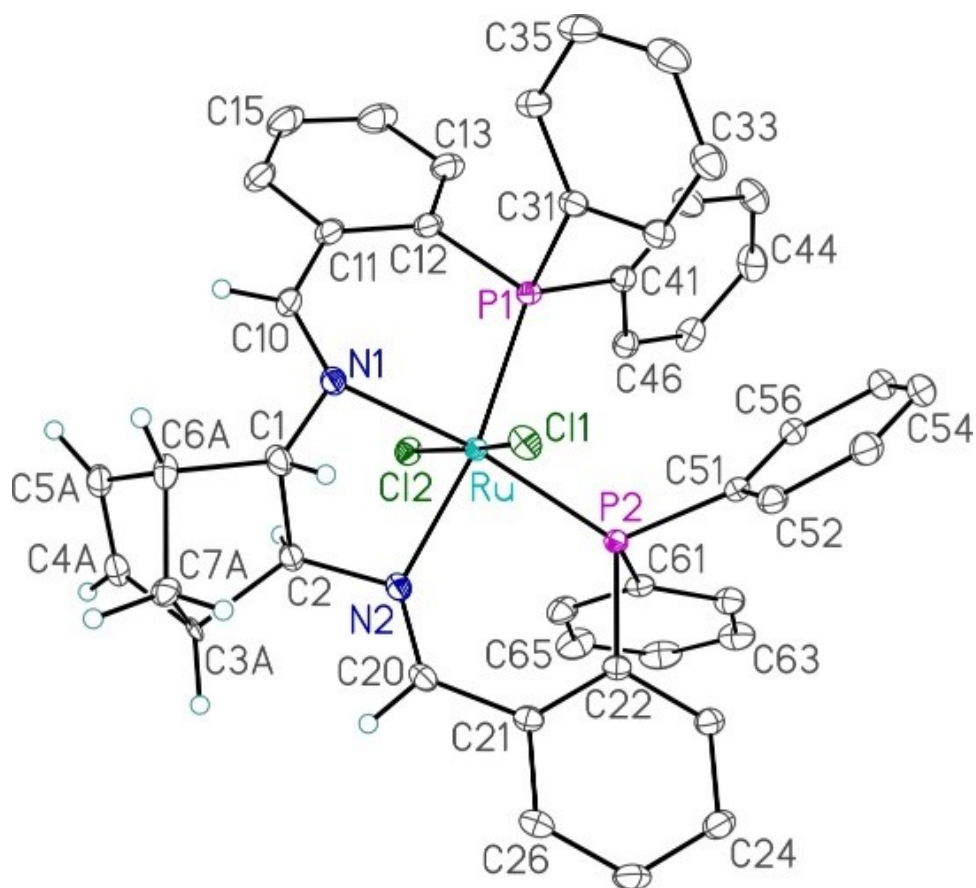
Figure 2-1. Perspective view of **121**. Non-hydrogen atoms are represented by Gaussian ellipsoids at the 30% probability level. Hydrogen atoms are shown with arbitrarily small thermal parameters, except for aromatic-group hydrogens, which are not shown.

We found that ROMP polymerization of **121** with $RuCl_2(=CHPh)(PCy_3)_2$ (**111**) as catalyst was very slow (5 mol% **111**, 40 °C, CH_2Cl_2), presumably because there was too much crowding between adjacent monomers in the polymer. Instead, we employed alt-ROMP to

polymerize **121**.[146, 147] Briefly, alt-ROMP occurs between a crowded, strained monomer and an uncrowded, unstrained monomer. The more reactive, strained monomer reacts with the metathesis catalyst, but does not polymerize because the resulting ruthenium-alkylidene is too crowded. Instead, the akylidene reacts with the less crowded monomer, typically *cis*-cyclooctene (COE) to generate a new, uncrowded alkylidene. This uncrowded alkylidene then reacts with the crowded, strained monomer, and so on.[146, 147] We found that 4 equiv. of COE smoothly underwent alt-ROMP with **121** employing 1 mol% of **111** as catalyst (40 °C, 20 h, CD$_2$Cl$_2$). Figure 2-2 shows the structures and NMR spectra of **121** and the resulting linear polymer **122**. The signals for the bridging methylene and olefin groups in **121**, as well as those for the olefin group in COE were absent in the ^{1}H NMR spectrum of the polymer. The ^{31}P NMR spectrum of the polymer contained major and minor broadened peaks, shifted ~2 ppm from those of **121**. We believe the slight shift resulted from ring opening during alt-ROMP, and the major and minor species arise from the *trans-* and *cis-* olefin geometries in the polymer.
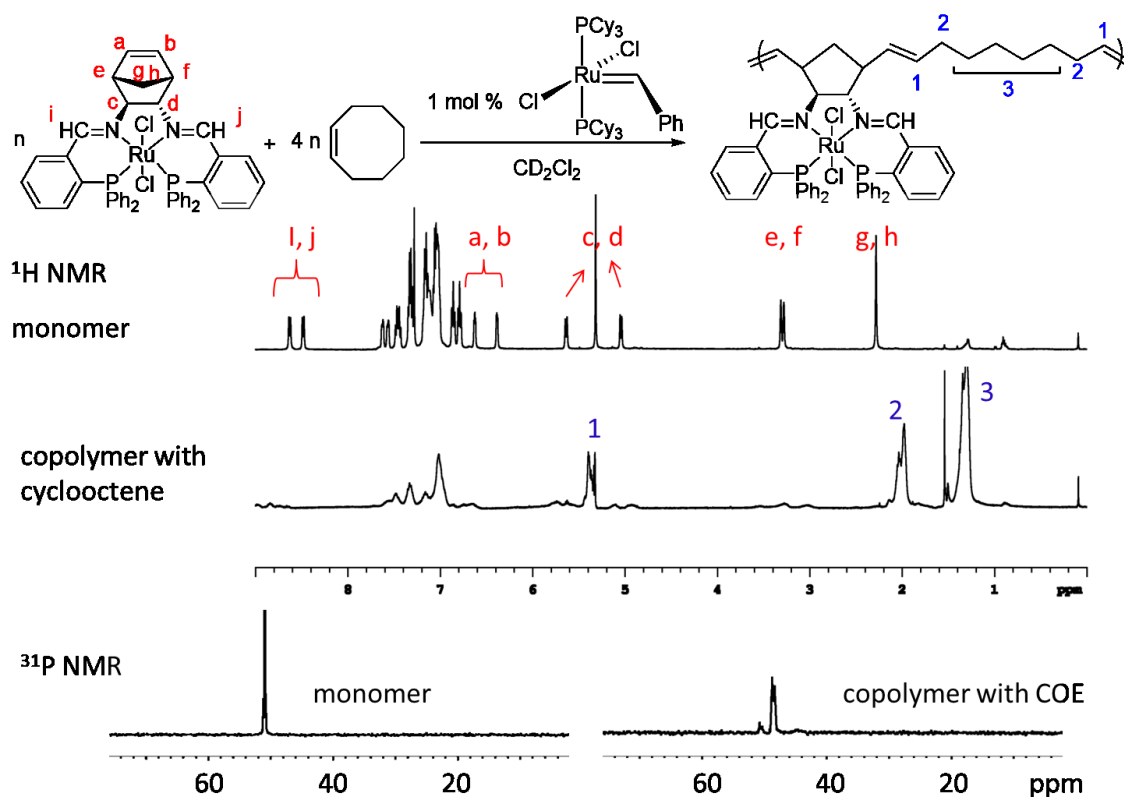
Figure 2-2. Alt-ROMP polymerization of **121** and COE; the NMR spectra of **121** and the linear polymer **122**.

Attempts to immobilize the polymeric catalyst (**122**) by depositing it as film on BaSO$_4$, as we did previously with the highly crosslinked 5,5'-bis(norimido)BINAP-Ru polymer framework,[147] were met with mixed results. Specifically, we evaluated **122**/BaSO$_4$ with the hydrogenation of methyl benzoate in THF (0.1 mol% Ru in **122**, 10 mol% KOtBu, 40 °C, 50 bar, THF, 4 h, Eq. 2-1).

$$\text{PhCO}_2\text{Me} \xrightarrow[\text{40 °C, 50 bar H}_2\text{, 4 h, THF}]{\substack{\text{0.1 mol\% [Ru] of \textbf{122} on BaSO}_4 \\ \text{10 mol\% KO}t\text{Bu}}} \text{PhCH}_2\text{OH} + \text{PhCO}_2\text{CH}_2\text{Ph} + \text{CH}_3\text{OH} \qquad \textbf{(2-1)}$$
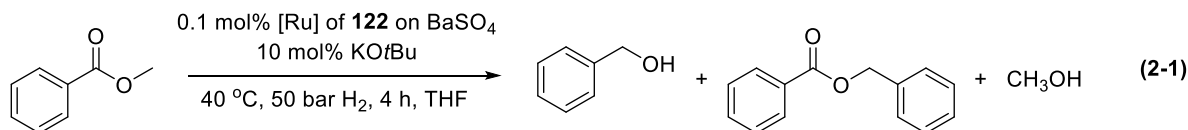
THF is often the solvent in which homogeneous ester hydrogenations operate with the highest rates and yields.[66, 80, 89] Although the first run reached 95% conversion (950 TON), the filtrate was deeply coloured, and the conversion of the 2nd run was significantly lower (65%). Not surprisingly, the solubility of the linear polymer **122** limited its isolation and reuse by filtration.

We expect that it is difficult to prevent polymers from dissolving under continuous stirring at 80°C in THF at 21 h per run. We therefore prepared the crosslinking agent **123** in one step by condensation of two equiv. of *cis*-5-norbornene-endo-2,3-dicarboxylic anhydride (Scheme 2-2) with ethylenediamine in acetic acid. The ROMP polymerization of **123** catalyzed by **111** was sluggish in CH$_2$Cl$_2$ at 40 °C. Presumably, the crowding around the olefin in the endo-norbornimide groups hindered the polymerization. The crosslinker **123** did, however, undergo alt-ROMP with **121** and COE. The optimized ratio of **121**:**123**:COE:**111** was 1:2:8:0.02. A 2:1 ratio of **121**:**123** was employed to form a highly crosslinked polymer to minimize dissolution in hot THF. This mixture underwent complete polymerization after 48 h in CD$_2$Cl$_2$ at 40 °C. NMR spectra recorded while the alt-ROMP was underway showed that the olefin groups in **121** and **123** polymerized at comparable rates. Specifically, 21% of **121**, 9% of the norimido groups in **123**, and 5% of COE had polymerized after 1.5 h. The corresponding conversions were 89%, 61% and 21% after 20 h. Both **121** and **123** were almost fully consumed after 48 h, with ~20% COE remaining in solution. The comparable rates for polymerization of **121** and **123** indicates that the resulting polymer more resembles an alternating copolymer rather than alternating blocks of **121** or **123**. Further, it is highly improbable that the crosslinked product is a linear, ladder polymer. It is more likely a three-dimensional framework crosslinked by **123**, and spaced by COE + **121**. The ^{1}H NMR spectrum of the framework contained highly broadened peaks, and did not contain signals from the

olefin- or bridging methylene groups arising from unreacted monomers. The peaks for **121** in the ^{31}P NMR spectrum of the polymer (Figure 2-3) were broadened and shifted up field by ~2.1 ppm from those of the unreacted monomer. After ~40 h reaction, the entire reaction mixture had converted into a uniform, static gel that could not be dissolved in CD_2Cl_2. This gel shrank to a compact, brittle piece of insoluble plastic upon evaporation of the solvent.

In previous reports,[146, 147] we utilized an inert, high surface area material such as $BaSO_4$, to support the polymerized catalysts. The functions of the support were to improve mass transport, to engender mechanical stability for long-term batch reactions with stirring, and to act as a filtration aid. The crosslinked polymer gel **121**/**123**/COE could not be diluted or dissolved after it formed, and so could not be deposited onto the $BaSO_4$ by simple solvent evaporation. Instead, we carried out the alt-ROMP of **121**, **123**, COE, and **111** directly in the presence of $BaSO_4$. Specifically, a solution of **121**, **123**, COE, and **111** was mixed with solid $BaSO_4$, with the reaction solution just covering the $BaSO_4$. The polymerization was allowed to proceed for 66 h heating at 40 °C. The resulting catalyst-polymer framework on $BaSO_4$ (**124**, Scheme 2-3) was ground with a mortar and pestle, washed with CH_2Cl_2, and dried under vacuum. An NMR study confirmed that ~7% of the Ru leached into the wash, presumably as lower molecular weight oligomers.
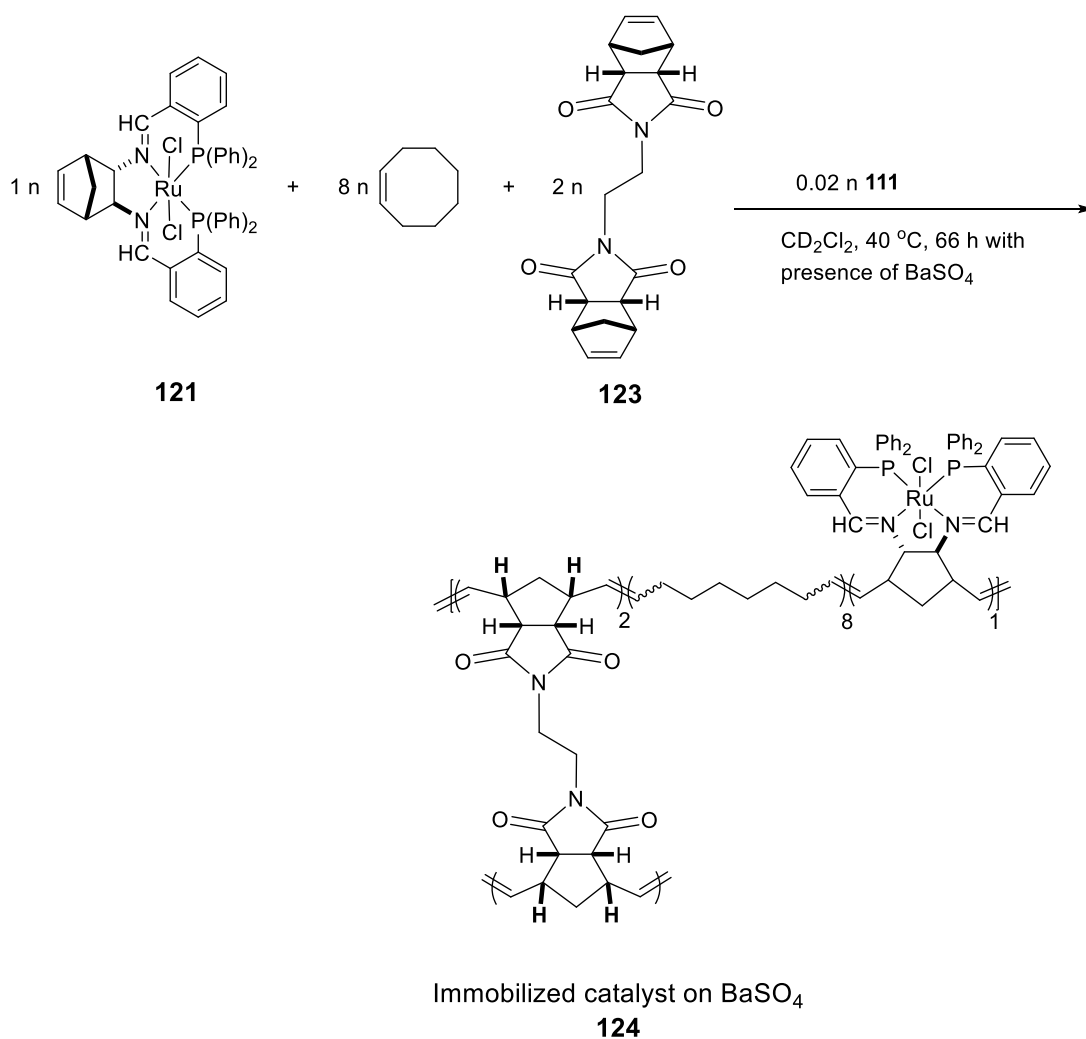
Scheme 2-3. The preparation of the crosslinked polymeric catalyst **124** dispersed on BaSO₄.
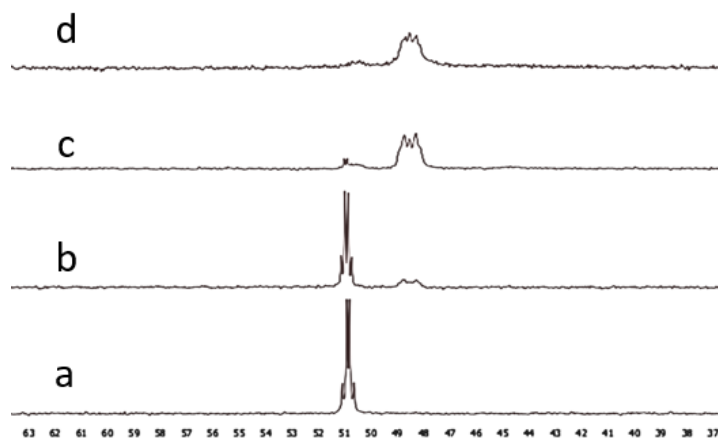
Figure 2-3. ³¹P NMR spectra recorded during polymerization of **121**, **123** and COE with 2 mol% **111** (40°C in CD₂Cl₂). Spectrum of (a) initial; (b) 1.5 h; (c) 20 h; (d) 48 h.

2.2.2 The Reusing Hydrogenation with the Supported Catalyst

We hydrogenated methyl benzoate with loadings of 40000 equiv. per run to evaluate **124** (0.0025 mol% Ru in **124**, 10 mol% KOtBu, 80 °C, 50 bar, THF, 21 h, Eq. 2-2). These conditions are in line with those utilized for high TON ester hydrogenations in the literature.[23-26] The product mixtures contained methyl benzoate, benzyl alcohol, and the transesterification product benzyl benzoate. The TON of the first run was 32960, corresponding to 82% conversion. The isolated yield after filtration was 30340 TON using an internal standard. Based upon the pressure drop, the hydrogenation was very rapid in the beginning, completing ~15000 turnovers (TO) during the first 1 h, ~20000 after 3 h, and ~33 000 after 21 h. Similar initial burst activity were reported for homogeneous ester hydrogenations.[86, 89, 109, 152] We found that a control homogeneous hydrogenation of methyl benzoate with the monomeric catalyst **121** (methyl benzoate : KO^{t}Bu : **121** = 25000 : 2500 : 1, 90 °C, 50 bar) proceeded with a similar burst followed by a slowdown (~14000 TO after 1h, ~16000 after 2h, ~17000 after 3h). Although the structure of **121** is modified by the ring opening polymerization, the similarity in turnover frequencies between **121** and the polymer indicates that mass transport does not significantly limit the rate of the polymerized catalyst. Presumably, the combination of the open framework structure of the polymer, the BaSO$_4$ support, and the 80–90 °C THF solvent minimized mass transport effects. We suggest this strategy be incorporated into future polymeric catalyst designs.
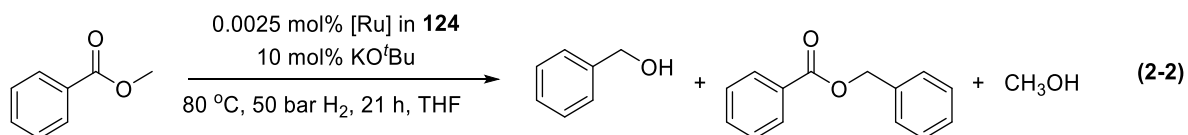
Adding more hydrogen and substrate after the homogeneous hydrogenation had no effect on the rate after the reaction had slowed. Thus, the slowdown is either due to product inhibition, a decrease in basicity of the medium as the hydrogenation proceeds, or catalyst decomposition. In contrast, the polymeric catalyst was easily reused after filtration, and the 2nd run proceeded with 29720 TO, and a similar initial burst in activity. Although some loss in activity occurred between the first and second runs, catalyst decomposition cannot explain the decrease in rate after the burst during the homogenous and heterogeneous hydrogenations.

In our prior mechanistic studies,[86, 186] we directly observed that alcohols inhibit ketone and ester hydrogenations by forming Ru-alkoxides, especially in the absence of base. We

expect that this inhibition is stronger for ester hydrogenations for two reasons. The first is that esters are intrinsically less reactive than ketones. The second is that the hydrogenation of a ketone forms one equiv. of a secondary alcohol, whereas the hydrogenation of a methyl ester forms 2 equiv. of primary alcohols. Primary Ru-alkoxides are more stable than secondary alkoxides because of steric crowding.[187] We therefore expect that the build up two equiv. of primary alcohols partially explains the decrease in rate over the course of these ester hydrogenations.

In other research, we reported two direct observations that may explain how the excess base increases the rates of these ester hydrogenations. The first is that base removes alkoxide ligands from these types of Ru compounds by an elimination reaction involving deprotonation of an N-H group.[86, 186, 187] We therefore expect that one role of the excess base in these ester hydrogenations is to minimize the inhibition by the 2 equiv. of primary alcohol products through this elimination reaction. In another study, we showed that the reducing power of these catalysts is dramatically increased by deprotonation of an N-H group. For example, we observed that the deprotonated version of Noyori's prototypal dihydride catalyst, $(BINAP)Ru(H)_2(NH^{(-)}CH(Ph)CH(Ph)NH_2)$, reduces imines on mixing at -80 °C in THF.[91] We propose that the combination of these two processes partially explain the need for excess base during active ester hydrogenations. As well, the basicity of these ester hydrogenations decreases as the medium changes from pure aprotic (THF + ester) to a protic medium as the two equiv. of alcohol products form. This decrease in basicity would limit the alkoxide elimination, and the catalyst activation the deprotonation of the N-H groups. We propose that the combination of primary alcohol product inhibition, and the decrease in reaction medium's basicity all contribute to the drop in rate after the initial burst in these ester hydrogenations. We suggest that the design of high turnover number ester hydrogenation catalysts in the future incorporate methods to minimize these types of inhibition.

Figure 2-4 plots TON versus run. The TONs of the first two runs were similar. The catalyst remained active in the subsequent runs, but gradually slowed. Run 5 proceeded with 14760 TO, with a total over the 5 runs = 121680, the highest TON reported for the hydrogenation of an ester with a molecular catalyst.[66, 79, 87, 89]
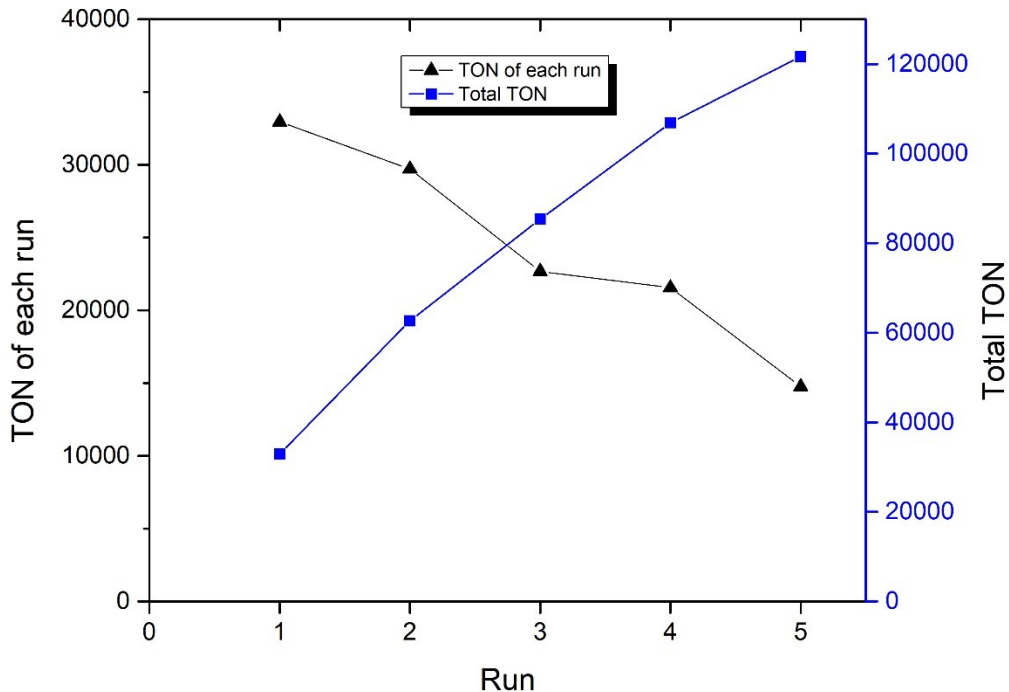
Figure 2-4. Turnovers per run, and total TON over five hydrogenations of methyl benzoate (0.0025 mol% Ru in **124**, 10 mol% KO*t*Bu, 80 °C, 50 bar, THF, 21 h).

The amounts of Ru leached during Runs 1 to 4 were 5.6%, 3.8%, 1.4%, 1.1% of the total catalyst loading, as determined by ICP-MS. These results show that although leaching was reduced by the crosslinked polymer, it was not eliminated. These results demonstrated the heterogeneity of the catalyst. Specifically, if the activity resulted from dissolved Ru complexes leached into solution, Run 4 occurred with an impossibly high ~2 million TON. The Ru leaching can be attributed to either/both dissolution of lower molecular weight oligomers over 21 h stirring in 80 °C THF per run, and/or some sort of active site decomposition. Further studies are required to study the mechanism of decomposition. Regardless, the total loss in Ru leaching was only 11.9%, much less than the 55% drop in activity between Run 1 and Run 5. We speculate that the gradual drop in activity over the 5 runs was due mainly to some sort of decomposition of the catalyst that did not release Ru out of the polymer framework. This long-term decomposition was either innate to the catalyst under these conditions, or it was caused by trace amounts of systematic impurities.

2.3 Conclusions

In summary, the majority of the reported immobilized molecular catalysts eventually resulted in less total TON compared to the homogeneous analogs in a single reaction. This fact minimizes the significance of heterogenizing those catalysts for real industrial production. We devised a convenient synthesis of a defined, dispersed Ru-PNNP crosslinked catalyst polymer framework utilizing alt-ROMP. The highest reported total TON for the hydrogenation of an ester was obtained by reusing the catalyst. The catalyst had similar activity to a homogeneous analog, indicating mass transport did not limit the activity. The study of this system provided insights into the mechanism of catalyst deactivation, how to minimize mass transport limitations, and guidelines for future catalyst design.

2.4 Experimental Details

2.4.1 General Information

Unless stated otherwise, all the synthetic experiments were carried out under an inert atmosphere (N_2 or Ar), using Schlenk techniques and a glovebox. High pressure hydrogenations were carried out in a high-pressure Parr 4750 reactor with an extra coned pressure fitting for adding and filtering reaction mixtures.

The gases N_2 (4.8), Ar (4.8), H_2 (5.0) were supplied by Praxair. Deuterated solvents were purchased from Sigma Aldrich and Cambridge Isotope Laboratories. All common solvents were used as received or distilled over proper drying agents under N_2 when it was necessary: CH_2Cl_2, $CHCl_3$ and hexanes were distilled over CaH_2; methanol was distilled over Mg/I_2; EtOH was dried over 3Å molecular sieves and distilled over CaO; THF was purified by distillation over Na/benzophenone. Triethylamine, pyridine, ethylenediamine, and piperidine were distilled over CaH_2. Norbornadiene and *cis*-cyclooctene were purified by simple fraction distillation. Methyl benzoate was obtained from Sigma Aldrich and fractionally distilled over CaH_2 prior to hydrogenation.

The following chemicals were obtained from suppliers and used without further purification: *trans*-3,6-endomethylene-1,2,3,6-tetrahydrophthaloyl chloride, *cis*-5-norbornene-endo-2,3-dicarboxylic anhydride, and 2-diphenylphosphinobenzaldehyde were

obtained from Sigma Aldrich; NaN_3 was obtained from Fisher Scientific Company; $NaBH_4$ were obtained from BDH Chemicals. 1st generation Grubbs catalyst was obtained from Strem Chemicals. $BaSO_4$ (white reflectance standard) was obtained from Eastman Chemical Co., Inc., washed with distilled CH_2Cl_2, dried under vacuum, and stored under nitrogen before use.

^1H, $^{13}C\{^1H\}$, and $^{31}P\{^1H\}$ NMR spectra were recorded with either a Varian Inova 500 MHz spectrometer, an Agilent/Varian 400 MHz spectrometer, or an Agilent VNMRS 700 MHz spectrometer. ^1H and ^{13}C Chemical shifts were recorded relative to TMS using the signals from the residual protons in the deuterated solvent as the internal standard. ^{31}P chemical shifts were reported relative to an H_3PO_4 external standard. Elemental analysis was carried out with a Flash 2000 Organic Elemental Analyzer made by Thermo Fisher. ICP-MS was carried out with a Perkin Elmer's Elan 6000 ICP-MS.

2.4.2 Catalyst Synthesis

trans-2,3-diaminonorborn-5-ene dihydrochloride (racemate) (119).

(2-3)
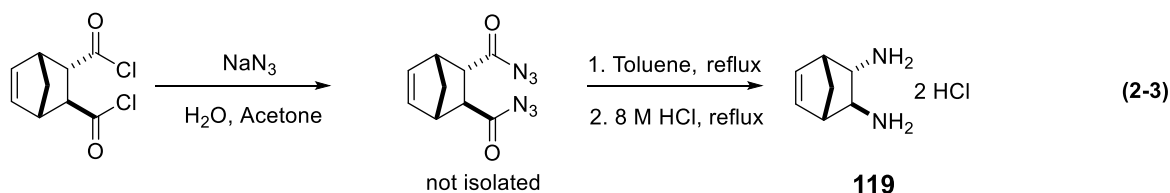
The whole experiment was carried out in apparatus open to air, following a modified literature procedure.[180] Solvents were used as received. The explosive diazide intermediate was not isolated (Eq. 2-2).

To an Erlenmeyer flask containing *trans*-3,6-endomethylene-1,2,3,6-tetrahydrophthaloyl chloride (3.085 g, 14.1 mmol), 7.5 mL acetone was added, followed by a solution of NaN_3 (2.747 g, 42.2 mmol) in deionized water (7.5 mL). The mixture was stirred for 1 h at rt. The aqueous solution was extracted with toluene (3 × 25 mL). The combined organic solution was washed with saturated $NaHCO_3$ (30 mL) and brine (30 mL), dried over Na_2SO_4, and filtered into a round-bottom flask. The solution was refluxed for 2 h, cooled down before adding 8 M HCl (120 mL), and reheated to reflux for 4 h. Over this period, the color of the solution slowly turned light purple. After the solution was cooled down to room temperature, the aqueous layer was separated and washed with diethyl ether (2 × 50 mL). After

removing the water under vacuum, the resultant brownish solid was washed with THF (2×20 mL), then dried under vacuum, and 1.811 g product was obtained with a yield of 65%.

^{1}H NMR (498.119 MHz, D_2O, 27 °C): δ 1.87–1.93 (2H, AB pattern, m, bridging CH_2), 3.16 (1H, m, CH), 3.21 (1H, m, CH), 3.29 (1H, m, CH), 3.88 (1H, m, CH), 6.34 (1H, m, CH, olefin), 6.53 (1H, m, CH, olefin).

$^{13}C\{^1H\}$ NMR (125.266 MHz, $CDCl_3$, 27 °C): δ 45.0 (CH_2), 45.1 (CH), 46.7 (CH), 55.6 (CH), 56.0 (CH), 134.1 (CH), 138.7 (CH).

Elemental Analysis calculated: C, 42.66; H, 7.16; N, 14.21. Found: C, 41.09; H, 6.91; N, 13.80.

_N,N'_-bis({(2-diphenylphosphino)phenyl}methylidene)bicyclo[2.2.1]hept-5-ene-2,3-diamine (racemate) (120).
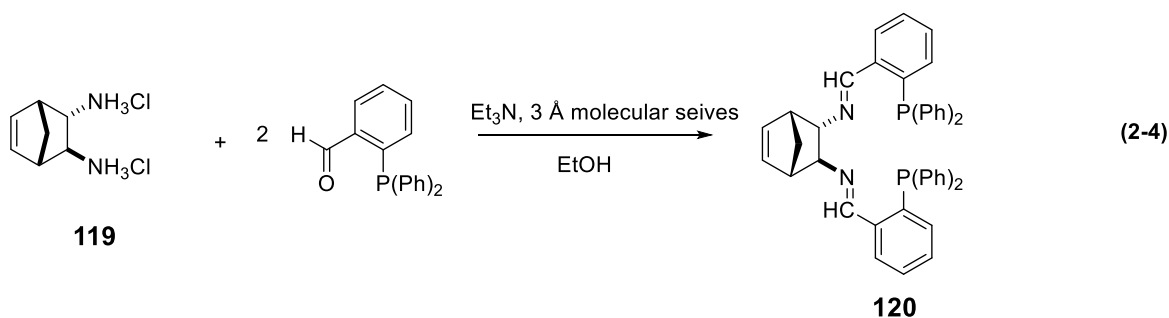
This synthesis was carried out under N_2, and all the liquid solvent/reagent were purified and degassed by purging N_2. The reaction was monitored by ^{1}H and $^{31}P\{^1H\}$ NMR and adjusted to make sure that the actual ratio of amine group with aldehyde is 1 to 1. The final weight of the diamine was ~15% "in excess" as the actual moles were lower than the calculated value, assuming the diamine was pure; this was probably because the compound was hygroscopic.

Compound **119** (248.6 mg, 1.26 mmol assuming no water uptake) was weighed into a Schlenk tube along with 3Å molecular sieves (565.6 mg, activated). The tube was degassed, then triethylamine (700 μL) and EtOH (5 mL) were added. 2-diphenylphosphinobenzaldehyde (731.6 mg, 2.52 mmol) was dissolved in EtOH (12 mL) under gentle heating and transferred to the Schlenk tube. The reaction was stirred for 16 h at rt, then an aliquot was taken for ^{1}H and $^{31}P\{^1H\}$ NMR to check the percentage of any unreacted starting materials. The aldehyde was 16% in excess, so another 39.6 mg diamine was added to the reaction. After another 24-h stirring, the reaction mixture was filtered through Celite, then pumped under vacuum to dry.

Dichloromethane (~10 mL) was added to dissolve the compound, and the resultant solution was washed with water three times, then dried over Na_2SO_4. After filtration and drying under high vacuum, 641 mg product was obtained with a yield of 76%.

^{1}H NMR (699.763 MHz, CD_2Cl_2, 27 °C): δ 1.43 (1H, m, bridging CH), 1.94 (1H, m, bridging CH), 2.38 (1H, m, CH next to olefin), 2.64 (1H, m, CH next to olefin), 2.76 (1H, m, CH next to imine), 3.35 (1H, m, CH next to imine), 6.04 (1H, dd, J=5.64 Hz, 2.82 Hz, olefin proton), 6.08 (1H, dd, J=5.64 Hz, 3.07 Hz, olefin proton), 6.82–7.79 (28H, aromatic), 8.43 (1H, d, J=3.71 Hz, imine), 8.61 (1H, d, J=4.10 Hz, imine)

^{13}C{^{1}H} NMR (175.972 MHz, CD_2Cl_2, 27 °C): δ 45.9 (CH_2), 49.4 (CH), 51.7 (CH), 78.7 (CH), 79.0 (CH), 129.4–137.5 (multiple aromatic CH), 137.7–140.1 (multiple aromatic C), 158.8–159.3 (multiple CH).

^{31}P{^{1}H} NMR (161.839 MHz, CD_2Cl_2, 27 °C): δ -11.6 (1P, s), -10.4 (1P, s)

Elemental Analysis calculated: C, 80.82; H, 5.73; N, 4.19. Found: C, 79.01; H, 5.72; N, 4.18.

Dichloro{N,N'-bis({(2-diphenylphosphino)phenyl}methylidene)bicyclo[2.2.1]-hept-5-ene-2,3-diamine}ruthenium (racemate) (121).

120 **115** **121** (2-5)
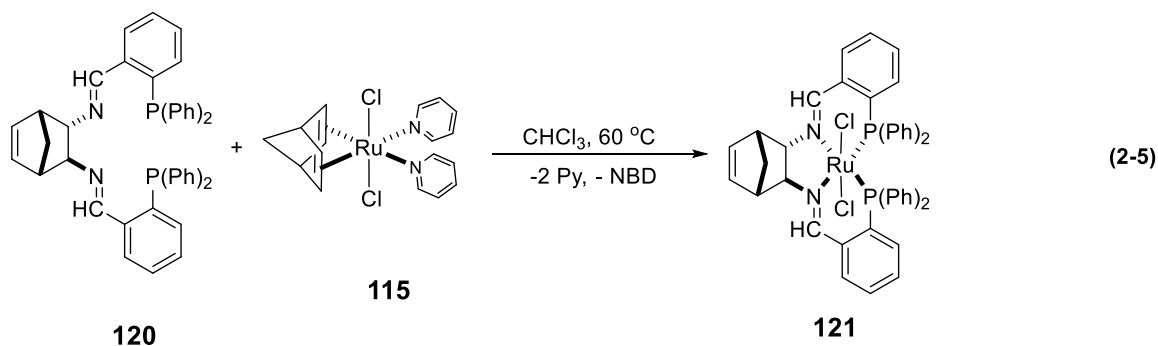
The complexation reaction (Eq. 2-5) was carried out by mixing **120** (387.0 mg, 0.58 mmol) and $RuCl_2(NBD)(Py)_2$, **115**[185] (243.1 mg, 0.58 mmol) in chloroform (15 mL, distilled) under N_2. The reaction mixture was heated at 60 °C for 4 days, after which the solution was pumped under high vacuum to dryness. The resultant dark red solid was purified by a column of neutral Al_2O_3 (30 cm^3 in bulk volume) with dichloromethane. The orange band on the column was collected and dried under vacuum, and 257 mg of red powdery compound was obtained after recrystallization using dichloromethane/hexane with a yield of 53%. Crystals for X-ray

crystallography were obtained by slowly adding hexane on the top of a solution of the product in DCM in an NMR tube and letting the tube sit for a few days.

^{1}H NMR (699.763 MHz, CD$_2$Cl$_2$, 27 °C): δ 2.28–2.31 (2H, AB pattern, m, bridging CH$_2$), 3.31 (1H, m, CH next to olefin), 3.34 (1H, m, CH next to olefin), 4.93 (1H, m, CH next to imine), 5.54 (1H, m, CH next to imine), 6.45 (1H, m, CH, olefin), 6.66 (1H, m, CH, olefin), 6.68–7.69 (28H, aromatic), 8.52 (1H, d, CH, J= 9.22 Hz, imine), 8.66 (1H, d, J= 9.34 Hz, CH, imine).

^{13}C{^{1}H} NMR (175.972 MHz, CD$_2$Cl$_2$, 27 °C): δ 38.2 (CH), 42.7 (CH), 48.9 (CH$_2$), 78.5 (CH), 79.2 (CH), 127.3–127.7 (multiple aromatic peaks), 129.0–130.1 (multiple aromatic peaks), 131.1–132.1 (multiple aromatic peaks), 134.0–134.1 (multiple aromatic peaks), 135.3–137.0 (multiple aromatic peaks), 141.1 (CH), 158.3 (CH), 158.9 (CH).

^{31}P{^{1}H} NMR (161.839 MHz, CD$_2$Cl$_2$, 27 °C): AB pattern, δ 51.6 (1P, d, J_{pp}= 27.5 Hz), 51.3 (1P, d, J_{pp}= 27.5 Hz).

Elemental Analysis calculated: C, 64.29; H, 4.56; N, 3.33. Found: C, 64.17; H, 4.77; N, 3.31.

1,2-N-di(cis-5-norbornene-2,3-endo-dicarboximido)-ethane (123).

123
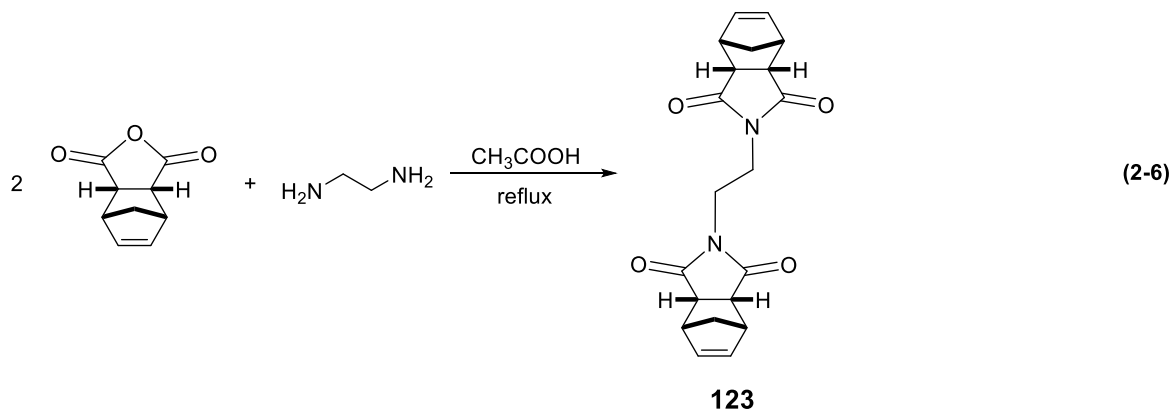
As shown in Eq. 2-6, *cis*-5-Norbornene-endo-2,3-dicarboxylic anhydride (2171.8 mg, 13.2 mmol), ethylenediamine (396.9 mg, 6.6 mmol), and acetic acid (32 mL, distilled) were refluxed at 125 °C for 4 h under N$_2$. The solution was poured into 250 mL water, and the product was extracted into DCM (2 × 150 mL). The combined DCM solution was washed with saturated NaHCO$_3$ (3 × 200 mL) and water (200 mL), dried over Na$_2$SO$_4$, and 2.54 g crude product was recovered after filtration and rotary evaporation. The crude product was

recrystallized in boiling EtOAc (290 mL), and 1.52 g crystalline product was obtained with a yield of 65%.

^{1}H NMR (498.118 MHz, CDCl$_3$, 27 °C): δ 1.52 (2H, m, bridging CH), 1.71 (2H, m, bridging CH), 3.23 (4H, m, α CH to carbonyl), 3.34 (4H, m, CH next to olefin), 3.47 (4H, s, CH$_2$), 6.06 (4H, m, olefin CH).

^{13}C{^{1}H} NMR (125.266 MHz, CDCl$_3$, 27 °C): δ 36.4 (CH$_2$), 44.7 (CH), 45.9 (CH), 52.3 (CH$_2$), 134.4 (CH), 177.6 (C=O).

Elemental Analysis calculated: C, 68.17; H, 5.72; N, 7.95. Found: C, 68.16; H, 5.79; N, 7.93.

Alt-ROMP polymerization of 121 and COE to 122, NMR study.

Catalyst monomer **121** (10.0 mg, 0.012 mmol, 1 equiv.), COE (6.0 μL, 0.046 mmol, 4 equiv.) and **111** (0.1 mg, 0.0001 mmol, 0.01 equiv.) were mixed in CD$_2$Cl$_2$ (0.8 mL) in an NMR tube. The NMR was taken after 20 h of heating at 40 °C.

Supported alt-ROMP polymer 122

Compound **121** (21.3 mg, 0.025 mmol, 1 equiv.), COE (13.2 μL, 0.100 mmol, 4 equiv.) and **111** (0.2 mg, 0.00024 mmol, in standard solution) were mixed in 0.8 mL CD$_2$Cl$_2$. The polymerization was completed after 48 h at 40 °C. The resulting polymer was diluted to 2 mL with DCM, then transferred to a slurry of BaSO$_4$ (3.76 g) in DCM (20 mL). The slurry was stirred for 30 min, then slowly pumped under high vacuum to remove the solvent, resulting a pink powder. The powder was washed with MeOH three times, then dried under high vacuum. The MeOH wash was collected and analyzed using ^{1}H NMR with 1,3,5- trimethoxybenzene as internal standard, indicating 53% of COE and 14% of Ru moiety dissolved in the MeOH. We suspect that these are lower molecular weight oligomers. The resulting supported catalyst had a loading of 0.0058 mmol Ru / g BaSO$_4$.

Hydrogenation with supported linear polymer catalyst (2 runs).

The hydrogenation was carried out in a customized high-pressure reactor. For the first run, 1.88 g methyl benzoate (1.35 mL, 1000 equiv.) was added to the reactor through a cannula, followed by supported catalyst (0.0107 mol Ru in **122**, 1 equiv., slurry in THF) and KO*t*Bu (120 mg, 100 equiv., THF solution) through a cannula, with 12 mL THF in total. The reactor

was sealed and pressurized. After 4 h at 50 bar H_2 under 40 °C, the reaction was stopped and filtered through a cannula filter under H_2. The next run was set up by adding methyl benzoate (1.35 mL, 1000 equiv.) and KOtBu (120 mg, 100 equiv.) in THF (12 mL) and the hydrogenation was carried out under the same conditions.

The filtrate from each run was pumped to dryness with a rotovap. Water (15 mL) was added to the mixture, then the mixture was extracted with diethyl ether twice. The ether layer was dried over Na_2SO_4 and the ether was removed with a rotovap. The conversions were determined by the ratio between each compound in the ^1H NMR spectra.

Polymerization study in an NMR tube.

Compound **121** (11.0 mg, 0.013 mmol, 1 equiv.), compound **123** (8.8 mg, 0.025 mmol, 2 equiv.), and 1st Generation Grubbs catalyst solution (0.22 mg **111**, 0.00026 mmol, 0.02 equiv., quantified with a standard solution in CD_2Cl_2) were placed in three separate NMR tubes under N_2. They were transferred into the same NMR tube after dissolving the solids in CD_2Cl_2; the total volume after mixing was 0.7 mL. *cis*-Cyclooctene (11.3 mg, 0.103 mol, 8 equiv.) was added to the NMR tube, an NMR of the reaction solution was recorded immediately. The tube was placed in a 40 °C oil bath, and NMR spectra were recorded after 1.5 h, 20 h, and 48 h. The reaction solution slowly turned into a gel in ~ 40 h, which could not flow anymore, as shown in Figure 2-5. However, the solution NMR spectra were still available with the gel.

Figure 2-5. A representative picture of an NMR tube containing the polymerized catalyst gel that does not flow with shaking.

Polymerization with the presence of BaSO₄ to make the immobilized catalyst 124.

The experiment was carried out under N_2. A polymerization solution was prepared first as describe above. It contained the following chemicals: **121** (21.2 mg, 0.025 mmol, 1 equiv.), **123** (17.7 mg, 0.049 mmol, 2 equiv.), **111** solution (0.4 mg **111**, 0.00049 mmol, 0.02 equiv., quantified with a standard solution in CD_2Cl_2), COE (22.2 mg, 0.201mol, 8 equiv.), and 1.3 mL CD_2Cl_2. An NMR spectrum was taken to confirm the ratio between each compound. 90% of this solution was transferred into a screwcap Schlenk tube with 4.0133 g BaSO₄ inside and 10% was left in the NMR tube as an indicator of the reaction process. Both the Schlenk tube and the NMR tube were placed in a 40 °C oil bath. The 10% solution in the NMR tube became a gel within 40 h. The reaction in the Schlenk tube was stopped after 66 h to make sure that the reaction had ended as it could not be monitored directly. The CD_2Cl_2 was removed under high vacuum, then the solid was ground with a mortar/pestle in the glovebox. Big chunks were broken into powder and the powder was ground as fine as possible. The resultant powder was washed with distilled DCM (3 × 20 mL), and 3.827 g supported catalyst was recovered after drying (some could not be recovered from the mortar). A picture of the powdery supported catalyst is shown in Figure 2-6. The wash was collected, and the DCM was removed under high vacuum. The residual was dissolved in $CDCl_3$ with 1,3,5-trimethoxybenzene and triphenylphosphine as internal standards. ^{31}P NMR spectra confirmed that 0.0015 mmol Ru complex leached out into the wash, corresponding to 6.6% of the total Ru initially in the Schlenk tube. The loading of the result supported catalyst was calculated as follows:

[90% × 0.025 mmol × (3.827 g / 4.013 g) – 0.0015mmol] / 3.827 g = 0.0053 mmol Ru / g BaSO₄.

Figure 2-6. BaSO$_4$ supported ester hydrogenation catalyst, **124**.

2.4.3 Catalytic Hydrogenation with Reusing the Catalyst

The whole process was carried out under Ar or H$_2$, and all the transfers were carried out using a cannula. The reaction was carried out in a high-pressure reactor with an extra pressure fitting where addition and filtration could be conducted. The reactor was assembled with a glass liner and a stir bar, then purged with Ar. The reactor was pressurized to 50 bar with H$_2$, evacuated, and purged with Ar again. Using Schlenk techniques, the supported catalyst **124** (0.2833 g, 0.0015 mmol Ru) was transferred with methyl benzoate (8.08 g, 7.48 mL, 59.4 mmol) as a slurry to the reactor under Ar, followed by KO^{t}Bu (665.4 mg, 5.9 mmol) solution in THF (16 mL). The reactor was sealed and pressurized gradually to 50 bar, and the valve on the reactor was closed to isolate it from the H$_2$ tank. The oil bath placed underneath it was set to 80 °C, and the stir rate was 600 rpm. (Note that the reactor would be re-pressurized if the pressure dropped below 40 bar as the reaction proceeded.) After 21 h, the reactor was cooled to rt, and the pressure was slowly released. The reaction mixture was filtered through a cannula filter into a pre-weighed flask under H$_2$ atmosphere, and once bubbles appeared from the cannula tip, the filtration was stopped. To set up the next run, methyl benzoate (8.08 g, 7.48 mL, 59.4 mmol) was added to the reactor immediately after the filtration, followed by KOtBu (665.4 mg, 5.9 mmol) solution in THF (16 mL). The reactor was pressurized and heated, as described

above, and the whole process was repeated for multiple runs. The collected filtrate was weighed with the flask, and the NMR of a weighed aliquot of the filtrate was taken in $CDCl_3$ with 1,3,5-trimethoxybenzene as the internal standard to calculate the conversion and yield. The details of each hydrogenation run are listed in Table 2-1.

A white solid was found in the bomb on completion of the reaction. After the last run (Run 5), the reaction mixture was cannulated into a side-arm flask under N_2, and a filtration was carried out to isolate the product. The remaining solid was washed with dry ether, and the organic compounds in the wash were combined with the filtrate of Run 5. Next, the solid was pumped to dry under high vacuum, and 0.714 g white powder was isolated. Its NMR confirmed the solid to be potassium benzoate with the remaining catalyst/$BaSO_4$ powder (0.283 g $BaSO_4$ would remain theoretically), without anything else visible in the NMR.

Table 2-1. Data of the reusing hydrogenation of methyl benzoate. (S:C:B = 40000:1:4000(KO*t*Bu), 80 °C, 50 bar, THF, 21 h)

	Total compound recovery[a]	Compound distribution[b]			Conv. (%)[c]	TON[d]	Isolated TON[e]
		Methyl benzoate	Benzyl benzoate	Benzyl alcohol			
Run 1	36820 (92%)	0.139	0.037	0.788	82.4	32960	30340
Run 2	39180 (98%)	0.209	0.048	0.695	74.3	29720	29110
Run 3	42850 (107%)	0.374	0.060	0.506	56.7	22680	24300
Run 4	40550 (101%)	0.391	0.069	0.470	53.9	21560	21860
Run 5	41030 (102%)	0.593	0.038	0.332	36.9	14760	15140
Total	200430[f]	NA	NA	NA	NA	121680 (60.8%)	120750 (60.2%)

[a] Total compound recovery = (methyl benzoate + benzyl benzoate × 2 + benzyl alcohol) recovered by filtration, reported as the molar ratio to the catalyst loading, and % to 40000 equiv. starting material. Determined by ^{1}H NMR with 1,3,5-trimethoxybenzene as an internal standard.
[b] molar ratio, (methyl benzoate + benzyl benzoate × 2 + benzyl alcohol) = 1,
[c] Conv., determined based on the integrated ratio between each compound in the ^{1}H NMR spectrum. Benzyl benzoate was considered as being formed from 1 starting ester + 1 alcohol product.
[d] TON = 40000 × conversion.
[e] Isolated TON = Isolated (benzyl alcohol + benzyl benzoate) / catalyst loading.
[f] The isolated potassium benzoate after Run 5 (~2000 equiv. to the catalyst loading) was not included.

2.4.4 ICP-MS to Determine the Leaching of the Catalyst in Heterogeneous Runs

A modified procedure was carried out based on the procedure of a previous study[147] in the same group. The procedure is described here using Run 1 as an example.

The filtrate of Run 1 was diluted using purified MeOH to a total weight of 29.3412 g. An aliquot (1.2274 g) was taken into a porcelain crucible, the crucible was placed on a hot plate, mild heating was applied to evaporate all the volatile solvents (THF and MeOH), then the temperature was increased slowly to evaporate the organic compounds. A white solid mixture with black stains remained in the crucible. The crucible with lid was placed on an open flame to destroy all the organics. Next, a few drops of trace-metal H_2SO_4 were added, and the sample was charred on an open flame again, until no more fumes evolved. (this process might take 1–2 h.) The residual was filled with saturated $K_2S_2O_8$ and left sitting for 20 h. The solution was transferred quantitively into a 25 mL volumetric flask, the flask was filled to the mark with 1 M trace-metal HNO_3, and a sample of this solution was submitted for ICP-MS. The Ru content was 0.0141 ppm for the sample of Run 1, which corresponded to 5.6% Ru leached out in Run 1.

2.4.5 NMR spectra of newly synthesized compounds:

trans-2,3-diaminonorborn-5-ene dihydrochloride (racemate) (119)
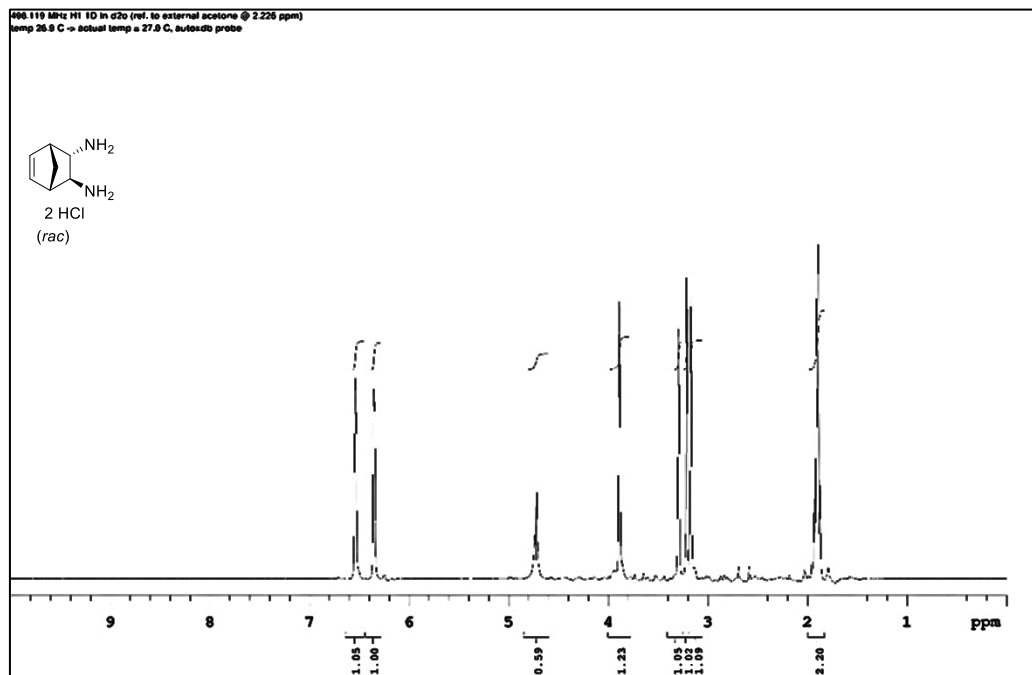
Figure 2-7. ^{1}H NMR spectrum of **119** in D$_2$O.
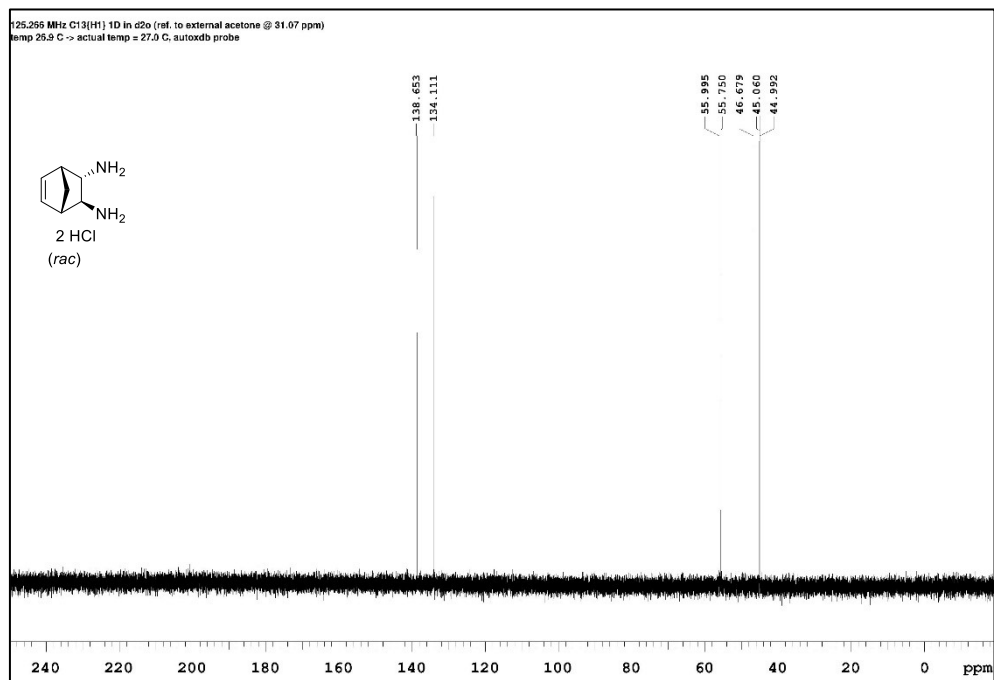
Figure 2-8. ^{13}C{^{1}H} NMR spectrum of **119** in D$_2$O.

N,*N'*-bis({(2-diphenylphosphino)phenyl}methylidene)bicyclo[2.2.1]hept-5-ene-2,3-diamine (racemate) (120)
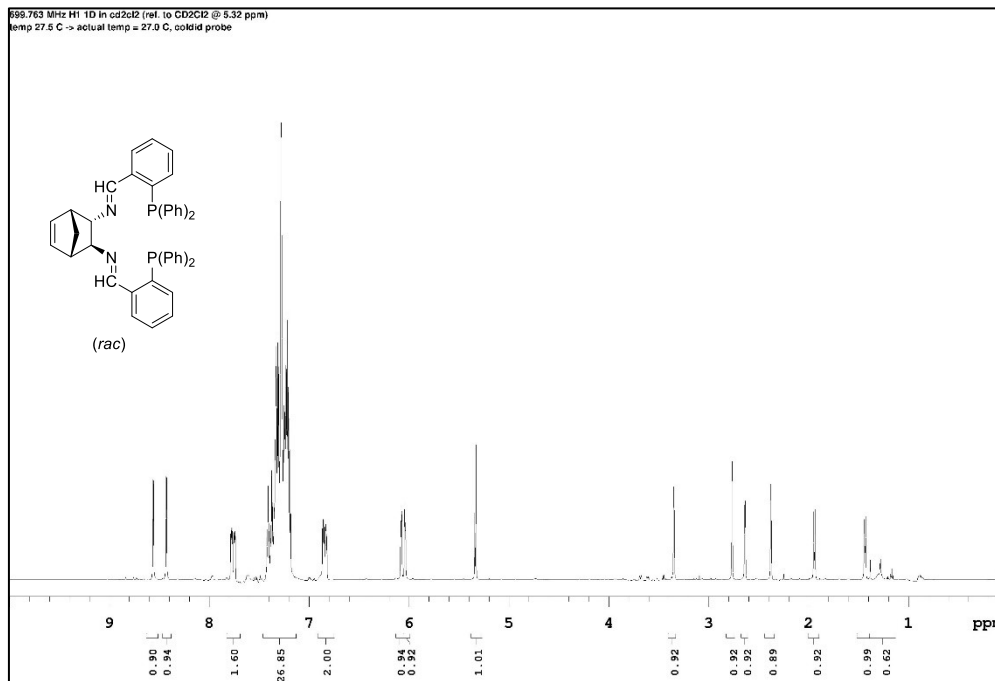
Figure 2-9. ^{1}H NMR spectrum **120** in CD$_2$Cl$_2$.
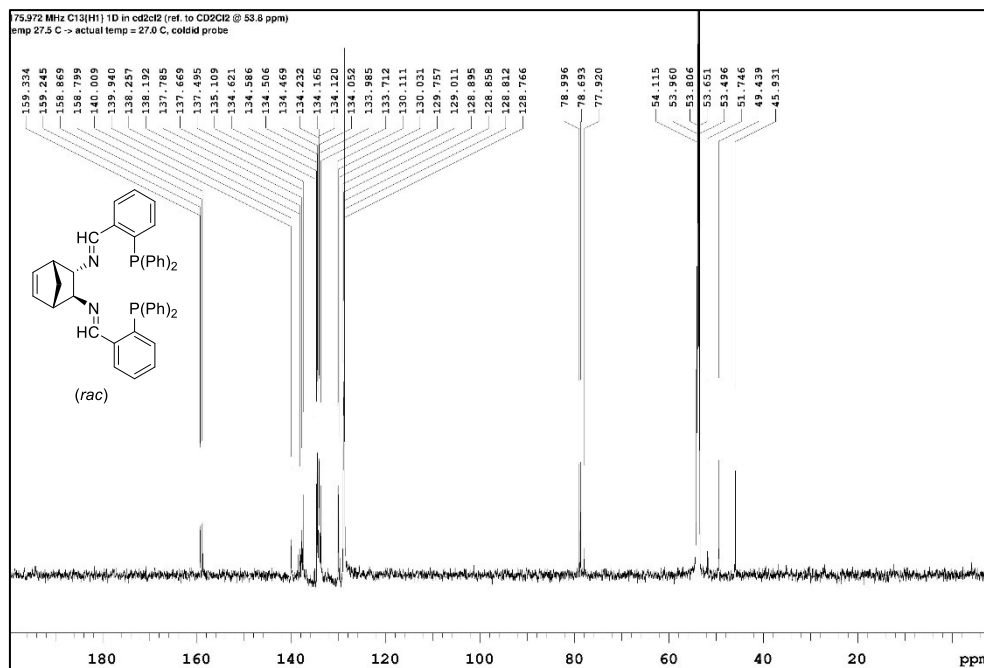
Figure 2-10. ^{13}C{^{1}H} NMR spectrum of **120** in CD$_2$Cl$_2$.
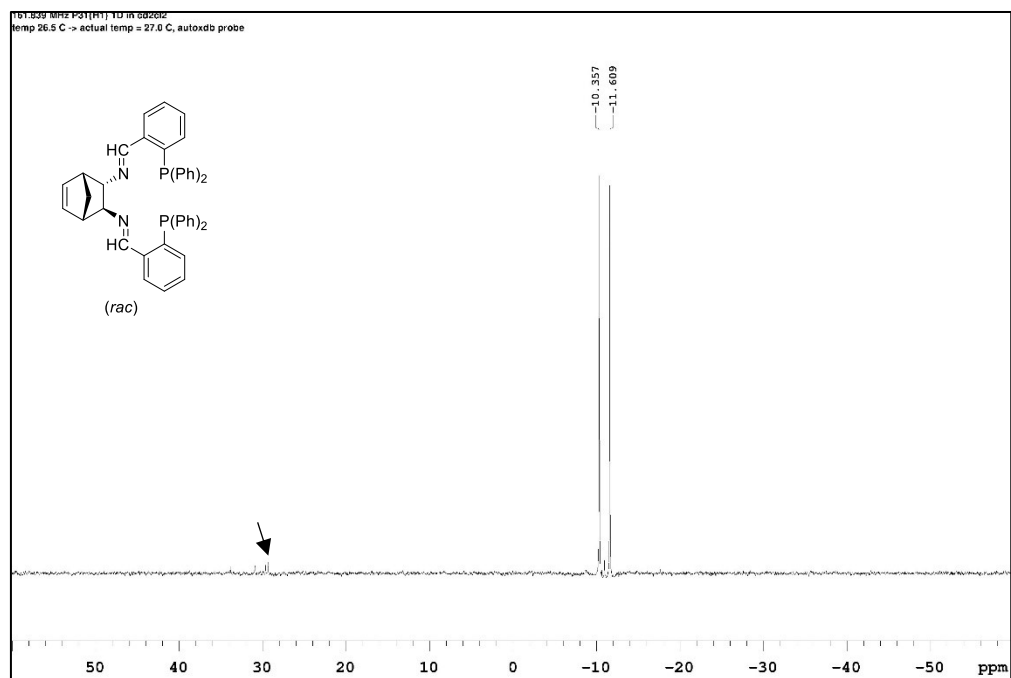
Figure 2-11. $^{31}P\{^1H\}$ NMR spectrum of **120** in CD$_2$Cl$_2$.

Dichloro{*N,N'*-bis({(2-diphenylphosphino)phenyl}pmethylidene)bicyclo[2.2.1]-hept-5-ene-2,3-diamine}Ruthenium (racemate) (121)
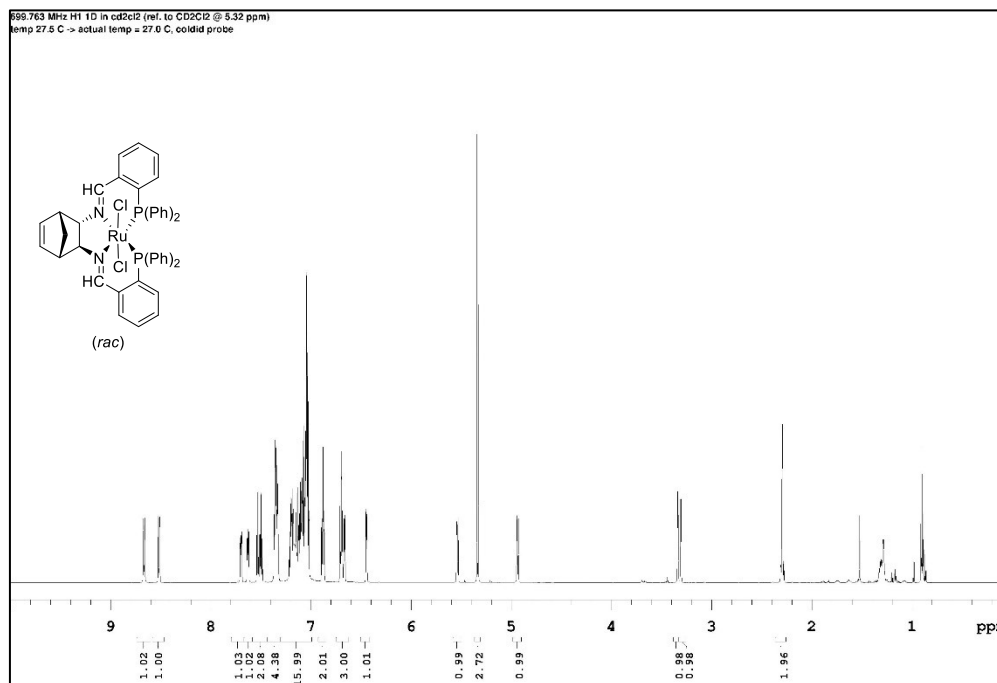
Figure 2-12. ^{1}H NMR spectrum of **121** in CD_2Cl_2. Some hexane could not be removed with high vaccum.
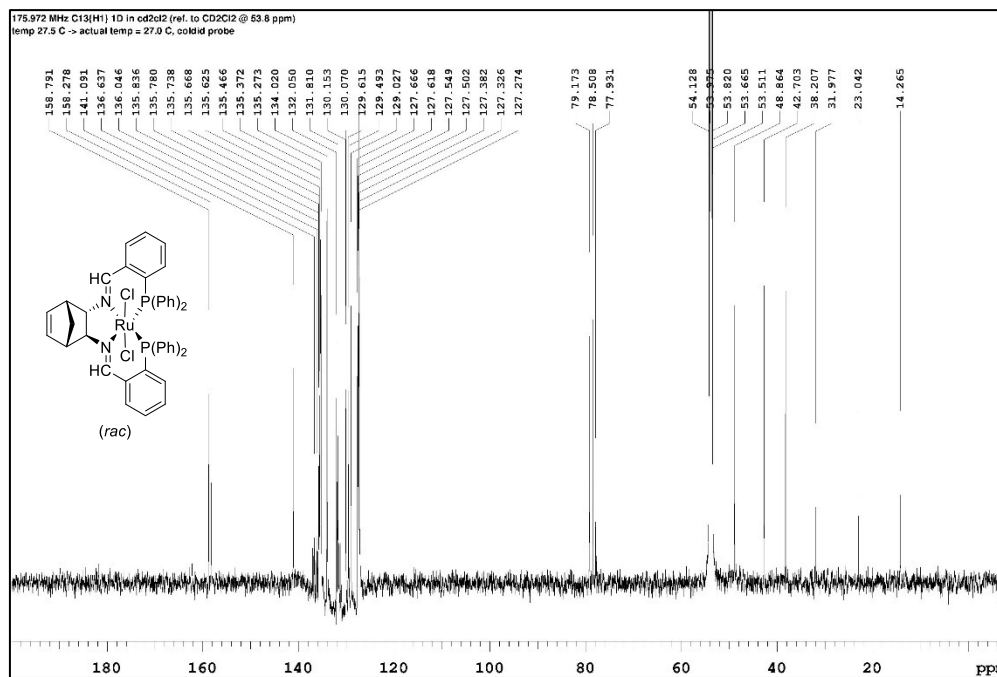
Figure 2-13. ^{13}C{^{1}H} NMR spectrum of **121** in CD_2Cl_2. Some hexane could not be removed with high vaccum.
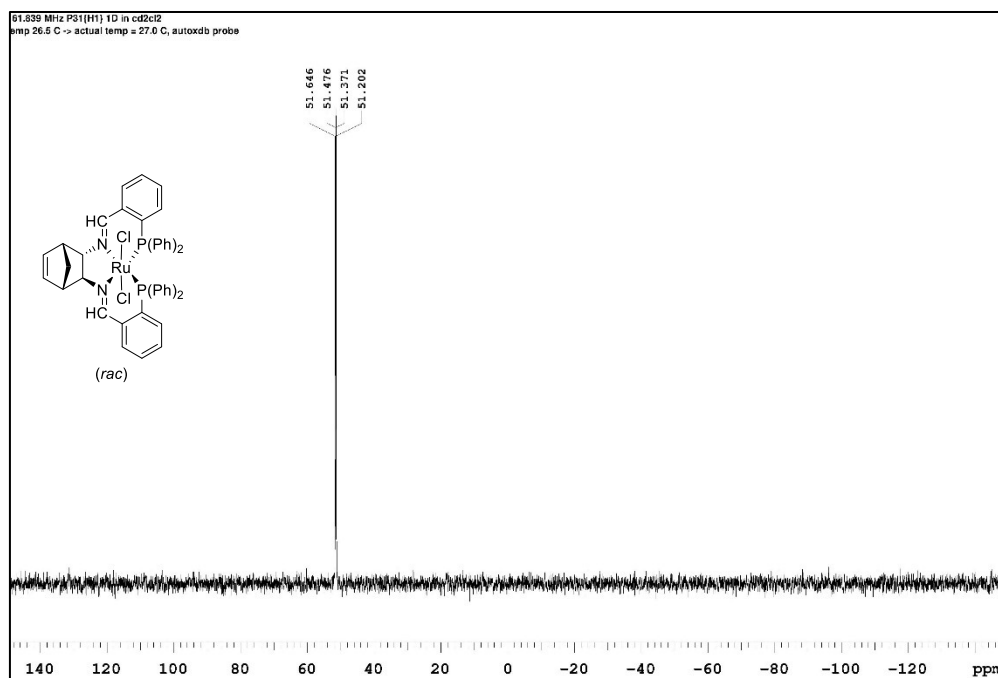
Figure 2-14. $^{31}P\{^1H\}$ NMR spectrum of **121** in CD_2Cl_2.

1,2-*N*-di(cis-5-norbornene-2,3-endo-dicarboximido)-ethane (123)
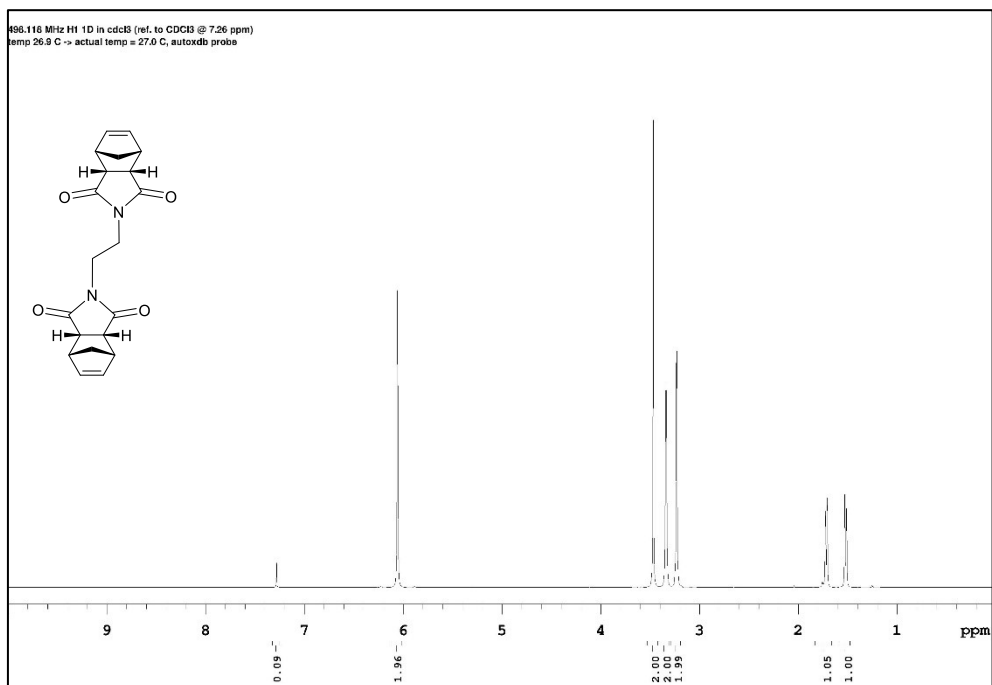
Figure 2-15. ^{1}H NMR spectrum of **123** in CDCl$_3$.
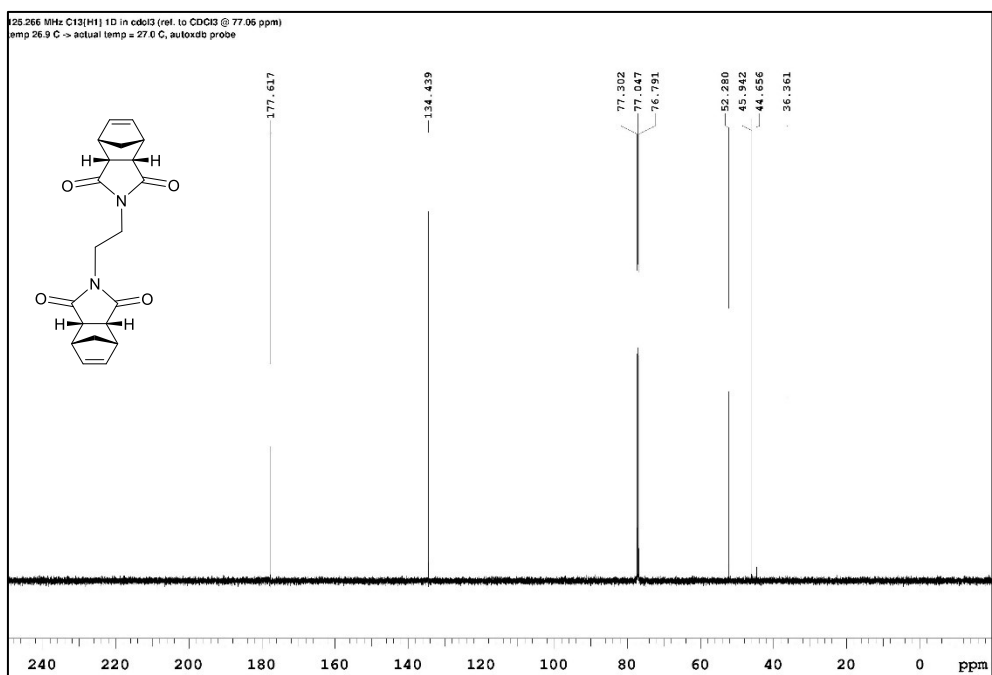
Figure 2-16. ^{13}C{^{1}H} NMR spectrum of **123** in CDCl$_3$.

Copolymerization of 121 (1 equiv.), 123 (2 equiv.), COE (8 equiv.) with 111 (0.02 equiv.) in CD₂Cl₂, at 40 °C:
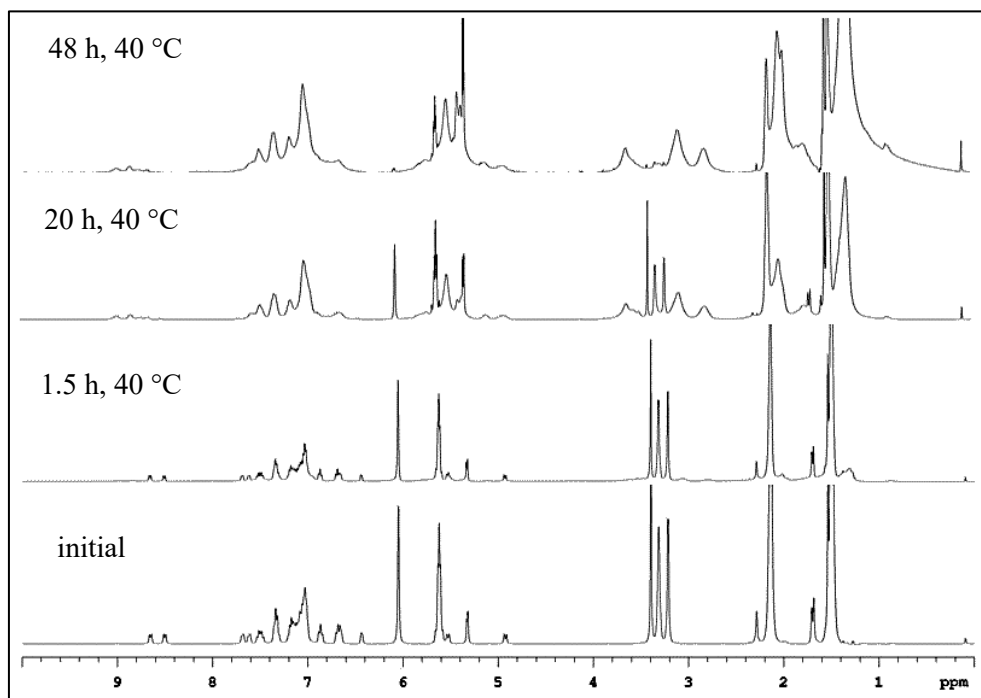
Figure 2-17. ^{1}H NMR spectra of the polymerization of **121**, COE, **123**, with 2 mol% **111**, From the bottom to the top: spectra recorded at initial, 1.5 h, 20 h, 48 h.
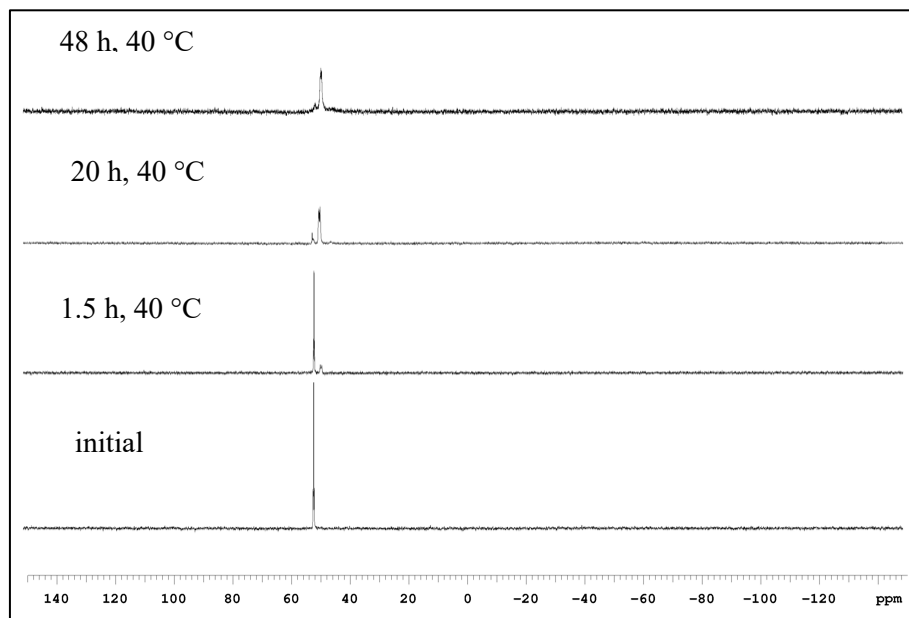
Figure 2-18. ^{31}P NMR spectra of polymerization of **121**, COE, **123**, with 2 mol% **111**, From the bottom to the top: spectra recorded at initial, 1.5 h, 20 h, 48 h.

2.4.6 Crystallographic Details of 121 (co-crystallized with 1 equiv. CH$_2$Cl$_2$)

Formula: C$_{46}$H$_{40}$Cl$_4$N$_2$P$_2$Ru (C$_{45}$H$_{38}$Cl$_2$N$_2$P$_2$Ru•CH$_2$Cl$_2$)

Crystallographic Experimental Details

A. Crystal Data

formula	C$_{46}$H$_{40}$Cl$_4$N$_2$P$_2$Ru
formula weight	925.61
crystal dimensions (mm)	0.31 × 0.25 × 0.06
crystal system	monoclinic
space group	*P*2$_1$/*n* (an alternate setting of *P*2$_1$/*c* [No. 14])
unit cell parameters[a]	
a (Å)	13.2651 (2)
b (Å)	15.0117 (3)
c (Å)	21.2637 (4)
β (deg)	105.3702 (6)
V (Å^3)	4082.80 (13)
Z	4
ρ_{calcd} (g cm^{-3})	1.506
μ (mm^{-1})	6.537

B. Data Collection and Refinement Conditions

diffractometer	Bruker D8/APEX II CCD[b]
radiation (λ [Å])	Cu Kα (1.54178) (microfocus source)
temperature (°C)	–100
scan type	ω and ϕ scans (1.0°) (5 s exposures)
data collection 2θ limit (deg)	147.91
total data collected	28679 (-16 ≤ h ≤ 16, -18 ≤ k ≤ 18, -26 ≤ l ≤ 26)
independent reflections	8268 (R_{int} = 0.0256)
number of observed reflections (*NO*)	7967 [$F_o^2 \geq 2\sigma(F_o^2)$]
structure solution method	Patterson/structure expansion (*DIRDIF–2008*[c])
refinement method	full-matrix least-squares on F^2 (*SHELXL–2014*[d])
absorption correction method	Gaussian integration (face-indexed)

range of transmission factors	0.7486–0.3333
data/restraints/parameters	8268 / 0 / 541
goodness-of-fit $(S)^e$ [all data]	1.039
final R indices[f]	
R_1 [$F_o^2 \geq 2\sigma(F_o^2)$]	0.0215
wR_2 [all data]	0.0555
largest difference peak and hole	0.556 and –0.520 e Å^{-3}

[a]Obtained from least-squares refinement of 9937 reflections with $7.30° < 2\theta < 147.42°$.

[b]Programs for diffractometer operation, data collection, data reduction and absorption correction were those supplied by Bruker.

[c]Beurskens, P. T.; Beurskens, G.; de Gelder, R.; Smits, J. M. M.; Garcia-Granda, S.; Gould, R. O. (2008). The *DIRDIF-2008* program system. Crystallography Laboratory, Radboud University Nijmegen, The Netherlands.

[d]Sheldrick, G. M. *Acta Crystallogr.* **2015**, *C71*, 3–8.

[e]$S = [\Sigma w(F_o^2 - F_c^2)^2/(n - p)]^{1/2}$ (n = number of data; p = number of parameters varied; $w = [\sigma^2(F_o^2) + (0.0260P)^2 + 2.3876P]^{-1}$ where $P = [\text{Max}(F_o^2, 0) + 2F_c^2]/3)$.

[f]$R_1 = \Sigma||F_o| - |F_c||/\Sigma|F_o|$; $wR_2 = [\Sigma w(F_o^2 - F_c^2)^2/\Sigma w(F_o^4)]^{1/2}$.

Table 2-2. Selected Interatomic Distances (Å) of **121**.

Atom1	Atom2	Distance	Atom1	Atom2	Distance
Ru	Cl1	2.4122(4)	C21	C26	1.403(2)
Ru	Cl2	2.4199(4)	C22	C23	1.400(2)
Ru	P1	2.2755(4)	C23	C24	1.387(2)
Ru	P2	2.2856(4)	C24	C25	1.383(3)
Ru	N1	2.1391(14)	C25	C26	1.385(3)
Ru	N2	2.1382(13)	C31	C32	1.397(2)
P1	C12	1.8477(17)	C31	C36	1.391(2)
P1	C31	1.8320(16)	C32	C33	1.391(2)
P1	C41	1.8330(16)	C33	C34	1.386(3)
P2	C22	1.8490(16)	C34	C35	1.382(3)
P2	C51	1.8368(16)	C35	C36	1.393(3)
P2	C61	1.8438(16)	C41	C42	1.396(2)
N1	C1	1.466(2)	C41	C46	1.393(2)
N1	C10	1.268(2)	C42	C43	1.390(3)
N2	C2	1.4658(19)	C43	C44	1.383(3)
N2	C20	1.273(2)	C44	C45	1.387(3)
C1	C2	1.550(2)	C45	C46	1.391(2)
C1	C6A	1.534(9)	C51	C52	1.400(2)
C1	C6B	1.625(8)	C51	C56	1.399(2)
C2	C3A	1.621(14)	C52	C53	1.394(2)
C2	C3B	1.484(16)	C53	C54	1.383(3)
C3A	C4A	1.504(16)	C54	C55	1.387(3)
C3A	C7A	1.555(18)	C55	C56	1.389(2)
C4A	C5A	1.318(6)	C61	C62	1.396(2)
C5A	C6A	1.526(8)	C61	C66	1.391(2)
C6A	C7A	1.553(10)	C62	C63	1.392(2)
C3B	C4B	1.51(2)	C63	C64	1.379(3)
C3B	C7B	1.563(17)	C64	C65	1.385(3)
C4B	C5B	1.322(6)	C65	C66	1.394(2)
C5B	C6B	1.512(7)			
C6B	C7B	1.526(10)			
C10	C11	1.469(3)			
C11	C12	1.413(2)			
C11	C16	1.398(3)			
C12	C13	1.395(3)			
C13	C14	1.393(3)			
C14	C15	1.377(3)			
C15	C16	1.384(3)			
C20	C21	1.470(2)			
C21	C22	1.409(2)			

Table 2-3. Selected Interatomic Angles (°) of **121**.

Atom1	Atom2	Atom3	Angle
Cl1	Ru	Cl2	171.228(13)
Cl1	Ru	P1	95.613(14)
Cl1	Ru	P2	87.437(14)
Cl1	Ru	N1	88.40(4)
Cl1	Ru	N2	85.79(4)
Cl2	Ru	P1	86.591(14)
Cl2	Ru	P2	100.419(13)
Cl2	Ru	N1	83.25(4)
Cl2	Ru	N2	90.54(4)
P1	Ru	P2	102.241(14)
P1	Ru	N1	86.62(4)
P1	Ru	N2	169.61(4)
P2	Ru	N1	170.53(4)
P2	Ru	N2	88.09(4)
N1	Ru	N2	83.12(5)
Ru	P1	C12	110.03(6)
Ru	P1	C31	118.80(5)
Ru	P1	C41	120.62(5)
C12	P1	C31	102.26(7)
C12	P1	C41	101.46(8)
C31	P1	C41	100.93(7)
Ru	P2	C22	112.95(5)
Ru	P2	C51	116.19(5)
Ru	P2	C61	121.80(5)
C22	P2	C51	100.97(7)
C22	P2	C61	96.40(7)
C51	P2	C61	104.99(7)
Ru	N1	C1	103.23(10)
Ru	N1	C10	134.45(13)
C1	N1	C10	121.67(15)
Ru	N2	C2	102.96(9)
Ru	N2	C20	135.98(11)
C2	N2	C20	120.46(14)
N1	C1	C2	104.34(13)
N1	C1	C6A	134.6(3)
N1	C1	C6B	120.4(3)
C2	C1	C6A	103.1(4)
C2	C1	C6B	100.3(3)
N2	C2	C1	105.14(12)

Atom1	Atom2	Atom3	Angle
N2	C2	C3A	124.1(6)
N2	C2	C3B	132.0(7)
C1	C2	C3A	102.9(6)
C1	C2	C3B	102.2(6)
C2	C3A	C4A	96.3(10)
C2	C3A	C7A	102.0(8)
C4A	C3A	C7A	99.8(9)
C3A	C4A	C5A	108.9(7)
C4A	C5A	C6A	108.5(5)
C1	C6A	C5A	105.6(5)
C1	C6A	C7A	100.3(5)
C5A	C6A	C7A	99.2(7)
C3A	C7A	C6A	94.9(9)
C2	C3B	C4B	110.2(10)
C2	C3B	C7B	99.8(10)
C4B	C3B	C7B	99.4(10)
C3B	C4B	C5B	108.0(8)
C4B	C5B	C6B	107.3(6)
C1	C6B	C5B	94.7(4)
C1	C6B	C7B	104.8(5)
C5B	C6B	C7B	100.1(6)
C3B	C7B	C6B	92.9(7)
N1	C10	C11	126.32(15)
C10	C11	C12	125.44(16)
C10	C11	C16	115.01(17)
C12	C11	C16	119.36(18)
P1	C12	C11	121.89(14)
P1	C12	C13	120.31(14)
C11	C12	C13	117.80(16)
C12	C13	C14	121.87(19)
C13	C14	C15	120.0(2)
C14	C15	C16	119.21(18)
C11	C16	C15	121.7(2)
N2	C20	C21	126.28(14)
C20	C21	C22	126.20(14)
C20	C21	C26	114.55(15)
C22	C21	C26	119.18(15)
P2	C22	C21	124.55(12)
P2	C22	C23	117.04(12)

(continued)

Atom1	Atom2	Atom3	Angle
C21	C22	C23	118.11(14)
C22	C23	C24	122.15(16)
C23	C24	C25	119.38(16)
C24	C25	C26	119.84(16)
C21	C26	C25	121.31(16)
P1	C31	C32	117.22(12)
P1	C31	C36	123.58(14)
C32	C31	C36	119.09(15)
C31	C32	C33	120.47(16)
C32	C33	C34	119.93(19)
C33	C34	C35	119.93(17)
C34	C35	C36	120.41(17)
C31	C36	C35	120.14(18)
P1	C41	C42	122.23(13)
P1	C41	C46	118.63(12)
C42	C41	C46	119.13(15)
C41	C42	C43	120.49(17)
C42	C43	C44	119.95(18)
C43	C44	C45	120.09(17)
C44	C45	C46	120.15(17)
C41	C46	C45	120.18(16)
P2	C51	C52	119.86(12)
P2	C51	C56	121.34(12)
C52	C51	C56	118.49(15)
C51	C52	C53	120.28(16)
C52	C53	C54	120.58(17)
C53	C54	C55	119.65(16)
C54	C55	C56	120.18(17)
C51	C56	C55	120.81(16)
P2	C61	C62	124.44(13)
P2	C61	C66	116.56(13)
C62	C61	C66	118.75(15)
C61	C62	C63	120.50(18)
C62	C63	C64	120.27(18)
C63	C64	C65	119.78(17)
C64	C65	C66	120.21(19)
C61	C66	C65	120.41(18)

Chapter 3

Exploratory Projects with Polymeric Ester Hydrogenation Catalysts

In this chapter, I report two exploratory projects derived from the polymeric RuPNNP catalyst discussed in Chapter 2. Part A involves the resolution of the norbornene-based RuPNNP catalysts and a preliminary study of their performance in the enantioselective ketone transfer hydrogenation and the enantioselective ester hydrogenation via dynamic kinetic resolution (DKR). In Part B, a neighboring base moiety is introduced into the chain of a polymeric Ru hydrogenation catalyst. The expectation was that this neighboring base would facilitate ester hydrogenations via intramolecular interactions. A brief background discussion is presented at the beginning of each part of this chapter.

3.1 Part A

3.1.1 Introduction

Chiral RuPNNPs are highly enantioselective catalysts for transfer hydrogenations of ketones,[179, 188, 189] olefin epoxidations,[180] Diels–Alder reactions,[190] and olefin cyclopropanations.[182] For example, Noyori et al reported that **125** (Scheme 3-1) catalyzes the transfer hydrogenation of acetophenone in 2-PrOH in up to 97% ee.[179]
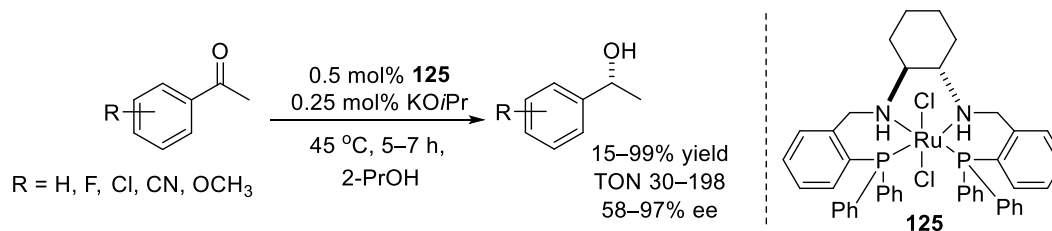
Scheme 3-1. Enantioselective ketone transfer hydrogenation with RuPNNP catalysts.[179]

The Bergens group recently found that **126** (Scheme 3-2) catalyzes the enantioselective hydrogenation of β-chiral esters via DKR. During this reaction, one enantiomer of the racemic ester is reduced faster than the other, and excess base catalyzes the racemization of the starting esters faster than the hydrogenation, driving the reaction to completion.
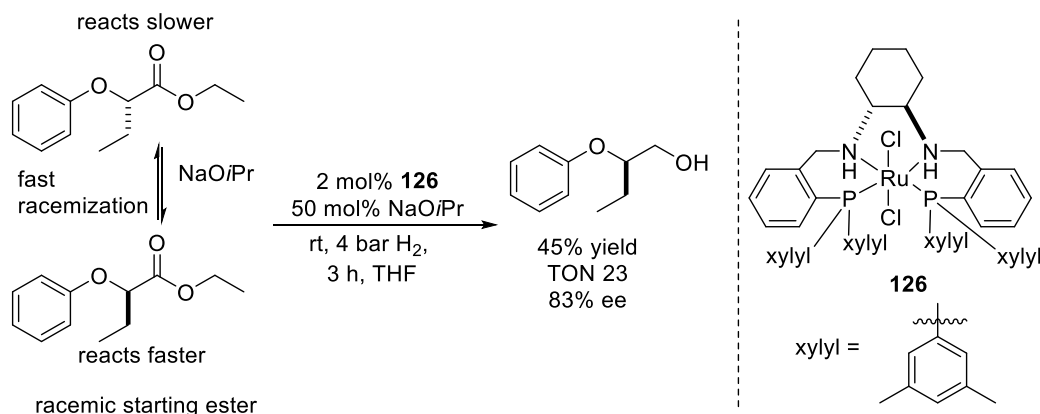
Scheme 3-2. Ester hydrogenation via dynamic kinetic resolution with a RuPNNP catalyst.[191]

The catalyst monomer dichloro{*N*,*N*'-bis({(2-diphenylphosphino)phenyl}-methylidene)bicyclo[2.2.1]-hept-5-ene-2,3-diamine}ruthenium (**121**) reported in Chapter 2 contains a PNNP ligand with a similar structure to these examples. The difference is the N, N backbone ligand. After olefin metathesis, a *trans*-1,2-disubstituted cyclopentane ring connects the nitrogen atom in the polymerized catalyst, whereas the literature examples contain a *trans*-1,2-disubstituted cyclohexane linker. In this chapter, I report the enantioselective synthesis of the PNNP ligands from the optically enriched starting material *trans*-2,3-diaminonorborn-5-ene dihydrochloride, the preparation of the corresponding ruthenium catalysts, as well as the preliminary results of the enantioselective catalysis using these chiral RuPNNP catalysts.

3.1.2 Results and Discussion

The synthesis of the optically enriched RuPNNP catalysts began with the resolution of *trans*-3,6-endomethylene-1,2,3,6-tetrahydrophthaloyl chloride **128** (Scheme 3-3). The asymmetric synthesis of **128** was reported previously, and the procedure involved a low-temperature diastereoselective Diels–Alder reaction between dimenthyl fumarate and cyclopentadiene catalyzed by Et$_2$AlCl, as shown in Scheme 3-3.[184, 192]
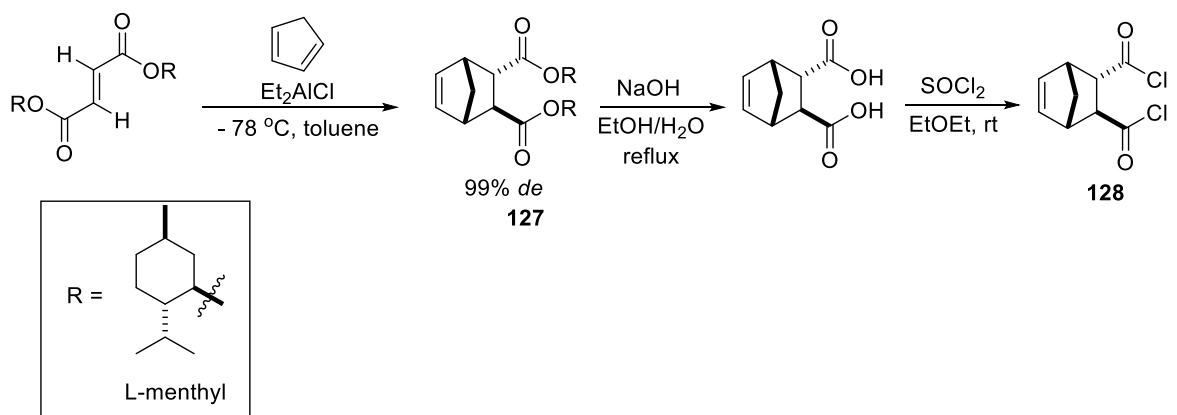
Scheme 3-3. Previously reported enantioselective synthesis of *trans*-3,6-endomethylene-1,2,3,6-tetrahydrophthaloyl chloride **128**.[184, 192]

The cycloaddition reaction proceeded in high de (99%) to **127**, and the chirality was retained during hydrolysis and conversion into the diacid chloride **128**. We developed a procedure that avoided the low temperature reaction. As shown in Scheme 3-4, instead of the diastereoselective cycloaddition, resolution of the racemic diacid chloride was carried out with L-menthol. After the esterification and recrystallization, one diastereomer of the dimenthyl ester **127** was isolated (71% yield) in high de (the other diastereomer could not be detected by ^{1}H NMR). Hydrolysis and reaction with thionyl chloride converted **127** to **128**.
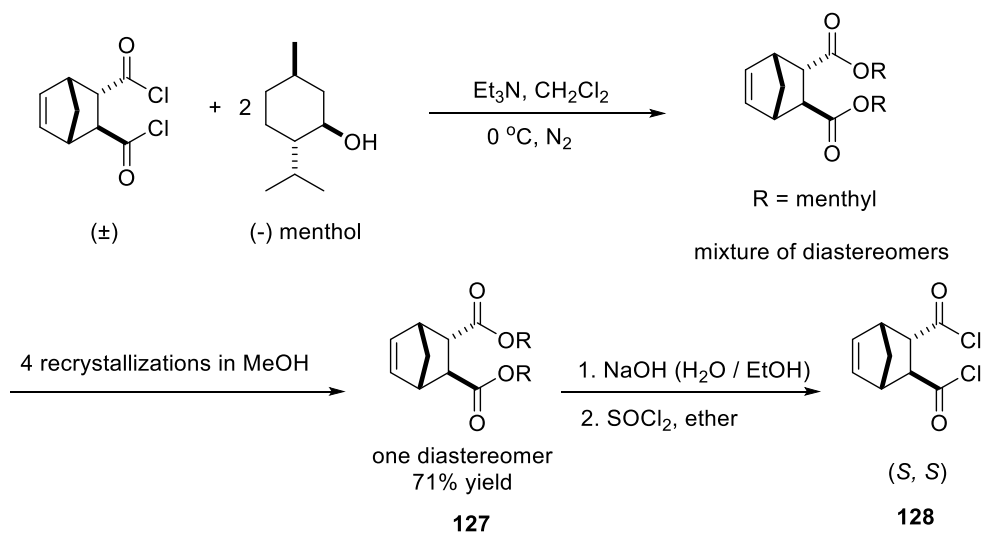
Scheme 3-4. The resolution of diacid chloride compound to optically enriched **128**.

The diacid chloride **128** was converted to the corresponding diacyl azide (Scheme 3-5), and then to the diamine HCl salt **129** via a Curtius rearrangement.
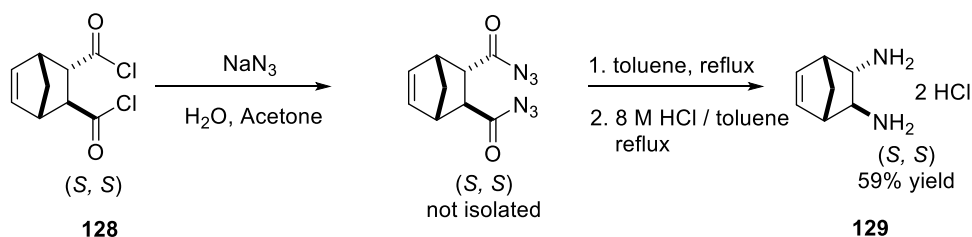
Scheme 3-5. Conversion of **128** to diamine salt **129**.

This reaction was reported previously by Lin et al,[184] who measured the optical rotation of **129** $[\alpha]_D = +51.2°(c\ 1.12, H_2O)$. No absolute ee determination was reported. The optical rotation of **129** prepared here from **127** was $[\alpha]_D = +62.5°(c\ 1.13, H_2O)$. We also determined the ee of **129** using (1R)-(-)-myrtenal as the chiral derivatizing agent. Condensation between the amine groups and the aldehyde resulted in diimine diastereomers (Scheme 3-6), and the imine protons were diagnostic in the ^{1}H NMR, indicating that the ee of **129** was 85%.
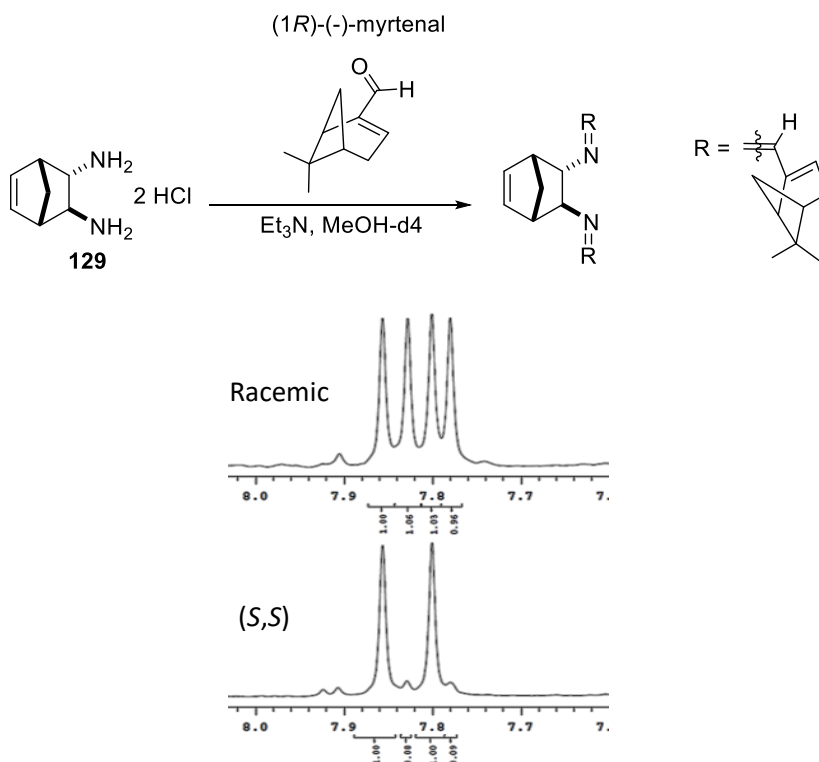
Scheme 3-6. (top) Condensation reaction to determine the ee of **129** using (R)-myrtenal. **(bottom)** Diagnostic peaks of imine protons made from **129** and racemic analog of **129**.

The ee of **129** was sufficient to perform preliminary studies with the RuPNNP catalysts. The partially resolved diamine reacted with 2-diphenylphosphinobenzaldehyde or 2-[bis(3,5-dimethylphenyl)phosphino]benzaldehyde to form the imine PNNP ligands **130** and **131** (Scheme 3-7). The corresponding amines **132** and **133** were prepared by the reduction of the imine ligands with NaBH$_4$.[179, 183, 189] As discussed for the racemic ligand **120** in Chapter 2, the optically enriched trans dichloride **134** was prepared by reaction between **130** and **115** at 60 °C in CHCl$_3$ for 3 days. Compound **135** was synthesized similarly, while **136** and **137** were synthesized by reacting **132** or **133** with **115** in DCM at 40 °C, followed by chromatographic purification using silica gel, with yields of 68% and 31%, respectively. The two amine ligands **132** and **133** react with **115** much faster than **130** and **131**, requiring only ~16 h at 40 °C in CH$_2$Cl$_2$. This is probably due to the less rigid sp^3 N and C atoms in **132** and **133**, which orient easier for the complexation. After purification, all four complexes showed two doublets in AB patterns in ^{31}P NMR.
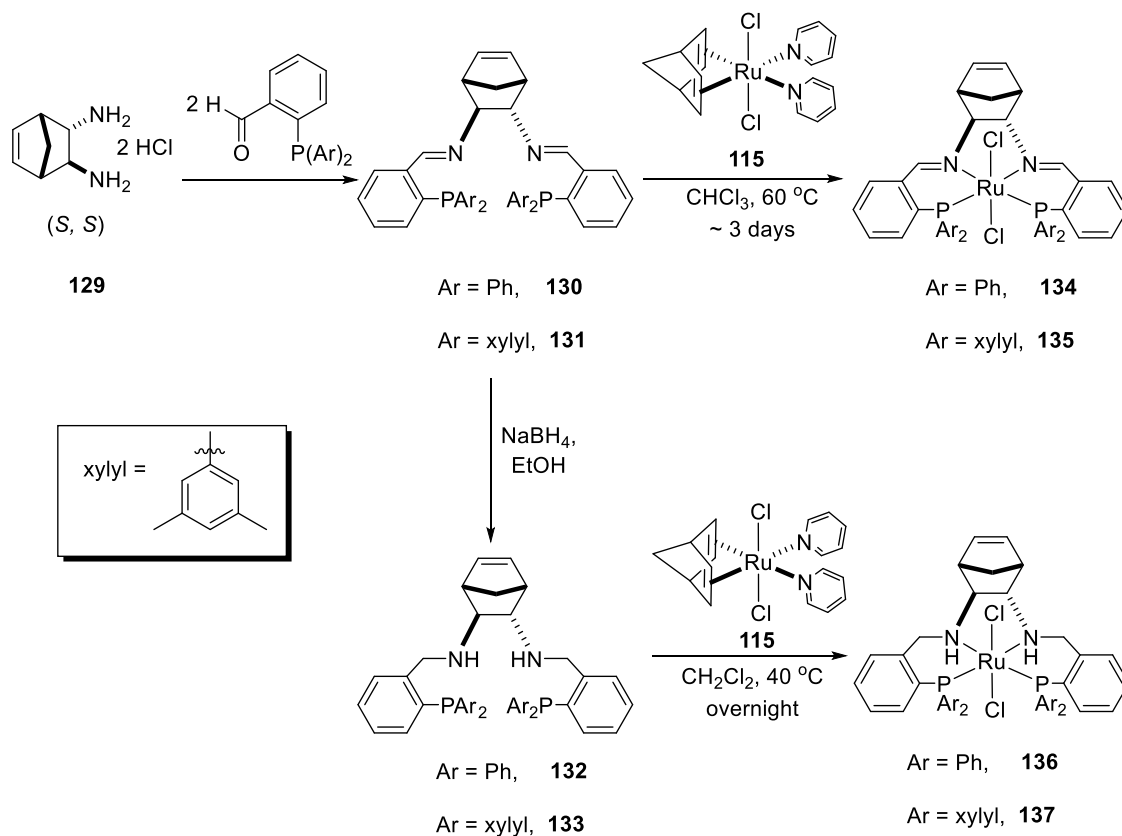
Scheme 3-7. The synthesis of optically enriched ligands and complexes.

The alt-ROMP of **135** and **137** proceeded smoothly with 5% 1st generation Grubbs (**111**) catalyst with 4 equiv. COE as a spacer in CD$_2$Cl$_2$ at 40 °C (Scheme 3-8).
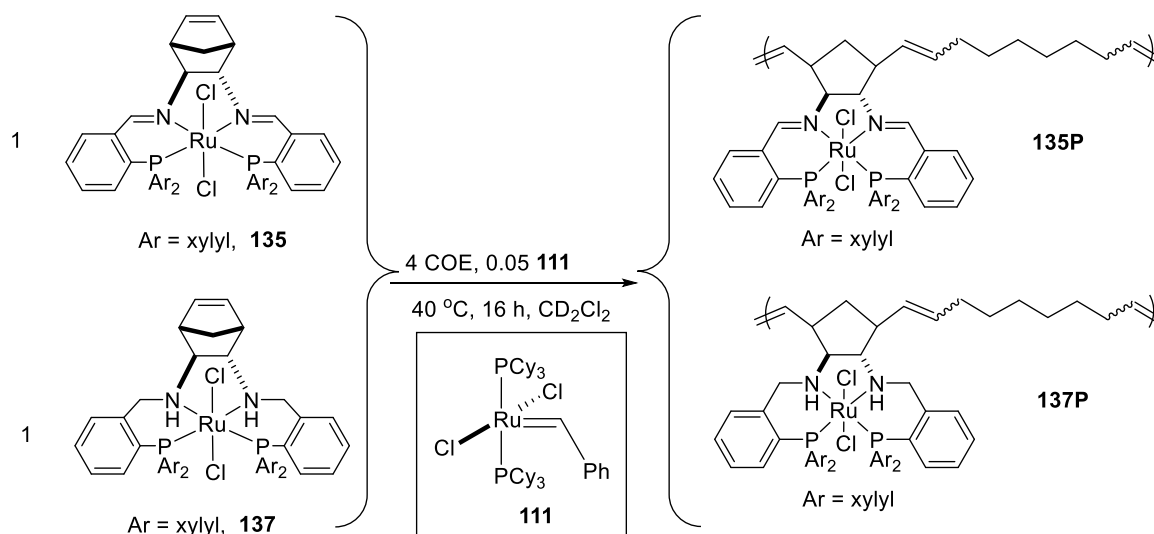
Scheme 3-8. The polymerization of **135** and **137**.
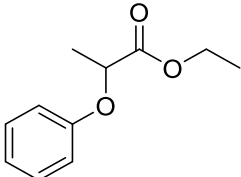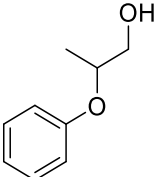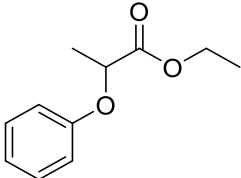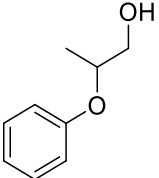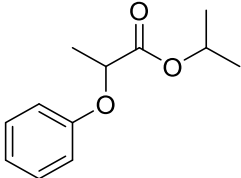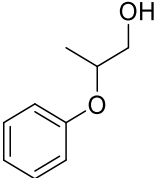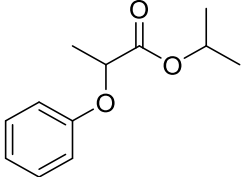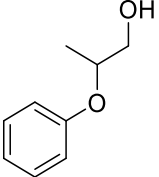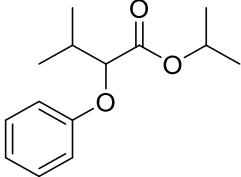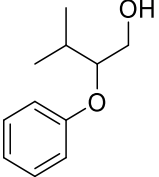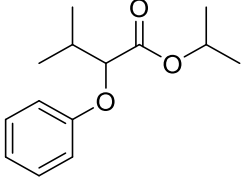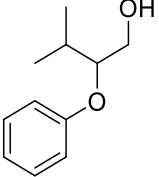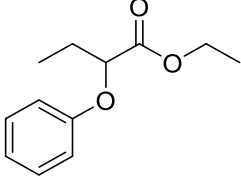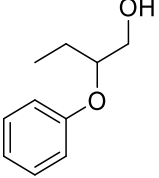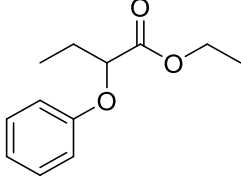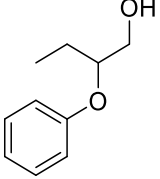
We evaluated these catalysts (Scheme 3-9) with the transfer hydrogenation reaction of acetophenone and with ester hydrogenations via DKR (Scheme 3-9). The enantioselective catalysis results are listed in Table 3-1. The highest enantioselectivity was 52% ee (60% normalized to the 85% ee of **129**, Table 3-1, Entry 1), obtained for the transfer hydrogenation of acetophenone in 2-PrOH using **134** (Scheme 3-9). The highest ee for ester hydrogenations via DKR with these catalysts was 39% (Table 3-1, Entry 12, with catalyst **137P**, Scheme 3-9).
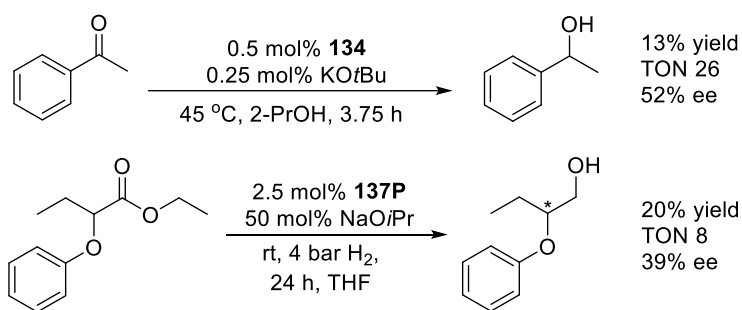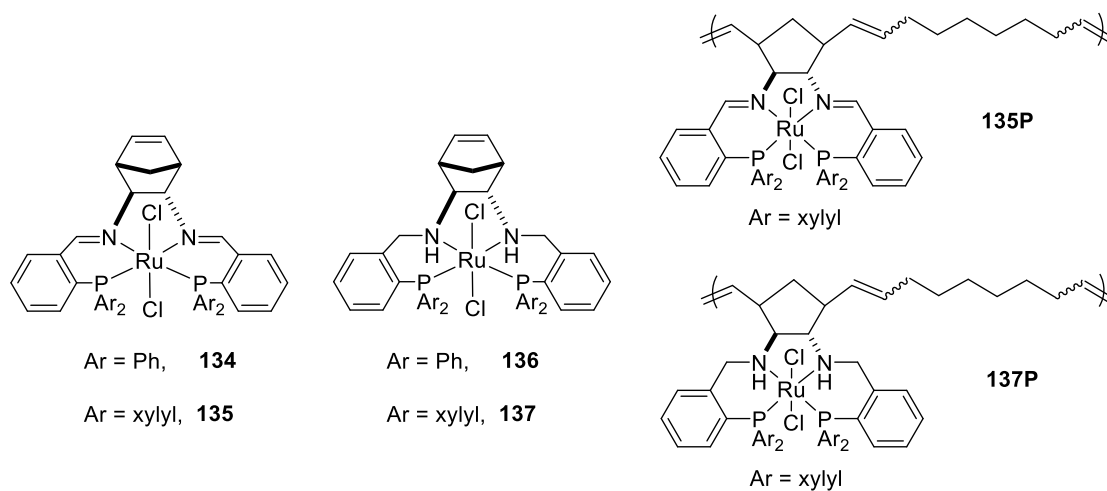
Scheme 3-9. Enantioselective catalysis carried out with RuPNNP catalysts.

Table 3-1. Enantioselective catalyses carried out with RuPNNP catalyst.

	Substrate	Catalyst /base	Product	Condi-tions	Yield (TON)	ee[a]	ee[b]
1		**134** (0.5 mol%) KO*t*Bu (0.25 mol%)		45 °C 2-PrOH 3.75 h	13% (26)	52%	60%
2		**136** (0.5 mol%) KO*t*Bu (0.25 mol%)		45 °C 2-PrOH 2 h	67% (134)	18%	21%
3		**137** (0.5 mol%) KO*t*Bu (0.25 mol%)		rt 2-PrOH 19 h	10% (20)	31%	36%
4		**137P** (0.5 mol%) KO*t*Bu (0.25 mol%)		rt 2-PrOH 21 h	5% (10)	22%	26%

#	Substrate	Catalyst	Product	Conditions			
5	(ethyl 2-phenoxypropanoate)	**135P** (2 mol%) NaO*i*Pr (50 mol%)	(2-phenoxypropan-1-ol)	rt THF 24 h 4 bar H$_2$	42% (21)	16% (S)	19% (S)
6	(ethyl 2-phenoxypropanoate)	**137P** (2.5 mol%) NaO*i*Pr (50 mol%)	(2-phenoxypropan-1-ol)	rt THF 21 h 4 bar H$_2$	46% (18)	36% (S)	42% (S)
7	(isopropyl 2-phenoxypropanoate)	**135P** (2 mol%) NaO*i*Pr (50 mol%)	(2-phenoxypropan-1-ol)	rt THF 24 h 4 bar H$_2$	17% (9)	0%	0%
8	(isopropyl 2-phenoxypropanoate)	**137P** (2.5 mol%) NaO*i*Pr (50 mol%)	(2-phenoxypropan-1-ol)	rt THF 21 h 4 bar H$_2$	12% (5)	0%	0%
9	(isopropyl 3-methyl-2-phenoxybutanoate)	**135P** (2 mol%) NaO*i*Pr (50 mol%)	(3-methyl-2-phenoxybutan-1-ol)	rt THF 24 h 4 bar H$_2$	0 (0)	NA	NA
10	(isopropyl 3-methyl-2-phenoxybutanoate)	**137P** (2.5 mol%) NaO*i*Pr (50 mol%)	(3-methyl-2-phenoxybutan-1-ol)	rt THF 21 h 4 bar H$_2$	0 (0)	NA	NA
11	(ethyl 2-phenoxybutanoate)	**135P** (2 mol%) NaO*i*Pr (50 mol%)	(2-phenoxybutan-1-ol)	rt THF 24 h 4 bar H$_2$	17% (9)	9% (S)	11% (S)
12	(ethyl 2-phenoxybutanoate)	**137P** (2.5 mol%) NaO*i*Pr (50 mol%)	(2-phenoxybutan-1-ol)	rt THF 21 h 4 bar H$_2$	20% (8)	39% (S)	46% (S)

13		**135P** (2 mol%) NaO*i*Pr (50 mol%)		rt THF 24 h 4 bar H$_2$	46% (23)	11%	13%
14		**137P** (2.5 mol%) NaO*i*Pr (50 mol%)		rt THF 21 h 4 bar H$_2$	37% (15)	27%	32%
15		**135P** (2 mol%) NaO*i*Pr (50 mol%)		rt THF 24 h 4 bar H$_2$	67% (34)	14%	16%
16		**137P** (2.5 mol%) NaO*i*Pr (50 mol%)		rt THF 21 h 4 bar H$_2$	49% (20)	20%	24%
17		**135P** (2 mol%) NaO*i*Pr (50 mol%)		rt THF 24 h 4 bar H$_2$	61% (31)	18%	21%
18		**137P** (2.5 mol%) NaO*i*Pr (50 mol%)		rt THF 21 h 4 bar H$_2$	52% (21)	25%	29%

a: ee obtained by gas chromatography with chiral column.
b: ee normalized to the ee of **129**.

In the transfer hydrogenation of ketones (Entry 1–4, Table 3-1), **136** was significantly more active than **134** (Entry 1 and 2), which probably is due to the existence of NH groups in **136**. Several studies[62, 183] imply that ruthenium catalysts similar to **134**, bearing imine PNNP ligands, are reduced to the amine analogs in a catalysis, resulting in the same active dihydride species in the hydrogenation or transfer hydrogenation of carbonyl compounds. Also, the significant difference in the ee between Entry 1 and 2 implies that the actual catalysts might be different. Further study is needed to discover the actual active species of **134** (and similar

catalysts) in the transfer hydrogenations. Polymer **137P** is less active and less enantioselective than monomer **137**. This is attributed to either or both factors: 1) the ROMP structurally changed the chemical environment around the ruthenium; 2) polymer **137P** has a slower mass transport than monomer **137** in solutions.

The ester hydrogenations via DKR were tested with the polymer catalysts **135P** and **137P**, which have a 5-member ring in the backbone (Entry 5–18, 2–2.5 mol% catalyst, 50 mol% NaO*i*Pr, rt, THF, 24 h, 4 bar H$_2$). Compared to **126** (Scheme 3-2) with a cyclohexyl backbone, these polymer catalysts exhibit similar activity but lower enantioselectivity (Entry 5 and 6). Polymer catalysts **135P** and **137P** have similar activities, but **137P** gave higher ee in these ester hydrogenations. The substrates with electron withdrawing substituents (Entry 15, 16, 17, and 18) are easier to reduce than the other substrates.

As indicated by these screening reactions, it was unlikely to obtain satisfactory ee with this substrate scope. Further development was not conducted within this PhD thesis. Here, we reported this preparation of the norbornene-based chiral ligands, the corresponding catalysts, as well as the preliminary results of their enantioselective catalysis.

3.2 Part B

3.2.1 Introduction

Excess base (ratios between base and catalyst are mostly between 10 to 10000, related to the catalyst loading) generally is required for high turnover number catalytic hydrogenation of esters using bifunctional catalysts. For example (Scheme 3-10), Zhou et al reported the ester hydrogenation with the highest TON (91000 in the hydrogenation of methyl benzoate) in the literature,[87] which required 100 to 10000 equiv. of KO*t*Bu to the catalyst. Numerous other examples are discussed in Chapter 1 as well.
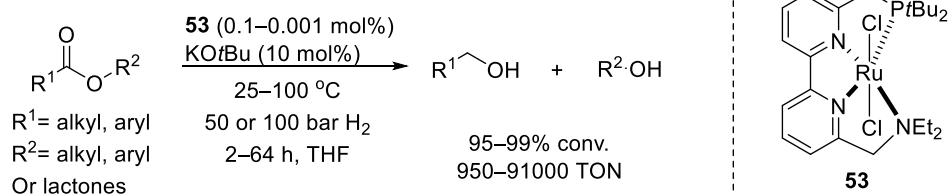
Scheme 3-10. Ester hydrogenation reported by Zhou et al.[87]

Several roles for the base have been investigated. One is to promote the dehydrohalogenation of the chloride precursor to form the dihydride species, probably via a Ru-amide intermediate, as exemplified in Scheme 3-11. While this mechanism explains the need for base to initiate these hydrogenations, it does not explain the observed dependence of the rate on base.[65, 66, 86, 90, 109]
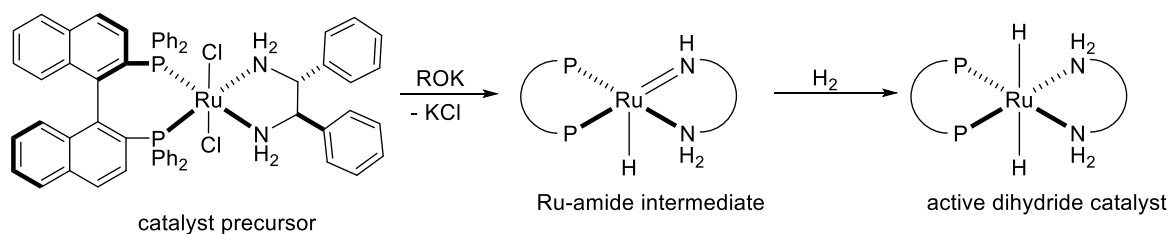
Scheme 3-11. The dehydrohalogenation of *trans*-RuCl$_2$((*R*)-BINAP)((*R, R*)-DPEN) for hydrogenations.

In 2001, Hartmann and Chen[193] proposed that an alkali metal is necessary for a ketone hydrogenation using Noyori's RuCl$_2$((*S*)-BINAP)((*S,S*)-DPEN) catalyst. The authors carried out ketone hydrogenations in 2-PrOH using 1,8-diazabicyclo[5.4.0]undec-7-ene (DBU) as the base, which deprotonated 2-PrOH to form isopropoxide. Under their experimental conditions (2 M acetophenone, 0.05 mol% Ru, 50 °C, 5 bar H$_2$, 2-PrOH), DBU (100 equiv.) did not promote the hydrogenation, but KO*t*Bu (10 equiv.) did. A mixture of 100 equiv. of DBU and 10 equiv. of KBAF (BAF = tetrakis(3, 5-bis(trifluoromethyl)phenyl)borate anion) did promote the hydrogenation. Addition of 18-crown-6, which strongly traps K$^+$, stopped the reaction. Based on these observations and modelling of the overall product forming kinetics, the authors proposed that deprotonation of an NH group forms a lone pair of electrons that can coordinate to K$^+$ in the axial position. This compound, **138** (Scheme 3-12), reduces a ketone through the outer-sphere hydride transfer via **139** and **140**, leaving one vacancy site for H$_2$ to coordinate to form **141**, which undergoes intramolecular deprotonation of η^2-H$_2$ to generate **138**. It is

important to note that these steps were tentative, and were based upon indirect measurements.
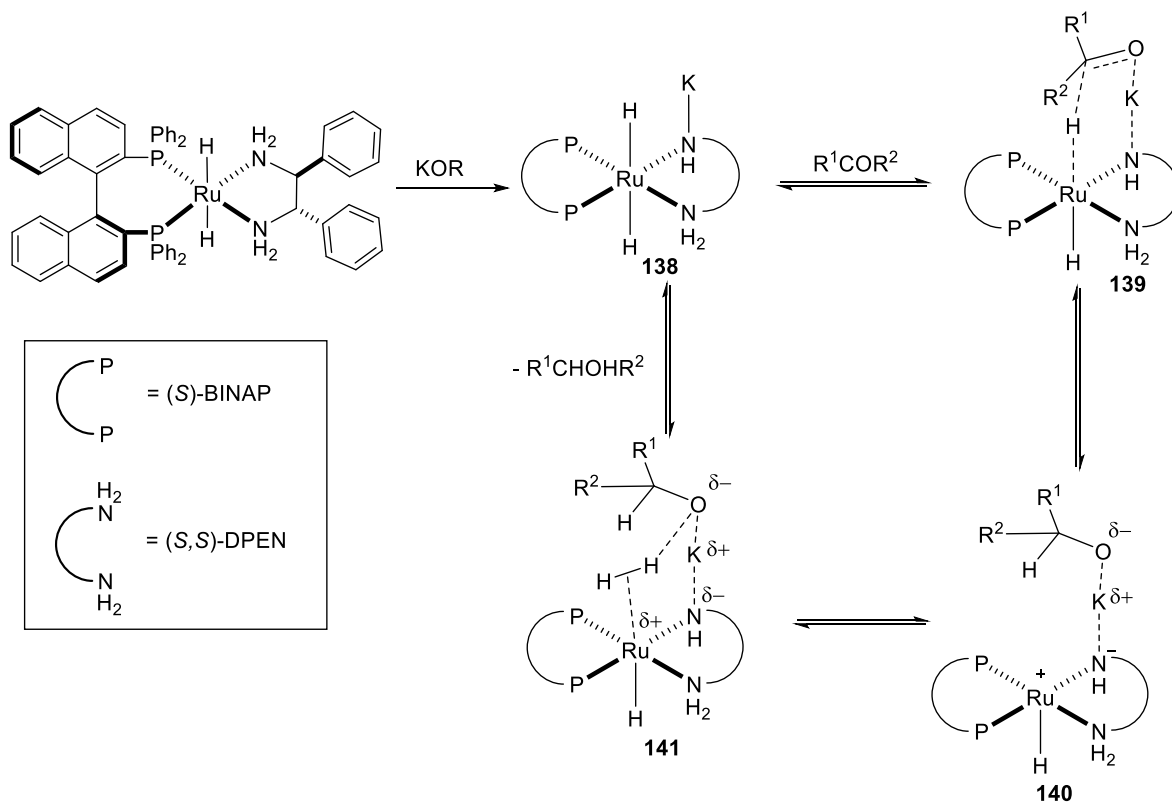
Scheme 3-12. Base-promoted mechanism of ketone hydrogenation catalyzed by Noyori's catalyst, proposed by Chen et al. from product-forming kinetics.[193]

Indeed, later reports implied that an alkali metal is not mandatory in these ketone hydrogenations. For example, Noyori and coworkers[194] reported their catalysts *trans*-RuH(η^1-BH$_4$)(diphosphine)(diamine) (**142**, Scheme 3-13), which catalyzed ketone hydrogenations in the absence of alkali metals in 2-PrOH. Specifically, complex **142** catalyzed the hydrogenation of acetophenone with a TON of almost 100000 (0.001mol% **142**, 45 °C, 8 bar H$_2$, 2-PrOH, 7 h).
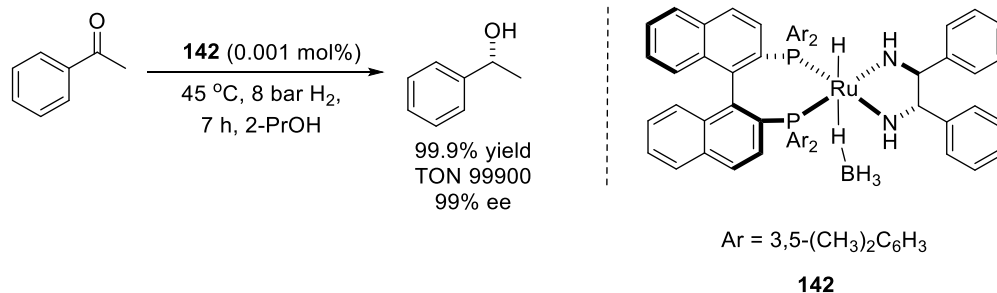
Scheme 3-13. Base-free catalytic system reported by Noyori et al.[194]

A later study[63] proved that 10 mM KO*t*Bu (~24 equiv. to Ru), using a similar catalyst **143** (Scheme 3-14), increased the TOF of a hydrogenation by 25 times (0.05 mol% **143**, 30 °C, 4 bar H_2, 2-PrOH). However, further increases in base concentration decreased the rate. When [KO*t*Bu] was between 20 to 130 mM (50–325 equiv. to **143**), the TOF was only 4~5 times higher than that without base.
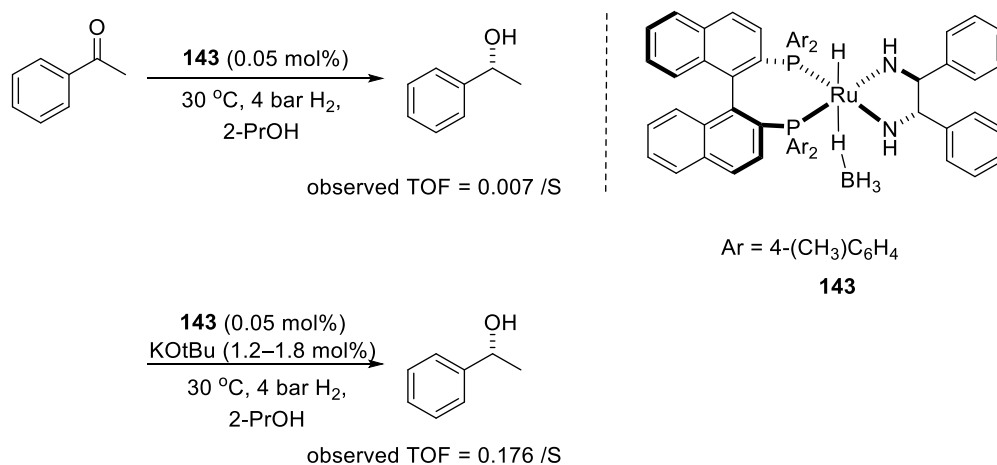
Scheme 3-14. Base-accelerated ketone hydrogenation reported by Noyori et al.[63]

The cation effect was studied by carrying out a ketone hydrogenation with **143** and a phosphazene base (Figure 3-1). In the presence of 1.1 mol% $M^+B(Ph)_4^-$ with different cations M^+ (0.056 mol% **143**, 1.1 mol% phosphazene, 30 °C, 8 bar H_2, 2-PrOH), the TOF was ~2 times higher compared to that in the absence of cations, but there was little difference between the cations. The rate constants with K^+, Na^+, and $(nC_4H_9)_4N^+$ were 40.6, 38.8, and 38.6 $M^{-1}s^{-1}$, respectively. Notably, both the protonated phosphazene base and $(n-C_4H_9)_4N^+$ are not Lewis acids.
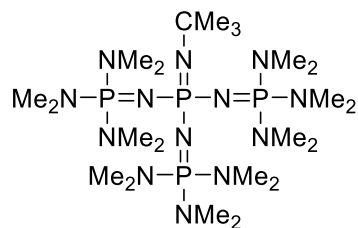
Figure 3-1. The phosphazene base used in Noyori's research.[63]

The authors proposed a mechanism by which the hydrogenation proceeds in two catalytic cycles, as shown in Scheme 3-15. The major difference between them is how the Ru-amide species (**144**) generates the active dihydride species (**148**). In Cycle 1, the amide was protonated to form the cationic species **145** that bonds to H_2 to form **146**. The splitting of H_2 is the rate-limiting process, and it is accelerated by base. However, if the concentration of base is too high, the formation of **145** is inhibited, and the reaction adapts to Cycle 2. In Cycle 2, H_2 coordinates to **144**, followed by the splitting of η^2-H_2 to regenerate the active dihydride species **148**. It is proposed that this pathway is slower than the cationic cycle.
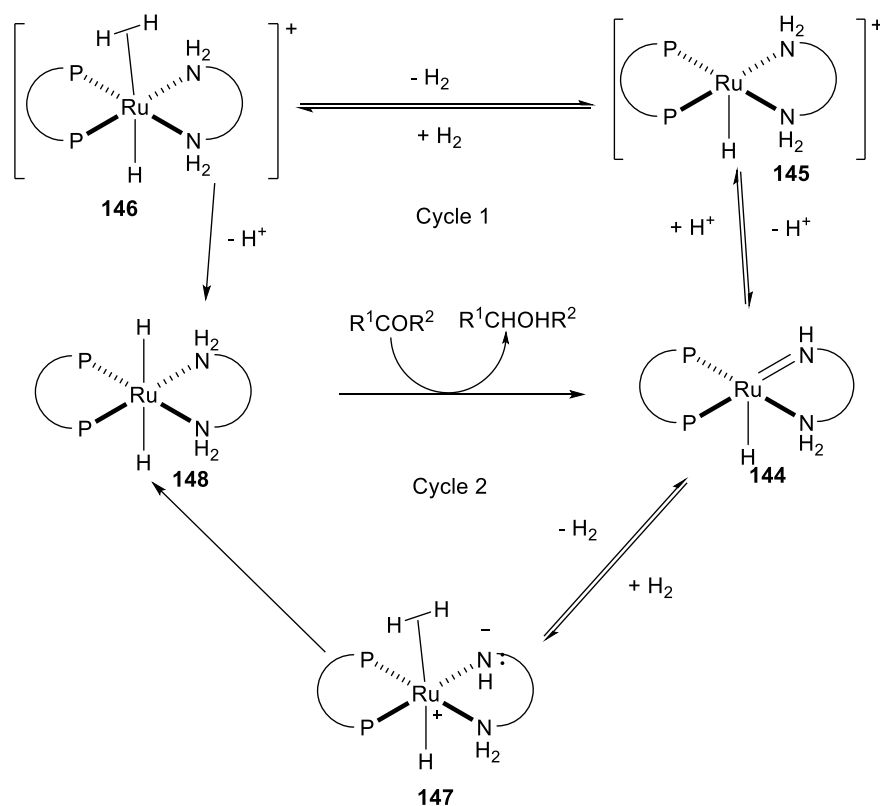
Scheme 3-15. The mechanisms of ketone hydrogenation proposed by Noyori et al.[63]

The research reported by the Morris group[195] showed that for ketone hydrogenations conducted in a protic solvent (2-PrOH, conditions are shown in Scheme 3-16), the TOF is increased ~4 times by the addition of 20 equiv. of KOtBu base.

without base: k = 0.9 M^{-1}s^{-1}
with 5.5 mol% KOtBu: k = 3.8 M^{-1}s^{-1}

Ar = 3,5-(CH$_3$)$_2$C$_6$H$_3$
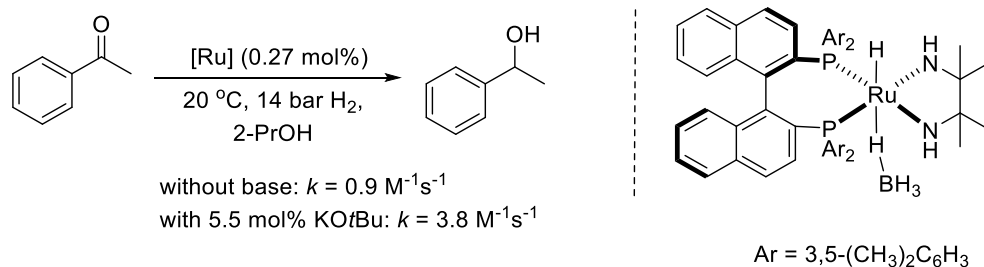
Scheme 3-16. Ketone hydrogenation in 2-PrOH solvent in the presence and absence of base, reported by Morris et al.[195]

The authors proposed that the formation of the putative Ru-alkoxide (**149,** Scheme 3-17) by the reaction between the amide (**144**) and an alcohol (solvent or product) competes with the regeneration of **148** and **144**. It was proposed further that the formation of this alkoxide was suppressed by lowering the acidity of the reaction media upon the addition of base.
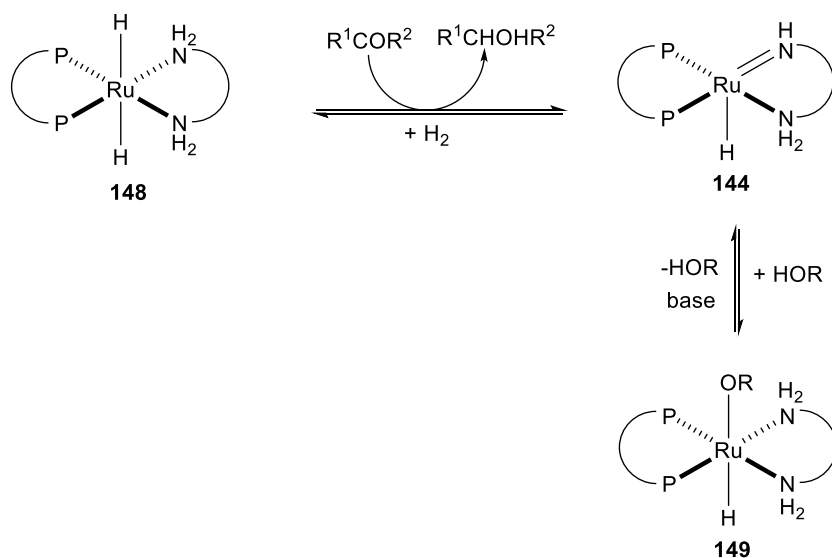
Scheme 3-17. Base-assisted regeneration of Ru amide intermediate proposed by Morris et al.[195]

The first conclusive characterizations of the alkoxide species in the Noyori hydrogenation were reported by Hamilton and Bergens.[186] As shown in Scheme 3-18, *trans-*

Ru((*R*)-BINAP))(H)(2-PrO)((*R,R*)-DPEN) (**151**) forms quickly at -80 °C by either treating *trans*-[Ru((*R*)-BINAP))(H)(η^2-H$_2$)((*R, R*)-DPEN)]$^+$ (**150**) with KO*t*Bu in PrOH, or by reacting the Ru-amide species [Ru((*R*)-BINAP))(H)((*R, R*)-NH(CH(Ph))$_2$NH$_2$)] (analog to **144**), with 2-PrOH in THF. The resultant alkoxide species **151** does not generate the active dihydride species in the absence of base in 2-PrOH at ~rt but quickly forms a hydrogen-bonding species (**152**) when treated with KO*t*Bu, which quickly generates the dihydride species (analog to **148**) even at -80 °C under H$_2$ (probably via the formation of **144**). In fact, **144** is made by reacting **151** with the stronger base ((CH$_3$)$_3$Si)$_2$NK, and **144** reacts quickly with H$_2$ to make **148**. In contrast to Morris' suggestion that **151** and **144** co-exist in equilibrium, the alkoxide formation was favored highly under these base-free conditions, and the dihydride forms in the presence of base.
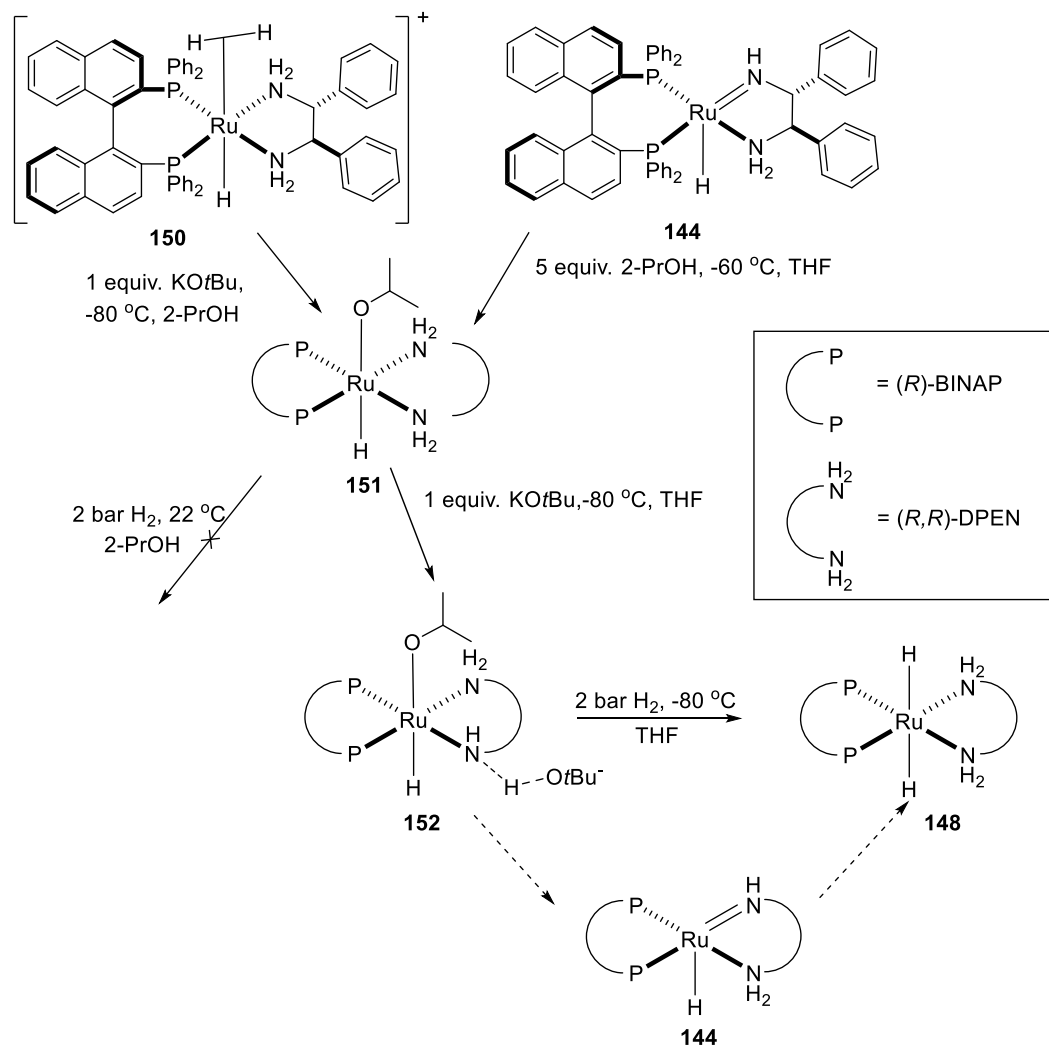
Scheme 3-18. Base-assisted mechanism for ketone hydrogenation reported by Bergens et al.[186]

This competition also was proposed for the hydrogenation of esters and lactones by Bergens' group.[86] The Ru-dihydride **148** underwent the stoichiometric bifunctional addition with γ-butyrolactone at even -80 °C. Product inhibition was observed during catalytic hydrogenations of esters with **148** as catalyst. This inhibition was attributed to the formation of the Ru hemiacetaloxides and Ru alkoxides, which were both observed experimentally, as shown in Scheme 3-19.
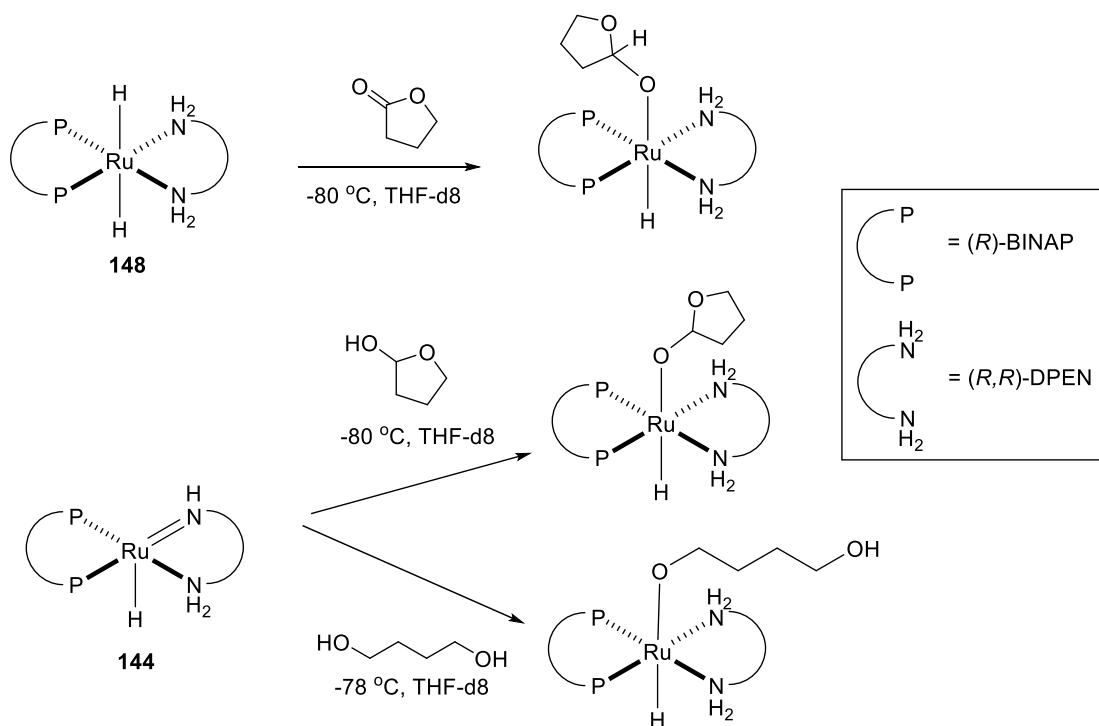
Scheme 3-19. The alkoxide and hemiacetaloxide formation during lactone hydrogenations reported by Bergens et al.[86]

The Bergens group confirmed a base-catalyzed bifunctional addition pathway for the hydrogenation of carbonyl compounds.[91] As shown in Scheme 3-20, the stoichiometric reduction of meso-cyclic imide **153** with the dihydride species **148** occurs in the presence of 0.2 equiv. KOH in THF-d8 at -80 °C to form **154**. However, no reaction was observed in the rigorous absence of KOH. It was found that the dihydride species **148** is deprotonated in strongly basic media to form the highly reactive species **155**. Also, the lone pair on N⁻ is located in the equatorial position, in contrast to the axial deprotonation proposed by Chen et al.[193] Compound **155** reduced imide or amide quantitatively upon mixing, which explains the necessity for the presence of base in the hydrogenation of carbonyls. Although KOH was not sufficiently basic to prepare **155** quantitatively, a lower concentration of **155** likely exists after the addition of KOH, which is responsible for the activity observed in the stoichiometric reduction. The deprotonation of NH to N⁻ increases the electron density of the ruthenium catalyst center, which increases the nucleophilicity of the hydride ligands, leading to a faster hydride addition to the carbonyl group. This research was the first report of the synthesis and characterization of the deprotonated species, and it proved experimentally that the deprotonated species **155** is much more reductive than the dihydride species **144**.

110
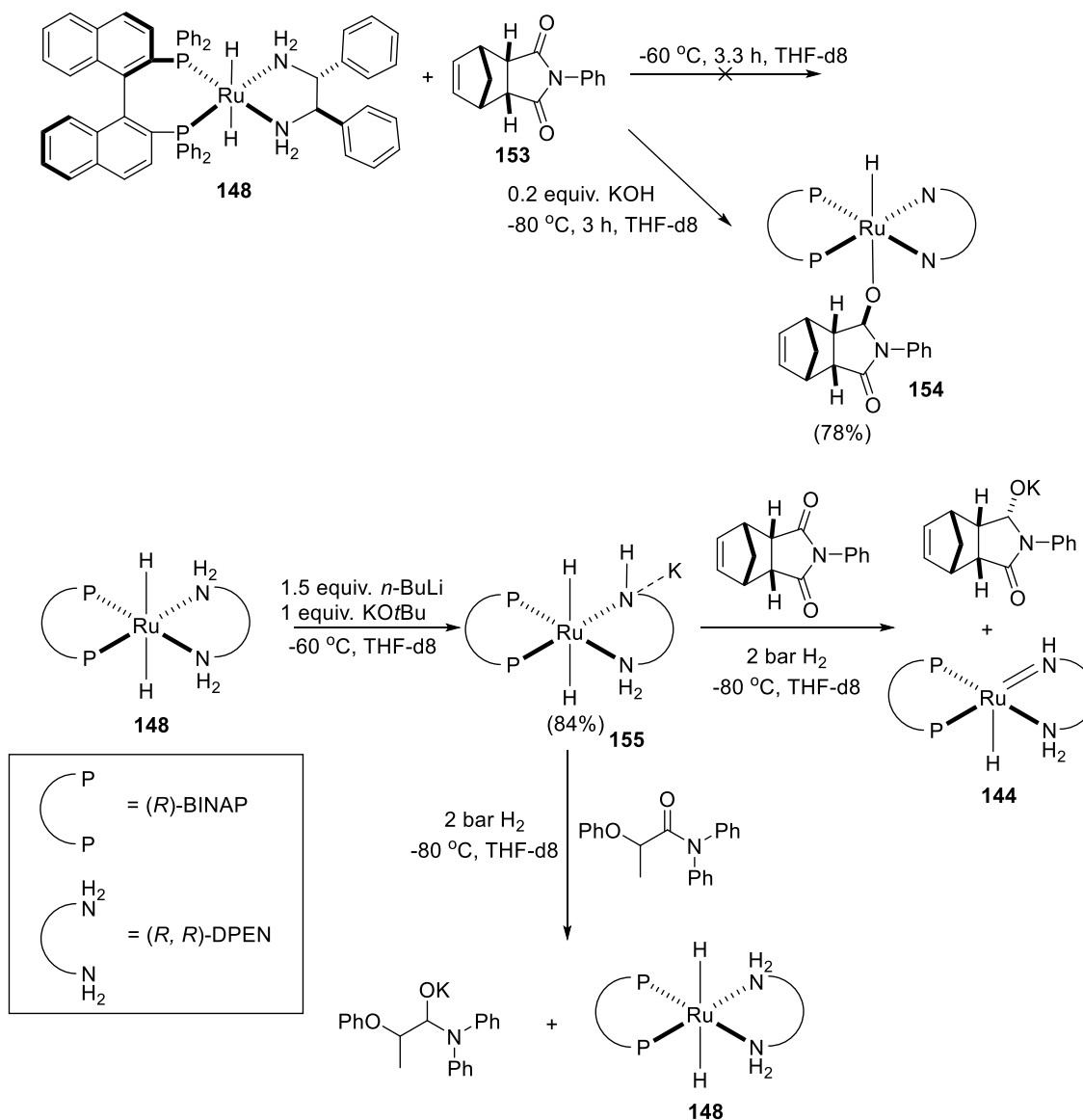
Scheme 3-20. Base-catalyzed bifunctional reduction of imides reported by Bergens et al.[91]

Dub and Gordon also proposed a mechanism for how base improves an ester hydrogenation reaction.[196] They observed that the ^{19}F peak of methyl trifluoroacetate in the ^{19}F NMR shifted upfield slightly and that another broad peak appeared in the spectrum when methyl trifluoroacetate mixed with 0.25 equiv. of NaOMe in MeOH. They speculated that base may activate the substrate via ionic interactions, shown in Scheme 3-21, where Na acts as a Lewis acid, making the carbonyl carbon more electrophilic towards the hydride addition.
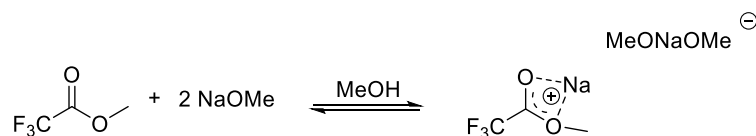
Scheme 3-21. Base-assisted ester activation proposed by Dub and Gordon.[196]

In summary, except for the recent hypothesis proposed by Dub and Gordon, the proposed mechanisms by which added base increases the rate of ester hydrogenations involves a direct reaction between the catalyst and base. The base either: 1) deprotonates a N-H group, thereby rendering the Ru dihydride species more nucleophilic; 2) accelerates activation of a dihydrogen ligand; or 3) decreases the concentration of inactive Ru-alkoxide species by a base-promoted elimination of the alkoxide ligand, also via deprotonation of a N-H group. I believe that the large relative concentrations of base often encountered in high TON and TOF ester hydrogenations are required to compensate for the low concentration of catalyst in these reactions. The requirement for high relative concentrations of base, e.g., KOtBu, adds to the cost and environmental impact of ester hydrogenations. Specifically, the potassium alkoxide must be shipped or prepared on site, purified, and kept rigorously dry before and during the hydrogenation. Further, the requirement for added base constrains the hydrogenation of base-sensitive substrates or products.

Intramolecular reactions are faster than their intermolecular analogs because of higher local concentrations and lower decreases in entropy.[197-200] In the following section, I report the use of alt-ROMP to synthesize a crosslinked, catalyst-base copolymer, in which the catalyst monomer **136** is copolymerized with a monomer containing a base-stable quaternary ammonium ion. The counter anion for the quaternary ammonium salt in the polymer will be exchanged with alkoxide, and the system will be evaluated with ester hydrogenations. The expectation is that the high relative concentrations of the alkoxide base and active ruthenium catalyst in the copolymer will accelerate the ester hydrogenation without the need for large concentrations of base dissolved in solution. Further, while the identity of the alkoxide anions associated with the quaternary sites in the polymer will change as product alcohols are formed by the ester hydrogenation, they will remain electrostatically bound to the polymer. For this reason, the concentration of free alkoxide in solution will be kept to a minimum, and flow reactions can be explored for hydrogenations that form base-sensitive products.

For this research, a spiro-quaternary ammonium ROMP monomer was prepared as a BF_4^-

salt. A monomer containing this group was targeted because a report by Marino and Kreuer[201] compared the stabilities of a large number of quaternary ammonium groups towards decomposition in aqueous base. These authors found that the spiro-quaternary ammonium cation (Figure 3-2) was the most stable among those examined by a large margin.

156
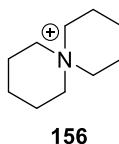
Figure 3-2. A spiro-quaternary ammonium cation with high stability to aqueous base.[201]

Presumably, **156** is resistant to E2-type eliminations of the tertiary amine (Hofmann elimination). Scheme 3-22 illustrates the general design concepts behind this project. The BF_4^- salt of the polymer will be activated by excess alkoxide and hydrogen gas to generate the alkoxide-Ru(dihydride) **157**. Intramolecular deprotonation of an N-H group in the Ru(dihydride) generates the active, anionic catalyst **158**. Based upon our direct observations of related compounds,[91] these species quickly reduce carboxylic acid derivatives to generate the corresponding alkoxides (or hemialkoxides) and neutral Ru-amides (**159**). Alkoxide-alcohol exchange followed by reaction between the Ru-amide and H_2 regenerates the alkoxide-dihydride **158**.
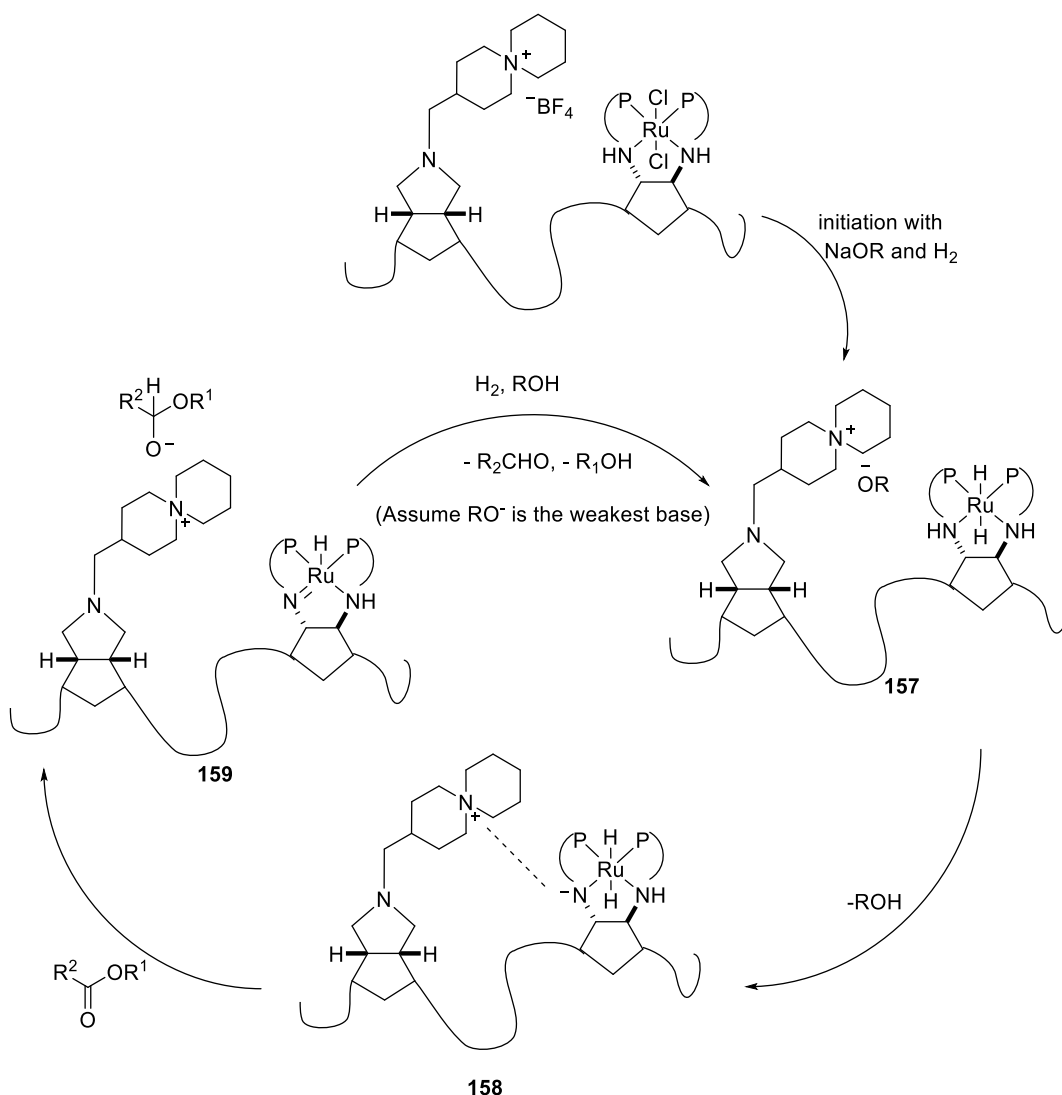
Scheme 3-22. Proposed neighboring base-assisted hydrogenation of esters.

3.2.2 Results and Discussion

Scheme 3-23 shows the synthesis we devised to prepare a ROMP-active monomer, **162**, bearing a spiro-quaternary amine similar to **156**. As expected from the differences in steric size, the condensation reaction between *cis*-5-norbornene-endo-2,3-dicarboxylic anhydride and 4-(aminomethyl)piperidine in acetic acid only occurred at the primary amine group, resulting in quantitative conversion to the *meso*-cyclic imine **160** (isolated yield = 86%). Subsequent reduction of the carbonyl groups with LiAlH₄ formed the *endo*-norbornene-polycyclic diamine **161** in 65% isolated yield. A base-promoted ring-closing dialkylation with 1,5-dibromopentane generated the spiro-quaternary ammonium group (65% isolated yield). Anion metathesis with AgBF₄ afforded the target ROMP-active spiro-quaternary ammonium

monomer **162** as the BF_4^{-1} salt after recrystallization (54% isolated yield).
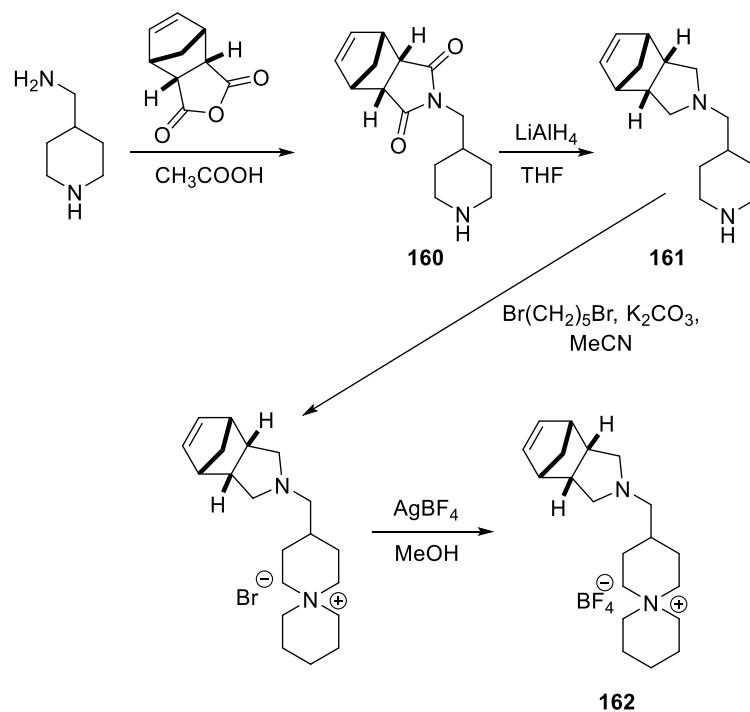
Scheme 3-23. The synthesis of a ROMP-active cationic monomer with quaternary ammonium.

The stability of **162** towards base was evaluated first in dry THF, the typical solvent used for ester hydrogenations. The reaction between **162** and 1 equiv. of KO^{t}Bu (~0.07 M) immediately resulted in a Hofmann elimination, as evidenced by the formation of a new species with a terminal olefin group (Scheme 3-24).
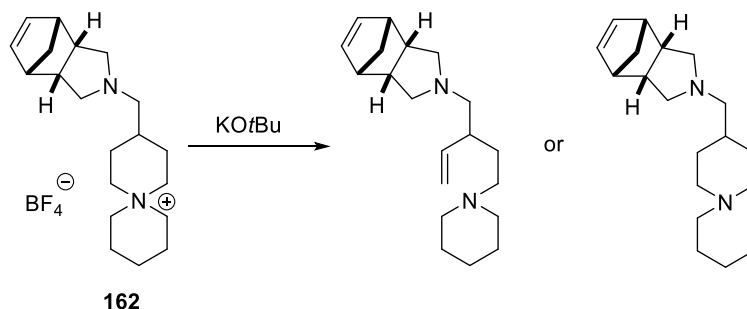
Scheme 3-24. Possible Hofmann elimination pathways for **162**.

Thus, the spiro-quaternary group is unstable towards alkoxide bases in non-protic media. There was no net reaction, however, between **162** and 1 equiv. of KOtBu in the presence

of 20 equiv. of 2-PrOH (rt, overnight). We suspect that **162** was less susceptible to Hofmann elimination in the presence of 2-PrOH because reaction with KO*t*Bu will generate the less basic alkoxide KO*i*Pr, and because alkoxides are generally less basic in protic media than they are in non-protic media.[195] Further, **162** was stable in a THF solution containing 24 equiv. of NaO*i*Pr (~0.5 M) at room temperature overnight. Having found conditions where **162** is stable and that are suitable for ester hydrogenations, I then turned my attention to preparing the copolymer with **136**.

Surprisingly, **162** underwent ROMP polymerization in the absence of COE with 2 mol % 1st generation Grubbs catalyst (**111**) in CD$_2$Cl$_2$ solvent at 40 °C over 23 h. The resulting polycationic polymer precipitated by the end of the polymerization and could not be dissolved in common solvents, including DMSO. Increasing the loading of **111** to 10 %, resulted in much less precipitate at the end of the polymerization. Presumably, increasing the loading of the ROMP catalyst decreased the length of the polycationic polymer, thereby increasing its solubility. Figure 3-3 shows the ^{1}H NMR of polymerization. After 18 h at 40 °C, the spectrum was broadened significantly, and the olefin peak position shifted. We found that the addition of 2-PrOH improved the solubility of the cationic polymer in DCM or chloroform solutions. Having found conditions to polymerize **162**, attention was turned to preparing the copolymer with **136**.
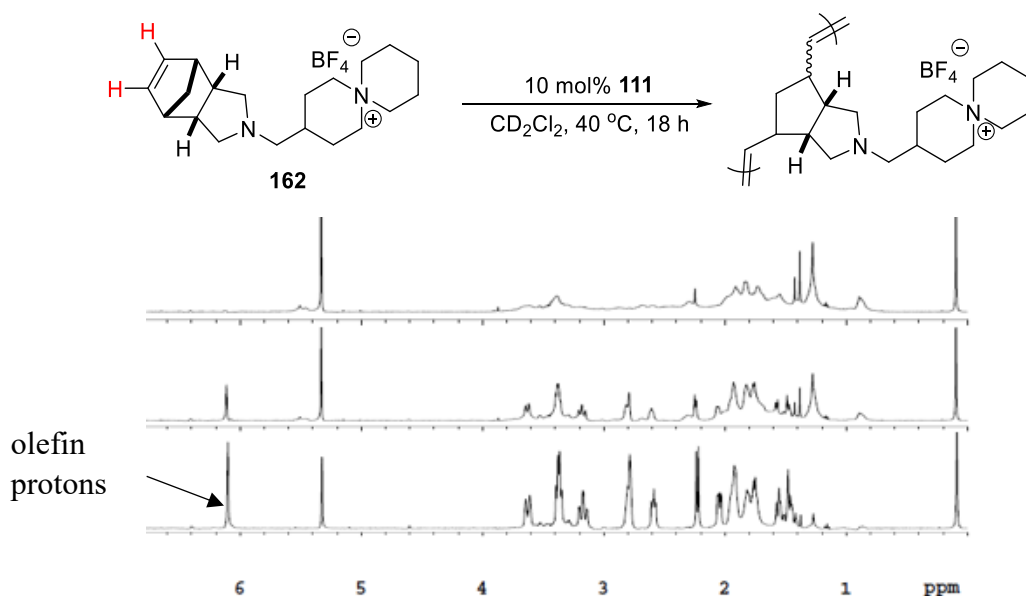
Figure 3-3. ^{1}H NMR spectra of the polymerization of **162** in CD$_2$Cl$_2$ with 10% Grubbs catalyst. Bottom: the monomer spectrum; middle: 1 h at 40 °C; top: 18 h at 40 °C.

An attempt to polymerize a mixture containing **136**, **162**, and 0.1 equiv. **111** (1:3:0.1) in CD$_2$Cl$_2$ at 40 °C without added COE resulted in **162** polymerizing 6–8 times faster than **136**, leaving most of **136** unreacted in solution when **162** was consumed. Polymers containing blocks of **162** or **136** are undesired because the alkoxide needs to be in close proximity to the Ru catalyst centre during ester hydrogenations.

Sequential addition was explored as a method to synthesize a copolymer of **162** and **136** with minimal block segments in the chain. Indeed, the target copolymer could be prepared by sequential addition using 3rd generation Grubbs catalyst (**163**, Figure 3-4).
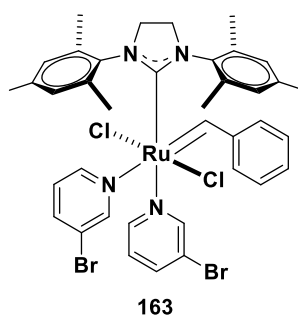
Figure 3-4. 3rd Generation Grubbs catalyst **163**.

Compound **163** was utilized because the rates of initiation are usually higher than the rates of propagation for this catalyst. Further, the catalyst is quite active, with propagation rates that are significantly higher than most ruthenium-based metathesis catalysts.[202, 203] As an illustration, the Grubbs group reported that a variety of norbornene derivatives are polymerized with **163** to form polymers with narrow polydispersity indices (between 1.04 and 1.10).[203] Narrow dispersity polymers form when the rate of initiation is faster than propagation. A sequential addition polymer cannot be prepared with control over the structure unless all or most of the polymer chains initiate first and then propagate at the same slower rate after initiation.

The polymerization was shown in Scheme 3-25. A stock solution containing 10 equiv. of **136**, 20 equiv. of **162**, and 30 equiv. of COE was prepared in CD$_2$Cl$_2$/2-PrOH-d$_8$ (2/1 in volume) solvent. Another solution was prepared containing 1 equiv. of **163** in CD$_2$Cl$_2$/2-PrOH-d$_8$ (2/1 in volume). Both solutions were precooled to -78 °C to prevent polymerization before mixing was complete. The stock solution of **136**, **162**, and COE was added in measured portions to the catalyst solution at -78 °C. The volume of each portion was calculated to contain

117

1 equiv. of **136**, 2 equiv. of **162**, and 3 equiv. of COE. After shaking the vessel at -78 °C, the polymerization solution was allowed to react at room temperature for 15 min. The reaction was monitored with ^{1}H and ^{31}P NMR spectroscopy after the first, second, fifth, eighth, and tenth additions. The reaction was cooled back to -78 °C before each next portion was added. In total, 10 portions were added. As shown in Figure 3-5, the ^{1}H NMR spectrum recorded ~15 min after the first addition showed that the monomers and metathesis catalyst were consumed, proving that **136**, **162**, and COE reacted. Similar observations were made after subsequent additions. As indicated by the ^{1}H NMR spectrum recorded ~15 min after 10th addition, only 1.3 equiv. of **136** (~13% of the total) and negligible amount of **162** remained unpolymerized, illustrating that most of **136** and **162** were polymerized closely within each addition.
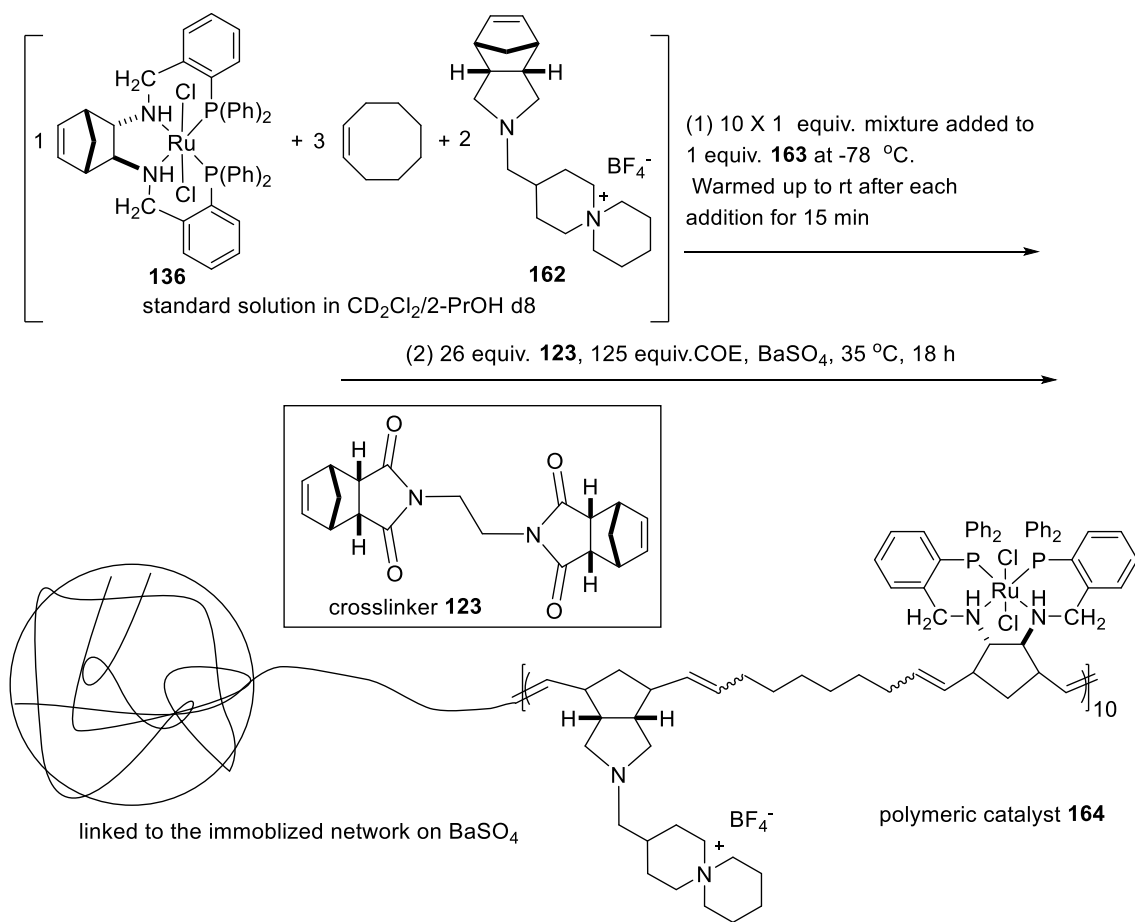
Scheme 3-25. Synthesis of the ROMP copolymer of **136**, **162**, and COE catalyst, supported on BaSO$_4$.
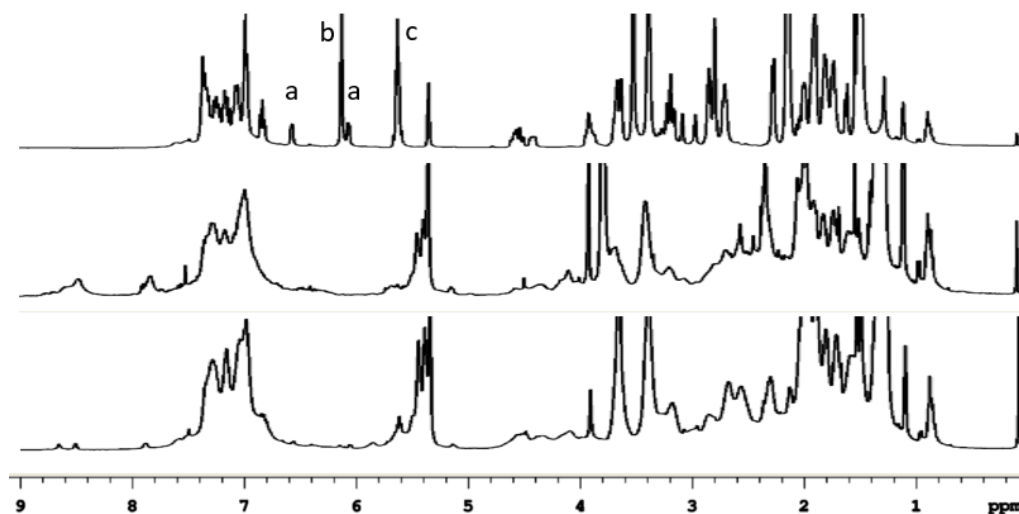
Figure 3-5. The ^{1}H NMR of the sequential addition polymerization; top: stock solution; middle: 1st addition; bottom: 10th addition. Peak a: olefin peaks of **136**; Peak b: olefin peaks of **162**; Peak c: olefin peaks of COE.

The resulting linear copolymer of **136**, **162** and COE was crosslinked with **123** as follows. The resulting linear polymer solution was added to an NMR tube containing 125 equiv. of COE and 26 equiv. of the crosslinker **123**, and this solution was transferred to a Schlenk tube containing BaSO$_4$. Further reaction in the presence of the BaSO$_4$ support at 35 °C for 18 h yielded the supported crosslinked cocatalyst polymer, **164**, which was washed with THF, filtered, and ground with a mortar and pestle. A rough estimation based on the ^{1}H, ^{31}P, and ^{19}F NMR spectra of the wash solution with internal standards indicated that ~14% of the cationic moiety and ~30% of the Ru catalyst leached out during washing. I believe that the leached ruthenium catalyst and cationic moiety mostly consisted of small molecular weight oligomers.

The catalyst **164** was tested in a reusing hydrogenation of methyl benzoate. The first run of the hydrogenation was conducted with excess alkoxide (175 equiv.) in order to initiate the catalyst and exchange the BF$_4^-$ to alkoxide. The second run was carried out in the absence of added base. The third run was carried out with extra base to make a direct comparison with the second run.

As shown in Scheme 3-26, all the hydrogenation runs were carried out with methyl benzoate (4200 equiv. to Ru) in dry THF at rt, 50 bar H$_2$. The first run was carried out with 175 equiv. KO*t*Bu and 1750 equiv. of 2-PrOH. The 2-PrOH was mixed with the KO*t*Bu first to generate the weaker base KO*i*Pr and in the protic medium. After 22 h, the first run gave a TON of 483 (11.5% conv.).

164
(0.024 mol% Ru loading)
50 bar H$_2$, rt, THF, 22 h

1st Run: 4.2 mol% KO*t*Bu
42.6 mol% 2-PrOH

2nd Run: 0 mol% KO*t*Bu
0 mol% 2-PrOH

3rd Run: 4.2 mol% KO*t*Bu
0 mol% 2-PrOH

TON:
1st Run 483
2nd Run 92
3rd Run 1919
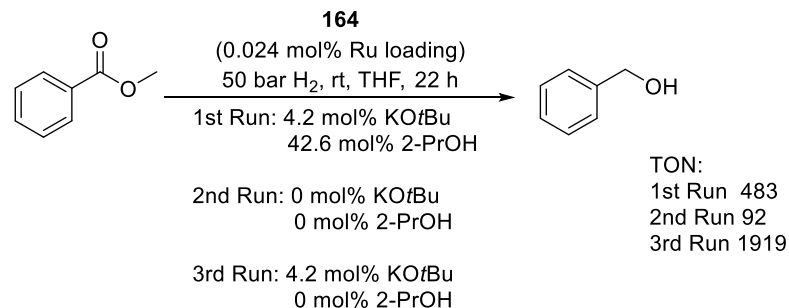
Scheme 3-26. Methyl benzoate hydrogenation with **164**.

After the filtration, the second run was set up with only substrate and solvent and with no base or 2-PrOH. After 22 h, only 2.2% product was present in the filtrate. There were two possibilities that may explain the low turnover of the second run. One possibility is that the neighbouring base in the copolymer did not act as a cocatalyst. The other possibility is that the heterogeneous catalyst was deactivated by the first run. A third run was carried out with the same S/C ratio and with 175 equiv. of KO*t*Bu. The third run produced the product with a TON of 1919 after 22 h at room temperature, proving that the catalyst remained active, and strongly suggesting that the second run did not work because of a lack of accessible base. Unfortunately, these results lead to the conclusion that the neighboring base in the copolymer did not assist the hydrogenation during these exploratory studies.

3.3 Conclusions

This chapter reports the preliminary results from two exploratory projects: 1) In one project, we successfully synthesized the optically enriched RuPNNP catalysts with norbornene backbone and their polymers. These catalysts did not exhibit a promising performance in the enantioselective transfer hydrogenation of ketones or ester hydrogenations via DKR. However, the possibility of finding better substrates for these catalysts is not excluded. 2) In the other project, a neighboring base was introduced to a polymeric ester hydrogenation catalyst. The proposed acceleration of the base moiety did not operate during initial evaluations. Future work will focus on developing other applications of this cationic copolymer. For example, the cationic moiety can be used in the immobilization of the polymer catalyst onto anionic solid supports via electrostatic interaction.

3.4 Experimental Details

3.4.1 General information

Experiments were carried out under N_2 or Ar atmosphere, unless otherwise stated. Solvents were distilled with proper drying agents, as illustrated in Chapter 2. Hydrogenations with single substrate were carried out in a Parr 4750 reactor. Substrate screening hydrogenations were carried out with a customized high-pressure reactor. The ee's were determined using a Hewlett Packard 5890 GC equipped with a 5970B MSD and a Supelco Beta DEX 225 capillary column.

For the chemicals that had been used in Chapter 2, the suppliers were the same as stated in Chapter 2. Other chemicals include: 4-(aminomethyl)piperidine, 1,5-dibromopentane from Sigma Aldrich and L-menthol from Aldrich, thionyl chloride from EMD Millipore corporation, 2-[bis(3,5-dimethylphenyl)phosphino]benzaldehyde from Sigma Aldrich, sodium borohydride from BDH Chemicals, sodium azide from Fisher Scientific.

3.4.2 Syntheses of New Compounds

The synthesis of optically enriched *trans*-2,3-diaminonorborn-5-ene dihydrochloride

Step 1. The preparation of di-(*L*)-menthyl (2*S*,3*S*)-[2.2.1]bicyclohept-5-ene-2,3-dicarboxylate, 127
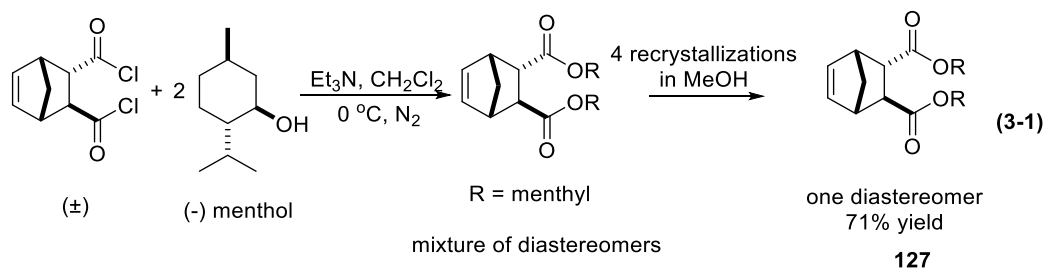
L-menthol (23.1 g, 147.8 mmol) and Et_3N (14.96 g, 147.8 mmol) were dissolved in a side-arm flask with 50 mL DCM. Racemic *trans*-3,6-endomethylene-1,2,3,6-tetrahydrophthaloyl chloride (10.792 g, 49.3 mmol) solution in 100 mL DCM was added dropwise to the flask in an ice bath. The reaction was allowed to warm up to rt and proceed for another 1 h at rt, then the reaction mixture was poured into water, and the organic layer was separated and washed

with water twice. The combined aqueous layer was back-extracted with diethyl ether (2 ×100 mL). The organic solutions were combined and dried over Na$_2$SO$_4$. After filtration and removing the solvent under vacuum, 30.5 g crude product with unreacted menthol was obtained. The resultant mixture was dissolved in 25 mL boiling MeOH, cooled down, and left in a fridge to recrystallize overnight, yielding a white solid after filtration. Another four recrystallizations with boiling MeOH were carried out, and 7.983 g product of one diastereomer was obtained with a yield of 71%. The ^{1}H NMR agrees the literature.[191]

^{1}H NMR (399.794 MHz, CDCl$_3$, 27 °C): δ 0.45–2.09 (38H), 2.68 (1H, m), 3.12 (1H, s), 3.28 (1H, s), 3.37 (1H, m), 4.59 (1H, m), 4.70 (1H, m), 6.04 (1H, m), 6.31 (1H, m).

Step 2. The hydrolysis of 127

127
(*S*, *S*)
(3-2)
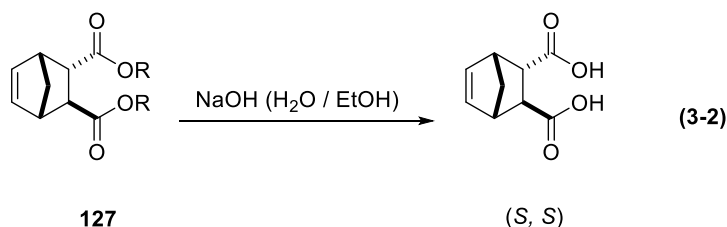
The diester **127** (3.2 g, 7.0 mmol) was hydrolyzed in a solution of NaOH (2.66 g, in EtOH/H$_2$O = 75 mL/29 mL) at reflux temperature for 13 h under N$_2$. The solution was pumped with a rotovap to remove the EtOH, the resultant aqueous mixture was washed with hexanes (5 × 30 mL), and then was acidified at 0 °C with concentrated HCl to pH = 1. This aqueous solution was extracted using diethyl ether (3 × 40 mL). The combined ether layer was dried over Na$_2$SO$_4$, filtered, and pumped to dry, yielding 1.1 g diacid product with a yield of 86%.

^{1}H NMR (399.796 MHz, CD$_3$OD, 27 °C): δ 1.43 (1H, m), 1.60 (1H, m), 2.58 (1H, m), 3.10 (1H, m), 3.22 (1H, m), 3.31 (1H, m), 6.09 (1H, m), 6.28 (1H, m).

Step 3. Converting to acid chloride 128

(*S*, *S*)
(3-3)

128
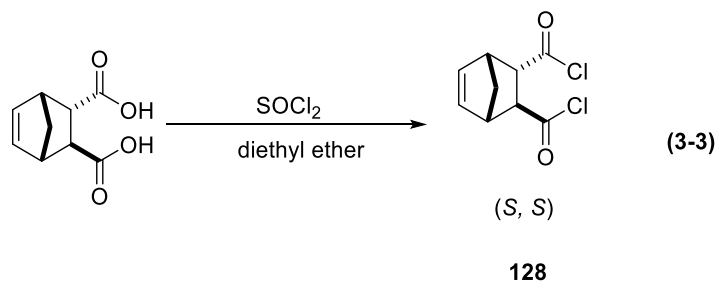
The diacid (1.1 g, 6.0 mmol) was dissolved in 10 mL dry diethyl ether and 22 mL thionyl chloride in a Schlenk tube. The reaction was carried out at rt for 2 days. The ether and excess thionyl chloride were removed using water aspirator vacuum with an acetone/dry ice cold trap. The ^{1}H NMR indicated a conversion close to 100%. The resultant oily diacid chloride product was not taken out of the Schlenk tube but was used directly in the next reaction to prepare the diamine.

^{1}H NMR (498.118 MHz, CDCl$_3$, 27 °C): δ 1.61 (1H, m), 1.67 (1H, m), 3.23 (1H, m), 3.48 (1H, m), 3.58 (1H, m), 3.88 (1H, m), 6.26 (1H, m), 6.41 (1H, m).

(*S,S*)-*trans*-2,3-diaminonorborn-5-ene dihydrochloride (129)

The procedure for the preparations of (*S,S*)-*trans*-2,3-diaminonorborn-5-ene dihydrochloride, was the same as for the racemate compound, **119**, in Chapter 2, with identical NMR spectra and close yields; these are not described again in this chapter.

The Syntheses of the Ligands

(*S,S*)-*N,N′*-bis({(2-diphenylphosphino)phenyl}methylidene)bicyclo[2.2.1]hept-5-ene-2,3-diamine (130)
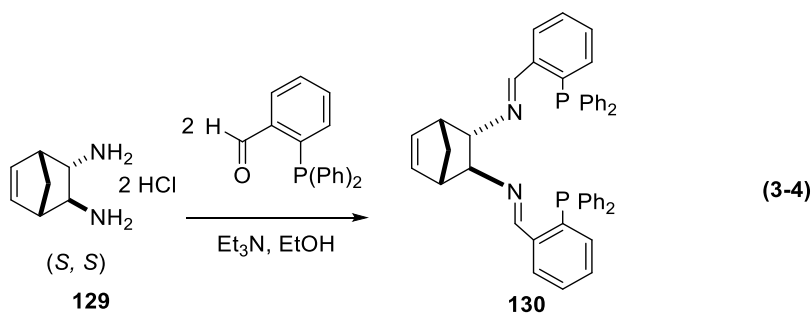
The synthesis of **130** was identical to the racemic analog, **120**, which was reported in Chapter 2.

(*S,S*)-*N,N′*-bis({(3,5-dimethylphenylphosphino)phenyl}methylidene)bicyclo[2.2.1]hept-5-ene-2,3-diamine (131)

(3-5)
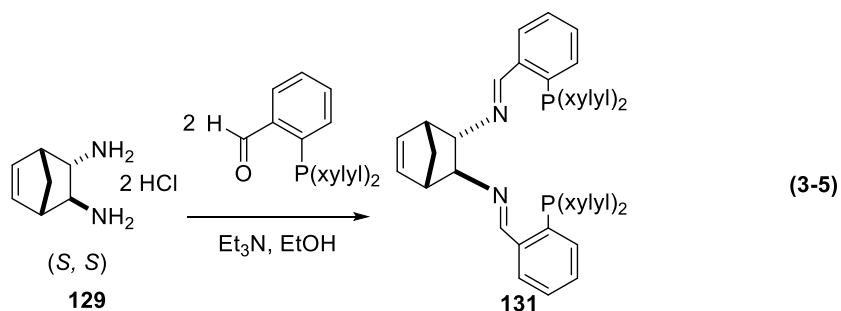
Ligand **131** was synthesized similarly to **130** with a quantitative yield, using 2-[bis(3,5-dimethylphenyl)phosphino]benzaldehyde and **129**.

^{1}H NMR (498.119 MHz, CD$_2$Cl$_2$, 27 °C): δ 1.45 (1H, m, bridging CH), 1.98 (1H, m, bridging CH), 2.17–2.27 (24H, overlapped singlets, CH$_3$), 2.36 (1H, m, CH next to olefin), 2.63 (1H, m, CH next to olefin), 2.90 (1H, m, CH next to imine), 3.48 (1H, m, CH next to imine), 6.04 (1H, dd, J=5.64 Hz, 2.82 Hz, olefin proton), 6.11 (1H, dd, J=5.64 Hz, 3.07 Hz, olefin proton), 6.83–7.81 (20H, aromatic), 8.54 (1H, d, J=3.9 Hz, imine), 8.66 (1H, d, J=4.4 Hz, imine).

^{31}P{^{1}H} NMR (201.641 MHz, CD$_2$Cl$_2$, 27 °C): δ -12.5 (1P, s), -11.6 (1P, s).

(*S*,*S*)-*N*,*N'*-bis{2-(diphenylphosphino)benzyl}bicyclo[2.2.1]hept-5-ene-2,3-diamine) (132)

(3-6)
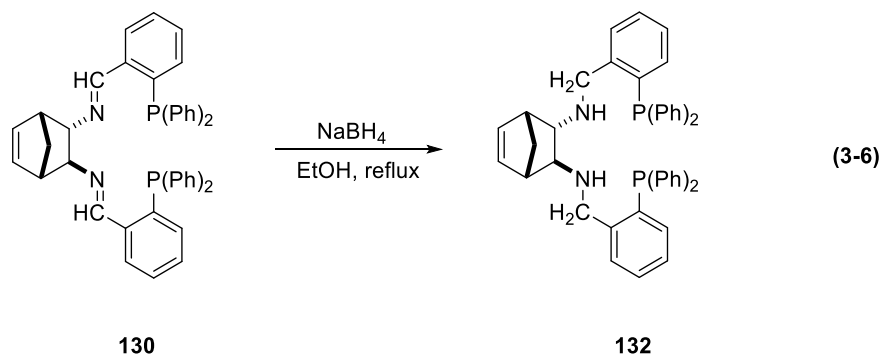
Compound **130** (526 mg, 0.79 mmol) and NaBH$_4$ (14.3 mmol) were heated in refluxing EtOH for 16 h under N$_2$. The reaction was quenched with 15 mL water and extracted with DCM (2 × 10 mL). The combined organic layer was washed with 10% NH$_4$Cl (2 × 10 mL) and water (2 × 10 mL), then dried over Na$_2$SO$_4$. After filtration and pumping, 335 mg product was obtained with a yield of 63%.

^{1}H NMR (498.119 MHz, CD$_2$Cl$_2$, 27 °C): δ 1.38 (1H, m, bridging CH), 1.47 (1H, m, bridging CH), 2.07 (1H, m, CH next to olefin), 2.43 (1H, m, CH next to olefin), 2.66 (2H, m,

CH next to NH), 3.86–3.99 (4H, m, 2 × CH$_2$), 5.91 (1H, m, olefin H), 6.02 (1H, m, olefin H), 6.85–7.53 (28H, aromatic).

^{31}P{^{1}H} NMR (201.641 MHz, CD$_2$Cl$_2$, 27 °C): δ -16.2 (1P, s), -16.0 (1P, s).

(S,S)-N,N'-bis{2-di(3,5-dimethylphenylphosphino)benzyl}bicyclo[2.2.1]hept-5-ene-2,3-diamine (133)
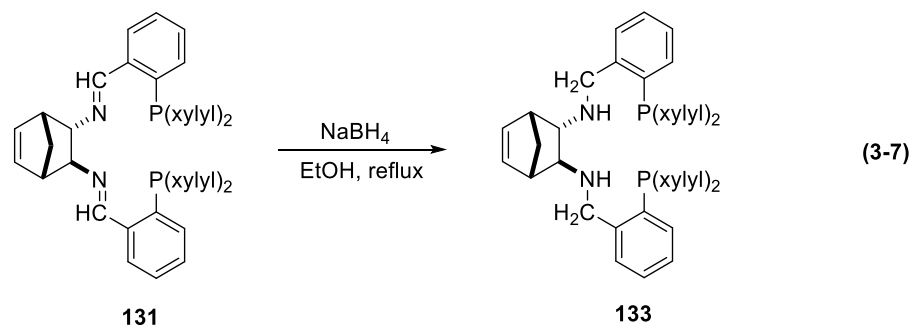
Ligand **133** was synthesized similarly to compound **132** from the reduction of **131**, with a yield of 88%.

^{1}H NMR (498.119 MHz, CDCl$_3$, 27 °C): δ 1.45 (1H, m, bridging CH), 1.51 (1H, m, bridging CH), 2.25–2.31 (24H, overlapped singlets, CH$_3$), 2.40 (1H, m, CH next to olefin), 2.50 (1H, m, CH next to olefin), 2.77 (1H, m, CH next to NH), 2.81 (1H, m, CH next to NH), 3.97–4.07 (4H, m, 2 × CH$_2$), 5.94 (1H, m, olefin H), 6.07 (1H, m, olefin H), 6.89–7.55 (20H, aromatic).

^{31}P{^{1}H} NMR (201.641 MHz, CD$_2$Cl$_2$, 27 °C): δ -16.0 (1P, s), -15.9 (1P, s).

The syntheses of ruthenium complexes

(S,S)-dichloro{N,N'-bis({(2-diphenylphosphino)phenyl}methylidene)bicyclo[2.2.1]hept-5-ene-2,3-diamine}ruthenium (134)
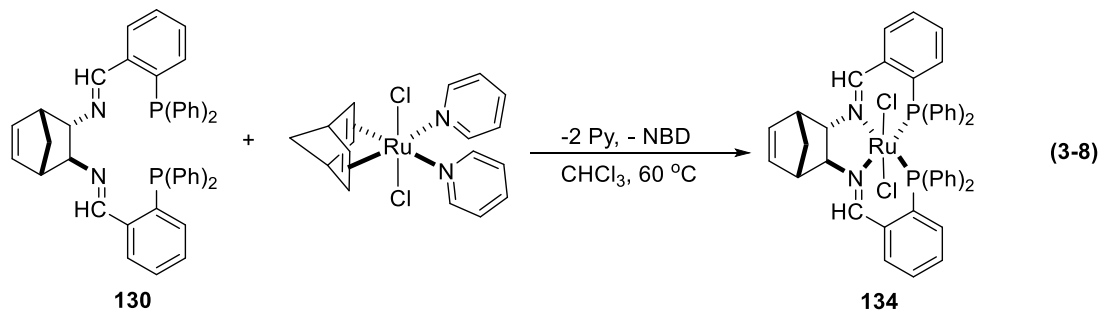
Ligand **134** was synthesized identically to the racemic analog, **121**, reported in Chapter 2.

(*S,S*)-dichloro{*N,N'*-bis({(2-(3,5-dimethylphenylphosphino))phenyl}methylidene)bicyclo[2.2.1]hept-5-ene-2,3-diamine}ruthenium, (135)
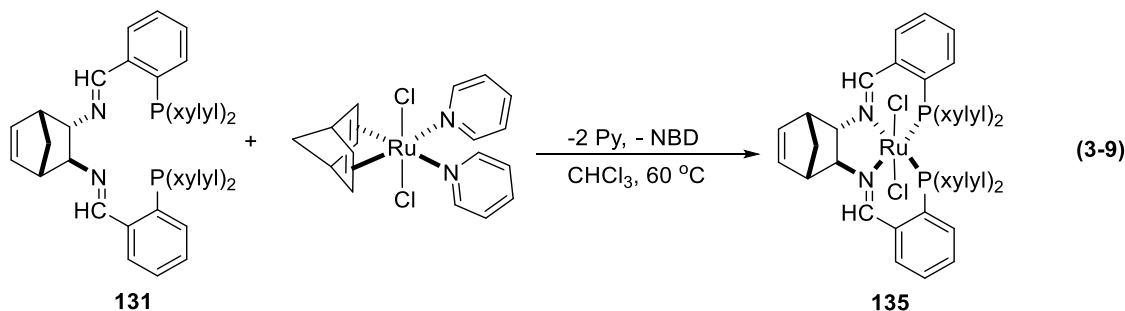
Complex **135** was synthesized similarly to **134**, with a yield of 50.0%.

^{1}H NMR (498.119 MHz, CDCl$_3$, 27 °C): δ 1.96, 1.99, 20.4, 2.10 (12H, s, CH$_3$) 2.25, 2.27 (2H, m, bridging CH), 3.25, 3.31 (2H, m, CH next to olefin), 5.06, 5.62 (2H, m, CH next to imine), 6.38, 6.61 (2H, m, olefin), 6.60, 6.74–7.59 (20H, aromatic), 8.47 (1H, d, *J*= 6.7 Hz, imine), 8.59 (1H, d, *J*= 6.4 Hz, imine).

^{31}P{^{1}H} NMR (201.641 MHz, CDCl$_3$, 27 °C): AB pattern, δ 49.8 (1P, d, *J*$_{pp}$= 27.7 Hz), 47.7 (1P, d, *J*$_{pp}$= 27.7 Hz).

[RuCl$_2$(*N,N'*-bis{2-(diphenylphosphino)benzyl}bicyclo[2.2.1]hept-5-ene-2,3-diamine)] (*S,S*) (136)
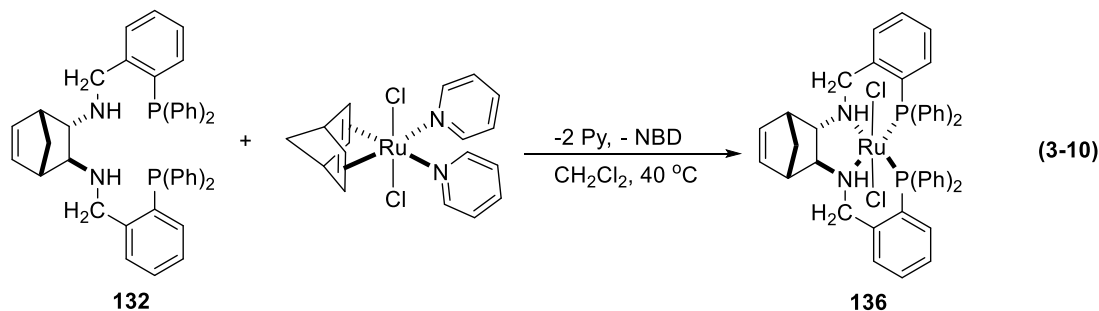
Ligand **132** (335 mg, 0.50 mmol) and RuCl$_2$(NBD)(Py)$_2$ (210 mg, 0.50 mmol) were dissolved in 15 mL DCM, and the solution was heated at 40 °C for 2 days. The reaction mixture was dried under high vacuum, followed by washing with hexanes (3 × 25 mL). The resultant compound was purified by two columns of silica (30 mL and 10 mL by volume, respectively) with DCM as the eluent, and 288 mg pure complex was obtained with a yield of 68%.

^{1}H NMR (498.119 MHz, CD$_2$Cl$_2$, 27 °C): δ 1.88 (1H, m, bridging CH), 2.05 (1H, m, bridging CH), 2.96 (1H, m, CH next to olefin), 3.09 (1H, m, CH next to olefin), 3.26 (1H, m,

NH), 3.68 (2H, m, 2 × CH next to N), 3.86–3.94 (2H, m, 2 × CH*H*), 4.43 (1H, m, NH,), 4.51–4.60 (2 × CH*H*), 6.07 (1H, m, olefin H), 6.57 (1H, m, olefin H), 6.85–7.34 (28H, aromatic)

^{31}P{^{1}H} NMR (201.641 MHz, CD$_2$Cl$_2$, 27 °C): AB pattern, δ 45.3 (1P, d, J_{pp}= 27.7 Hz), 45.7 (1P, d, J_{pp}= 27.7 Hz).

[RuCl$_2$(*N*,*N*'-bis{2-((3,5-dimethylphenylphosphino))benzyl}bicyclo[2.2.1]hept-5-ene-2,3-diamine)] (*S*,*S*) (137)

133   **137**   **(3-11)**
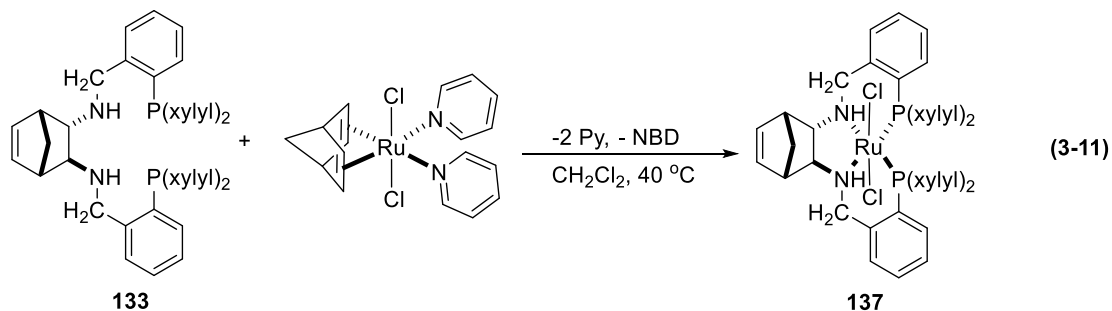
Complex **137** was synthesized similarly to **136**, but with a lower yield of 31.4%. It was likely that **137** decomposes partially on the silica column.

^{1}H NMR (498.119 MHz, CD$_2$Cl$_2$, 27 °C): δ 1.87 (1H, m, bridging CH), 1.95 & 2.06 (24H, overlapped singlets, CH$_3$), 2.04 (1H, m, bridging CH), 2.96 (1H, m, CH next to olefin), 3.08 (1H, m, CH next to olefin), 3.26 (1H, m, NH), 3.68 (2H, m, 2 × CH next to N), 3.87–3.91 (2H, m, 2 × CH*H*), 4.42 (1H, m, NH,), 4.50–4.57 (2 × CH*H*), 6.07 (1H, m, olefin H), 6.56 (1H, m, olefin H), 6.70–7.31 (20H, aromatic).

^{31}P{^{1}H} NMR (201.641 MHz, CD$_2$Cl$_2$, 27 °C): AB pattern, δ 45.6 (1P, d, J_{pp}= 28.7 Hz), 46.1 (1P, d, J_{pp}= 28.7 Hz).

Compounds in Part B

4-(piperidin-4-ylmethyl)-4-azatricyclo[5.2.1.0^{2,6}]dec-8-ene-3,5-dione (160)

^{1}H NMR labeling
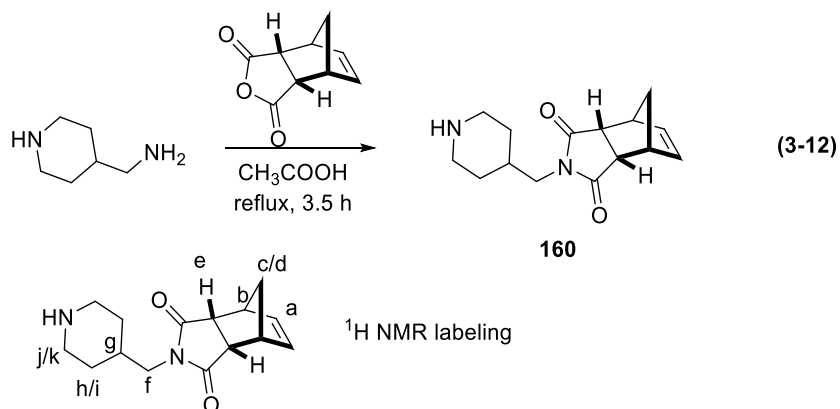
4-(Aminomethyl)piperidine (2105 mg, 18.4 mmol) were weighed into a 3-neck flask charged with a condenser and an additional funnel. A *cis*-5-norbornene-endo-2,3-dicarboxylic anhydride (3023 mg, 18.4 mmol) solution in 30 mL acetic acid was added dropwise into the flask with heating, followed by another 20 mL acetic acid to wash the funnel. After addition, the temperature was brought up to reflux, and the heating was stopped after 3.5 h. As much acetic acid as possible was removed under high vacuum, resulting in an oily crude product with acetic acid residual (7.680 g). The ^{1}H NMR indicated that this conversion was quantitative. To remove the acetic acid, 1780 mg of the crude product was dissolved in 50 mL DCM, then washed with 2.1 M Na_2CO_3 (3 × 60 mL) and water (1× 60 mL). The organic layer was separated and dried over Na_2SO_4. After filtration and pumping, 0.966 g product was obtained with a yield of 86%.

^{1}H NMR (498.119 MHz, CDCl$_3$, 27 °C): δ 1.07–1.15 & 1.54–1.56 (4H, multiplet, H$_{h/i}$), 1.54–1.56 (1H, multiplet, H$_{c/d}$), 1.69 (1H, multiplet, H$_g$), 1.74 (1H, multiplet, H$_{c/d}$), 1.93 (1H, singlet, NH), 2.52 & 3.05 (4H, multiplet, H$_{j/k}$), 3.22 (2H, d, *J*= 7.05 Hz, H$_f$), 3.26 (2H, multiplet, $_e$), 3.39 (2H, multiplet, H$_b$), 6.11 (2H, multiplet, H$_a$).

^{13}C{^{1}H} NMR (125.266 MHz, CDCl$_3$, 27 °C): δ 31.2, 35.1, 44.3, 44.8, 45.8, 46.0, 52.4, 134.6, 177.9.

HRMS (ESI): Calculated: 260.1525; found: 261.1596 (+ 1 H$^+$).

4-(piperidin-4-ylmethyl)-4-azatricyclo[5.2.1.0^{2,6}]dec-8-ene (161)
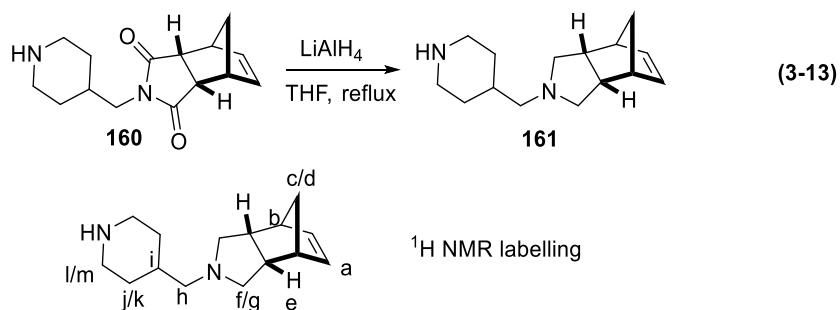
LiAH$_4$ (0.4646 g, 16.6 mmol) was added into a 3-neck flask, followed by 18 mL dry THF. 4-(piperidin-4-ylmethyl)-4-azatricyclo[5.2.1.0^{2,6}]dec-8-ene-3,5-dione **160** (1.052 g, 4.0 mmol) was dissolved in 10 mL THF, then the solution was added through an additional funnel to the same 3-neck flask dropwise over 30 min, and another 5 mL THF was added to wash the additional funnel. The reaction was heated to reflux for 15 min, then allowed to cool to rt and stay at rt for 16 h. The reaction mixture was quenched in an ice bath by dropwise addition of water (0.46 mL), 1 M KOH (0.46 mL), and water (1.38 mL). The mixture was filtered, and the solid was washed with DCM (3 × 20 mL). The combined organic solution was dried over Na$_2$SO$_4$, and 1.032 g crude product was obtained. The crude product was dissolved in DCM/diethyl ether mixture (2 ml/19 ml), then filtered through a filter paper. The resultant solution was pumped to dry, then the solid was dissolved in 30 mL diethyl ether and filtered again. After removing the ether, 602 mg product was obtained with a yield of 65%.

^{1}H NMR (498.118 MHz, CDCl$_3$, 27 °C): δ 1.08 & 1.70 (4H, multiplet, H$_{j/k}$), 1.46 (1H, multiplet, H$_i$), 1.52 (1H, multiplet, H$_{c/d}$), 1.64 (1H, multiplet, H$_{c/d}$), 1.85 (2H, multiplet, H$_e$), 2.16 (2H, doublet, J= 3.23Hz, H$_h$), 2.57 & 3.06 (4H, multiplet, H$_{l/m}$), 2.75 & 2.88 (4H, multiplet, H$_{f/g}$), 2.77 (2H, multiplet, H$_b$), 6.10 (2H, multiplet, H$_a$).

^{13}C{^{1}H} NMR (125.266 MHz, CDCl$_3$, 27 °C): δ 31.0, 31.7, 35.3, 44.8, 46.4, 53.5, 57.1, 62.9, 137.1.

HRMS (ESI): Calculated: 232.1939; found: 233.2013 (+ 1 H$^+$).

Converting 37 to quaternary ammonium bromide, 4-[6-azonia-spiro[5.5]undecyl]-4-azatricyclo[5.2.1.0²,⁶]dec-8-ene-3,5-dione bromide

(3-14)

¹H NMR labelling
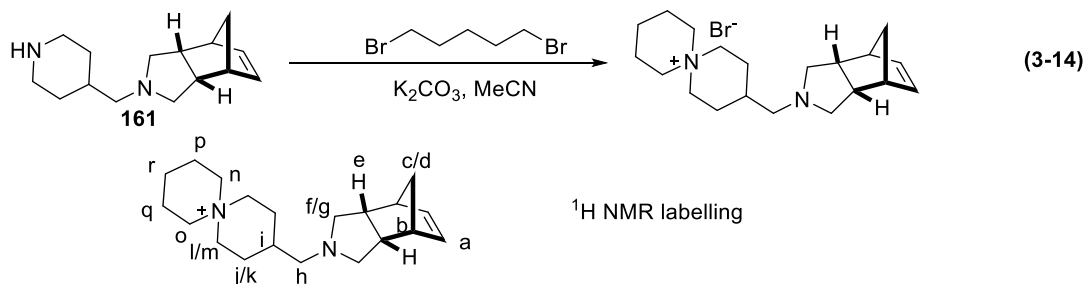
Compound **161** (369.6 mg, 1.6 mmol), K_2CO_3 (1435 mg, 10.4 mmol), 1,5-dibromopentane (366.8 mg, 1.6 mmol), and MeCN (17 mL) were added into a Schlenk tube. The mixture was heated at 80 °C for 20 h, then pumped to dry. The resultant solid was washed with EtOH (15 mL + 15 mL + 5 mL) and DCM (30 mL). The combined organic solution was pumped to dry. The resultant solid was recrystallized with DCM (5 mL) and ether (46 mL), and 396 mg product was obtained with a yield of 65%.

¹H NMR (498.118 MHz, CDCl₃, 27 °C): δ 1.46–1.53 (3H, multiplet, $H_{c/d}$ & one set of $H_{j/k}$), 1.61 (1H, multiplet, $H_{c/d}$), 1.80–2.04 (13H, H_e, H_i, $H_{j/k}$, H_p, H_q, & H_r), 2.28 (2H, doublet, J= 6.96 Hz, $H_{c/d}$), 2.70 & 2.84 (4H, multiplet, $H_{f/g}$), 3.61–3.94 (8H, multiplet, l/m, H_n & H_o), 6.09 (2H, multiplet, H_a).

¹³C{¹H} NMR (125.266 MHz, CDCl₃, 27 °C): δ 19.5, 19.9, 21.2, 24.3, 32.1, 45.0, 46.2, 53.3, 54.2, 57.0, 58.5, 60.6, 63.6, 136.8.

HRMS (ESI): Calculated: 301.2644; found: 301.2637.

Ion exchange to BF₄⁻ salt 38, 4-[6-azonia-spiro[5.5]undecyl]-4-azatricyclo[5.2.1.0²,⁶]dec-8-ene-3,5-dione tetrafluoroborate (162)

(3-15)
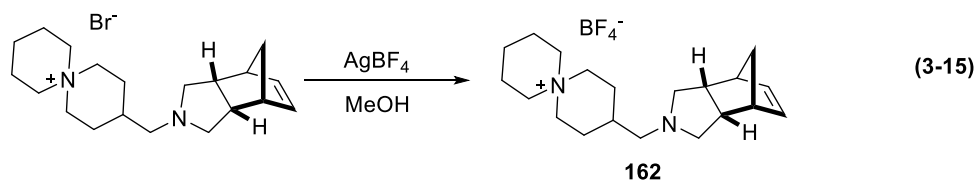
An effort was made to keep the reaction in the dark, to minimize the decomposition of AgBr byproduct. Dark oily impurities were observed during this reaction, and they were removed by filtration and recrystallizations.

As shown in Eq. 3-15, the bromide salt (160 mg, 0.42 mmol) and AgBF$_4$ (83.3 mg, 0.43 mmol) were dissolved in MeOH (10 mL) and stirred for 10 min. The resultant mixture was filtered to remove the precipitate, and the filtrate was dried under vacuum. The resultant solid was recrystallized twice with MeOH/diethyl ether and DCM/diethyl ether, and 88.8 mg solid was obtained after drying, with a yield of 54%.

The ^{1}H NMR and ^{13}C NMR are identical to those of the bromide compound.

^{19}F NMR (376.319 Hz, MeOH-d4, 27 °C): δ -154.3– -154.2 (4F, multiple peaks coupled to ^{11}B and ^{10}B, BF$_4^-$).

HRMS (ESI): Calculated: 301.2644; found: 301.2637.

3.4.3 Other Experiments for Part A

An example of the transfer hydrogenation (with 137 as the catalyst)

In a Schlenk tube under N$_2$, **137** (8.0 mg, 0.0084 mmol) was dissolved in 2-PrOH (8 mL). Acetophenone (200 mg, 1.66 mmol) and KOtBu (0.5 mg, 0.0044 mmol) were transferred into the Schlenk tube with 2-PrOH (7 mL + 1 mL, to a final volume of 16 mL). The tube was sealed, and the reaction was stirred at rt for 19 h. An aliquot was taken, and the solvent was removed by vacuum. The conversion was determined using the ratio between the starting material and the product in the ^{1}H NMR spectra. The ee was determined by chiral GC-MS.

An example of the ester hydrogenation via DKR (with 13P as the catalyst)

The hydrogenation was set up in a customized screening reactor, in which eight reactions can be carried out at the same time under the same pressure and temperature. Eight different ester substrates (0.34 mmol) were weighed into eight test tubes separately, then the tubes were placed into the high-pressure screening reactor and purged with Ar for 20 min. The pre-prepared polymer catalyst solution of **137P** (0.0043 mmol Ru in 0.125 mL CD$_2$Cl$_2$) was added into each tube, followed by a NaOiPr solution (0.085 mmol / mL, 2 mL). The reactor was purged with H$_2$ for 0.5 h, then the reaction was carried out at rt under 4 bar H$_2$ for 24 h. Next, the contents in each test tube were filtered through a florisil plug with DCM. The conversion and ee were determined using ^{1}H NMR and chiral GC-MS, respectively.

3.4.4 Other Experiments for Part B

Preparation of the polymer catalyst with cation

A solvent mixture (1.4 mL CD_2Cl_2 and 0.7 mL 2-PrOH$_{d8}$) and two NMR tubes were prepared: Tube A contained **136** (21.0 mg, 0.0249 mmol), **162** (19.0 mg, 0.0490), COE (8.16 mg, 0.074 mmol), and 1.5 mL solvent mixture. Tube B contained **163** (2.2 mg, 0.00249 mmol). The two tubes were cooled to -78 °C, then 1/10 of the solution in Tube A was transferred into Tube B. Then, Tube B was shaken to mix, left at rt for 15 min, and cooled again before the next addition of Tube A. Another nine additions were carried out in the same manner to consume the solution in Tube A. ^{1}H and ^{31}P NMR spectra were taken after the 1st, 2nd, 5th, 8th, and 10th additions. Crosslinker (23 mg, 0.065 mmol) and COE (34 mg, 0.309 mmol) were added at -78 °C. Then, 14/15 of the solution was shaken and transferred to a Schlenk tube with 5.05 g $BaSO_4$. The Schlenk tube was placed in an oil bath and heated at 35 °C for 18 h, along with the 1/15 solution left in the NMR tube, which was used as a reference. The Schlenk tube was pumped under high vacuum for 1 h at 30 °C, then the catalyst in the Schlenk tube was ground in a glovebox and washed with THF (3 × 15 mL). The wash was pumped to dry, and the residual solid was analyzed by ^{1}H, ^{31}P, and ^{19}F NMR. The leaching of the ruthenium catalyst was ~30%, and the leaching of the cation was ~14%. The ruthenium loading was 0.0032 mmol / g $BaSO_4$.

Catalytic hydrogenation using polymer catalyst with cation

To minimize the moisture content, THF and methyl benzoate were distilled over Na/benzophenone and CaH_2, respectively, followed by passing through 10 wt% Al_2O_3 (neutral, activated), and 2-PrOH was distilled over CaO. After drying, 16 mL methyl benzoate were diluted by THF to a total volume of 80 mL; this served as the stock solution.

The hydrogenation procedure was similar to the reusing hydrogenation described in Chapter 2. The polymer catalyst on $BaSO_4$ (1.39 g, 0.0044 mmol catalyst) was transferred into the high-pressure reactor with the stock solution (11.7 mL, 18.5 mmol ester). KOtBu (85.7 mg, 0.77 mmol) was reacted with 2-PrOH (456 mg, 7.6 mmol), then the resultant solution was transferred to the reactor. The reactor was sealed, pressurized to 50 bar H_2, and the reaction was carried out for 22 h with stirring. The first run was stopped, and the reaction mixture was filtered with the catalyst remaining in the reactor, then another 11.7 mL stock solution was added under H_2 to set up the second run without extra base. After the filtration of the second

run, the third run was set up by adding stock solution (11.7 mL, 18.5 mmol ester) and KO*t*Bu (87.7 mg, 0.78 mmol). After each run, an NMR of the aliquot with 1,3,5-trimethoxybenzene as the internal standard. Conversion was calculated based on the ratio between each compound. TON = 4200 × conversion.

Chapter 4

Glancing Angle Deposited Ni Nanopillars Coated with Conformal, Thin Layers of Pt by a Novel Electrodeposition: Application to the Oxygen Reduction Reaction

4.1 Introduction

4.1.1 Fuel Cell

A fuel cell is a device that converts the chemical energy from the oxidation of fuels directly into electricity via electrochemical processes.[204] A schematic diagram of a H_2/O_2 fuel cell with an alkaline electrolyte is shown in Figure 4-1. The fuel, H_2, is oxidized to protons and electrons at the anode. The released electrons travel through the external circuit to the cathode, where oxygen is reduced to HO^-. The electrolyte between the anode and cathode transports hydroxide and separates the fuel and oxidants. Fuel cells are classified generally based upon their electrolytes.[205] Common types of fuel cells include proton exchange membrane fuel cells, alkaline membrane fuel cells, solid oxide fuel cells, phosphoric acid fuel cells, etc.[204]

The only emission by a H_2/O_2 fuel cell is water, so there are no concerns with fuel cells regarding air pollution and CO_2.[206, 207] The efficiency of a fuel cell is generally higher than that of a combustion engine as it is not limited by the Carnot cycle. In addition, the operation of a fuel cell can be much quieter and requires fewer moving parts than a combustion engine.[208, 209] These advantages make fuel cells good candidates for a variety of applications, such as power stations, vehicles, and portable devices.[210, 211]

The first fuel cell was constructed in the late 1830s when Grove and Schönbein

---

demonstrated the principles with H_2/O_2 electrochemical cells.[212, 213] Almost a hundred years later, the first fuel cell for practical use was developed by Francis Thomas Bacon (a direct descendant of Francis Bacon, the famous 16th century philosopher). Fuel cells drew more attention after their application in NASA's Gemini and Apollo programs in the 1960s.[214, 215] With the developments in catalysis, electrolytes, fuel sources, and system engineering, fuel cells are becoming cheaper, more efficient, and more commercially applicable. The first fuel cell powered vehicle model available for consumers was manufactured by Honda in 2007.[216] According to the 2016 Fuel Cell Technologies Market Report released by the US Department of Energy,[217] more than 62000 fuel cell systems were shipped worldwide with above 500 MW output in 2016, and the market is growing rapidly.
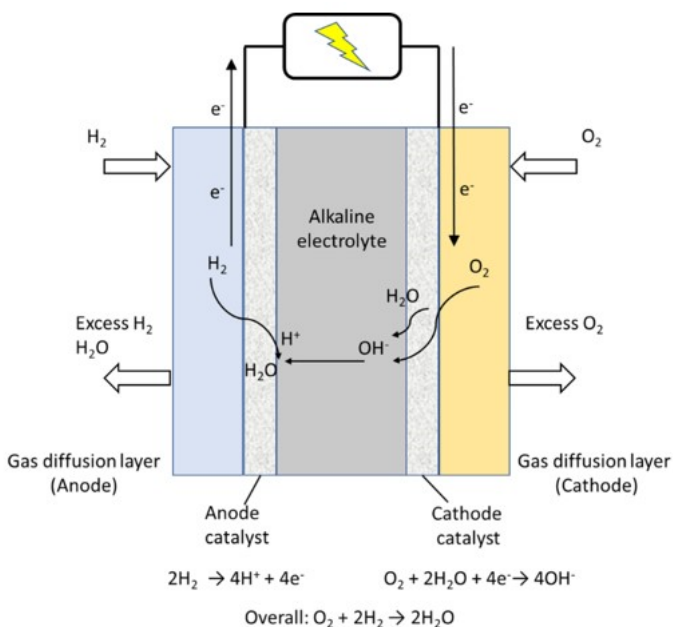
Figure 4-1. Schematic of a typical hydrogen–oxygen fuel cell with an alkaline electrolyte.

4.1.2 Oxygen Reduction Reaction (ORR) and Pt-based Catalysts

The half reactions at the anode and cathode of a fuel cell depend on the type of electrolyte and fuel. This dissertation is focusing only on polyelectrolyte membrane fuel cells with H_2 or alcohols fuels. The interested reader is directed to recent review papers.[218-222]

For H_2/O_2 fuel cells with proton exchange membranes, the reactions are as follows:[204]

Overall: $H_2 + 1/2\ O_2 \rightarrow H_2O$

Anode: $H_2 \rightarrow 2\ H^+ + 2\ e^-$

Cathode: $1/2\ O_2 + 2\ e^- + 2\ H^+ \rightarrow H_2O$
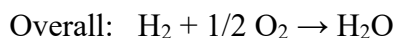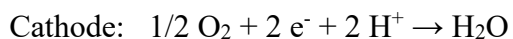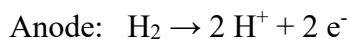
If the fuel cell is operating with a hydroxide exchange membrane, the reactions are:[204]

Overall: $H_2 + 1/2\ O_2 \rightarrow H_2O$

Anode: $H_2 + 2\ OH^- \rightarrow 2\ H_2O + 2\ e^-$

Cathode: $1/2\ O_2 + 2\ e^- + H_2O \rightarrow 2\ OH^-$
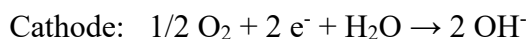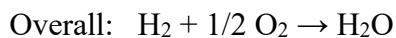
  To date, Pt-based catalysts remain the most active for the cathode half reaction in fuel cells.[223] The reduction of oxygen is the kinetically limiting process of H_2/O_2 fuel cells, and the cathode requires more Pt than the anode.[224] Thus, numerous studies have been dedicated to improving the efficiencies or lowering the costs of ORR catalysts. Commercially available Pt catalysts commonly are made by dispersing Pt onto carbon black materials.

  It is recognized widely that ORR may occur via two pathways: the complete 4-electron pathway and the incomplete 2-electron pathway.[225] Table 4-1 summarizes these pathways.

Table 4-1. ORR Pathways in Acidic or Alkaline Media.[225]

Electrolyte	Reaction	E^0 (V)
Acidic	4-e⁻ pathway: $O_2 + 4\ H^+ + 4e^- \rightarrow 2\ H_2O$	1.229
	2-e⁻ pathway: $O_2 + 2\ H^+ + 2e^- \rightarrow H_2O_2$	0.695
	$H_2O_2 + 2\ H^+ + 2e^- \rightarrow 2\ H_2O$	1.776
Alkaline	4-e⁻ pathway: $O_2 + 2\ H_2O + 4e^- \rightarrow 4\ OH^-$	0.401
	2-e⁻ pathway: $O_2 + H_2O + 2e^- \rightarrow HO_2^- + OH^-$	-0.076
	$HO_2^- + H_2O + 2e^- \rightarrow 3\ OH^-$	0.878

  The 4-electron reduction pathways are preferred because of their higher efficiency.[226] The 4-electron pathway for ORR is heavily studied in the literature. Due to the complexity of the ORR process and the limitations of surface characterization techniques, the mechanism of ORR still is not understood fully on the molecular level.[224, 227] Nevertheless, DFT calculations provide valuable insights into the detailed process of the ORR. Nørskov and coworkers[228]

studied the pathways of ORR on Pt (111) surfaces in acid media. Based upon their calculations, three pathways, called the "dissociative", "associative", and "peroxo" mechanisms, were proposed. Those pathways were studied further by Keith and Jacob,[229] as shown in Figure 4-2.
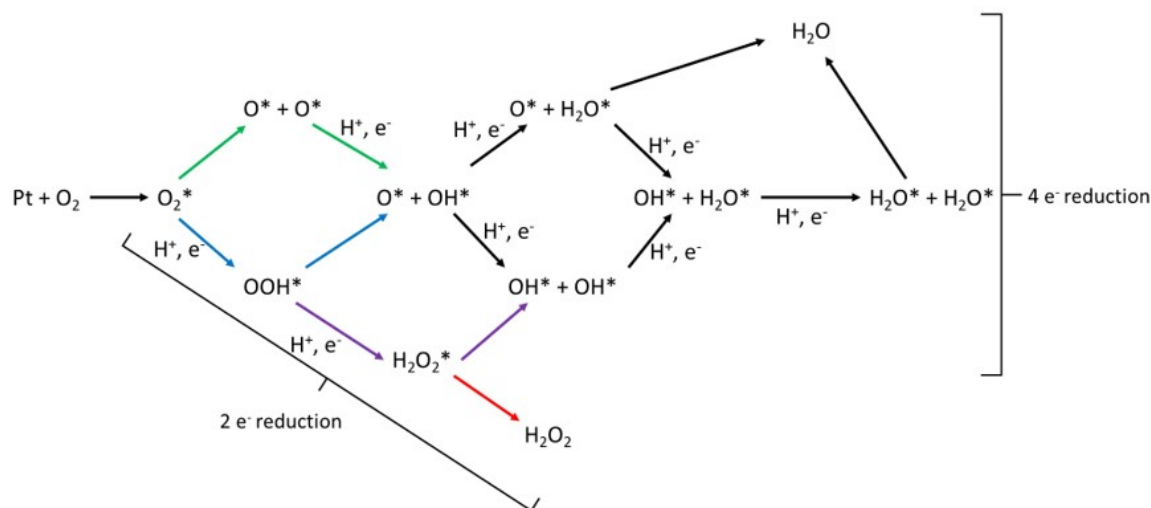
Figure 4-2. The mechanism of ORR under acidic conditions. "*" represents the adsorption of a species onto the surface.[229]

The reduction starts with the binding of O_2 on to the surface of Pt, forming O_2*. In the dissociative mechansim, represented by green + black arrows, the O_2* dissociates to O* first, then the O* combines with a proton and an electron to form OH*. The OH* may combine further with protons and electrons to form H_2O*, which is released from the Pt surface. In the associative mechanism, O_2* forms OOH*, shown with blue arrows. In the peroxo mechanism, shown with purple arrows, the OOH* in the dissociative mechanism is reduced by a proton and an electron to H_2O_2*, which then splits to two OH*. A branched 2-electron reduction may occur, in which the H_2O_2* species escapes from the Pt surface, as represented by the red arrow.

A "volcano plot" was reported by Nørskov and coworkers by plotting the ORR activity of different metals with respect to their calculated oxygen binding energies.[228] It indicated that, to obtain good activity, the binding between the catalyst surface and oxygen should be neither too strong, which would block the dissociation of oxygen species, nor too weak, which would affect the interaction between O_2 and the catalyst surface. It suggested that Pt is the best single metal candidate for catalyzing ORR, but a 0.2 eV decrease with respect to the oxygen binding energy of Pt will lead to the optimum energy profile of an ORR catalyst. This goal in catalyst

design can be achieved by the synergy of Pt and other metals in Pt alloy catalysts.

Numerous results[230-234] have proven experimentally that certain Pt alloys have superior ORR activities to bare Pt/C catalysts. More intrinsically, the band theory describes the energy diagram of electrons in solid state substances, which is applied also to analyze the behavior of ORR catalysts.[235-237] As shown in Figure 4-3, when an oxygen species is adsorbed onto the catalyst surface, the d-band of the catalyst hybridizes with the σ orbital to form a bonding state and an antibonding state. The position of the d-band center with respect to the Fermi level of a catalyst is the key parameter in this evaluation. A higher (or lower) d-band center results in a less (or more) occupation of the antibonding states, which means a stronger (or weaker) binding between the adsorbate and the catalyst surface. The d-band theory helps to find the optimum composition and morphology of a catalyst to approach the ideal oxygen binding energy of a catalyst.
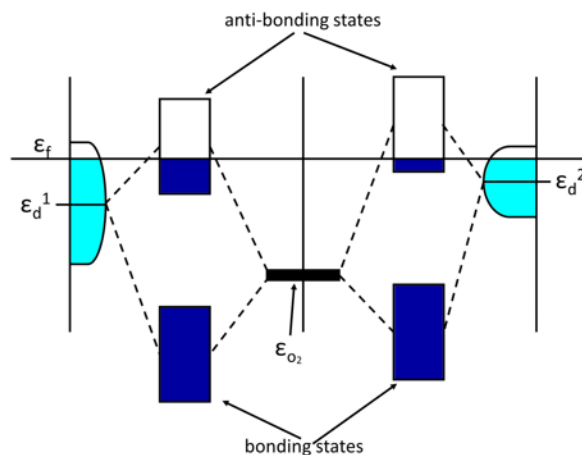
Figure 4-3. Schematic representation of the coupling of an O_2 adsorbate level (ε_{O2}) with a lower d-band center (ε_d^1) or a higher d-band center (ε_d^2) of a catalyst. Less filling of the anti-bonding state indicates a stronger binding between O_2 and the catalyst, in other words, higher binding energy in the "volcano plot". [235-237]

A benefit of the d-band theory is that the d-band center can be measured experimentally by photoemission spectroscopy. Nørskov and coworkers[238] studied different Pt-based alloy compositions with both experimentally measured ORR activity and the predicted ORR activity, based on the DFT simulation and the experimentally measured d-band center. The simulated activities of Pt_3Ti, Pt_3Fe, Pt_3Co (the subscript indicates the composition) exhibit excellent agreement with the measured activities of these alloys, whereas the simulated activity

of Pt_3Ni is significantly higher than the experimental results. Although they do not match perfectly, the d-band theory has been successful in providing important hints for the search of catalysts that are more active than Pt.

Two parameters commonly are used to evaluate the performance of a Pt-based catalyst for ORR:

1) The specific activity (mA cm^{-2}), which is the current density at a certain potential normalized to the electrochemical active surface area (ECSA) of a catalyst. The ECSA commonly is obtained by hydrogen underpotential deposition or CO-stripping.[239] Specific activity reflects the intrinsic activity, guiding the optimization of the composition and surface structure of a catalyst.

2) The mass activity (A mg^{-1}), which is the current at a certain potential normalized to the Pt (or other precious metal, if applicable) loading of a catalyst. This number provides an economic evaluation of a catalyst, which is particularly important for the catalyst implementation. Mostly, these two parameters are obtained at 0.9 V_{RHE} (RHE = reversible hydrogen electrode). Pt alloy catalysts often show improvement over Pt catalyst in both the specific activity and the mass activity of the resultant catalyst. This strategy to prepare highly active catalysts with low Pt loading has been discussed widely in the literature.

The relationship between the ORR activity and the electronic structure of Pt_3Ni was studied extensively by Stamenkovic, Markovic, and coworkers.[233] Three low-index surfaces (111), (100), (110) of Pt_3Ni and pure Pt were investigated. The Pt atom is dominant in the surface of a Pt_3Ni material, and the bulk ratio between Pt and Ni is balanced by the Pt depletion in the next few layers inside. Thus, for example, $Pt_3Ni(111)$ and pure $Pt(111)$ have the same top-layer composition; however, their electronic structures are influenced greatly by the underlying layers. Based on the DFT calculations, the d-band center of $Pt_3Ni(111)$ has a downshift of 0.34 eV compared to $Pt(111)$, resulting in a weaker binding with oxygen species. This relationship was investigated experimentally. Specifically, the fractional coverage of $Pt_3Ni(111)$ by OH at 0.9 V_{RHE} was ~50% less than $Pt(111)$ in 0.1 M $HClO_4$ at 60 °C . The ORR rate of $Pt_3Ni(111)$ was accelerated greatly by the weaker adsorption of OH on Pt. The specific activity of $Pt_3Ni(111)$ is ~10 times higher than that of $Pt(111)$ (measured at 0.9 V vs RHE in 0.1 M $HClO_4$ solution, 60 °C). The comparison between different surfaces of Pt_3Ni indicated that the $Pt_3Ni(111)$ has better activity than $Pt_3Ni(110)$ and $Pt_3Ni(100)$; this was

attributed to the structure-sensitive adsorption behavior between Pt and oxygen-containing species. This report, both experimentally and theoretically, demonstrated that a $Pt_3Ni(111)$-rich morphology is a desired structure in the catalyst design of ORR.

Carpenter and coworkers[240] reported a method to synthesize PtNi nanoparticles (NPs) by reducing $Pt(acac)_2$ and $Ni(acac)_2$ in DMF at 200 °C. NPs with different compositions were obtained by tuning the ratio between the Pt and Ni precursors. The best catalyst was Pt_1Ni_1, whose specific activity reached 3.0 mA cm^{-2}, and whose mass activity reached 0.68 A mg^{-1} in 0.1 M $HClO_4$.

The Strasser group[232] prepared PtNi nanoparticles (NPs) using a similar method by heating $Pt(acac)_2$ and $Ni(acac)_2$ in DMF at 120 °C for a controlled time, followed by adding the Vulcan XC-72 carbon support. The near surface compositions of the resultant NPs were controlled by the reaction time. The best catalyst was obtained after 42 h heating, with a near surface of 41 at.% (percent of atom) of Pt. The specific activity of this catalyst reached 3.14 mA cm^{-2}, and the mass activity reached 1.45 A mg^{-1}, which are both more than 10 times higher than the commercial Pt/C catalysts. In a later study,[241] the same group synthesized three octahedral PtNi NPs with different bulk ratios ($Pt_{1.5}Ni_1$, Pt_1Ni_1, $Pt_1Ni_{1.5}$). They found that Pt was enriched in the edges and corners of the NPs, whereas Ni atoms are segregated in the (111) facet of the NPs. The resulting NPs on the Vulcan carbon support exhibit excellent initial activity, which could be improved further by dealloying in 0.1 M $HClO_4$ with 25 cycles potential sweep between 0.06 and 1.0 V_{RHE}. The dealloying process electrochemically changed the composition and structure of a catalyst by dissolving the metal atoms on the surface, resulting in octahedral nanoparticles with Pt-rich concave surfaces. The highest specific activity was ~3.8 mA cm^{-2}, with a mass activity ~1.7 A mg^{-1} obtained from the catalyst with Pt_1Ni_1 ratio. The authors attributed this exceptional activity to the maintained octahedral structure with Pt(111) facets as well as the underlying Ni providing favored electronic effects.

PtFe and PtCo nanowire catalysts were reported by Stamenkovic, Sun, and coworkers.[231] PtFe catalysts are more active than PtCo catalysts. PtFe nanowires (NWs) were synthesized by reducing $Pt(acac)_2$ in a solution of 1-octadencene and oleylamine in the presence of $Fe(CO)_5$ at 115 °C. The resulting NWs were 2.5 nm in diameter and 30–100 nm in length. Using the seed-mediated growth method, the 2.5 nm NWs further grew to 6.3 nm in a solution of $Fe(CO)_5$, $Pt(acac)_2$, 1-octadencene, oleylamine, and oleic acid at 240 °C. The resultant NWs

were dispersed on a carbon support (Ketjen EC-300J). The best catalyst had a composition of $Pt_{44}Fe_{56}$, and the specific activity reached 3.9 mA cm^{-2}. No significant activity loss was detected in the stability test, which was carried out by measuring the ORR activity after 4000 potential sweeps between 0.6 and 1.0 V_{RHE}.

Catalysts with specific activities >10 mA cm^{-2} were reported by Huang and coworkers. They found that Mo-doping Pt_3Ni catalysts lead to significantly improved activity.[230] The synthesis started with the preparation of the Pt_3Ni NPs through the reduction of $Pt(acac)_2$ and $Ni(acac)_2$, then the Pt_3Ni NPs were doped in the solution of $Mo(CO)_6$, $Pt(acac)_2$, and $Ni(acac)_2$ in DMF at 170 °C for 48 h. The specific activity of this Mo-Pt_3Ni catalyst was 10.3 mA cm^{-2}, and its mass activity was 2.08 A mg^{-1}. It has an octahedral shape, with Mo atoms sitting near the edges and vertices. Only ~6% decrease in the specific activity and the mass activity was observed after 8000 potential cycles (0.6–1.1 V_{RHE}) in O_2 saturated 0.1 M $HClO_4$. Mo-Pt_3Ni NPs exhibit better performance in both activity and stability than those of the pristine Pt_3Ni NPs. The calculation results indicated that the oxygen binding energy around the Mo atoms was 0.15 eV less than the Pt(111) facet, which was in a favored position in the volcano plot. The Mo-Pt and Mo-Ni bonds are strong, and Mo held Pt and Ni better than themselves, which explains the outstanding stability of this catalyst.

The state-of-the-art ORR catalysts were reported by Duan and coworkers.[242] First, Pt/NiO core/shell nanowires (NWs) were synthesized by heating the solution containing $Pt(acac)_2$, $Ni(acac)_2$, $W(CO)_6$, 1-octadecene, oleylamine, and polyvinylpyrrolidone at 140 °C for 6 h. The obtained NWs were reduced under Ar/H_2: 97/3 gas flow at 450 °C in the presence of a carbon black support. The following dealloying process (160 potential cycles 0.05–1.1 V_{RHE} in 0.1 M $HClO_4$) removed the Ni atoms on the NW surface, resulting in NWs with a Pt(111)-dominated surface. The diameter of the NWs also shrank from ~5 nm to ~2.2 nm after the dealloying. Notably, the author recognized this catalyst as a non-alloyed Pt catalyst. The resultant NWs (J-PtNWs) have a highly jagged surface, with a mass-specific ECSA of 118 m^2/g$_{pt}$, which is the largest mass-specific ECSA ever reported. The specific activity of the J-PtNWs was 11.5 mA cm^{-2}, and the mass activity was 13.6 A mg^{-1} (0.9 V_{RHE}), which are both the highest reported in the literature. This mass activity was ~50 times higher than a commercial Pt/C catalyst and 30 times higher than the U.S. Department of Energy 2020 target (0.44 A mg^{-1}, set in 2016), illustrating a promising implementation of the catalyst. This mass

activity only dropped by 12% after treating the catalyst with 6000 cyclic voltammetry scans (0.6–1.0 V_{RHE}, O_2 saturated 0.1 M $HClO_4$). Other than the high mass-specific ECSA, the author attributed the exceptionally high activity to the ORR-favorable rhombic geometry of Pt atoms on the catalyst surface. This less-coordinated, more strained rhombic structure of Pt decreases the binding energy of oxygen species compared to the face centered cubic Pt(111) surface, resulting in a better ORR activity.

In summary, cathode catalysts of fuel cells play an important role in the performance of a fuel cell. Pt-based catalysts exhibit the highest activities, especially Pt-based nanomaterials. However, few papers reported the actual cell performance of these catalysts. Also, nanomaterials are subject to structural decomposition,[243] which may affect the lifetime of the catalysts. The current manufacture of nanomaterials also causes environmental concerns.[244] There is room for improvement in their activity, durability, and manufacturing costs.

4.1.3 Glancing Angle Deposition and Its Application in Fuel Cell Catalysis

The glancing angle deposition (GLAD) is a physical vapor deposition (PVD) technique.[245] Figure 4-4 is a schematic illustration of a GLAD process. Under high vacuum, a vapor-phased atom stream hits a solid substrate, and the atoms condense onto the substrate. Microstructural control is achieved by the precise motion of the substrate relative to the incoming vapor flux.[246, 247] Two angular parameters, α and φ, commonly are used to describe a GLAD process, where α is the oblique deposition angle, defined as the angle between the substrate normal and the vaper flux, and φ represents the rotation about the axis perpendicular to the substrate. During the deposition, the obliquely incident atoms are able only to nucleate onto the highest points of the substrate surface due to a self-shadowing effect. With increasing flux deposition, this self-shadowing effect leads to columnar or pillar-shaped growth. The porosity and nanopillar spacing can be controlled by changing α. Further morphology control can be achieved by modulation of substrate rotation in φ and allows access to various structures (e.g., vertical columns, slanted posts, chevrons, square spirals, helices, and combinations thereof). The high level of morphology control, inherent to GLAD, leads to well-tailored nanostructures that can be used in a variety of applications, including electrocatalysis. Moreover, large area GLAD films have been prepared in a prototype roll-to-roll system that can be extended further to mass production of these materials.[248]
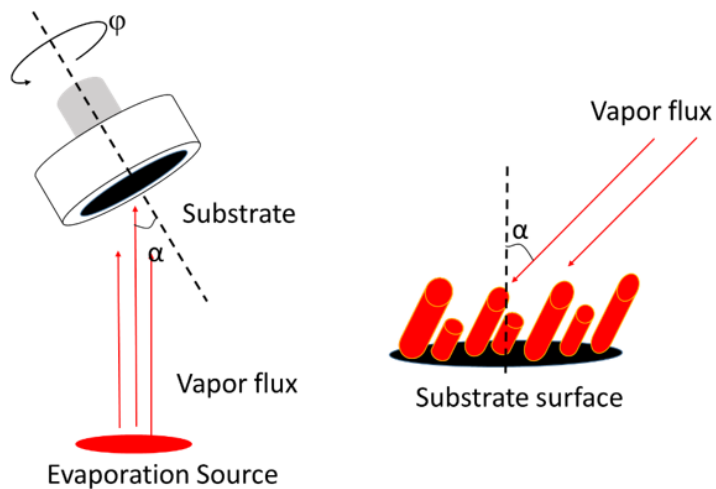
Figure 4-4. Schematic illustration of a GLAD process.[246]

We previously reported the first study of alcohol oxidation with GLAD-based electro catalysts.[249] Specifically, Pt was deposited electrochemically onto 500 nm long Ni_{GLAD} nanopillars supported on Si wafers (Ni_{GLAD}/Si). Two Pt deposition methods were compared. The first was a traditional potentiostatic deposition from Pt salts dissolved in acidic electrolytes. This deposition mainly placed the Pt on the tops of the Ni_{GLAD} nanopillars to give a layered structure with Ni below and Pt on the top (referred to herein as $Pt_{Tr}Ni_{GLAD}$/Si). The second Pt deposition was an unconventional, self-limiting, galvanostatic one ($J = (-) \ 100 \ mA \ cm^{-2}$, normalized to the geometric area of the Si support under the Ni_{GLAD}), with a Pt counter electrode (CE) as the source of Pt in a 2.0 M NH_4Cl electrolyte[250, 251] to result in a conformal Pt coating on the Ni_{GLAD}/Si. This core-layer catalyst is referred to as Ni_{GLAD}[Pt]/Si. Both $Pt_{Tr}Ni_{GLAD}$/Si and the core-layer Ni_{GLAD}[Pt]/Si were more active for the electro-oxidation of 2-PrOH in base than Pt foil or Ni_{foam}[Pt] (made by a similar Pt CE deposition on a Ni foam)[250]. At low potentials, (50–300 mV_{RHE}) the electrochemically active surface atom-normalized activity of Ni_{GLAD}[Pt]/Si was higher than the unsupported Pt and Pt–Ru nanoparticles as well. Interestingly, the Ni_{GLAD}/Si substrate without added Pt was also active towards 2-PrOH electro-oxidation at low potentials.

The use of GLAD materials as oxygen reduction electro-catalysts was reported recently.[252-259] The Gall group reported various studies of GLAD-based electrodes in PEM fuel

cells.[252-255] For example, 100 to 500 nm GLAD Pt nanorods were sputtered at $\alpha = 87°$ directly onto gas diffusion layers and incorporated into polymer electrolyte membrane (PEM) fuel cells as cathodes. These were compared to Pt cathodes prepared at normal incidence ($\alpha = 0°$). The GLAD Pt cathode had a lower ECSA but a higher porosity than the cathode prepared at $\alpha = 0°$. The mass specific activity of the GLAD-based cell was higher than that of the $\alpha = 0°$ system, suggesting that mass transport was more facile in the GLAD-based cathode.[255] In another report, Pt sputtered onto 500 nm GLAD carbon nanorods were incorporated into a fuel cell and etched in situ by applying cell voltages between 1.2 and 1.7 V. The etching improved the performance of the cell, suggesting that mass transport was also more facile in the etched cathode.[254]

The Brett group has collaborated with the research groups of Wilkinson and Dahn to report Pt sputtered on GLAD annealed niobium oxide and titanium nanopillars, respectively.[256, 257] Both reports showed catalyst surface enhancement factors on the order of 11 to 13 due to the high surface area of the supports. Room temperature ORR studies in 0.1 M $HClO_4$ showed that Pt/GLAD Ti could achieve current densities of 0.5 mA cm^{-2}, while the annealed niobium oxide-supported Pt displayed current densities ≥ 1 mA cm^{-2} at 0.9 V_{RHE}. Moreover, the latter catalyst withstood aggressive electrochemical testing up to 1.4 V_{RHE}, and its morphology was stable at 1000 °C.

In most cases, the initial use of basic conditions to study a newly developed combinatory catalyst would minimize significant changes in structure and composition due to dissolution. The use of alkaline electrolytes thereby allows for convenient screening of the near as-prepared structure, activity, and durability of ORR electro-catalysts. Furthermore, the results of such studies are relevant to the development of alkaline fuel cells.[260]

A great deal of attention has been focused on the study of ORR in alkaline media using Pt as a catalyst in binary and ternary combinations with non-noble transition metals. For instance, Garcia-Contreras et al[261] reported that PtNi and PtNiCo made by chemical vapor deposition were both more active than Pt in KOH solution, with the latter giving the best activity. A comparative theoretical and experimental survey of ORR in 0.1 M KOH by Pasti et al. showed that the Pt-In alloy was 2.6 times more active than Pt.[262] More recently, Jaeger and coworkers[263] showed that a Pt-C(Mo_2C) catalyst was more active than Pt/Vulcan carbon towards ORR in base.

This study presents the first ORR study in alkaline media on GLAD Ni supports over which Pt was electrochemically deposited using a rotating disc electrode. Using the versatile GLAD deposition methodology, we have been able to cast Ni on a bare glassy carbon electrode with control over shape, quantity, and distribution. Here, a higher value of α than for our previous studies with Ni_{GLAD}/Si ($\alpha = 85°$) was set to decrease the surface density of the nanopillars in an attempt to facilitate the mass transport of O_2 in the catalyst layer.[264, 265] As well, in the present work, we used a modified version of the Pt CE deposition with the working electrode rotating at high rates to prepare Ni_{GLAD}[Pt]/GC core-layer nanopillars with minimal mass transport effects. This technique appears to deposit controlled amounts of Pt uniformly over the Ni particles. The resulting structures survived fast WE rotation during ORR tests in the absence of binders such as Nafion®. This approach is beneficial for mechanistic studies, for benchmarking catalysts, and for testing novel catalyst materials, while avoiding intrinsic complications (e.g., mass transport and stability problems) commonly encountered with binding agents.

4.2 Results and Discussion

Figure 4-5 shows top (A) and 45° oblique side (B) views SEM images of the as-prepared Ni_{GLAD}/GC deposit. The Ni nanopillars appear polycrystalline. They are columnar, roughly perpendicular to the surface of the glassy carbon, ~500 nm tall, and widen with increasing height. The average maximum diameter is ~200 nm, while the nanopillars are distributed evenly on the surface. The typical mass of the Ni deposits was 62.5 μg (1.06×10^{-6} mole Ni), or 500 μg cm^{-2} (8.35×10^{-6} mole cm^{-2}), as determined by ICP-MS after dissolution of the Ni deposit.
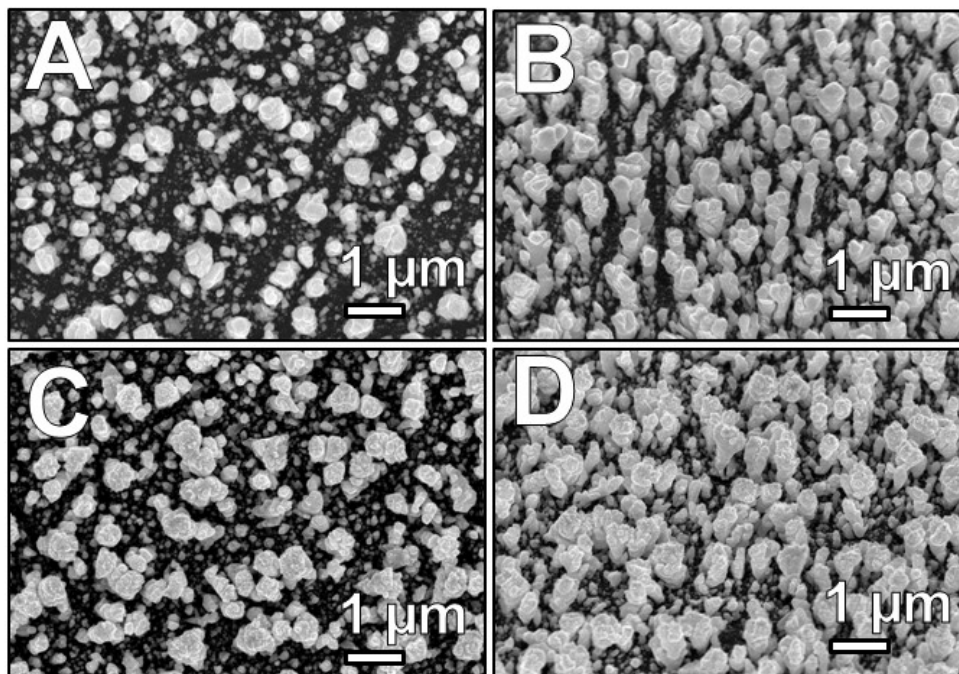
Figure 4-5. Scanning electron micrographs showing the (a) top-down and (b) 45 degree oblique side view of Ni_{GLAD}/GC, as well as the (c) top-down and (d) 45 degree oblique side view of as prepared Ni_{GLAD}[Pt]/GC.

Figure 4-6 shows typical voltammograms (five consecutive cycles) for the Ni_{GLAD}/GC substrate in 1.0 M KOH and 0–0.40 V_{RHE} (sweep rate = 10 mV s^{-1}). This range covers the reversible, 2-electron Ni/α-Ni(OH)$_2$ conversion, and it avoids the irreversible formation of β-Ni(OH)$_2$ at higher potentials.[266-269] The first scan displays a weak anodic wave at ~0.05 V on the forward sweep, which disappeared in the subsequent cycles. This anodic peak likely arises from the oxidation of adsorbed hydrogen that would have formed during the initial polarization at 0 V. [267] Unlike previous reports with bulk polycrystalline Ni that typically contain a well-defined anodic peak at ~0.23 V,[266-269] the anodic sweeps for Ni_{GLAD}/GC showed merely an oxidative region with two broad peaks at ~0.12 and ~0.25 V, ascribable to the Ni/α–Ni(OH)$_2$ conversion. A similar broadening was observed previously in the CVs of Ni_{GLAD}/Si in base. [250] This broadening likely is due to differences in the nature and distribution of the active sites on the Ni_{GLAD} nanopillars and on bulk, polycrystalline Ni. A previous study reported only slight differences in the peak potentials of the anodic waves in the Ni (110), (100), and (010) crystal faces, [268] further suggesting that the broad nature of this wave is a unique property of Ni_{GLAD}/GC or Ni_{GLAD}/Si. A large reduction peak at ~0.06 V is the prevailing feature of the cathodic scan, which is due to the reduction of α-Ni(OH)$_2$ to Ni.[266-269] The cathodic features

146

of the CVs did not change appreciably with cycling. The evolution of H_2 over Ni_{GLAD}/GC commences at ~0.02 V, which is more positive than that over bulk, polycrystalline Ni. [251] The charge under the 5th sweep of the cathodic wave, down to the onset of the H_2 evolution, was used to approximate the ECSA of the Ni_{GLAD}/GC. For a typical sample, this charge was ~1182 μC. Assuming a 2-electron process for the Ni/α-$Ni(OH)_2$ couple, this charge corresponds to 6.1×10^{-9} surface atoms of Ni, compared to 1.1×10^{-6} mole total Ni (63 μg) in the deposit. Considering the approximations in the literature,[268] this charge would correspond to ECSA of ~2.3 cm^2 (on 0.126 cm^2 GC). After characterization by CV, we washed the Ni_{GLAD}/GC electrode and cell with deoxygenated H_2O under an atmosphere of nitrogen, added 2.0 M NH_4Cl electrolyte, and then carried out the WE_{rot}/CE_{Pt} deposition in the same cell without exposing the Ni_{GLAD}/GC to air.
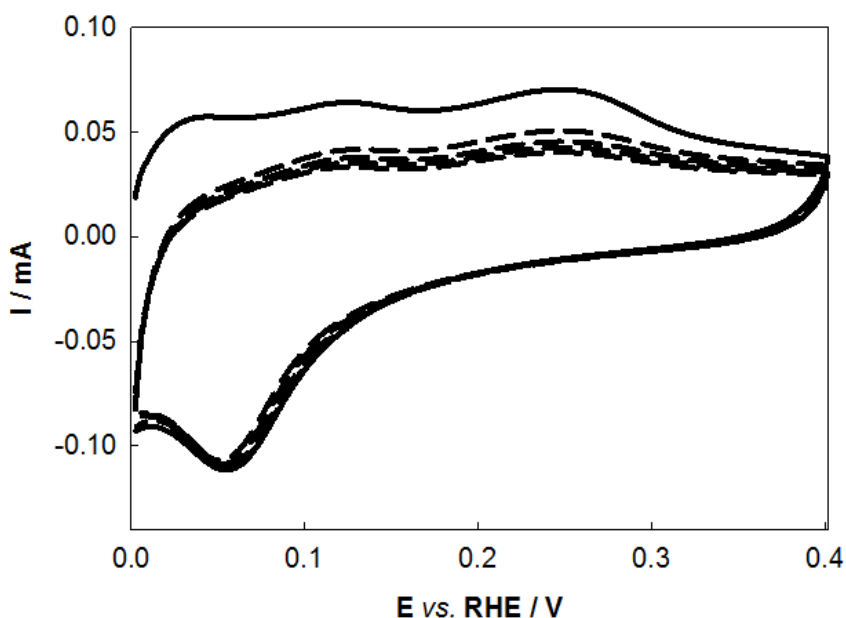
Figure 4-6. The first five sweeps of the cyclic voltammogram for the Ni_{GLAD}/GC substrate in 1.0 M KOH under N_2 at 25 °C. Potential sweep rate was 10 mV s^{-1}.

The deposition was carried out galvanostatically in 2.0 M NH_4Cl with a Pt black gauze CE as the Pt source. The CE was exposed to H_2 (1 atm) before the deposition in order to reduce the surface Pt oxides.[249-251] As was the case in 1.0 M KOH, H_2 evolution at the Ni_{GLAD}/GC WE started at lower overpotentials than at bulk, polycrystalline Ni in 2.0 M NH_4Cl. Indeed, the H_2 evolution at Ni_{GLAD}/GC was significant, and the gas bubbles blocked the electrolyte access to

the WE even at the beginning of the deposition when little or no Pt existed on the surface. Therefore, we performed the depositions at a high rate of WE rotation (ω = 1700 rpm) to dislodge the bubbles continuously as they formed. This high rate of rotation also would minimize the mass transport effects on the distribution of the Pt deposit within the catalyst layer. As well, we used a lower current density than in our previous reports (j = (-) 64 mA cm$^{-2}_{GC}$ or j_{ECSA} = (-) 5.5 mA cm^{-2} Ni$_{surf}$ (using the initial ECSA of the Ni$_{GLAD}$ deposit).[249] Under these conditions, we expected to obtain a more uniform deposit of Pt on Ni$_{GLAD}$. We note that the nature of the Ni$_{GLAD}$/GC deposit, i.e. with the Ni nanopillars attached directly to the surface of the GC disc, uniquely allowed the rotating WE deposition without the need of binders such as Nafion$^{\circledR}$ that could interfere with the deposition and activity measurements of the resulting electrocatalysts. The potential of the WE increases (decreasing the overpotential) as the Ni surface is covered progressively by Pt until it levels out when the Ni is covered by Pt.[249] As can be seen in Figure 4-5C and D (SEM for a Ni$_{GLAD}$[Pt]/GC), there appear to be no significant changes in the overall shape and morphology of the GLAD pillars before and after the rotating deposition. Thus, it is likely that Pt has been deposited uniformly, over the Ni$_{GLAD}$ nanopillars. Closer inspection of the nanopillars before and after Pt deposition reveals the appearance of some fine structures that are presumably due to partial surface deposition of Pt, which is also consistent with the E$_{WE}$ changes over the course of electrodeposition (Figure 4-7).
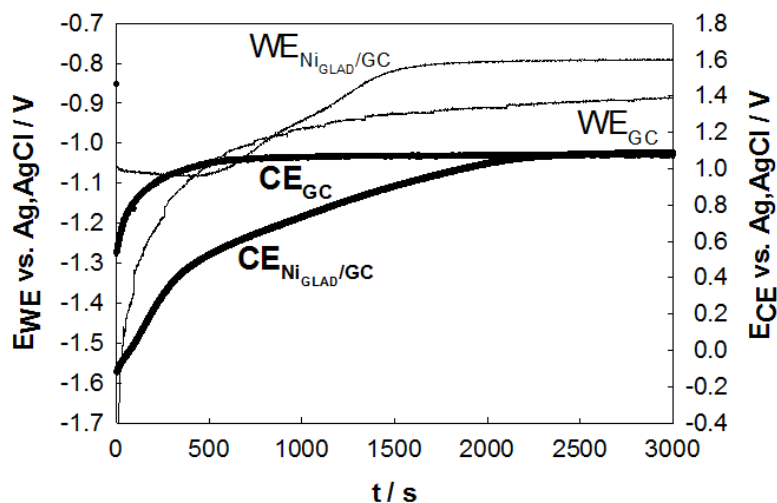
Figure 4-7. Potential profile of the working electrodes (E$_{WE}$) and counter electrodes during the Pt counter electrode depositions for a bare GC and Ni$_{GLAD}$/GC electrodes.

Figure 4-7 shows profiles of E vs. time during the WE_{rot}/CE_{Pt} deposition for both the WE and CE. For comparison, the same procedure was carried out over a bare GC disk to prepare a control [Pt]/GC electrode. The initial stages (up to ~400 s) of the deposition over the Ni_{GLAD}/GC largely represent H_2 evolution over the rotating Ni_{GLAD}/GC, with E_{WE} ranging from -1.06 to -1.08 V vs Ag/AgCl (4.0 M KCl). The Pt deposition largely begins once the Pt black CE potential rises to values adequate to dissolve significant amounts of Pt in 2.0 M NH_4Cl (~0.47 V).[249-251] Starting at 410 s, we believe a mixed H_2 evolution system exists over Ni_{GLAD}[Pt]/GC, with H_2 evolution occurring over both Pt and Ni, and then mainly (or merely) over Pt when the Ni is fully covered with Pt (i.e., after t = 1500 s). The E_{WE} increased almost linearly in the mixed potential region for ~1200 s and then leveled off asymptotically towards -0.81 V vs Ag/AgCl (4.0 M KCl). This behavior of E_{WE} with time indicates that the Pt coverage increases almost linearly during the early stages of the WE_{rot}/CE_{Pt} dep (~1200 s). As expected, the initial WE potential is significantly more negative over bare GC than over Ni_{GLAD}/GC. Also, the polarization of the CE initiates at potentials larger than 0.47 V, suggesting that the electrodissolution from the CE and Pt deposition onto the WE started almost immediately. Indeed, E_{WE} over GC started to increase at the onset of the deposition. Over bare GC, the initial surge in E_{WE} likely is due to nucleation and growth of the Pt deposit. The WE potential increase levels off much earlier over [Pt]/GC than over Ni_{GLAD}[Pt]/GC (around 1000 s). We note, however, that the overall deposition time for both electrodes (start of the potential increase up to the plateau) seems quite similar and is roughly 1000±50 s. The difference in the WE potentials near the end of the depositions likely reflects differences in the overpotentials for hydrogen evolution over the [Pt]/GC and Ni_{GLAD}[Pt]/GC surfaces.

Figure 4-8 shows a typical voltammogram of a Ni_{GLAD}[Pt]/GC catalyst in 1.0 M KOH (100 mV s^{-1}) and a typical voltammogram of [Pt]/GC. The CVs were recorded without exposing the Ni_{GLAD}[Pt]/GC WE to air after the WE_{rot}/CE_{Pt} deposition. For both electrodes, typical features of Pt are observed,[270] with H desorption (anodic) and adsorption (cathodic) below 0.45 V vs RHE, while oxide formation (anodic) and stripping (cathodic) are at potentials higher than 0.5 V vs RHE. We note, however, that the oxide stripping peak over Ni_{GLAD}[Pt]/GC is at ~0.53 V, compared to ~0.71 V over [Pt]/GC. Using the charge under the cathodic wave and assuming that the Pt electrochemistry is dominant,[271] the ECSA of the Ni_{GLAD}[Pt]/GC is ~0.76 cm^2; similarly, 0.75 cm^2 was obtained for [Pt]/GC. The CV of [Pt]/GC was stable over

the course of these experiments in the absence of binder, showing that this deposition approach can be used successfully over bare carbon surfaces as well.
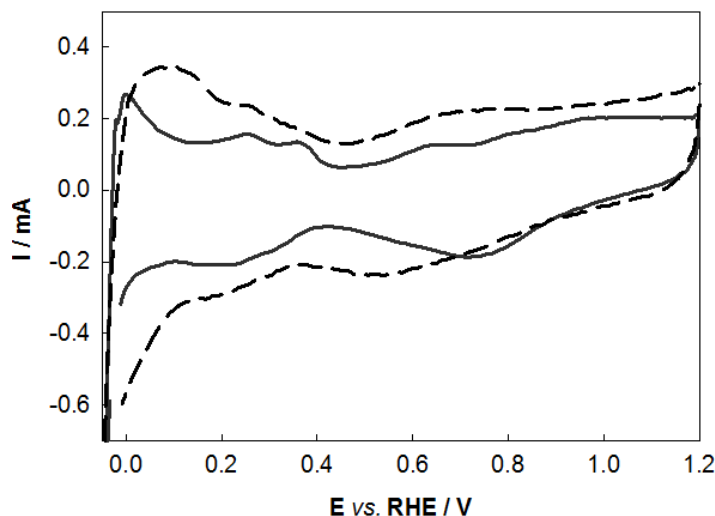
Figure 4-8. Typical cyclic voltammograms for the [Pt]/GC (solid) and Ni_{GLAD}[Pt]/GC (dashed) electrodes in 1.0 M KOH under N_2 (25 °C) at 100 mV s^{-1}.

Figure 4-9 compares the ORR activities of the Ni_{GLAD}[Pt]/GC and [Pt]/GC electrodes in O_2-saturated 1.0 M KOH. The figure shows the 5th negative going (cathodic) and positive going (anodic sweeps) (ω = 1600 rpm, 1.00 to 0.50 V, 10 mV sec^{-1}) of the hydrodynamic CVs corrected for the baseline CV (measured in the absence of O_2). The current densities are normalized to the estimated ECSA of the deposits. We note that, based on the charges under the H adsorption/desorption regions (Figure 4-8), the ECSA of the Ni_{GLAD}[Pt]/GC and [Pt]/GC electrodes were 0.76 and 0.75 cm^{-2}, respectively. As such, both electrodes produced similar mass transport controlled activities. The onset of the ORR was ~30 mV less negative over Ni_{GLAD}[Pt]/GC, resulting in about a 2–3 fold superior activity for Ni_{GLAD}[Pt]/GC over [Pt]/GC and 0.75–0.90 V vs RHE (cathodic sweeps). Comparing the anodic sweeps showed similar improvements, somewhat better. This signifies the role of Ni_{GLAD} structures in improving sluggish ORR activity of Pt. In 2013 Kariuki et al[272] reported that Pt-Ni (both deposited by GLAD) nanorods gave similar ORR activity improvements compared with Pt in acidic electrolytes. Table 4-2 summarizes key data of the two catalysts where the ECSA and mass normalized activities have been reported at 0.9 V vs RHE of the anodic scans.
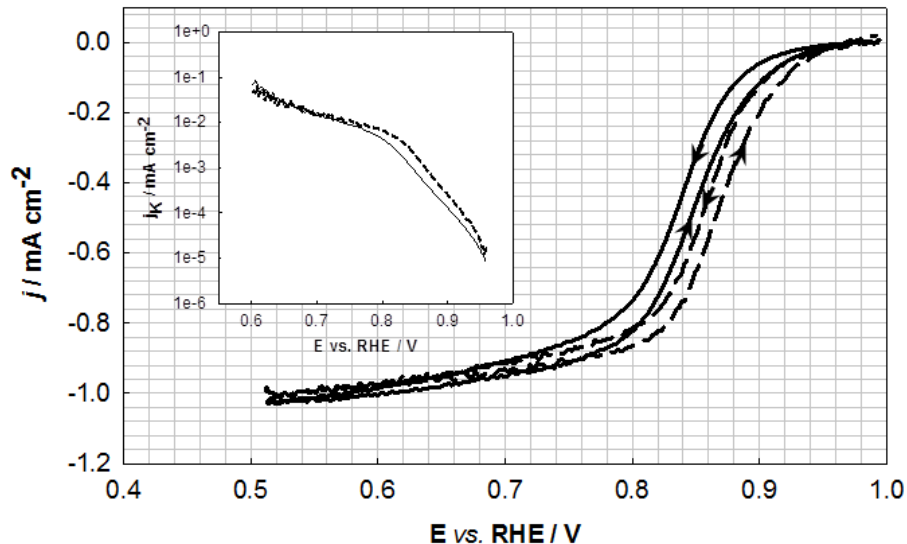
Figure 4-9. The baseline-corrected 5th cathodic and anodic sweeps of the hydrodynamic CVs of the [Pt]/GC (solid) and Ni_{GLAD}[Pt]/GC (dashed) electrodes in O_2-saturated 1.0 M KOH at 25 °C, 1600 rpm, and 10 mV s^{-1}. Current densities are normalized to electrochemical active surface area. Inset: Tafel plots extracted from the anodic sweeps. The data are not iR corrected.

Figure 4-9 (inset) displays mass transport corrected Tafel plots of the cathodic sweeps (i.e., negative going) of the logarithm of the kinetic current density normalized to the ECSA vs. E_{WE}, $j_{ECSAkinetic}$, $(j_{obs} \times j_{lim})/(j_{lim} - j_{obs})$. For both electrodes, there were two regions of the Tafel plots with different slopes, indicating a change in the rate-determining step with overpotential. At low overpotentals, down to E_{WE} ~0.80 V, the Tafel slopes were 63 and 58 mV dec^{-1}, while at E_{WE} between ~0.80 V and ~0.60 V, Tafel slopes of as large as 172 and 227 mV dec^{-1} were obtained for [Pt]/GC and Ni_{GLAD}[Pt]/GC, respectively. Other authors also have reported two regions with different Tafel slopes for ORR over Pt in KOH electrolytes,[272, 273] typically 60 mV dec^{-1} down to E_{WE} = ~0.80 V and ~121 mV dec^{-1} at E_{WE} < ~0.80 V. The reasons for the overly large Tafel slope at large overpotentials for Ni_{GLAD}[Pt]/GC are unknown at this point. We note that it has been hypothesized that such high Tafel slopes would be indicative of the rate determining step being the adsorption of O_2.[273] This hypothesis is consistent with the relative ORR activities of Ni_{GLAD}[Pt]/GC and [Pt]/GC and their corresponding O_2-free voltammetry (Figure 4-8), where the oxide stripping peak for Ni_{GLAD}[Pt]/GC appeared at about 0.2 V less positive than that for the [Pt]/GC. Such a shift is suggestive of a stronger O_2 adsorption energy with Ni present in the Ni_{GLAD}[Pt]/GC catalyst, as has been documented also in the well-known volcano plots for Pt alloys activities as a function of the oxygen binding

151

energies.[228] Further investigations are required, however, to fully explain the differences in ORR activity between $Ni_{GLAD}[Pt]/GC$ and $[Pt]/GC$.

Table 4-2. Some Key Parameters for the $[Pt]/GC$ and $Ni_{GLAD}[Pt]/GC$ Electrodes.

Catalyst	ORR onset V_{RHE}	ECSA / cm^2	ECSA activity mA cm^{-2}	Mass activity A g^{-1}
[Pt]/GC	0.93	0.75	0.105	5.53
Ni$_{GLAD}$[Pt]/GC	0.96	0.76	0.202	13.23

Moderate-term potentiostatic ORR's (E = 0.85 V vs RHE) over 5000 s were carried out with the $[Pt]/GC$ and $Ni_{GLAD}[Pt]/GC$ electrodes (not shown) as a preliminary comparison of the durability of these catalysts. The $Ni_{GLAD}[Pt]/GC$ retained its initial performance and also showed some improvement (-4.80×10^{-2} mA at t = 0 and -5.47×10^{-2} mA at t = 5000 s), while the activity of the $[Pt]/GC$ electrode decreased by 38% after 5000 s (-2.06×10^{-2} mA at t = 0 and -1.27×10^{-2} mA at t = 5000 s, respectively). This result is consistent with the report of Zhang et al[274] who overviewed influences of metal oxide supports in sustaining the ORR activity of Pt. Figure 4-10 shows the baseline CVs in O_2-free 1 M KOH for $[Pt]/GC$ (A) and $Ni_{GLAD}[Pt]/GC$ (B) before and after the moderate-term ORR tests. The before and after ECSA of the $Ni_{GLAD}[Pt]/GC$ were 0.76 cm^2 and ~0.74 cm^2, respectively, and the corresponding values for $[Pt]/GC$ were both ~0.75 cm^2. Thus, the ECSA of both surfaces were not changed significantly by moderate-term potentiostatic ORR's.

These results show that the deposition method described in this work gives rise to Pt particles that are attached strongly to the GC support. On this basis, we propose that the superior ORR activity and moderate-term durability of the $Ni_{GLAD}[Pt]/GC$ over $[Pt]/GC$ are due to the promotional effects of the Ni_{GLAD} support on the Pt layer, rather than catalyst decomposition.
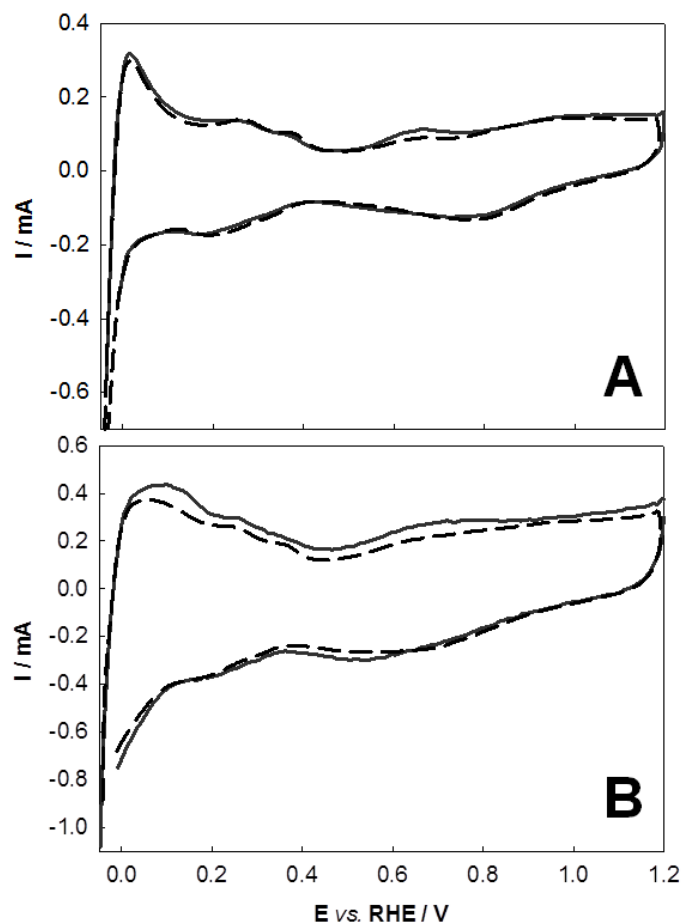
Figure 4-10. Cyclic voltammograms before (solid) and after (dash) 5000 s ORR at 0.85 (RHE) for the [Pt]/GC (A) and Ni_{GLAD}[Pt]/GC (B) electrodes in 1.0 M KOH under N_2 (25 °C) at 100 mV s^{-1}.

4.3 Experimental Details

The following chemicals were used as received from the supplier: Nitrogen (Praxair, pre-purified), oxygen (Praxair, pre-purified), concentrated sulfuric acid (Caledon), hydrochloric acid (EMD chemicals), nitric acid (EMD chemicals), perchloric acid (Anachemia Corporation), potassium permanganate (Fisher Scientific), 30% hydrogen peroxide (Fisher Scientific), potassium hydroxide (Caledon Laboratory Chemicals), ammonium chloride (Caledon Laboratory chemicals), ethanol (Greenfield Ethanol Incorporated), and potassium hexachloroplatinate (Aithica Chemical Corporation). The following materials were used as received from the supplier: platinum gauze (Alfa Aesar, 52 mesh woven from 0.1 mm wire, 99.9% metals basis) and nickel metal chunks (Cerac, Inc., 99.9% purity). The glassy carbon

discs (Pine Research Instrumentation, 5 mm outer diameter × 4 mm thick, 0.196 cm^2 geometric surface area) were polished and cleaned as described below before use.

Triply distilled H$_2$O was used to prepare all aqueous solutions and was itself prepared by distilling a mixture of alkaline KMnO$_4$ and doubly distilled H$_2$O. 2-Propanol (ACS reagent grade, Sigma-Aldrich) was distilled under N$_2$ from Mg. Analytical grade reagents were used to prepare all electrolyte solutions. All aqueous solutions were saturated with N$_2$ gas by purging for 30 min before use. All electrochemical experiments were carried out under N$_2$ using standard Schlenk techniques. Rinse water and electrolytes were transferred under flushing N$_2$ with cannulas. ORR experiments were carried out in O$_2$-saturated 1.0 M KOH under an atmosphere of O$_2$. All glassware was cleaned with Piranha solution (5:1 by volume concentrated H$_2$SO$_4$ and 30% H$_2$O$_2$), rinsed thoroughly with triply distilled H$_2$O, and then dried at 80°C. The platinum-blacked gauze counter electrodes were prepared as described previously.[249]

The electrochemical experiments were performed with a Solartron SI 1287 Electrochemical Interface controlled by CorrWare for Windows Version 2-3d software. During the rotating WE depositions, the potential of the Pt CE was recorded with a Radio Shack multimeter. Rotating disc electrode experiments were performed with a Pine Research Instrumentation Modulated Speed Rotator equipped with an AFE6MB RRDE shaft and E5TQ series Change-Disk tip. The shaft and tip were connected to the reaction flask with a Pine AC01TPA6M Gas-Purged Bearing Assembly.

SEM was performed with a Hitachi S-4800 instrument. ICP-MS data were measured with an Agilent 7500 ce ICPMS coupled with a Cetac ASX-510 autosampler. Samples were prepared by dissolving the deposits in aqua regia, evaporating the resulting solution to dryness with a hot plate, followed by quantitatively making up the residue in 0.3 M HNO$_3$.

Preparation of GLAD nickel nanopillars on glassy carbon (Ni$_{GLAD}$/GC)

The glassy carbon (GC) discs were polished with a Pine Research Instrumentation polishing kit (5, 0.3, and/or 0.05 μm alumina slurry with a nylon or rayon microcloth) and cleaned with acetone, iso-propanol, and water before being placed in the high vacuum deposition chamber (Kurt J. Lesker). The deposition chamber was evacuated to below 0.1 mP, and Ni was deposited from Ni metal chunks via electron beam deposition. The flux rate was maintained at

1 nm s^{-1} while a film of ~500 nm vertical nanopillars was deposited at α = 88˚. The substrates were rotated constantly in φ at a rate of one rotation every 10 nm of film growth. The Ni$_{GLAD}$/GC discs were stored under glass in air.

Characterization of GLAD catalysts by CV and the Rotating WE, Pt-CE deposition (WE$_{rot}$/CE$_{Pt}$ dep)

The experiments of GLAD catalyst characterization, Pt-CE deposition, and ORR measurements typically were completed on the same day to minimize ageing effects on the activity and characteristics of the resulting electrodes. The Ni$_{GLAD}$/GC disc was loaded into the RRDE tip under air using a homemade, hands-free mounting tool that also removed the outer 0.5 mm-thick ring of the Ni$_{GLAD}$ deposit, leaving 0.126 cm^2 of the GC covered with Ni$_{GLAD}$. The Ni$_{GLAD}$/GC WE was cleaned with triply distilled water and then fitted to a 100 mL, three neck flask with a Pine AC01TPA6M Gas-Purged Bearing Assembly. The Pt black CE (in a glass filter tube with a coarse sinter tip) and the H$_2$ (1 atm)/1.0 M KOH/Pt RHE reference electrode were fitted to the flask through holes in rubber septa. All gases were handled with needles attached to feed- and bubbler- lines. The vessel was flushed with N$_2$ for 20 min and then filled with ~50 mL, N$_2$-saturated 1.0 M KOH through a cannula. Immediately after immersion, the E$_{WE}$ was held at -0.10 V$_{RHE}$ for 180 s, after which the CV was recorded to characterize the Ni$_{GLAD}$ surface (E = 0–0.40 V, 10 mV s^{-1}, 5 sweeps). Next, the KOH solution was removed through a cannula, and with rapid N$_2$ flushing, the CE was replaced with an unprotected, fresh Pt black gauze, and the RHE was replaced with a Ag/AgCl (4.0 M KCl) reference electrode, both fitted with rubber septa. Using cannulas, the vessel was washed three times with N$_2$-saturated H$_2$O (~50 mL each), emptied, and the Pt CE surface was reduced by exposure to a stream of H$_2$ (1 atm) for 10 min. The H$_2$ was flushed with N$_2$, and 30 mL of N$_2$-saturated 2.0 M NH$_4$Cl was added through a cannula. Thereafter, the WE was rotated at ω = 1700 rpm, and the current density was set to j = (-) 64 mA cm^{-2}$_{GC,}$ considering the total area of the GC disc (0.196 cm^2). After the deposition, the NH$_4$Cl solution was removed through a cannula. Under flushing N$_2$, the CE was exchanged for a Pt black gauze in a filter tube with a coarse sinter, and the reference electrode was exchanged for an RHE. Both electrodes were fitted through rubber septa. Using cannulas, the reaction vessel and working electrode were rinsed three times (~50 mL each) with N$_2$-saturated triply distilled water, then ~50 mL aqueous

1.0 M KOH was introduced to the vessel. Next, voltammetry was conducted to characterize the $Ni_{GLAD}[Pt]/GC$ catalyst (11.6 µg; ICP-MS). The same steps were carried out with a bare GC electrode to prepare the [Pt]/GC electrodes (14.5 µg; ICP-MS). The GC surface was polished (with a 5, 0.3, and/or 0.05 µm alumina slurry with a nylon or rayon microcloth) and cleaned with acetone, iso-propanol, and water.

ORR measurements

The $Ni_{GLAD}[Pt]/GC$ electrode was characterized by CV in 1.0 M KOH under N_2, as described above. Then, oxygen (1 atm) was bubbled through the electrolyte for 30 min to saturate it while the WE was at open circuit. The ORR measurements were carried out at room temperature at the scan rates, rotation rates, and potential limits described in the text (Figure 4-9). The $Ni_{GLAD}[Pt]/GC$ catalyst layers were washed with triply-distilled water and stored in air between uses.

4.4 Conclusions

Glancing angle deposition (GLAD) was employed to cast Ni nanopillars on glassy carbon disc supports. Then, a unique, rapid rotating WE_{rot}/CE_{Pt} galvanostatic deposition approach was used to incorporate Pt. This resulted in uniform deposition of Pt over the Ni structures, while SEM indicated that trace amounts of Pt also have been deposited as an overlayer. It is noteworthy that the underlying morphology of the Ni_{GLAD} did not change appreciably after the deposition. Preliminary tests showed that the $Ni_{GLAD}[Pt]$ on GC was 2–3 fold more active towards the ORR than [Pt] on GC under identical conditions. Typically, for both catalyst layers, the Tafel plots showed two distinctive slope regions, similar to bulk polycrystalline Pt, demonstrating the change in the ORR mechanism with potential. Moderate-term potentiostatic ORR studies showed that the Pt layer at the Ni_{GLAD} support was more durable, which should be of interest in the development of commercial catalysts for alkaline fuel cells.

The preparation of the Ni_{GLAD} deposit on GC is easy to perform, reproducible, and reasonably fast (about one hour is required for the simultaneous deposition on multiple GC electrodes). We emphasize, however, that this methodology is in its preliminary stages, and investigations are underway to optimize the conditions. As well, this approach was extended

to ORR studies in acidic media by the Bergens group.[275] Finally, we believe that the report of the highly active Pt$_3$Ni nanoframes for ORR in acid by Chen et al[276] encourages attempts towards different approaches for making Pt-Ni systems that are active, durable, and easy to fabricate.

Chapter 5

Concluding Remarks

Chapter 2 describes the preparation and study of an efficient, heterogenized ester hydrogenation catalyst. The catalyst was polymerized via altROMP of a well-defined RuPNNP monomer, dichloro{*N,N*'-bis({(2-diphenylphosphino)phenyl}methylidene)bicyclo[2.2.1]-hept-5-ene-2,3-diamine}ruthenium (**121**), cyclooctene and a crosslinking reagent **123**. The resulting crosslinked framework was prepared over BaSO$_4$. This supported catalyst had activity that was similar to the homogeneous analog, indicating that mass transport did not limit the rate of hydrogenation over the heterogenized catalyst. The catalyst was tested over five consecutive hydrogenations of methyl benzoate (0.0025 mol% catalyst, 10 mol% KO*t*Bu, 80 °C, 50 bar, THF, 21 h), which led to a total TON above 120000. This is the highest TON reported for an ester hydrogenation. The total Ru leaching over the first four runs was 11.9%, proving that the reaction was heterogeneous.

An initial burst of activity occurred during these hydrogenations, than the activity dropped off as the reaction proceeded. Once the reaction rate slowed down, it could not be restored by replenishing the hydrogen and substrate. However, a similar burst of was observed after filtering the heterogeneous reaction and resetting the hydrogenation. I attribute the deactivation to either product inhibition via the formation of Ru alkoxide species and/or the decrease in basicity during the reaction.

Future research on this system should focus on improving its stability. The mechanism of deactivation should be addressed. X-ray photoelectron spectroscopy (XPS) spectra and even solid state NMR spectra of the supported catalyst before and after the hydrogenation reaction may help to reveal the changes of the catalyst during the hydrogenation. Another important goal is to develop catalysts that intrinsically resist product inhibition. There are a few catalysts that are not strongly inhibited by alcohol formation or even catalyzing ester hydrogenations in alcohol solvents (e.g., **21**, **53,** and **70** in Chapter 1). The scope of the hydrogenation should be

expanded to the real products/intermediates in fine chemical industry. Some examples are shown in Scheme 5-1.
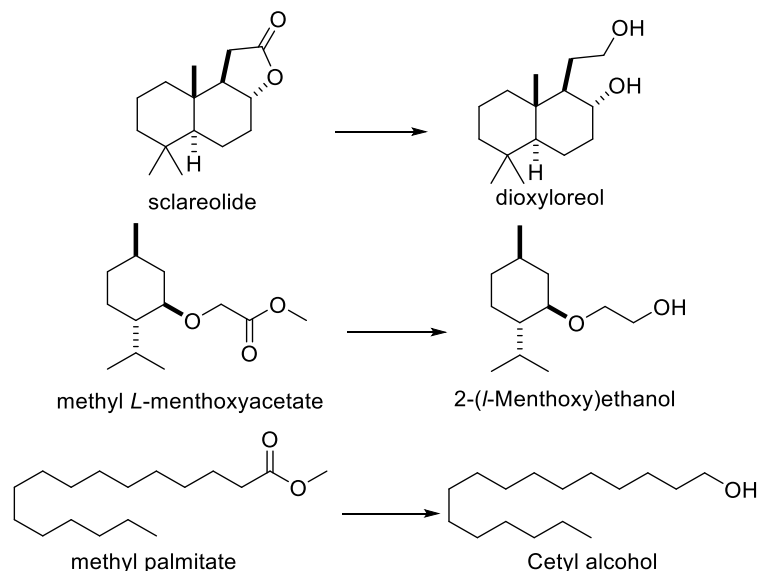
Scheme 5-1. Examples of alcohol products in the fine chemical industry that can be obtained by the hydrogenation of esters/lactones. Dioxyloreol is the precursor to make Cetalox®;[277] 2-(l-menthoxy)ethanol is a cooling agent;[30] cetyl alcohol is used as an emollient or thickening agent in cosmetic industry.[278]

Chapter 3, Part A describes a novel method to prepare the optically enriched starting material *trans*-2,3-diaminonorborn-5-ene dihydrochloride (**129**), avoiding the low-temperature Diels–Alder reaction between dimenthyl fumarate and cyclopentadiene. Optically enriched ligands **130**, **131**, **132,** and **133** were prepared. The Ru complexes (**134**, **135**, **136,** and **137**) bearing these ligands were prepared and studied for the enantioselective transfer hydrogenation of ketones and the enantioselective hydrogenation of β-chiral esters via dynamic kinetic resolution (DKR). Moderate ee's were obtained within these exploratory reactions. The highest ee (52%) was obtained for the transfer hydrogenation of acetophenone using **134** in 2-PrOH (0.5 mol% **134**, 0.25 mol% KO*t*Bu, 45 °C 2-PrOH 3.75 h). The polymer catalysts with imine ligand (**135P**) and amine ligand (**137P**) showed similar activity in the ester hydrogenations via DKR (2–2.5 mol% catalyst, 50 mol% NaO*i*Pr, rt, THF, 24 h, 4 bar H$_2$), but **137P** gave higher ee's (up to 39%).

Despite the modest ee's obtained in these catalyses, the possibility that other substrates may lead to better ee's with these catalysts is not excluded. For example, β-chiral esters without alkoxy groups and β-chiral lactones may also be hydrogenated by these catalysts via DKR.

159

More screening reactions may help to find better substrate/catalyst/condition combinations. Figure 5-1 shows some possible substrates for this exploration.
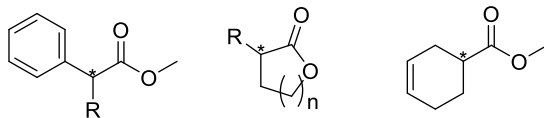
Figure 5-1. Substrate candidates for the enantioselective hydrogenation of esters/lactones via DKR.

Excess base (2 mol% to 10 mol% of the substrate) generally is needed for the hydrogenation of esters. Mechanistically, a base deprotonates the NH group in bifunctional hydrogenation catalysts, rendering the hydride group in the catalyst more nucleophilic and accelerating the reaction. A base also can suppress the formation of the inactive Ru alkoxide, minimizing the product inhibition. In Part B of Chapter 3, I tried to address the issue of using excess base in the hydrogenation of esters by copolymerizing a neighboring cation with a catalyst monomer. I expected that the neighboring cation bearing an alkoxide counterion would co-catalyze an ester hydrogenation via an intramolecular interaction. A stable quaternary ammonium cationic monomer **162** was synthesized, and the desired polymer was prepared by a sequential addition of **136**, **162,** and COE to 3rd Generation Grubbs catalyst at -78 °C. However, the resultant polymer did not exhibit any advantages in the hydrogenation without excess base. Our hypothesis was not supported by our experimental results.

Although the neighboring cation did not assist a hydrogenation, it may have other uses. For example, this cation can be used to prepare polymer catalysts with cations, and the cation may be used potentially in the immobilization of the polymer catalyst onto negatively charged surfaces. Similar strategies used in the immobilization of cationic Rh catalysts for the hydrogenation of olefins are reported in the literature. For example, [Rh((R,S_p)-(JosiPhos)(COD)]BF$_4$ (JosiPhos = 2-(diphenylphosphino)ferrocenyl]ethyldicyclohexyl-phosphine) was immobilized on Al-MCM-41 electrostatically (a acidic mesoporous aluminosilicate) as a reusable catalyst for the enantioselective hydrogenation of olefins.[279] Other anionic solid supports include alumina-phosphotungstic acid,[280] hectorite,[281] ion-exchange resins,[282, 283] etc. Also, monomer **162** may copolymerize with other monomers (e.g., COE), resulting polymeric materials with good mechanical properties, conductivities, and

alkaline stability, which can be good candidate materials for the hydroxide exchange membranes in fuel cells.[201]

In Chapter 4, I reported a thin film Pt catalyst supported on nanopillar structured Ni for oxygen reduction reaction under alkaline conditions. Evenly distributed Ni nanopillars with heights ~500 nm and maximum diameters ~200 nm were deposited on glassy carbon electrodes via glancing angle deposition (GLAD). The resulting Ni nanopillars were coated with thin Pt film by a counter electrode Pt deposition, in which Pt in the counter electrode was dissolved into the experimental media and reduced onto the Ni nanopillars. The deposited Pt thin layer did not change the shape and morphology of the nanopillars significantly.

The activity of the resultant Ni_{GLAD}[Pt] showed an ECSA activity of 0.202 mA cm^{-2} and a mass activity of 13.23 A g^{-1}, which were both 2–3 times higher than the [Pt] catalyst deposited on bare glassy carbon in the same way. In the durability test, Ni_{GLAD}[Pt] also performed better than [Pt] on glassy carbon. The activity of Ni_{GLAD}[Pt] was improved slightly by ~14% after a 5000 s ORR test at 0.85 V_{RHE}, whereas [Pt] on glassy carbon was deactivated by 38%. This easy-prepared Pt-Ni catalyst system is in its preliminary stages, and more investigations are needed to improve its activity.

Bibliography

1. Solomon, S., Stratospheric ozone depletion: A review of concepts and history. *Reviews of Geophysics* **1999,** *37* (3), 275-316.

2. Lindström, B.; Pettersson, L. J., A Brief History of Catalysis. *Cattech* **2003,** *7* (4), 130-138.

3. Chambers, P. J.; Pretorius, I. S., Fermenting knowledge: the history of winemaking, science and yeast research. *EMBO reports* **2010,** *11* (12), 914-920.

4. Mellor, J. W., History of the water problem. *The Journal of Physical Chemistry* **1902,** *7* (8), 557-567.

5. Wisniak, J., The history of catalysis. from the beginning to nobel prizes. *Educación Química* **2010,** *21* (1), 60-69.

6. History of catalysis. In *Encyclopedia of Catalysis*; John Wiley & Sons, Inc., **2002**.

7. Piumetti, M., *A brief history of the science of catalysis - I: From the early concepts to single-site heterogeneous catalysts*. *Chimica oggi* **2014**, 32, 22-27.

8. Cook, E., Peregrine Phillips, The inventor of the contact process for sulphuric acid. *Nature* **1926,** *117*, 419.

9. Burwell, R. L., Heterogeneous catalysis before 1934. In *Heterogeneous Catalysis*; American Chemical Society, **1983**.

10. Economic importance of catalysts. In *Industrial Catalysis*; Wiley‑VCH Verlag GmbH & Co. KGaA, **2015**.

11. Transition metal catalysis in the pharmaceutical industry. In *Applications of Transition Metal Catalysis in Drug Discovery and Development*; John Wiley & Sons, Inc., **2012**.

12. Introduction. In *Catalysis*; Wiley‑VCH Verlag GmbH & Co. KGaA, **2008**.

13. Anastas, P.; Eghbali, N., Green chemistry: principles and practice. *Chem. Soc. Rev.* **2010,** *39* (1), 301-312.

14. Sheldon, R. A., Green chemistry and resource efficiency: towards a green economy. *Green Chemistry* **2016,** *18* (11), 3180-3183.

15. Anastas, P. T.; Kirchhoff, M. M.; Williamson, T. C., Catalysis as a foundational pillar of green chemistry. *Applied Catalysis A: General* **2001,** *221* (1), 3-13.

16. Anastas, P. T.; Kirchhoff, M. M., Origins, current status, and future challenges of green chemistry. *Acc. Chem. Res.* **2002,** *35* (9), 686-694.

17. H. Clark, J., Green chemistry: challenges and opportunities. *Green Chemistry* **1999,** *1* (1), 1-8.

18. Anastas, P. T.; Bartlett, L. B.; Kirchhoff, M. M.; Williamson, T. C., The role of catalysis in the design, development, and implementation of green chemistry. *Catal. Today* **2000,** *55* (1), 11-22.

19. Werkmeister, S.; Junge, K.; Beller, M., Catalytic hydrogenation of carboxylic acid esters, amides, and nitriles with homogeneous catalysts. *Organic Process Research & Development* **2014,** *18* (2), 289-302.

20. Pritchard, J.; Filonenko, G. A.; van Putten, R.; Hensen, E. J. M.; Pidko, E. A., Heterogeneous and homogeneous catalysis for the hydrogenation of carboxylic acid derivatives: history, advances and future directions. *Chem. Soc. Rev.* **2015,** *44* (11), 3808-3833.

21. Catalytic reductions. In *Green Chemistry and Catalysis*; Wiley‑VCH Verlag GmbH & Co. KGaA, **2007**.

22. W. Gribble, G., Sodium borohydride in carboxylic acid media: a phenomenal reduction system. *Chem. Soc. Rev.* **1998,** *27* (6), 395-404.

23. Smith, A. M.; Whyman, R., Review of methods for the catalytic hydrogenation of carboxamides. *Chem. Rev.* **2014,** *114* (10), 5477-5510.

24. Xie, J.-H.; Liu, X.-Y.; Xie, J.-B.; Wang, L.-X.; Zhou, Q.-L., An additional coordination group leads to extremely efficient chiral iridium catalysts for asymmetric hydrogenation of ketones. *Angew. Chem. Int. Ed.* **2011,** *50* (32), 7329-7332.

25. Blaser, H.-U.; Malan, C.; Pugin, B.; Spindler, F.; Steiner, H.; Studer, M., Selective hydrogenation for fine chemicals: recent trends and new developments. *Adv. Synth. Catal.* **2003,** *345* (1-2), 103-151.

26. Noyori, R.; Ohkuma, T., Asymmetric catalysis by architectural and functional molecular engineering: practical chemo- and stereoselective hydrogenation of ketones. *Angew. Chem. Int. Ed.* **2001,** *40* (1), 40-73.

27. Zhao, B.; Han, Z.; Ding, K., The N-H functional group in organometallic catalysis. *Angew. Chem. Int. Ed.* **2013,** *52* (18), 4744-4788.

28. Kim, D.; Le, L.; Drance, M. J.; Jensen, K. H.; Bogdanovski, K.; Cervarich, T. N.; Barnard, M. G.; Pudalov, N. J.; Knapp, S. M. M.; Chianese, A. R., Ester hydrogenation catalyzed by cnn-pincer complexes of ruthenium. *Organometallics* **2016,** *35* (7), 982-989.

29. Thakur, D. S.; Carrick, W. J.; US Patent 9,120,086, 2015.

30. Kuriyama, W.; Matsumoto, T.; Ogata, O.; Ino, Y.; Aoki, K.; Tanaka, S.; Ishida, K.; Kobayashi, T.; Sayo, N.; Saito, T., Catalytic hydrogenation of esters. development of an efficient catalyst and processes for synthesising (R)-1,2-propanediol and 2-(l-menthoxy)ethanol. *Organic Process Research & Development* **2012,** *16* (1), 166-171.

31. Adkins, H.; Folkers, K., The catalytic hydrogenation of esters to alcohols. *JACS* **1931,** *53* (3), 1095-1097.

32. Folkers, K.; Adkins, H., The catalytic hydrogenation of esters to alcohols. II. *JACS* **1932,** *54* (3), 1145-1154.

33. Rieke, R. D.; Thakur, D. S.; Roberts, B. D.; White, G. T., Fatty methyl ester hydrogenation to fatty alcohol part I: correlation between catalyst properties and activity/selectivity. *Journal of the American Oil Chemists' Society* **1997,** *74* (4), 333-339.

34. Fairweather, N. T.; Gibson, M. S.; Guan, H., Homogeneous hydrogenation of fatty acid methyl esters and natural oils under neat conditions. *Organometallics* **2015,** *34* (1), 335-339.

35. Adkins, H.; Burgoyne, E. E.; Schneider, H. J., The copper—chromium oxide catalyst for hydrogenation1. *JACS* **1950,** *72* (6), 2626-2629.

36. Hattori, Y.; Yamamoto, K.; Kaita, J.; Matsuda, M.; Yamada, S. J. J. o. t. A. O. C. S., The development of nonchromium catalyst for fatty alcohol production. *Journal of the American Oil Chemists' Society* **2000,** *77* (12), 1283-1288.

37. Jürgen, L.; Tiberius, R., Fatty methyl ester hydrogenation: application of chromium free catalysts. *Stud. Surf. Sci. Catal.* **1999**, *121*, 215-220.

38. Hattori, Y.; Yamamoto, K.; Kaita, J.; Matsuda, M.; Yamada, S. J. J. o. t. A. O. C. S., The development of nonchromium catalyst for fatty alcohol production. *Journal of the American Oil Chemists' Society* **2000,** *77* (12), 1283-1288.

39. Yin, A.; Wen, C.; Dai, W.-L.; Fan, K., Surface modification of HMS material with silica sol leading to a remarkable enhanced catalytic performance of Cu/SiO2. *Appl. Surf. Sci.* **2011,** *257* (13), 5844-5849.

40. Yin, A.; Guo, X.; Dai, W.-L.; Li, H.; Fan, K., Highly active and selective copper-containing HMS catalyst in the hydrogenation of dimethyl oxalate to ethylene glycol. *Applied Catalysis A: General* **2008,** *349* (1), 91-99.

41. Yin, A.; Guo, X.; Fan, K.; Dai, W.-L., Influence of copper precursors on the structure evolution and catalytic performance of Cu/HMS catalysts in the hydrogenation of dimethyl oxalate to ethylene glycol. *Applied Catalysis A: General* **2010,** *377* (1), 128-133.

42. Deshpande, V. M.; Patterson, W. R.; Narasimhan, C. S., Studies on ruthenium-tin boride catalysts I. Characterization. *Journal of Catalysis* **1990,** *121* (1), 165-173.

43. Deshpande, V. M.; Ramnarayan, K.; Narasimhan, C. S., Studies on ruthenium-tin boride catalysts II. Hydrogenation of fatty acid esters to fatty alcohols. *J. Catal.* **1990,** *121* (1), 174-182.

44. Miyake, T.; Makino, T.; Taniguchi, S.-i.; Watanuki, H.; Niki, T.; Shimizu, S.; Kojima, Y.; Sano, M., Alcohol synthesis by hydrogenation of fatty acid methyl esters on supported Ru–Sn and Rh–Sn catalysts. *Applied Catalysis A: General* **2009,** *364* (1), 108-112.

45. Sánchez, M. A.; Mazzieri, V. A.; Sad, M. R.; Pieck, C. L., Influence of the operating conditions and kinetic analysis of the selective hydrogenation of methyl oleate on Ru–Sn–B/Al2O3 catalysts. *Reaction Kinetics, Mechanisms and Catalysis* **2012,** *107* (1), 127-139.

46. Sánchez, M. A.; Mazzieri, V. A.; Oportus, M.; Reyes, P.; Pieck, C. L., Influence of Ge content on the activity of Ru–Ge–B/Al2O3 catalysts for selective hydrogenation of methyl oleate to oleyl alcohol. *Catal. Today* **2013,** *213*, 81-86.

47. Zheng, J.; Lin, H.; Wang, Y.-n.; Zheng, X.; Duan, X.; Yuan, Y., Efficient low-temperature selective hydrogenation of esters on bimetallic Au–Ag/SBA-15 catalyst. *J. Catal.* **2013,** *297*, 110-118.

48. Liu, K.; Pritchard, J.; Lu, L.; van Putten, R.; Verhoeven, M. W. G. M.; Schmitkamp, M.; Huang, X.; Lefort, L.; Kiely, C. J.; Hensen, E. J. M.; Pidko, E. A., Supported nickel–rhenium catalysts for selective hydrogenation of methyl esters to alcohols. *Chem. Commun.* **2017,** *53* (70), 9761-9764.

49. Grey, R. A.; Pez, G. P.; Wallo, A.; Corsi, J., Homogeneous catalytic hydrogenation of carboxylic acid esters to alcohols. *J. Chem. Soc., Chem. Commun.* **1980,** (16), 783-784.

50. Pez, G. P.; Grey, R. A.; Corsi, J., Anionic metal hydride catalysts. 1. Synthesis of potassium hydrido(phosphine)ruthenate complexes. *JACS* **1981,** *103* (25), 7528-7535.

51. Grey, R. A.; Pez, G. P.; Wallo, A., Anionic metal hydride catalysts. 2. Application to the hydrogenation of ketones, aldehydes, carboxylic acid esters, and nitriles. *JACS* **1981,** *103* (25), 7536-7542.

52. Bianchi, M.; Menchi, G.; Francalanci, F.; Piacenti, F.; Matteoli, U.; Frediani, P.; Botteghi, C., Homogeneous catalytic hydrogenation of free carboxylic acids in the presence of cluster ruthenium carbonyl hydrides. *J. Organomet. Chem.* **1980,** *188* (1), 109-119.

53. Matteoli, U.; Blanchi, M.; Menchi, G.; Prediani, P.; Piacenti, F., Homogeneous catalytic hydrogenation of dicarboxylic acid esters. *J. Mol. Catal.* **1984,** *22* (3), 353-362.

54. Matteoli, U.; Menchi, G.; Bianchi, M.; Piacenti, F., Homogeneous catalytic hydrogenation dicarboxylic acid esters. II. *J. Organomet. Chem.* **1986,** *299* (2), 233-238.

55. Yoshinori, H.; Hiroko, I.; Sugio, N.; Keisuke, W., Selective hydrogenation of cyclic ester to α,ω-diol catalyzed by cationic ruthenium complexes with trialkylphosphine ligands. *Chem. Lett.* **1992,** *21* (10), 1983-1986.

56. Nomura, K.; Ogura, H.; Imanishi, Y., Ruthenium catalyzed hydrogenation of methyl phenylacetate under low hydrogen pressure. *J. Mol. Catal. A: Chem.* **2002,** *178* (1), 105-114.

57. T. Teunissen, H.; J. Elsevier, C., Ruthenium catalysed hydrogenation of dimethyl oxalate to ethylene glycol. *Chem. Commun.* **1997,** (7), 667-668.

58. van Engelen, M. C.; Teunissen, H. T.; de Vries, J. G.; Elsevier, C. J., Suitable ligands for homogeneous ruthenium-catalyzed hydrogenolysis of esters. *J. Mol. Catal. A: Chem.* **2003,** *206* (1), 185-192.

59. T. Teunissen, H., Homogeneous ruthenium catalyzed hydrogenation of esters to alcohols‡. *Chem. Commun.* **1998,** (13), 1367-1368.

60. vom Stein, T.; Meuresch, M.; Limper, D.; Schmitz, M.; Hölscher, M.; Coetzee, J.; Cole-Hamilton, D. J.; Klankermayer, J.; Leitner, W., Highly versatile catalytic hydrogenation of carboxylic and carbonic acid derivatives using a Ru-Triphos complex: molecular control over selectivity and substrate scope. *JACS* **2014,** *136* (38), 13217-13225.

61. Zhang, J.; Leitus, G.; Ben-David, Y.; Milstein, D., Efficient homogeneous catalytic hydrogenation of esters to alcohols. *Angew. Chem. Int. Ed.* **2006,** *118* (7), 1131-1133.

62. Saudan, L. A.; Saudan, C. M.; Debieux, C.; Wyss, P., Dihydrogen reduction of carboxylic esters to alcohols under the catalysis of homogeneous ruthenium complexes: high efficiency and unprecedented chemoselectivity. *Angew. Chem. Int. Ed.* **2007,** *119* (39), 7617-7620.

63. Sandoval, C. A.; Ohkuma, T.; Muñiz, K.; Noyori, R., Mechanism of asymmetric hydrogenation of ketones catalyzed by BINAP/1,2-Diamine−Ruthenium(II) complexes. *JACS* **2003,** *125* (44), 13490-13503.

64. Abdur-Rashid, K.; Lough, A. J.; Morris, R. H., Ruthenium dihydride RuH2(PPh3)2((R,R)-cyclohexyldiamine) and ruthenium monohydride RuHCl(PPh3)2((R,R)-cyclohexyldiamine): active catalyst and catalyst precursor for the hydrogenation of ketones and imines. *Organometallics* **2000,** *19* (14), 2655-2657.

65. Carpenter, I.; Eckelmann, S. C.; Kuntz, M. T.; Fuentes, J. A.; France, M. B.; Clarke, M. L., Convenient and improved protocols for the hydrogenation of esters using Ru catalysts derived from (P,P), (P,N,N) and (P,N,O) ligands. *Dalton Transactions* **2012,** *41* (34), 10136-10140.

66. Tan, X.; Wang, Y.; Liu, Y.; Wang, F.; Shi, L.; Lee, K.-H.; Lin, Z.; Lv, H.; Zhang, X., Highly efficient tetradentate ruthenium catalyst for ester reduction: especially for hydrogenation of fatty acid esters. *Org. Lett.* **2015,** *17* (3), 454-457.

67. Zhang, J.; Balaraman, E.; Leitus, G.; Milstein, D., Electron-rich PNP- and PNN-type ruthenium(II) hydrido borohydride pincer complexes. synthesis, structure, and catalytic dehydrogenation of alcohols and hydrogenation of esters. *Organometallics* **2011,** *30* (21), 5716-5724.

68. Ito, M.; Ootsuka, T.; Watari, R.; Shiibashi, A., Himizu, A, Ikariya, T.; Catalytic hydrogenation of xarboxamides and esters by well-defined Cp*Ru complexes bearing a protic amine ligand. *JACS.* **2011,** *133* (12), 4240-4242.

69. Díez-González, S.; Nolan, S. P., Stereoelectronic parameters associated with N-heterocyclic carbene (NHC) ligands: A quest for understanding. *Coord. Chem. Rev.* **2007,** *251* (5), 874-883.

70. Crudden, C. M.; Allen, D. P., Stability and reactivity of N-heterocyclic carbene complexes. *Coord. Chem. Rev.* **2004,** *248* (21), 2247-2273.

71. Hopkinson, M. N.; Richter, C.; Schedler, M.; Glorius, F., An overview of N-heterocyclic carbenes. *Nature* **2014,** *510*, 485.

72. O, W. W. N.; Lough, A. J.; Morris, R. H., The hydrogenation of molecules with polar bonds catalyzed by a ruthenium(ii) complex bearing a chelating N-heterocyclic carbene with a primary amine donor. *Chem. Commun.* **2010,** *46* (43), 8240-8242.

73. O, W. W. N.; Morris, R. H., Ester hydrogenation catalyzed by a ruthenium(II) complex bearing an N-heterocyclic carbene tethered with an "NH2" group and a DFT study of the proposed bifunctional mechanism. *ACS Catalysis* **2013,** *3* (1), 32-40.

74. Fogler, E.; Balaraman, E.; Ben-David, Y.; Leitus, G.; Shimon, L. J. W.; Milstein, D., New CNN-type ruthenium pincer NHC complexes. mild, efficient catalytic hydrogenation of esters. *Organometallics* **2011,** *30* (14), 3826-3833.

75. Sun, Y.; Koehler, C.; Tan, R.; Annibale, V. T.; Song, D., Ester hydrogenation catalyzed by Ru-CNN pincer complexes. *Chem. Commun.* **2011,** *47* (29), 8349-8351.

76. Westerhaus, F. A.; Wendt, B.; Dumrath, A.; Wienhöfer, G.; Junge, K.; Beller, M., Ruthenium catalysts for hydrogenation of aromatic and aliphatic esters: make use of bidentate carbene ligands. *ChemSusChem* **2013,** *6* (6), 1001-1005.

77. Junge, K.; Wendt, B.; Jiao, H.; Beller, M., Iridium-catalyzed hydrogenation of carboxylic acid esters. *ChemCatChem* **2014,** *6* (10), 2810-2814.

78. Hydrogenation of Esters. In *Sustainable Catalysis*.

79. Spasyuk, D.; Smith, S.; Gusev, D. G., From esters to alcohols and back with ruthenium and osmium catalysts. *Angew. Chem. Int. Ed.* **2012,** *51* (11), 2772-2775.

80. Spasyuk, D.; Smith, S.; Gusev, D. G., Replacing phosphorus with sulfur for the efficient hydrogenation of esters. *Angew. Chem. Int. Ed.* **2013,** *52* (9), 2538-2542.

81. Spasyuk, D.; Vicent, C.; Gusev, D. G., Chemoselective hydrogenation of carbonyl compounds and acceptorless dehydrogenative coupling of alcohols. *JACS* **2015,** *137* (11), 3743-3746.

82. Gusev, D. G., Dehydrogenative coupling of ethanol and ester hydrogenation catalyzed by pincer-type ynp complexes. *ACS Catalysis* **2016,** *6* (10), 6967-6981.

83. Hasanayn, F.; Baroudi, A.; Bengali, A. A.; Goldman, A. S., Hydrogenation of dimethyl carbonate to methanol by trans-[Ru(H)2(PNN)(CO)] catalysts: DFT evidence for ion-pair-mediated metathesis paths for C–OMe bond cleavage. *Organometallics* **2013,** *32* (23), 6969-6985.

84. Hasanayn, F.; Harb, H., A metathesis model for the dehydrogenative coupling of amines with alcohols and esters into carboxamides by Milstein's [Ru(PNN)(CO)(H)] catalysts. *Inorg. Chem.* **2014,** *53* (16), 8334-8349.

85. Chen, X.; Jing, Y.; Yang, X., Unexpected direct hydride transfer mechanism for the hydrogenation of ethyl acetate to ethanol catalyzed by SNS pincer ruthenium complexes. *Chemistry – A European Journal* **2016,** *22* (6), 1950-1957.

86. Takebayashi, S.; Bergens, S. H., Facile bifunctional addition of lactones and esters at low temperatures. the first intermediates in lactone/ester hydrogenations. *Organometallics* **2009,** *28* (8), 2349-2351.

87. Li, W.; Xie, J.-H.; Yuan, M.-L.; Zhou, Q.-L., Ruthenium complexes of tetradentate bipyridine ligands: highly efficient catalysts for the hydrogenation of carboxylic esters and lactones. *Green Chemistry* **2014,** *16* (9), 4081-4085.

88. Fogler, E.; Garg, J. A.; Hu, P.; Leitus, G.; Shimon, L. J. W.; Milstein, D., System with potential dual modes of metal–ligand cooperation: highly catalytically active pyridine-based PNNH–Ru pincer complexes. *Chemistry – A European Journal* **2014,** *20* (48), 15727-15731.

89. Filonenko, G. A.; Aguila, M. J. B.; Schulpen, E. N.; van Putten, R.; Wiecko, J.; Müller, C.; Lefort, L.; Hensen, E. J. M.; Pidko, E. A., Bis-N-heterocyclic carbene aminopincer ligands enable high activity in Ru-catalyzed ester hydrogenation. *JACS* **2015,** *137* (24), 7620-7623.

90. Tan, X.; Wang, Q.; Liu, Y.; Wang, F.; Lv, H.; Zhang, X., A new designed hydrazine group-containing ruthenium complex used for catalytic hydrogenation of esters. *Chem. Commun.* **2015,** *51* (61), 12193-12196.

91. John, J. M.; Takebayashi, S.; Dabral, N.; Miskolzie, M.; Bergens, S. H., Base-catalyzed bifunctional addition to amides and imides at low temperature. a new pathway for carbonyl hydrogenation. *JACS* **2013,** *135* (23), 8578-8584.

92. Le, L.; Liu, J.; He, T.; Kim, D.; Lindley, E. J.; Cervarich, T. N.; Malek, J. C.; Pham, J.; Buck, M. R.; Chianese, A. R., Structure–function relationship in ester hydrogenation catalyzed by ruthenium CNN-pincer complexes. *Organometallics* **2018,** *37* (19), 3286-3297.

93. Wang, Z.; Chen, X.; Liu, B.; Liu, Q.-b.; Solan, G. A.; Yang, X.; Sun, W.-H., Cooperative interplay between a flexible PNN-Ru(ii) complex and a NaBH4 additive in the efficient catalytic hydrogenation of esters. *Catalysis Science & Technology* **2017,** *7* (6), 1297-1304.

94. Stadler, B. M.; Puylaert, P.; Diekamp, J.; van Heck, R.; Fan, Y.; Spannenberg, A.; Hinze, S.; de Vries, J. G., Inexpensive ruthenium NNS-complexes as efficient ester hydrogenation catalysts with high C=O vs. C=C selectivities. *Adv. Synth. Catal.* **2018,** *360* (6), 1151-1158.

95. Zell, T.; Ben-David, Y.; Milstein, D., Unprecedented iron-catalyzed ester hydrogenation. mild, selective, and efficient hydrogenation of trifluoroacetic esters to alcohols catalyzed by an iron pincer complex. *Angew. Chem. Int. Ed.* **2014,** *53* (18), 4685-4689.

96. Werkmeister, S.; Junge, K.; Wendt, B.; Alberico, E.; Jiao, H.; Baumann, W.; Junge, H.; Gallou, F.; Beller, M., Hydrogenation of esters to alcohols with a well-defined iron complex. *Angew. Chem. Int. Ed.* **2014,** *53* (33), 8722-8726.

97. Chakraborty, S.; Dai, H.; Bhattacharya, P.; Fairweather, N. T.; Gibson, M. S.; Krause, J. A.; Guan, H., Iron-based catalysts for the hydrogenation of esters to alcohols. *JACS* **2014,** *136* (22), 7869-7872.

98. Elangovan, S.; Wendt, B.; Topf, C.; Bachmann, S.; Scalone, M.; Spannenberg, A.; Jiao, H.; Baumann, W.; Junge, K.; Beller, M., Improved second generation iron pincer complexes for effective ester hydrogenation. *Adv. Synth. Catal.* **2016,** *358* (5), 820-825.

99. Gajewski, P.; Gonzalez-de-Castro, A.; Renom-Carrasco, M.; Piarulli, U.; Gennari, C.; de Vries, J. G.; Lefort, L.; Pignataro, L., Expanding the catalytic scope of (cyclopentadienone)iron complexes to the hydrogenation of activated esters to alcohols. *ChemCatChem* **2016,** *8* (22), 3431-3435.

100. Shvo, Y.; Czarkie, D.; Rahamim, Y.; Chodosh, D. F., A new group of ruthenium complexes: structure and catalysis. *JACS* **1986,** *108* (23), 7400-7402.

101. Blum, Y.; Czarkie, D.; Rahamim, Y.; Shvo, Y., (Cyclopentadienone)ruthenium carbonyl complexes - a new class of homogeneous hydrogenation catalysts. *Organometallics* **1985,** *4* (8), 1459-1461.

102. Korstanje, T. J.; Ivar van der Vlugt, J.; Elsevier, C. J.; de Bruin, B., Hydrogenation of carboxylic acids with a homogeneous cobalt catalyst. *Science* **2015,** *350* (6258), 298-302.

103. Srimani, D.; Mukherjee, A.; Goldberg, A. F. G.; Leitus, G.; Diskin-Posner, Y.; Shimon, L. J. W.; Ben David, Y.; Milstein, D., Cobalt-catalyzed hydrogenation of esters to alcohols: unexpected reactivity trend indicates ester enolate intermediacy. *Angew. Chem. Int. Ed.* **2015,** *54* (42), 12357-12360.

104. Yuwen, J.; Chakraborty, S.; Brennessel, W. W.; Jones, W. D., Additive-free cobalt-catalyzed hydrogenation of esters to alcohols. *ACS Catalysis* **2017,** *7* (5), 3735-3740.

105. Junge, K.; Wendt, B.; Cingolani, A.; Spannenberg, A.; Wei, Z.; Jiao, H.; Beller, M., Cobalt pincer complexes for catalytic reduction of carboxylic acid esters. *Chemistry – A European Journal* **2018,** *24* (5), 1046-1052.

106. Elangovan, S.; Garbe, M.; Jiao, H.; Spannenberg, A.; Junge, K.; Beller, M., Hydrogenation of esters to alcohols catalyzed by defined manganese pincer complexes. *Angew. Chem. Int. Ed.* **2016,** *55* (49), 15364-15368.

107. Espinosa-Jalapa, N. A.; Nerush, A.; Shimon, L. J. W.; Leitus, G.; Avram, L.; Ben-David, Y.; Milstein, D., Manganese-catalyzed hydrogenation of esters to alcohols. *Chemistry – A European Journal* **2017,** *23* (25), 5934-5938.

108. Widegren, M. B.; Harkness, G. J.; Slawin, A. M. Z.; Cordes, D. B.; Clarke, M. L., A highly active manganese catalyst for enantioselective ketone and ester hydrogenation. *Angew. Chem. Int. Ed.* **2017,** *56* (21), 5825-5828.

109. van Putten, R.; Uslamin, E. A.; Garbe, M.; Liu, C.; Gonzalez-de-Castro, A.; Lutz, M.; Junge, K.; Hensen, E. J. M.; Beller, M.; Lefort, L.; Pidko, E. A., Non-pincer-type manganese complexes as efficient catalysts for the hydrogenation of esters. *Angew. Chem. Int. Ed.* **2017,** *56* (26), 7531-7534.

110. McMorn, P.; Hutchings, G. J., Heterogeneous enantioselective catalysts: strategies for the immobilisation of homogeneous catalysts. *Chem. Soc. Rev.* **2004,** *33* (2), 108-122.

111. Copéret, C.; Basset, J.-M., Strategies to immobilize well-defined olefin metathesis catalysts: supported homogeneous catalysis vs. surface organometallic chemistry. *Adv. Synth. Catal.* **2007,** *349* (1-2), 78-92.

112. Altava, B.; Burguete, M. I.; García-Verdugo, E.; Luis, S. V., Chiral catalysts immobilized on achiral polymers: effect of the polymer support on the performance of the catalyst. *Chem. Soc. Rev.* **2018,** *47* (8), 2722-2771.

113. Song, C. E.; Lee, S.-g., Supported chiral catalysts on inorganic materials. *Chem. Rev.* **2002,** *102* (10), 3495-3524.

114. Pal, N.; Bhaumik, A., Mesoporous materials: versatile supports in heterogeneous catalysis for liquid phase catalytic transformations. *RSC Advances* **2015,** *5* (31), 24363-24391.

115. Zamboulis, A.; Moitra, N.; Moreau, J. J. E.; Cattoën, X.; Wong Chi Man, M., Hybrid materials: versatile matrices for supporting homogeneous catalysts. *J. Mater. Chem.* **2010,** *20* (42), 9322-9338.

116. Collis, A. E. C.; Horváth, I. T., Heterogenization of homogeneous catalytic systems. *Catalysis Science & Technology* **2011,** *1* (6), 912-919.

117. Vural Gürsel, I.; Noël, T.; Wang, Q.; Hessel, V., Separation/recycling methods for homogeneous transition metal catalysts in continuous flow. *Green Chemistry* **2015,** *17* (4), 2012-2026.

118. Li, C.; Wang, W.; Yan, L.; Ding, Y. J. F. o. C. S.; Engineering, A mini review on strategies for heterogenization of rhodium-based hydroformylation catalysts. *Frontiers of Chemical Science and Engineering* **2018,** *12* (1), 113-123.

119. Dewaele, A.; Verpoort, F.; Sels, B., Opportunities of immobilized homogeneous metathesis complexes as prominent heterogeneous catalysts. *ChemCatChem* **2016,** *8* (19), 3010-3030.

120. Hübner, S.; de Vries, J. G.; Farina, V., Why does industry not use immobilized transition metal complexes as catalysts? *Adv. Synth. Catal.* **2016,** *358* (1), 3-25.

121. Munirathinam, R.; Huskens, J.; Verboom, W., supported catalysis in continuous-flow microreactors. *Adv. Synth. Catal.* **2015,** *357* (6), 1093-1123.

122. Grubbs, R. H.; Kroll, L. C., Catalytic reduction of olefins with a polymer-supported rhodium(I) catalyst. *JACS* **1971,** *93* (12), 3062-3063.

123. Mashima, K.; Kusano, K.-h.; Sato, N.; Matsumura, Y.-i.; Nozaki, K.; Kumobayashi, H.; Sayo, N.; Hori, Y.; Ishizaki, T., Cationic BINAP-Ru(II) halide complexes: highly efficient catalysts for stereoselective asymmetric hydrogenation of .alpha.- and .beta.-functionalized ketones. *The Journal of Organic Chemistry* **1994,** *59* (11), 3064-3076.

124. Noyori, R.; Ohta, M.; Hsiao, Y.; Kitamura, M.; Ohta, T.; Takaya, H., Asymmetric synthesis of isoquinoline alkaloids by homogeneous catalysis. *JACS* **1986,** *108* (22), 7117-7119.

125. Ohkuma, T.; Ooka, H.; Hashiguchi, S.; Ikariya, T.; Noyori, R., Practical enantioselective hydrogenation of aromatic ketones. *JACS* **1995,** *117* (9), 2675-2676.

126. Ohkuma, T.; Koizumi, M.; Doucet, H.; Pham, T.; Kozawa, M.; Murata, K.; Katayama, E.; Yokozawa, T.; Ikariya, T.; Noyori, R., Asymmetric hydrogenation of alkenyl, cyclopropyl, and aryl ketones. RuCl2(xylbinap)(1,2-diamine) as a precatalyst exhibiting a wide scope. *JACS* **1998,** *120* (51), 13529-13530.

127. Hashiguchi, S.; Fujii, A.; Takehara, J.; Ikariya, T.; Noyori, R., Asymmetric transfer hydrogenation of aromatic ketones catalyzed by chiral ruthenium(II) complexes. *JACS* **1995,** *117* (28), 7562-7563.

128. Noyori, R.; Hashiguchi, S., Asymmetric transfer hydrogenation catalyzed by chiral ruthenium complexes. *Acc. Chem. Res.* **1997,** *30* (2), 97-102.

129. Ikariya, T.; Blacker, A. J., Asymmetric transfer hydrogenation of ketones with bifunctional transition metal-based molecular catalysts. *Acc. Chem. Res.* **2007,** *40* (12), 1300-1308.

130. Bayston, D. J.; Fraser, J. L.; Ashton, M. R.; Baxter, A. D.; Polywka, M. E. C.; Moses, E., Preparation and use of a polymer supported binap hydrogenation catalyst. *The Journal of Organic Chemistry* **1998,** *63* (9), 3137-3140.

131. Ohkuma, T.; Takeno, H.; Honda, Y.; Noyori, R., Asymmetric hydrogenation of ketones with polymer-bound BINAP/diamine ruthenium catalysts. **2001,** *343* (4), 369-375.

132. Li, X.; Chen, W.; Hems, W.; King, F.; Xiao, J., Asymmetric hydrogenation of ketones with polymer-supported chiral 1,2-diphenylethylenediamine. *Org. Lett.* **2003,** *5* (24), 4559-4561.

133. Li, X.; Chen, W.; Hems, W.; King, F.; Xiao, J., Asymmetric transfer hydrogenation of ketones with a polymer-supported chiral diamine. *Tetrahedron Lett.* **2004,** *45* (5), 951-953.

134. Li, X.; Wu, X.; Chen, W.; Hancock, F. E.; King, F.; Xiao, J., Asymmetric transfer hydrogenation in water with a supported Noyori−Ikariya catalyst. *Org. Lett.* **2004,** *6* (19), 3321-3324.

135. ter Halle, R.; Schulz, E.; Lemaire, M., Heterogeneous enantioselective catalytic reduction of ketones. *Synlett* **1997,** *1997* (11), 1257-1258.

136. Sun, Q.; Jin, Y.; Zhu, L.; Wang, L.; Meng, X.; Xiao, F.-S., Superhydrophobic, chiral, and mesoporous TsDPEN copolymer coordinated to ruthenium species as an efficient catalyst for asymmetric transfer hydrogenation. *Nano Today* **2013,** *8* (4), 342-350.

137. Zhang, Y.; Wei, S.; He, Y.; Nawaz, F.; Liu, S.; Zhang, H.; Xiao, F.-S., Solvothermal synthesis of carboxyl and amido functionalized mesoporous resins for water treatments. *J. Mater. Chem.* **2010,** *20* (22), 4609-4614.

138. Arakawa, Y.; Haraguchi, N.; Itsuno, S., Design of novel polymer-supported chiral catalyst for asymmetric transfer hydrogenation in water. *Tetrahedron Lett.* **2006,** *47* (19), 3239-3243.

139. Arakawa, Y.; Chiba, A.; Haraguchi, N.; Itsuno, S., Asymmetric transfer hydrogenation of aromatic ketones in water using a polymer-supported chiral catalyst containing a hydrophilic pendant group. *Adv. Synth. Catal.* **2008,** *350* (14-15), 2295-2304.

140. Xie, Y.; Wang, M.; Wu, X.; Chen, C.; Ma, W.; Dong, Q.; Yuan, M.; Hou, Z., A pH-responsive soluble-polymer-based homogeneous ruthenium catalyst for highly efficient asymmetric transfer hydrogenation (ATH). *CHEMPLUSCHEM* **2016,** *81* (6), 541-549.

141. Judkins, C. M. G.; Knights, K. A.; Johnson, B. F. G.; Miguel, Y. R. d.; Raja, R.; Thomas, J. M., Immobilisation of ruthenium cluster catalysts via novel derivatisations of ArgoGel resins. *Chem. Commun.* **2001,** (24), 2624-2625.

142. Gibson, S. E.; Hales, N. J.; Peplow, M. A., Chromium carbonyl complexes as novel traceless linkers. *Tetrahedron Lett.* **1999,** *40* (7), 1417-1418.

143. Canali, L.; Cowan, E.; L. Gibson, C.; C. Sherrington, D.; Deleuze, H., Remarkable matrix effect in polymer-supported Jacobsen's alkene epoxidation catalysts. *Chem. Commun.* **1998,** (23), 2561-2562.

144. Canali, L.; Sherrington, D. C.; Deleuze, H., Synthesis of resins with pendently-bound chiral manganese–salen complexes and use as heterogeneous asymmetric alkene epoxidation catalysts. *React. Funct. Polym.* **1999,** *40* (2), 155-168.

145. Smith, K.; Liu, C.-H., Asymmetric epoxidation using a singly-bound supported Katsuki-type (salen)Mn complex. *Chem. Commun.* **2002,** (8), 886-887.

146. Ralph, C. K.; Akotsi, O. M.; Bergens, S. H., A Reusable polymeric asymmetric hydrogenation catalyst made by ring-opening olefin metathesis polymerization. *Organometallics* **2004,** *23* (7), 1484-1486.

147. Ralph, C. K.; Bergens, S. H., A highly reusable catalyst for enantioselective ketone hydrogenation. Catalyst-organic frameworks by alternating ROMP assembly. *Organometallics* **2007,** *26* (7), 1571-1574.

148. Corkum, E. G.; Hass, M. J.; Sullivan, A. D.; Bergens, S. H., A highly reusable rhodium catalyst-organic framework for the intramolecular cycloisomerization of 1,6-enynes. *Org. Lett.* **2011,** *13* (13), 3522-3525.

149. Corkum, E. G.; Kalapugama, S.; Hass, M. J.; Bergens, S. H., Solvent-free isomerization of allylic alcohols catalyzed by a rhodium catalyst-organic framework. *RSC Advances* **2012,** *2* (8), 3473-3476.

150. Adkins, H.; Wojcik, B.; Covert, L. W., The catalytic hydrogenation of esters to alcohols. III. *JACS* **1933,** *55* (4), 1669-1676.

151. Fan, G.; Zhou, Y.; Fu, H.; Ye, X.; Li, R.; Chen, H.; Li, X., Highly efficient hydrogenation of methyl propionate to propanol over hydrous zirconia supported ruthenium. *Chin. J. Chem .* **2011,** *29* (2), 229-236.

152. Bergbreiter D. E.; The use of soluble polymers to effect homogeneous catalyst separation and reuse. *Catal. Today.* **1998,** *42* (4), 389-397.

153. Tanimu, A.; Jaenicke, S.; Alhooshani, K., Heterogeneous catalysis in continuous flow microreactors: a review of methods and applications. *Chem. Eng. J.* **2017,** *327*, 792-821.

154. Hübner, S.; de Vries, J. G.; Farina, V., Why does industry not use immobilized transition metal complexes as catalysts? *Adv. Synth. Catal.* **2016,** *358* (1), 3-25.

155. Insoluble resin-supported catalysts. In *Recoverable and Recyclable Catalysts*. John Wiley & Sons, Ltd, **2009**

156. Barbaro, P.; Liguori, F., Ion exchange resins: catalyst recovery and recycle. *Chem. Rev.* **2009,** *109* (2), 515-529.

157. Pugin, B.; Blaser, H.-U. J. T. i. C., Immobilized complexes for enantioselective catalysis: when will they be used in industry? *Top. Catal.* **2010,** *53* (13), 953-962.

158. Dioos, B. M. L.; Vankelecom, I. F. J.; Jacobs, P. A., Aspects of immobilisation of catalysts on polymeric supports. *Adv. Synth. Catal.* **2006,** *348* (12-13), 1413-1446.

159. Mastrorilli, P.; Nobile, C. F., Supported catalysts from polymerizable transition metal complexes. *Coord. Chem. Rev.* **2004,** *248* (3), 377-395.

160. Ding, S.-Y.; Wang, W., Covalent organic frameworks (COFs): from design to applications. *Chem. Soc. Rev.* **2013,** *42* (2), 548-568.

161. Feng, X.; Ding, X.; Jiang, D., Covalent organic frameworks. *Chem. Soc. Rev.* **2012,** *41* (18), 6010-6022.

162. Dumont, W.; Poulin, J. C.; Dang Tuan, P.; Kagan, H. B., Asymmetric catalytic reduction with transition metal complexes. II. Asymmetric catalysis by a supported chiral rhodium complex. *JACS* **1973,** *95* (25), 8295-8299.

163. Shi, L.; Wang, X.; Sandoval, C. A.; Wang, Z.; Li, H.; Wu, J.; Yu, L.; Ding, K., Development of a continuous-flow system for asymmetric hydrogenation using self-supported chiral catalysts. *Chemistry – A European Journal* **2009,** *15* (38), 9855-9867.

164. Wang, X.; Shi, L.; Li, M.; Ding, K., Heterogenization of Shibasaki's Binol/La catalyst for enantioselective epoxidation of α,β-unsaturated ketones with multitopic binol ligands: The Impact of Bridging Spacers. *Angew. Chem. Int. Ed.* **2005,** *117* (39), 6520-6524.

165. Wang, T.; Lyu, Y.; Chen, X.; Li, C.; Jiang, M.; Song, X.; Ding, Y., Ru coordinated with BINAP in knitting aryl network polymers for heterogeneous asymmetric hydrogenation of methyl acetoacetate. *RSC Advances* **2016,** *6* (34), 28447-28450.

166. Sun, Q.; Meng, X.; Liu, X.; Zhang, X.; Yang, Y.; Yang, Q.; Xiao, F.-S., Mesoporous cross-linked polymer copolymerized with chiral BINAP ligand coordinated to a ruthenium species as an efficient heterogeneous catalyst for asymmetric hydrogenation. *Chem. Commun.* **2012,** *48* (85), 10505-10507.

167. Wang, T.; Lyu, Y.; Xiong, K.; Wang, W.; Zhang, H.; Zhan, Z.; Jiang, Z.; Ding, Y., Chiral BINAP-based hierarchical porous polymers as platforms for efficient heterogeneous asymmetric catalysis. *Chinese Journal of Catalysis* **2017,** *38* (5), 890-897.

168. Fan, Q.-h.; Ren, C.-y.; Yeung, C.-h.; Hu, W.-h.; Chan, A. S. C., Highly effective soluble polymer-supported catalysts for asymmetric hydrogenation. *JACS* **1999,** *121* (32), 7407-7408.

169. Pugin, B.; Blaser, H.-U., The immobilization of rhodium-4-(diphenylphosphino)-2-(diphenylphosphinomethyl)-pyrrolidine (rh-ppm) complexes: a systematic study. *Adv. Synth. Catal.* **2006,** *348* (12-13), 1743-1751.

170. Pu, L., Rigid and sterically regular chiral 1,1′-binaphthyl polymers in asymmetric catalysis. *Chemistry - A European Journal* **1999,** *5* (8), 2227-2232.

171. Yu, H.-B.; Hu, Q.-S.; Pu, L., Synthesis of a rigid and optically active poly(BINAP) and its application in asymmetric catalysis. *Tetrahedron Lett.* **2000,** *41* (11), 1681-1685.

172. Wang, X.; Lu, S.-m.; Li, J.; Liu, Y.; Li, C., Conjugated microporous polymers with chiral BINAP ligand built-in as efficient catalysts for asymmetric hydrogenation. *Catalysis Science & Technology* **2015,** *5* (5), 2585-2589.

173. den Heeten, R.; Swennenhuis, B. H. G.; van Leeuwen, P. W. N. M.; de Vries, J. G.; Kamer, P. C. J., Parallel synthesis and screening of polymer-supported phosphorus-stereogenic aminophosphane–phosphite and –phosphinite ligands. *Angew. Chem. Int. Ed.* **2008,** *47* (35), 6602-6605.

174. Swennenhuis, B. H. G.; Chen, R.; van Leeuwen, P. W. N. M.; de Vries, J. G.; Kamer, P. C. J., Supported chiral monodentate ligands in rhodium-catalysed asymmetric hydrogenation and palladium-catalysed asymmetric allylic alkylation. *Eur. J. Org. Chem.* **2009,** *2009* (33), 5796-5803.

175. Pugin, B.; Landert, H.; Spindler, F.; Blaser, H.-U., More than 100,000 turnovers with immobilized Ir-diphosphine catalysts in an enantioselective imine hydrogenation. *Adv. Synth. Catal.* **2002,** *344* (9), 974-979.

176. Ohkuma, T.; Takeno, H.; Honda, Y.; Noyori, R., asymmetric hydrogenation of ketones with polymer-bound BINAP/diamine ruthenium catalysts. *Adv. Synth. Catal.* **2001,** *343* (4), 369-375.

177. Li, X. G.; Wu, X. F.; Chen, W. P.; Hancock, F. E.; King, F.; Xiao, J. L., Asymmetric transfer hydrogenation in water with a supported Noyori-Ikariya catalyst. *Org. Lett.* **2004,** *6* (19), 3321-3324.

178. Heutz, F. J. L.; Erken, C.; Aguila, M. J. B.; Lefort, L.; Kamer, P. C. J., Heterogeneous hydrogenation of esters under mild conditions using solid-supported phosphorus–ruthenium catalysts. *ChemCatChem* **2016,** *8* (11), 1896-1900.

179. Gao, J.-X.; Ikariya, T.; Noyori, R., A Ruthenium(II) Complex with a C2-symmetric diphosphine/diamine tetradentate ligand for asymmetric transfer hydrogenation of aromatic ketones. *Organometallics* **1996,** *15* (4), 1087-1089.

180. M. Stoop, R.; Mezzetti, A., Asymmetric epoxidation of olefins . The first enantioselective epoxidation of unfunctionalised olefins catalysed by a chiral ruthenium complex with H2O2 as oxidant. *Green Chemistry* **1999,** *1* (1), 39-41.

181. Schotes, C.; Mezzetti, A., Asymmetric Diels-Alder reactions of unsaturated beta-ketoesters catalyzed by chiral ruthenium PNNP complexes. *JACS* **2010,** *132* (11), 3652-+.

182. Bachmann, S.; Furler, M.; Mezzetti, A., Cis-selective asymmetric cyclopropanation of olefins catalyzed by five-coordinate [RuCl(PNNP)]+ complexes. *Organometallics* **2001,** *20* (10), 2102-2108.

183. Li, T.; Churlaud, R.; Lough, A. J.; Abdur-Rashid, K.; Morris, R. H., Dihydridoamine and hydridoamido complexes of ruthenium(II) with a tetradentate P−N−N−P donor ligand. *Organometallics* **2004,** *23* (26), 6239-6247.

184. Lin, Z.-C.; Chen, C., Asymmetric synthesis of a new Salen type-titanium complex as the catalyst for asymmetric trimethylsilylcyanation of aldehydes. **2010,** *57* (4A), 726-737.

185. Leong, C. G.; Akotsi, O. M.; Ferguson, M. J.; Bergens, S. H., A ruthenium catalyst that does not require an N–H ligand to achieve high enantioselectivity for hydrogenation of an alkyl-aryl ketone. *Chem. Commun.* **2003,** (6), 750-751.

186. Hamilton, R. J.; Bergens, S. H., An unexpected possible role of base in asymmetric catalytic hydrogenations of ketones. synthesis and characterization of several key catalytic intermediates. *JACS* **2006,** *128* (42), 13700-13701.

187. Takebayashi, S.; Dabral, N.; Miskolzie, M.; Bergens, S. H., Experimental investigations of a partial Ru–O bond during the metal–ligand bifunctional addition in Noyori-Type enantioselective ketone hydrogenation. *JACS* **2011,** *133* (25), 9666-9669.

188. Gao, J.-X.; Yi, X.-D.; Xu, P.-P.; Tang, C.-L.; Zhang, H.; Wang, H.-L.; Ikariya, T.; Cationic rhodium complexes with chiral tetradentate ligands as catalysts for enantioselective reduction of simple ketones. *J. Mol. Catal. A. Chem.* **2000,** *159*, 3-9.

189. Rautenstrauch, V.; Hoang-Cong, X.; Churlaud, R.; Abdur-Rashid, K.; Morris, R. H., Hydrogenation versus transfer hydrogenation of ketones: two established ruthenium systems catalyze both. *Chemistry - A European Journal* **2003,** *9* (20), 4954-4967.

190. Schotes, C.; Mezzetti, A., Asymmetric Diels−Alder reactions of unsaturated β-ketoesters catalyzed by chiral ruthenium pnnp complexes. *JACS* **2010,** *132* (11), 3652-3653.

191. Endean, R. T.; Rasu, L.; Bergens, S. H., Enantioselective hydrogenations of esters with dynamic kinetic resolution. *ACS Catal.* **2019,** *9* (7), 6111-6117.

192. Furuta, K.; Iwanaga, K.; Yamamoto, H., Asymmetric diels-alder reaction. Cooperative blocking effect in organic synthesis. *Tetrahedron Lett.* **1986,** *27* (37), 4507-4510.

193. Hartmann, R.; Chen, P., Noyori's hydrogenation catalyst needs a lewis acid cocatalyst for high activity. *Angew. Chem. Int. Ed.* **2001,** *40* (19), 3581-3585.

194. Ohkuma, T.; Koizumi, M.; Muñiz, K.; Hilt, G.; Kabuto, C.; Noyori, R., trans-RuH(η-BH4)(binap)(1,2-diamine): A catalyst for asymmetric hydrogenation of simple ketones under base-free conditions. *JACS* **2002,** *124* (23), 6508-6509.

195. Abdur-Rashid, K.; Clapham, S. E.; Hadzovic, A.; Harvey, J. N.; Lough, A. J.; Morris, R. H., Mechanism of the hydrogenation of ketones catalyzed by trans-dihydrido(diamine)ruthenium(ii) complexes. *JACS* **2002,** *124* (50), 15104-15118.

196. Dub, P. A.; Scott, B. L.; Gordon, J. C., Why does alkylation of the N–H functionality within M/NH bifunctional Noyori-Type catalysts lead to turnover? *JACS* **2017,** *139* (3), 1245-1260.

197. Morawetz, H., Kinetics of intramolecular and intermolecular reactions involving two functional groups attached to polymers. In *Pure Appl. Chem.*, 1974; Vol. 38, p 267.

198. Karaman, R., A general equation correlating intramolecular rates with 'attack' parameters: distance and angle. *Tetrahedron Lett.* **2010,** *51* (39), 5185-5190.

199. Sanchez, J.; McCormick, A. V., Intramolecular vs. intermolecular condensation rates in the acidic polymerization of octaethoxytrisiloxane. *J. Non-Cryst. Solids* **1994,** *167* (3), 289-294.

200. Armstrong, A. A.; Amzel, L. M., Role of entropy in increased rates of intramolecular reactions. *JACS* **2003,** *125* (47), 14596-14602.

201. Marino, M. G.; Kreuer, K. D., Alkaline stability of quaternary ammonium cations for alkaline fuel cell membranes and ionic liquids. *CHEMSUSCHEM* **2015,** *8* (3), 513-523.

202. Love, J. A.; Morgan, J. P.; Trnka, T. M.; Grubbs, R. H., A practical and highly active ruthenium-based catalyst that effects the cross metathesis of acrylonitrile. *Angew. Chem. Int. Ed.* **2002,** *41* (21), 4035-4037.

203. Choi, T.-L.; Grubbs, R. H., Controlled living ring-opening-metathesis polymerization by a fast-initiating ruthenium catalyst. *Angew. Chem. Int. Ed.* **2003,** *42* (15), 1743-1746.

204. Kirubakaran, A.; Jain, S.; Nema, R. K., A review on fuel cell technologies and power electronic interface. *Renewable and Sustainable Energy Reviews* **2009,** *13* (9), 2430-2440.

205. McLean, G. F.; Niet, T.; Prince-Richard, S.; Djilali, N., An assessment of alkaline fuel cell technology. *Int. J. Hydrogen Energy* **2002,** *27* (5), 507-526.

206. Mehta, V.; Cooper, J. S., Review and analysis of PEM fuel cell design and manufacturing. *J. Power Sources* **2003,** *114* (1), 32-53.

207. Das, V.; Padmanaban, S.; Venkitusamy, K.; Selvamuthukumaran, R.; Blaabjerg, F.; Siano, P., Recent advances and challenges of fuel cell based power system architectures and control – A review. *Renewable and Sustainable Energy Reviews* **2017,** *73*, 10-18.

208. Haseli, Y., Maximum conversion efficiency of hydrogen fuel cells. *Int. J. Hydrogen Energy* **2018,** *43* (18), 9015-9021.

209. Daud, W. R. W.; Rosli, R. E.; Majlan, E. H.; Hamid, S. A. A.; Mohamed, R.; Husaini, T., PEM fuel cell system control: A review. *Renewable Energy* **2017,** *113*, 620-638.

210. Sulaiman, N.; Hannan, M. A.; Mohamed, A.; Majlan, E. H.; Wan Daud, W. R., A review on energy management system for fuel cell hybrid electric vehicle: Issues and challenges. *Renewable and Sustainable Energy Reviews* **2015,** *52*, 802-814.

211. Cheng, J.; He, G.; Zhang, F., A mini-review on anion exchange membranes for fuel cell applications: Stability issue and addressing strategies. *Int. J. Hydrogen Energy* **2015,** *40* (23), 7348-7360.

212. Andújar, J. M.; Segura, F., Fuel cells: History and updating. A walk along two centuries. *Renewable and Sustainable Energy Reviews* **2009,** *13* (9), 2309-2322.

213. Cook, B. Introduction to fuel cells and hydrogen technology *Engineering Science & Education Journal*, **2002**, 205-216.

214. McNicol, B. D.; Rand, D. A. J.; Williams, K. R., Fuel cells for road transportation purposes — yes or no? *J. Power Sources* **2001,** *100* (1), 47-59.

215. Ortiz-Rivera, E. I.; Reyes-Hernandez, A. L.; Febo, R. A. In *Understanding the history of fuel cells*, 2007 IEEE Conference on the History of Electric Power, 3-5 Aug. 2007; 117-122.

216. Wang, Y.; Chen, K. S.; Mishler, J.; Cho, S. C.; Adroher, X. C., A review of polymer electrolyte membrane fuel cells: Technology, applications, and needs on fundamental research. *Applied Energy* **2011,** *88* (4), 981-1007.

217. https://www.energy.gov/sites/prod/files/2017/10/f37/fcto_2016_market_report.pdf

218. Mahato, N.; Banerjee, A.; Gupta, A.; Omar, S.; Balani, K., Progress in material selection for solid oxide fuel cell technology: A review. *Prog. Mater Sci.* **2015,** *72*, 141-337.

219. Lanzini, A.; Madi, H.; Chiodo, V.; Papurello, D.; Maisano, S.; Santarelli, M.; Van herle, J., Dealing with fuel contaminants in biogas-fed solid oxide fuel cell (SOFC) and molten carbonate fuel cell (MCFC) plants: degradation of catalytic and electro-catalytic active surfaces and related gas purification methods. *Prog. Energy Combust. Sci.* **2017,** *61*, 150-188.

220. Jun, A.; Kim, J.; Shin, J.; Kim, G., Perovskite as a cathode material: a review of its role in solid-oxide fuel cell technology. *ChemElectroChem* **2016,** *3* (4), 511-530.

221. Afif, A.; Radenahmad, N.; Cheok, Q.; Shams, S.; Kim, J. H.; Azad, A. K., Ammonia-fed fuel cells: a comprehensive review. *Renewable and Sustainable Energy Reviews* **2016,** *60*, 822-835.

222. Yuan, H.; Hou, Y.; Abu-Reesh, I. M.; Chen, J.; He, Z., Oxygen reduction reaction catalysts used in microbial fuel cells for energy-efficient wastewater treatment: a review. *Materials Horizons* **2016,** *3* (5), 382-401.

223. Chen, W.; Huang, J.; Wei, J.; Zhou, D.; Cai, J.; He, Z.-D.; Chen, Y.-X., Origins of high onset overpotential of oxygen reduction reaction at Pt-based electrocatalysts: A mini review. *Electrochem. Commun.* **2018,** *96*, 71-76.

224. Sui, S.; Wang, X.; Zhou, X.; Su, Y.; Riffat, S.; Liu, C.-j., A comprehensive review of Pt electrocatalysts for the oxygen reduction reaction: Nanostructure, activity, mechanism and carbon support in PEM fuel cells. *Journal of Materials Chemistry A* **2017,** *5* (5), 1808-1825.

225. Ge, X.; Sumboja, A.; Wuu, D.; An, T.; Li, B.; Goh, F. W. T.; Hor, T. S. A.; Zong, Y.; Liu, Z., Oxygen reduction in alkaline media: from mechanisms to recent advances of catalysts. *ACS Catalysis* **2015,** *5* (8), 4643-4667.

226. Lu, F.; Zhang, Y.; Liu, S.; Lu, D.; Su, D.; Liu, M.; Zhang, Y.; Liu, P.; Wang, J. X.; Adzic, R. R.; Gang, O., Surface proton transfer promotes four-electron oxygen reduction on gold nanocrystal surfaces in alkaline solution. *JACS* **2017,** *139* (21), 7310-7317.

227. Nie, Y.; Li, L.; Wei, Z., Recent advancements in Pt and Pt-free catalysts for oxygen reduction reaction. *Chem. Soc. Rev.* **2015,** *44* (8), 2168-2201.

228. Nørskov, J. K.; Rossmeisl, J.; Logadottir, A.; Lindqvist, L.; Kitchin, J. R.; Bligaard, T.; Jónsson, H., Origin of the overpotential for oxygen reduction at a fuel-cell cathode. *The Journal of Physical Chemistry B* **2004,** *108* (46), 17886-17892.

229. Keith, J. A.; Jacob, T., Theoretical studies of potential-dependent and competing mechanisms of the electrocatalytic oxygen reduction reaction on Pt(111). *Angew. Chem. Int. Ed.* **2010,** *49* (49), 9521-9525.

230. Huang, X.; Zhao, Z.; Cao, L.; Chen, Y.; Zhu, E.; Lin, Z.; Li, M.; Yan, A.; Zettl, A.; Wang, Y. M.; Duan, X.; Mueller, T.; Huang, Y., High-performance transition metal–doped Pt$_3$Ni octahedra for oxygen reduction reaction. *Science* **2015,** *348* (6240), 1230-1234.

231. Guo, S.; Li, D.; Zhu, H.; Zhang, S.; Markovic, N. M.; Stamenkovic, V. R.; Sun, S., FePt and CoPt nanowires as efficient catalysts for the oxygen reduction reaction. *Angew. Chem. Int. Ed.* **2013,** *125* (12), 3549-3552.

232. Cui, C.; Gan, L.; Li, H.-H.; Yu, S.-H.; Heggen, M.; Strasser, P., Octahedral PtNi nanoparticle catalysts: exceptional oxygen reduction activity by tuning the alloy particle surface composition. *Nano Lett.* **2012,** *12* (11), 5885-5889.

233. Stamenkovic, V. R.; Fowler, B.; Mun, B. S.; Wang, G.; Ross, P. N.; Lucas, C. A.; Marković, N. M., Improved oxygen reduction activity on Pt$_3$Ni(111) via increased surface site availability. *Science* **2007,** *315* (5811), 493-497.

234. Choi, S.-I.; Xie, S.; Shao, M.; Odell, J. H.; Lu, N.; Peng, H.-C.; Protsailo, L.; Guerrero, S.; Park, J.; Xia, X.; Wang, J.; Kim, M. J.; Xia, Y., Synthesis and characterization of 9 nm Pt–Ni octahedra with a record high activity of 3.3 A/mgPt for the oxygen reduction reaction. *Nano Lett.* **2013,** *13* (7), 3420-3425.

235. Rossmeisl, J.; Karlberg, G. S.; Jaramillo, T.; Nørskov, J. K., Steady state oxygen reduction and cyclic voltammetry. *Faraday Discuss.* **2009,** *140* (0), 337-346.

236. Hammer, B., Reactivity of a stepped surface NO dissociation on Pd(211). *Faraday Discuss.* **1998,** *110* (0), 323-333.

237. Jiao, Y.; Zheng, Y.; Jaroniec, M.; Qiao, S. Z., Design of electrocatalysts for oxygen- and hydrogen-involving energy conversion reactions. *Chem. Soc. Rev.* **2015,** *44* (8), 2060-2086.

238. Stamenkovic, V.; Mun, B. S.; Mayrhofer, K. J. J.; Ross, P. N.; Markovic, N. M.; Rossmeisl, J.; Greeley, J.; Nørskov, J. K., Changing the activity of electrocatalysts for oxygen reduction by tuning the surface electronic structure. *Angew. Chem. Int. Ed.* **2006,** *118* (18), 2963-2967.

239. Liu, M.; Zhao, Z.; Duan, X.; Huang, Y., Nanoscale structure design for high-performance pt-based orr catalysts. *Adv. Mater.* **2019,** *31* (6), 1802234.

240. Carpenter, M. K.; Moylan, T. E.; Kukreja, R. S.; Atwan, M. H.; Tessema, M. M., Solvothermal synthesis of platinum alloy nanoparticles for oxygen reduction electrocatalysis. *JACS* **2012,** *134* (20), 8535-8542.

241. Cui, C.; Gan, L.; Heggen, M.; Rudi, S.; Strasser, P., Compositional segregation in shaped Pt alloy nanoparticles and their structural behaviour during electrocatalysis. *Nature Materials* **2013,** *12*, 765-771.

242. Li, M.; Zhao, Z.; Cheng, T.; Fortunelli, A.; Chen, C.-Y.; Yu, R.; Zhang, Q.; Gu, L.; Merinov, B. V.; Lin, Z.; Zhu, E.; Yu, T.; Jia, Q.; Guo, J.; Zhang, L.; Goddard, W. A.; Huang, Y.; Duan, X., Ultrafine jagged platinum nanowires enable ultrahigh mass activity for the oxygen reduction reaction. *Science* **2016,** *354* (6318), 1414-1419.

243. Baldizzone, C.; Gan, L.; Hodnik, N.; Keeley, G. P.; Kostka, A.; Heggen, M.; Strasser, P.; Mayrhofer, K. J. J., Stability of dealloyed porous Pt/Ni nanoparticles. *ACS Catalysis* **2015,** *5* (9), 5000-5007.

244. Wiesner, M. R.; Lowry, G. V.; Alvarez, P.; Dionysiou, D.; Biswas, P., Assessing the risks of manufactured nanomaterials. *Environmental Science & Technology* **2006,** *40* (14), 4336-4345.

245. Introduction: glancing angle deposition technology. In *Glancing Angle Deposition of Thin Films*. John Wiley & Sons, Ltd, **2014**

246. Hawkeye, M. M.; Brett, M. J., Glancing angle deposition: Fabrication, properties, and applications of micro- and nanostructured thin films. *Journal of Vacuum Science & Technology A* **2007,** *25* (5), 1317-1335.

247. Taschuk, M. T.; Hawkeye, M. M.; Brett, M. J., Chapter 13 - glancing angle deposition. In *Handbook of Deposition Technologies for Films and Coatings (Third Edition)*; Elsevier Inc., **2010**.

248. Krause, K. M.; Taschuk, M. T.; Brett, M. J., Glancing angle deposition on a roll: towards high-throughput nanostructured thin films. *Journal of Vacuum Science & Technology A* **2013,** *31* (3), 031507.

249. Francis, S. A.; Tucker, R. T.; Brett, M. J.; Bergens, S. H., Structural and activity comparison of self-limiting versus traditional Pt electro-depositions on nanopillar Ni films. *J. Power Sources* **2013,** *222*, 533-541.

250. Francis, S. A.; Bergens, S. H., Low Pt-loading Ni–Pt and Pt deposits on Ni: Preparation, activity and investigation of electronic properties. *J. Power Sources* **2011,** *196* (18), 7470-7480.

251. Menard, L. N.; Bergens, S. H., An unexpected, self-regulating codeposition of nickel and platinum forming deposits with surfaces enriched in platinum. *J. Power Sources* **2009,** *194* (1), 298-302.

252. Gasda, M. D.; Eisman, G. A.; Gall, D., Nanorod PEM fuel cell cathodes with controlled porosity. *J. Electrochem. Soc.* **2010,** *157* (3), B437-B440.

253. Gasda, M. D.; Eisman, G. A.; Gall, D., Pore Formation by in situ etching of nanorod PEM fuel cell electrodes. *J. Electrochem. Soc.* **2010,** *157* (1), B113-B117.

254. Gasda, M. D.; Eisman, G. A.; Gall, D., Sputter-deposited Pt/CrN nanoparticle PEM fuel cell cathodes: limited proton conductivity through electrode dewetting. **2010,** *157* (1), B71-B76.

255. Gasda, M. D.; Teki, R.; Lu, T.-M.; Koratkar, N.; Eisman, G. A.; Gall, D., Sputter-deposited Pt PEM fuel cell electrodes: particles vs layers. *J. Electrochem. Soc.* **2009,** *156* (5), B614-B619.

256. Bonakdarpour, A.; Tucker, R. T.; Fleischauer, M. D.; Beckers, N. A.; Brett, M. J.; Wilkinson, D. P., Nanopillar niobium oxides as support structures for oxygen reduction electrocatalysts. *Electrochim. Acta* **2012,** *85*, 492-500.

257. Bonakdarpour, A.; Fleischauer, M. D.; Brett, M. J.; Dahn, J. R., Columnar support structures for oxygen reduction electrocatalysts prepared by glancing angle deposition. *Applied Catalysis A: General* **2008,** *349* (1), 110-115.

258. Khudhayer, W. J.; Kariuki, N. N.; Wang, X.; Myers, D. J.; Shaikh, A. U.; Karabacak, T., Oxygen reduction reaction electrocatalytic activity of glancing angle deposited platinum nanorod arrays. *J. Electrochem. Soc.* **2011,** *158* (8), B1029-B1041.

259. Khudhayer, W. J.; Kariuki, N.; Myers, D. J.; Shaikh, A. U.; Karabacak, T., GLAD Cr nanorods coated with SAD Pt thin film for oxygen reduction reaction. *J. Electrochem. Soc.* **2012,** *159* (6), B729-B736.

260. Spendelow, J. S.; Wieckowski, A., Electrocatalysis of oxygen reduction and small alcohol oxidation in alkaline media. *Phys. Chem. Chem. Phys.* **2007,** *9* (21), 2654-2675.

261. García-Contreras, M. A.; Fernández-Valverde, S. M.; Vargas-García, J. R., Pt, PtNi and PtCoNi film electrocatalysts prepared by chemical vapor deposition for the oxygen reduction reaction in 0.5M KOH. *J. Alloys Compd.* **2010,** *504*, S425-S428.

262. Pašti, I. A.; Gavrilov, N. M.; Baljozović, M.; Mitrić, M.; Mentus, S. V., Oxygen reduction reaction of Pt–In alloy: Combined theoretical and experimental investigations. *Electrochim. Acta* **2013,** *114*, 706-712.

263. Jäger, R.; Härk, E.; Kasatkin, P. E.; Lust, E., Investigation of a carbon-supported Pt electrode for oxygen reduction reaction in 0.1M KOH aqueous solution. *J. Electrochem. Soc.* **2014,** *161* (9), F861-F867.

264. Krause, K. M.; Thommes, M.; Brett, M. J., Pore analysis of obliquely deposited nanostructures by krypton gas adsorption at 87K. *Microporous Mesoporous Mater.* **2011,** *143* (1), 166-173.

265. Debe, M. K., Effect of electrode surface area distribution on high current density performance of PEM fuel cells. *J. Electrochem. Soc.* **2011,** *159* (1), B53-B66.

266. Hahn, F.; Beden, B.; Croissant, M. J.; Lamy, C., In situ uv visible reflectance spectroscopic investigation of the nickel electrode-alkaline solution interface. *Electrochim. Acta* **1986,** *31* (3), 335-342.

267. Machado, S. A. S.; Avaca, L. A., The hydrogen evolution reaction on nickel surfaces stabilized by H-absorption. *Electrochim. Acta* **1994,** *39* (10), 1385-1391.

268. Beden, B.; Floner, D.; Léger, J. M.; Lamy, C., A voltammetric study of the formation on hydroxides and oxyhydroxides on nickel single crystal electrodes in contact with an alkaline solution. *Surf. Sci.* **1985,** *162* (1), 822-829.

269. Seghiouer, A.; Chevalet, J.; Barhoun, A.; Lantelme, F., Electrochemical oxidation of nickel in alkaline solutions: a voltammetric study and modelling. *J. Electroanal. Chem.* **1998,** *442* (1), 113-123.

270. Jiang, J.; Kucernak, A., Solid polymer electrolyte membrane composite microelectrode investigations of fuel cell reactions. II: voltammetric study of methanol oxidation at the nanostructured platinum microelectrode|Nafion® membrane interface. *J. Electroanal. Chem.* **2005,** *576* (2), 223-236.

271. Conway, B. E.; Angerstein-Kozlowska, H., The electrochemical study of multiple-state adsorption in monolayers. *Acc. Chem. Res.* **1981,** *14* (2), 49-56.

272. Kariuki, N. N.; Khudhayer, W. J.; Karabacak, T.; Myers, D. J., GLAD Pt–Ni alloy nanorods for oxygen reduction reaction. *ACS Catalysis* **2013,** *3* (12), 3123-3132.

273. Marković, N. M.; Gasteiger, H. A.; Ross, P. N., Oxygen reduction on platinum low-index single-crystal surfaces in alkaline solution: rotating ring disk Pt(hkl) studies. *The Journal of Physical Chemistry* **1996,** *100* (16), 6715-6721.

274. Zhang, Z.; Liu, J.; Gu, J.; Su, L.; Cheng, L., An overview of metal oxide materials as electrocatalysts and supports for polymer electrolyte fuel cells. *Energy & Environmental Science* **2014,** *7* (8), 2535-2558.

275. Wang, C.; Moghaddam, R. B.; Sorge, J. B.; Xu, S.; Brett, M. J.; Bergens, S. H., Oxygen reduction over dealloyed Pt layers on glancing angle deposited Ni nanostructures. *Electrochim. Acta* **2015,** *176*, 620-626.

276. Chen, C.; Kang, Y.; Huo, Z.; Zhu, Z.; Huang, W.; Xin, H. L.; Snyder, J. D.; Li, D.; Herron, J. A.; Mavrikakis, M.; Chi, M.; More, K. L.; Li, Y.; Markovic, N. M.; Somorjai, G. A.; Yang, P.; Stamenkovic, V. R., Highly crystalline multimetallic nanoframes with three-dimensional electrocatalytic surfaces. *Science* **2014,** *343* (6177), 1339-1343.

277. Hydrogenation. In *Applied Homogeneous Catalysis with Organometallic Compounds*; Wiley‑VCH Verlag GmbH & Co. KGaA. **2018**

278. C. Smolinske, S., *CRC Handbook of Food, Drug, and Cosmetic Excipients*. 2018.

279. Hems, W. P.; McMorn, P.; Riddel, S.; Watson, S.; Hancock, F. E.; Hutchings, G. J., Asymmetric hydrogenation using chiral Rh complexes immobilised with a new ion-exchange strategy. *Organic & Biomolecular Chemistry* **2005,** *3* (8), 1547-1550.

280. Augustine, R.; Tanielyan, S.; Anderson, S.; Yang, H., A new technique for anchoring homogeneous catalysts. *Chem. Commun.* **1999,** (13), 1257-1258.

281. Mazzel, M.; Marconi, W.; Riocci, M., Asymmetric hydrogenation of substituted acrylic acids by Rhʹ-aminophosphine chiral complex supported on mineral clays. *J. Mol. Catal.* **1980,** *9* (4), 381-387.

282. Simons, C.; Hanefeld, U.; Arends, I. W. C. E.; Maschmeyer, T.; Sheldon, R. A., Comparison of supports for the electrostatic immobilisation of asymmetric homogeneous catalysts. *J. Catal.* **2006,** *239* (1), 212-219.

283. Barbaro, P.; Bianchini, C.; Giambastiani, G.; Oberhauser, W.; Bonzi, L. M.; Rossi, F.; Dal Santo, V., Recycling asymmetric hydrogenation catalysts by their immobilisation onto ion-exchange resins. *Dalton Transactions* **2004,** (12), 1783-1784.